Institute of Animal Reproduction and Food Research
Polish Academy of Sciences

MTech Manohara Mahadeva

Membrane potential sets the tempo: Bioelectricity controls the rate of somitogenesis in chick embryos through mechanics

A doctoral thesis was undertaken in the Team of Reproductive Pathology and Translational Medicine at the Institute of Animal Reproduction and Food Research Polish Academy of Sciences

under the supervision of

dr hab. Magdalena Kowacz

This work was supported by the project Sonata Bis 2020/38/E/NZ3/00039 funded by the National Science Centre, Poland

Olsztyn 2025

Vote of thanks

Science is my passion, and becoming a scientist was my childhood dream. This PhD is a major milestone in my career. The journey was interesting and challenging, and I felt very happy every time I learned something new. This achievement was only possible because of the wholehearted support, constant motivation, and encouragement I received from so many people.

The most important person in this journey was my supervisor, dr hab. Magdalena Kowacz. First of all, I would like to thank her for choosing me for this fascinating project. She was my mentor, guide, and teacher, or, as we respectfully say in our language, GURU. It would not have been possible for me to learn so much without her enthusiastic and strong support in every aspect of my Ph.D. I express my sincere and deepest gratitude for her patience, especially when I made silly mistakes multiple times, and for believing in my skills and learning abilities. She became my inspiration. Her unique way of thinking about science, her criticism, and her strong feedback shaped me into a critical thinker and changed my perspective on physics. Being her first PhD student, I had the opportunity to understand the challenges of setting up a lab for biophysical studies. I am grateful for this invaluable experience. I also thank her for organizing internships for me and supporting me in learning embryo culturing methods, something I never imagined I would work on in my life.

I am also grateful to Dr. Sebastian Niestępski, a postdoc researcher in our lab, whose constant support in setting up the lab, building experimental setups, optimizing methods, and analyzing data, made my workflow easier and faster. I thank him for his valuable suggestions for all my experiments, manuscripts and thesis preparation. His attention to detail with experimental methods made me to be precise during data acquisition. I sincerely thank him for always making time to help, he never refused any of my requests. His kind support throughout my PhD, even with administrative tasks, made my life much easier at the institute.

I sincerely thank the Doctoral School of the Institute of Animal Reproduction and Food Research, Polish Academy of Sciences, for providing the necessary infrastructure, resources, and a supportive working environment to carry out my PhD work. I would like to thank prof. dr hab. Aneta Andronowska, the head of the doctoral school, for organizing coursework and supporting with all the paperwork, including internship applications. Without her help, things would not have been smooth.

I would like to thank prof. dr hab. Dariusz Skarżyński and all the members of the Team of Reproductive Pathology & Translation Medicine for creating an amazing work environment. I sincerely thank Dr. Beenu Moza Jalali for her kind hearted support and encouragement in the early days of my PhD. Her suggestions strengthened me and helped me especially with manuscript writing process. I thank Karolina Łukasik for her friendliness, which made me to feel at home in Poland, and Paweł Likszo, for his kind help in the lab.

I Sincerely thank prof. Raquel P. Andrade from Portugal for training me in embryo work. Our discussions further fuelled my curiosity in developmental biology. I also thank Gil, Tomas, Cristina, and Nisia for helping me learn embryo culturing techniques.

I extend my heartfelt thanks to all my friends. Mamata, my senior and very good friend, was someone I could speak with in Kannada (my mother tongue) and share Indian food with, something I never expected in Poland. Her experiences and suggestions gave me confidence that I could survive here. She also introduced me to her Polish friends Marcin and Adam, the first people I befriended in Poland. I am grateful to Abhi, Yashi, Rose, Costanza, Ewelina, Saumya, Ranjini, Tanya, Ola, Bia, and Mafalda, wonderful friends who made me feel included from the very beginning, even when I was the only guy in the group. Many thanks to Abhi, Yashi, Saumya, and Rose for always being there to help me. I really thank Parcival for our late-night parties and endless scientific discussions. Prutha, thank you for cooking together with me and for our long conversations about life and science. I also thank my small lunch group, Reshma, Karolina, and Priman. It was always relaxing to spend time with you. Reshma (Achoo), thank you for your delicious kerala food, you made the last months of my PhD truly memorable. I am grateful for your company and our interesting scientific conversations. I also thank my non-PhD Polish friends Matteo, Piotr, Martin, and Ola for their companionship. To my Indian friends, Amrutha, Priya, Puneeth, Naveen, Soma, Amith, Kiran, Hemanth, Gaja, Subhash, Sukanya, Divya, Sharadhi, Sumanth, Deepshika, Saurabh, Mahesh, Pavi akka, Puppy akka, Vidya, Yashaswini, and Mamatha, thank you for your encouragement throughout this journey. I would also like to thank my mentor, Dr. Gautam V Soni, the person who inspired me to become a researcher.

Finally, I thank my family for their constant support and encouragement. My Dad, Mom, and Atthe were proud and happy that I was pursuing a Ph.D. Special thanks go to my sisters Latha and Anu, and my brother Sachi, who stood firmly by my decision to go for higher studies. They took care of my entire family in my absence, allowing me to focus on building my career. Without them, it would not have been possible to complete this Ph.D. I know it was difficult for them to send me so far away, and I am deeply grateful for their sacrifices. I feel privileged to be a part of such a loving family.

With sincere gratitude,

Mano

Table of Contents

List of abbreviations

ANCOVA	Analysis of Covariance
APW	Artificial Pond Water
D	Width of extracellular voltage zone
ΔL	Change in aspiration length
ΔP	Change in pressure
ΔV_i	Change in intracellular voltage
ΔV_m	Change in membrane potential
ΔV_z	Change in extracellular voltage
E	Young's modulus
EC	Embryo clock
ECM	Extracellular matrix
EDL	Electrical double layer
EZ	Exclusion zone
ID	Inner diameter
L	Aspiration length
L_C	Aspiration length at control condition
L_D	Aspiration length at depolarized condition
L_H	Aspiration length at hyperpolarized condition
L_O	Initial aspiration length
L(t)	Somite growth rate
n	Number of somite pairs
NT	Neural tube
OD	Outer diameter
PC	Pennett-Compton
PSM	Presomitic mesoderm
$\varphi(\eta)$	Dimensionless factor, defined as pipette wall function.
η	Ratio of thickness and inner radius of pipette
R	Pipette radius

R_O	Initial pipette radius
S	Somite
SS	Somite Stage
TMP	Transmembrane potential
TFs	Transcription factors
τ	Periodicity of somite formation
V_i	Intracellular voltage
V_m	Membrane potential
V_z	Extracellular voltage
Wnt	Wingless-related integration site signaling pathway
YAP	Yes-associated protein
ZEV	Zone of extracellular voltage

Abstract

The question of what ticks the life clock is intriguing. Yet, we still lack a clear answer. For instance, in early embryogenesis, the formation of tissue blocks, called somites, is a crucial, tightly regulated, and time-bounded developmental process known as somitogenesis. During this process, somites are sequentially generated from paraxial mesoderm along the embryonic body axis. The periodicity of somite formation is strictly specific to tissue and species types; however, what sets this rhythm for somite segmentation, and the mechanism that brings the synchronicity between temporal periodicity and somite growth remains elusive. Somite segmentation involves migration, self-assembly of a fixed number of cells, which subsequently undergo proliferation and differentiation to acquire specific size and structure. To maintain proportionality of the developing body and produce somites of consistent size at precise intervals, these processes must be strictly coordinated in space and time. All these fundamental processes have been shown to be individually regulated by membrane potential of cells (V_m).

V_m is the electric potential difference between cytosol and extracellular space, generated due to an unequal distribution of ions across the semipermeable membrane. It has negative values with a magnitude specific to a given cell type and function. The cells undergoing proliferation, migration, and self-organization are more depolarized (less negative) in comparison to differentiated cells. Also, these active cells are softer than their quiescent counterparts, and are exposed to specific conditions of their microenvironment - enriched in CO_2 and K^+. Therefore, in this study, we aimed to examine whether the periodicity of somite segmentation (cell migration/self-assembly) and concurrent somite growth (cell proliferation) can be controlled by altering V_m. We ask the question whether the effects of V_m are mediated by tissue mechanics, and if microenvironment plays functional role in defining respective cellular properties. For that purpose, we used early-stage chick embryos as an experimental model and i) mapped V_m and stiffness patterns of somites along the embryonic body axis (the data that were not available for vertebrate embryos); ii) followed by V_m modifications with the use of physiologically relevant stimuli and iii) measurements of tissue mechanics and markers of somitogenesis progression (segmentation time and somites spatial expansion) in response to altered V_m.

As they grow into developmentally advanced stages, somites become hyperpolarized and stiffer. Apart from this, we observed step-like changes in V_m between specific somite groups, mirroring the previously reported onset of biochemical and morphological transitions. Induced modifications in V_m set new tempo for somite segmentation and synchronously adjust the somite size without disturbing its regular aspect ratio. In particular, induced depolarization has accelerated the rate of somitogenesis, by promoting proliferation and migration/self-assembly, and softened the somite-forming cells (a characteristic related to enhanced proliferation and motility), while hyperpolarization has increased their stiffness and slowed down the process. Very notably, we could promote unprecedented, nearly 30% acceleration of somite segmentation time without disturbing overall body pattern. A linear and an exponential dependence of periodicity of somite formation and somite growth rate on V_m was observed, respectively. The linear correlation between changes in somite stiffness and induced changes in V_m, as revealed in this work, suggests that V_m-dependent modifications in the rate of somitogenesis might be associated with alterations in cell stiffness. Furthermore, environmental stimuli, CO_2 and KCl, physiologically enriched in the vicinity of embryonic cells, were shown here to contribute to cell depolarization - V_m characteristic promoting developmental processes under study. For CO_2 specifically, which role in the cell electrophysiology is not widely recognized, we used algal cells to prove its general depolarizing action, not specific to a given cell type.

Our results show the ability of V_m to orchestrate the processes involved in somitogenesis and suggest that this might be mediated through V_m-related alterations in cell mechanics, with microenvironment playing functional role in defining V_m during development. The characteristics such as cell proliferation, migration/self-assembly, depolarized membrane potentials, CO_2- and K^+-enriched microenvironment and softened tissue are the features that are common to embryogenesis, tumorigenesis, and tissue regeneration. The unravelled correlations between V_m, cell stiffness, microenvironmental compositions, and somitogenesis from our study may therefore provide valuable insights into fundamental mechanisms that control both physiological and pathological conditions.

Streszczenie

Pytanie, co napędza zegar życia, jest intrygujące. Nadal jednak brakuje nam jednoznacznej odpowiedzi. Na przykład we wczesnej embriogenezie formowanie bloków tkankowych, zwanych somitami, stanowi kluczowy, ściśle regulowany i ograniczony czasowo proces rozwojowy określany jako somitogeneza. Podczas tego procesu somity są kolejno generowane z mezodermy przyosiowej wzdłuż osi ciała zarodka. Okresowość tworzenia somitów jest ściśle specyficzna dla rodzaju tkanki i gatunku; jednak to, co ustala ten rytm segmentacji somitów oraz mechanizm synchronizacji między czasową periodycznością a wzrostem somitów, pozostaje niejasne. Segmentacja somitów obejmuje migrację, samoorganizację określonej liczby komórek, które następnie ulegają proliferacji i różnicowaniu, aby uzyskać specyficzny rozmiar i strukturę. Aby zachować proporcjonalność rozwijającego się ciała i produkować somity o stałym rozmiarze w precyzyjnych odstępach czasu, procesy te muszą być ściśle skoordynowane w przestrzeni i czasie. Wszystkie te fundamentalne procesy, jak wykazano, są indywidualnie regulowane przez potencjał błonowy komórek (V_m).

V_m to różnica potencjału elektrycznego między cytoplazmą a przestrzenią zewnątrzkomórkową, powstająca w wyniku nierównego rozkładu jonów po obu stronach półprzepuszczalnej błony. V_m ma wartości ujemne, o wielkości specyficznej dla danego typu komórki i jej funkcji. Komórki podlegające proliferacji, migracji i samoorganizacji są bardziej zdepolaryzowane (mniej ujemne) w porównaniu do komórek zróżnicowanych. Ponadto komórki te są bardziej miękkie od tych zróżnicowanych i znajdują się w specyficznych warunkach mikrośrodowiska – wzbogaconego w CO_2 i K^+. Dlatego w niniejszej pracy postanowiliśmy sprawdzić, czy okresowość segmentacji somitów (migracja/samoorganizacja komórek) i jednoczesny wzrost somitów (proliferacja komórek) mogą być kontrolowane poprzez zmianę V_m. Zadajemy pytanie, czy efekty wywołane zmianami V_m związane są z wpływem potencjału na mechanikę tkankową oraz czy mikrośrodowisko odgrywa funkcjonalną rolę w definiowaniu właściwości komórkowych. W tym celu użyliśmy embrionów kurzych jako modelu eksperymentalnego i: i) wykonaliśmy mapowanie V_m i sztywności somitów wzdłuż osi ciała zarodka (dane wcześniej niedostępne dla kręgowców); ii) przeprowadziliśmy modyfikacje V_m z użyciem fizjologicznie istotnych bodźców oraz

iii) zmierzyliśmy mechanikę tkanek i markery postępu somitogenezy (czas segmentacji i przestrzenną ekspansję somitów) w odpowiedzi na zmieniony V_m.

Wraz z rozwojem, somity zyskują stopniowo bardziej negatywny potencjał błonowy oraz większą sztywność. Oprócz tego zaobserwowaliśmy skokowe zmiany V_m pomiędzy określonymi grupami somitów, odzwierciedlające wcześniej rozpoznane rozpoczęcie zmian biochemicznych i morfologicznych. Indukowane modyfikacje V_m ustalały nowe tempo segmentacji somitów i synchronicznie dostosowywały ich rozmiar, bez zakłócania regularnych proporcji ciała wczesnego zarodka. W szczególności, depolaryzacja przyspieszała tempo somitogenezy poprzez promowanie proliferacji i migracji/samoorganizacji oraz zmiękczała komórki tworzące somity (cecha związana ze zwiększoną proliferacją i ruchliwością), natomiast hiperpolaryzacja zwiększała ich sztywność i spowalniała proces. Co bardzo istotne, udało się uzyskać bezprecedensowe, blisko 30% przyspieszenie czasu segmentacji somitów bez zaburzania ogólnych proporcji ciała. Zaobserwowano odpowiednio liniową i wykładniczą zależność okresowości formowania somitów oraz tempa ich wzrostu od V_m. Liniowa korelacja między zmianami sztywności somitów a indukowanymi zmianami V_m, ujawniona w niniejszej pracy, sugeruje, że modyfikacje tempa somitogenezy zależne od V_m mogą być związane ze zmianami sztywności komórek. Ponadto wykazano, że bodźce środowiskowe, CO_2 i KCl, fizjologicznie wzbogacone w otoczeniu komórek embrionalnych, przyczyniają się do depolaryzacji komórek – charakterystyki V_m wspierającej badany wczesny etap rozwoju zarodka. W przypadku CO_2, którego rola w elektrofizjologii komórki nie jest szeroko rozpoznana, użyliśmy komórek alg, aby udowodnić jego ogólne działanie depolaryzujące, niespecyficzne dla określonego typu komórki.

Wyniki przedstawione w tej pracy pokazują zdolność V_m do kontroli procesów związanych z somitogenezą i sugerują, że może się ona odbywać poprzez zmiany w mechanice komórek zależne od V_m, przy czym mikrośrodowisko odgrywa funkcjonalną rolę w definiowaniu V_m podczas rozwoju. Cechy takie jak proliferacja komórek, migracja/samoorganizacja, zdepolaryzowany potencjał błonowy, środowisko wzbogacone w CO_2 i K^+ oraz zmiękczona tkanka są wspólne dla embriogenezy, nowotworzenia i regeneracji tkanek. Odkryte w niniejszej pracy korelacje między V_m, sztywnością komórek, składem mikrośrodowiska a somitogenezą mogą zatem

dostarczyć cennych wskazówek dotyczących fundamentalnych mechanizmów kontrolujących zarówno procesy fizjologiczne, jak i patologiczne.

List of publications included in the doctoral dissertation

- original article:

Mahadeva, M., Niestępski, S., & Kowacz, M. (2024). ***Dependence of cell's membrane potential on extracellular voltage observed in Chara globularis.*** Biophysical Chemistry, 307, 107199. DOI: 10.1016/j.bpc.2024.107199. PMID: 38335807. IF 2.2

- original article:

Mahadeva, M., Niestepski, S., & Kowacz, M. (2025). ***Modifying membrane potential synchronously controls the somite's formation periodicity and growth***. Developmental Biology, 517, 317-326. DOI: 10.1016/j.ydbio.2024.11.002. PMID: 39521163. IF 2.1

- original article:

Mahadeva, M., Niestepski, S., & Kowacz, M. ***Bioelectric control of tissue mechanics: Effect of membrane potential on somite deformability in chick embryos.***

Status: Submitted

Chapter 1

Introduction

1.1 General introduction and aims

The developmental processes including somitogenesis, morphogenesis, and organogenesis that are involved in the embryonic development are tightly regulated and occur at precise time and space intervals. In particular, somitogenesis is a rhythmic process, in which pairs of tissue blocks, known as somites, derived from presomitic mesoderm (PSM), are generated on either side of neural tube along the rostral-caudal axis of embryos at a fixed time interval. After they segment, somites grow and mature into predefined structures with their dimension proportional to overall body size (Dale & Pourquié, 2000; Pourquié, 2003b). Both periodicity of somite formation and somite growth must work in a coordinated manner to develop regular body pattern. However, what sets the clock period and the mechanism that brings synchronicity between the tempo of somite segmentation and its growth are not clearly understood (Carraco et al., 2022; Ishimatsu et al., 2018). The periodicity of somite formation varies depending on the tissue and species types (Carraco et al., 2022). Several models have been developed to explain the control mechanisms that are involved in somitogenesis, such as clock and wavefront model (Cooke & Zeeman, 1976), cell cycle model (Primmett et al., 1989; Stern et al., 1988), traction-based model (Bard, 1990), clock and induction model (Schnell & Maini, 2000), clock and trail model (Kerszberg & Wolpert, 2000), and delayed coupling model (Morelli et al., 2009). The most accepted one is the clock and wavefront model (Naoki & Matsui, 2020). It has been reported that the timing of somite segmentation is regulated by oscillations of gene expression pattern referred to as molecular embryo clock (EC) or segmentation clock, which is known to be driven by intricate signaling pathways (Dequéant et al., 2006; Hubaud & Pourquié, 2014; Krol et al., 2011; Masamizu et al., 2006; Palmeirim et al., 1997). Yet, there is no clear explanations on the parameters that are setting up the segmentation clock for the periodic emergence of somites and their simultaneous scaling with body length (Naoki & Matsui, 2020). Studies have experimentally shown the possibility of controlling the pace of somite segmentation by manipulating gene expressions. Shortening the somite segmentation time however resulted in smaller somites, while slowing down the pace of somite formation led to larger ones (Harima et al., 2013; Schröter & Oates, 2010). The

opposite behavior of somite segmentation period and size variations was modeled by a study, which attempted to explain respective somite scaling (Juul et al., 2019). It has also been suggested that the somite size scales with the length of PSM, supported by substantial modifications in respective clock gene oscillation dynamics (Lauschke et al., 2013), indicating that the segmentation period and somite growth are tightly coupled. It has been shown that the species-specific segmentation timing is related to the speed of biochemical reactions, the slower their progression, the longer the segmentation period (Matsuda et al., 2020). Furthermore, a recent study has shown that mass-specific metabolic rates scale with the rate of segmentation period (Diaz-Cuadros et al., 2023). However, exact mechanism setting up the timing of somite formation and how somites adjust their size to this tempo is still unclear. Therefore, it is essential to pay attention to the fundamental processes that are involved in somitogenesis. Somite segmentation occurs by migrating and reorganizing of a fixed number of cells from PSM into spherically shaped tissue blocks. Then cells within somites undergo proliferation and growth to achieve required somite size, and differentiation to acquire particular structures to perform predefined functions (Alvarez et al., 1989; Blomberg et al., 2008; Nakamura et al., 2007). One of the crucial aspects of somitogenesis is the ability of somite-forming cells to cooperate for motility, proliferation, and differentiation that should work in an orchestrated manner to produce somite segments at right time and develop to its right size. Studies have demonstrated that cell migration and the pattern formation during tissue regeneration and embryo development can be controlled by membrane potential (V_m) (Fukumoto et al., 2005; Levin, 2012; Nishiyama et al., 2008). Additionally, cell proliferation and differentiation have been experimentally shown to be regulated by altering V_m (Blackiston et al., 2009; Cone & Tongier, 1971).

V_m is a crucial feature of healthy cells. Its proper maintenance keeps cells in homeostasis and it also regulates cell cycle, volume, and growth, while failure in this system may results in dysfunctional or diseased cells (Abdul Kadir et al., 2018). V_m is the electric potential difference generated due to the existence of ion concentration gradients between cell interior and exterior. This electrochemical gradient is sustained by active and passive transportation of ions through ion channels and energy consuming ion pumps embedded within membrane. The electrochemical gradient across the membrane exists mainly, due to the fact that K^+ ions move out of the cytosol at a faster rate than Na^+ ions penetrate into the cell. Recent studies have recognized the presence of voltage

beyond the cell membrane, a gradient of voltage within a few nanometers in the vicinity of cells, and have shown the correlation between this voltage and V_m (Hughes et al., 2022; Hughes et al., 2021). Supporting this, it has been shown that V_m comprises both intracellular and extracellular voltage components and the application of external electric field near the cell can induce changes in overall transmembrane potential (Vodovnik et al., 1992). The emergence of these voltages is also consistent with Ling's theory, which proposes that the transmembrane potential consists of both intracellular and extracellular voltage components explained by ion adsorption near the inner and outer surface of the cell membrane (Tamagawa & Ikeda, 2018). The magnitude of V_m is specific for a given type of cell and its function. Proliferative cells like in early developing embryos and tumors, for example, are depolarized compared to quiescent cells (Binggeli & Weinstein, 1986). Apart from being depolarized, mitotically active cells have common features of their microenvironments, enriched in CO_2 and K^+ in comparison with differentiated cells (Chen et al., 2022; Kikuchi et al., 2019; Oginuma et al., 2017). This indicates that chemical compositions of extracellular space may contribute to defining V_m and play functional role during development. In the context of bioelectricity relating to embryonic development, it has been demonstrated that existing endogenous extraembryonic electric fields influence the development of embryos by supporting cell migration (Hotary & Robinson, 1990). The importance of electric fields and V_m in the course of embryonic development has been recognized for some time; however, the field of developmental bioelectricity is recently gaining significant attention (George & Bates, 2022; Levin, 2021). Bioelectric patterns in developing tissue have been suggested to regulate cell proliferation and differentiation by altering gene expression, signaling pathways and cell's reaction to external stimuli (Levin, 2012, 2014, 2021; McLaughlin & Levin, 2018; McMillen & Levin, 2024; Tassinari et al., 2022; Whited & Levin, 2019). Moreover, V_m has been recognized as responsible for early body pattering, growth, regeneration, and even pathological deviations (Zhang & Levin, 2025). Additionally, tissue and organ formation has been shown to have a relationship with V_m during development (George & Bates, 2022). Unlike excitable cells, non-excitable cells do not show quick changes in V_m, however, there are evidences showing that the observed changes and patterns of V_m across cells influence developmental processes (Harris, 2021; Levin, 2014, 2021). It was first observed in early 1970's that the depolarization could enhance the rate of neural cell division (Cone & Cone, 1976; Stillwell et al., 1973). Calcium, potassium, sodium, and chloride, ions that

contribute to determining V_m of cells, have been shown to play roles in controlling the cell division (Blackiston et al., 2009). Ion fluxes and V_m gradient are essential features to promote cell migration, would healing, and tissue regeneration (Campetelli et al., 2012). Apart from this, alterations in V_m have also been shown to affect the cell stiffness (Callies et al., 2011; He & Dallos, 1999, 2000), a key feature that controls cell division (Fujii et al., 2021), tissue morphogenesis (Huang et al., 2024), and contributes to organ formation during development (Majkut et al., 2013; Thompson et al., 2019). Supporting this, being depolarized, mitotically active cells are softer than fully formed or matured functional cells (Chowdhury et al., 2010). This suggests a correlation between bioelectricity, cellular processes that are involved in development, and the mechanical characteristics of cells. All these evidences prompted us to ask whether V_m is playing a regulatory role during development and is carrying out this process via altering the mechanical properties of cells. Therefore, we i) explore the role of V_m during the developmental events, somitogenesis in particular, involving time-specific segmentation of somites (cell migration/self-assembly) and somite growth (cell proliferation); ii) examine whether tissue mechanics is involved in V_m-related alteration in the rate of somitogenesis.

1.2 Research hypothesis and objectives

Hypothesis

Based on the literature data, it is known that cell migration, self-assembly, and proliferation, which are involved in the somite formation process, can be regulated by modifying membrane potential. Also, cells going through these processes are softer than quiescent cells. Therefore, in this study we hypothesized that **"membrane potential may control the rate of somitogenesis, and this process could possibly be mediated by biomechanical alterations of somite-forming cells".**

Objectives

This study was conducted to explore the contribution of bioelectricity in the field of developmental biology by employing biophysical methods. For this purpose, we used chick embryo as an experimental model. Objectives of this study include the following.

1. Mapping of V_m and stiffness patterns of somite-forming cells along the embryonic body axis, the data that were not available for vertebrate embryos.
2. Exploring the possibilities of altering the cell's membrane potential by changing the chemical compositions of cell's microenvironment using physiologically relevant stimuli.
3. Assessment of whether modulation of V_m of somite-forming cells can control the somitogenesis rate.
4. Investigating the effect of V_m modification on the deformability of somite-forming cells

Chapter 2

Dependence of cell's membrane potential on extracellular voltage observed in *Chara globularis*

Manohara Mahadeva[1], Sebastian Niestępski[1], Magdalena Kowacz[1]*

[1]Department of Reproductive Immunology & Pathology, Institute of Animal Reproduction and Food Research Polish Academy of Sciences, 10-748 Olsztyn, Poland

***Corresponding author**

Published in: Biophysical Chemistry volume 307, Article number: 107199 (2024),

DOI: 10.1016/j.bpc.2024.107199

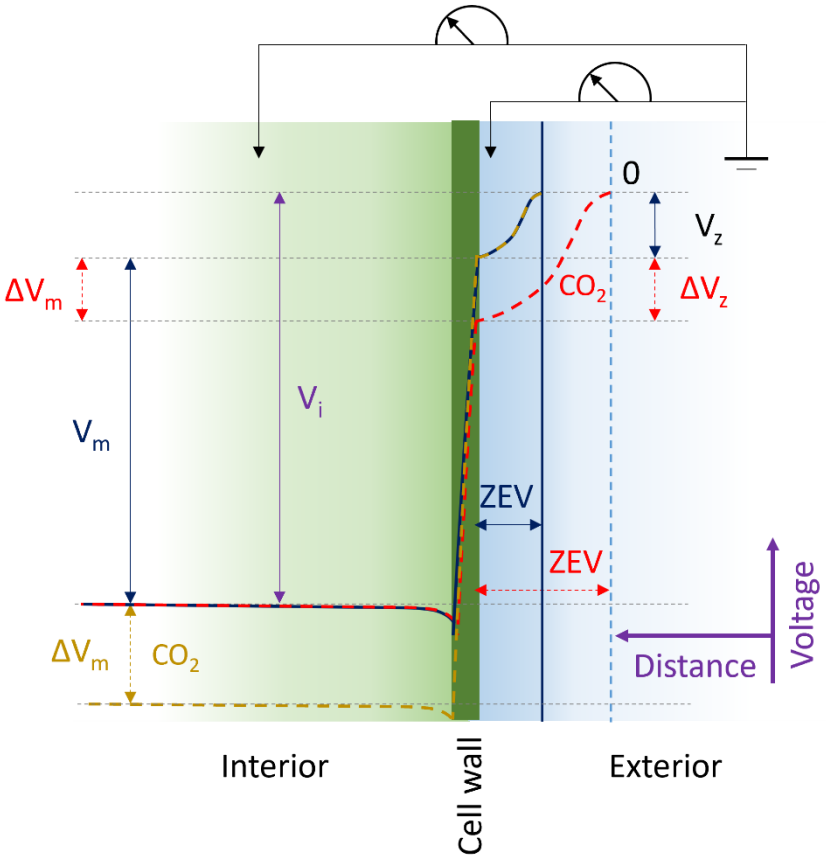

2.1 Introduction

Membrane potential is a fundamental characteristic of a healthy cell, determined by an unequal distribution of ions across the semipermeable membrane (Kempson, 2012). The unequal distribution is controlled by ion channels and energy-consuming ion pumps embedded within the cell membrane. Mainly, K^+ ions move out from the cytosol at a higher rate than Na^+ ions penetrate into the cell, creating a difference in electric voltage across the cell membrane (McCormick, 2014). However, the existence of an ion concentration gradient and an electric potential difference across a gel membrane (an abiotic system, resembling plant cell wall and/or animal cytoskeleton from its porous structure and negative surface charge (Fels et al., 2009; Michel et al., 2010), has been experimentally showed (Kowacz & Pollack, 2020) . In our recent study, a negative voltage gradient, emerging adjacent to the charged hydrogel surface within a few hundred micrometers from its interface in the solution, has been experimentally demonstrated and theoretical explanation for the mechanism behind the phenomenon has been provided (Kowacz et al., 2023). It should be noted that voltage extending over such large distance in ionic solution is not expected from the perspective of classical electrostatic theory due to charge screening effect (Kowacz et al., 2023). The presence of voltage near the hydrogel has been substantiated by visual observation of the exclusion of colloids away from the gel surface. This region of voltage gradient has been termed the depletion zone or exclusion zone (EZ). Many studies have provided evidence for the development of EZ adjacent to hydrophilic and ion-exchanging surfaces in both biological and synthetic systems (Chai et al., 2009; Florea et al., 2014; Kowacz & Pollack, 2020; Kowacz et al., 2023; Li & Pollack, 2020; Pedregal-Cortés et al., 2019; Sharma & Pollack, 2020; Zheng et al., 2006; Zheng & Pollack, 2003). The formation of these zones is facilitated by the selective exchange of ions between the zone-inducing surface and its surrounding medium, driven by electrical and chemical forces (Kowacz & Pollack, 2020; Kowacz et al., 2023). We have suggested in our previous work that the formation of the depletion zone near the gel surface is controlled by the liquid junction potential across the gel/water interface due to the generation of electric repulsive force between the negatively charged gel surface and the negative terminal of the liquid junction. The separation of ionic charges with different diffusion speeds plays a crucial role in generating voltage near the hydrogel (Kowacz et al., 2023). Namely, it is the charge separation that generates diffusion (or liquid junction) potential within the

aqueous solution (Shim et al., 2021; Shin et al., 2017). For example, when atmospheric CO_2 dissolves in an aqueous solution, it dissociates into H^+ and HCO_3^- ions. Charge separation within the solution occurs due to the distinct diffusion rates of the dissolved ions (with a diffusivity of 9.3×10^{-9} m^2 s−1 for H^+ ions and 1.2×10^{-9} m^2 s^{-1} for HCO_3^- ions). As rapidly diffusing H^+ move in a specific direction due to the chemical gradient (out of equilibrium conditions) following them counterions (HCO_3^-) are left behind and the ionic charges become physically separated in space (Shin et al., 2017). Charge separation translates into electric potential difference - junction potential.

Living cells are subjected to local chemical gradients, including those generated by fast diffusing protons and their slower counterions. Therefore, local charge separation at the cell interface (next to, but not necessarily across the membrane), accompanied by voltage generation, can be expected. Recent studies have recognized the presence of voltage beyond the cell membrane, but only within a few nanometers of the region adjacent to red blood cells, and have shown its close relation to their membrane potential (Hughes et al., 2022; Hughes et al., 2021). This suggests that a cell's membrane potential may include an extracellular voltage component that exists away from the cell membrane, prompting us to examine the membrane potential of a cell from a different perspective. The voltage near the red blood cells was described as an electrical double layer (EDL) (Hughes et al., 2021). However, there is a substantial difference in the size between the EDL and the depletion zone having a voltage gradient adjacent to the gel surface. The depletion zone is larger by three orders of magnitude compared to EDL. Additionally, the behavior of the voltage within the depletion zone is completely different from that of the EDL in response to the external modifications in the ionic concentration of the bulk. The thickness of the depletion zone and its voltage increase with increase in ion concentration of the solution (Kowacz et al., 2023), whereas the EDL exhibits the exact opposite behavior (Hatsuki et al., 2013). In this work, we aim to explore the existence of extracellular voltage in living system and its behavior towards contributing to the cell membrane potential. We use *Chara globularis* as our experimental model. *Chara* is widely utilized as a model for electrophysiological measurements due to its large single-cell size and ease of manipulation (Kamiya, 1986; Kamiya & Kamiya, 1981; Shimmen et al., 1994; Tazawa & Shimmen, 2001). Membrane potential of Chara species has been known for many decades, including its responses to environmental modifications such as changes in light/dark conditions, pH, and salinity

of the extracellular solution (Baudenbacher et al., 2005; Bulychev & Kamzolkina, 2006; Hope, 1965; Lucas, 1982; Lucas & Ogata, 1985; Shimmen et al., 1994; Shimmen & Tazawa, 1981). Despite the extensive studies on *Chara*, none of them have mentioned extracellular voltage next to *Chara* cells.

In our previous work on hydrogel, we demonstrated that the voltage near the hydrogel can be modulated by external stimuli, such as CO_2 (Kowacz et al., 2023). CO_2 as an external stimulant may possibly have an impact on the membrane potential of cells. For example, proliferative cells such as embryos and tumors always experience a higher extracellular CO_2 concentration than other cells and tend to be depolarized compared to terminally differentiated cells (Kikuchi et al., 2019; Kirkegaard et al., 2013; Levin, 2012; Oginuma et al., 2017). The apparent correlation between cell function, its membrane potential and microenvironment, brings the idea about possible bioelectrical modification of cell's behavior by means of modulating chemistry of its environment (Sundelacruz et al., 2009) . Therefore, we examine whether an elevated level of CO_2 is merely present in the cell's surrounding or it is also causing the cell's depolarization. We aim to determine whether the cell's depolarization, if induced by increased CO_2 level, is dependent on the extracellular voltage present adjacent to the cell. To achieve this, our study aims to accomplish the following: (i) assess the feasibility of manipulating extracellular voltage using external CO_2 in an algal cell model system, and (ii) investigate the influence of changes in extracellular and intracellular CO_2 concentrations on the cell's membrane potential in relation to extracellular voltage.

2.2 Results and discussion

Extracellular voltage and membrane potential of algal cells

Extracellular and cytoplasmic modifications, such as changes in ionic concentration, can influence the membrane potential of living cells (Hodgkin & Horowicz, 1959). To explore the changes in the cell's membrane potential in response to extracellular and intracellular modifications, we have used algal cells (*Chara globularis*) as our experimental model system, and employed the microelectrode technique for measuring cellular voltages. The resting membrane potentials (V_m) of internodal (a: axial, b: branch, and c: non-corticated) (Fig. 2.S1 a, b, and c) cells measured against artificial pond water (pH 7.3) as a reference under microscope light during the day were as

follows: a: (-184.52 ± 15.66) mV, b: (-180.20 ± 13.16) mV, and c: (-189.28 ± 12.52) mV (Fig. 2.1). These measured membrane potentials are in agreement with previously reported values for Chara cells (Beilby, 2016; Beilby et al., 2022; Hope, 1965; Johnson et al., 2002; Shepherd & Goodwin, 1992; Shimmen, 2002; Tester et al., 1987; Tester & Tester, 1988; Walker et al., 1979). The cortex cells (Fig. 2.S1 d) of *C. globularis* exhibited a lower membrane potential of (-88.68 ± 6.09) mV (Fig. 2.1). To the best of our knowledge, this is the first report of the membrane potential observed in cortex cells that show very similar ultrastructure, but are smaller in volume in relation to the internodal cells they surround (Swetha Balakrishnan, 2020). It has been suggested that cell volume is directly proportional to the concentration of impermeable intracellular anions, including anionic metabolites, and that these anions are among the factors that determine membrane potential of a cell (Kay, 2017; Kay & Blaustein, 2019). An augmented metabolic rate in a cell raises the concentration of impermeable anions, leading to an increase in both the negative membrane potential and cell volume (Jakobsson, 1980). Therefore, cell metabolism, cell voltage, and cell volume are interrelated. Thus, less negative membrane potential of the cortex cells, correlating with their smaller volume, may reflect their lower metabolic activity. Further in this work we will show experimental evidence supporting notion of different metabolic rates of internodal and cortex cells.

During the measurement of the algal cell's membrane potential, as we were slowly approaching the cell with the microelectrode, a negative voltage was observed at a distance of (4.67 ± 1.21) μm from the cell wall with reference to the bulk solution (Fig. 2.1, inset). A gradient of negative voltage was recorded throughout this micron-sized region, which we refer to as the zone of extracellular voltage (ZEV) or simply "the zone". At the immediate vicinity of the cell wall, a maximum negative voltage of (-18.04 ± 1.99) mV was observed (Fig. 2.1, inset). The voltage of (-18.67 ± 1.51) mV was measured at a distance of (4.83 ± 0.75) μm from the cell wall, even in the presence of a pH buffer in APW. The similarity in values of V_z and the width of the zone, both with and without the presence of a buffer in APW, suggests that the recorded voltage and the expanded zone were not influenced by changes in pH near the cell wall or within the bulk. Notably, the voltage gradient persisted despite the absence of any physical barrier between the zone and the bulk solution. We are reporting the existence of the extracellular voltage (V_z) phenomenon in algal cells for the first time. The presence of

this zone of extracellular voltage indicates a localized electrochemical environment near the cell membrane/wall. This suggests that there is an electric potential beyond the cell membrane that must be considered when defining the membrane potential of a cell.

In order to understand the effect of the extracellular voltage on the cell membrane potential, it is necessary to consider the way in which the potential is actually measured. In our experiments, the potential difference is measured between a reference electrode placed in the bulk solution and the measuring electrode positioned either inside the cell or immediately outside it. Therefore, any changes induced in the cell's immediate environment, on the way of charge passage from the cell interior or its interfacial zone to the reference electrode (Veech et al., 2019), will necessarily affect the readings on both intracellular and extracellular electrodes relative to the reference. In the following sections, we will demonstrate the effect of an increase in ion concentration within the cell interior and exterior (induced by internal or external stimulations) on the zone of extracellular voltage and its correlation with the cell's membrane potential.

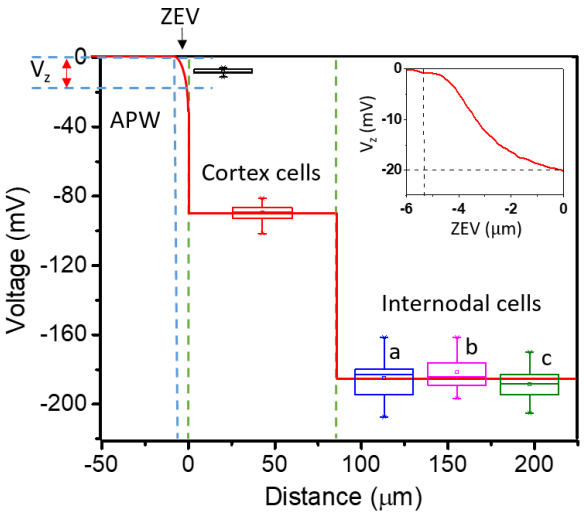

Fig. 2.1. Extracellular voltage and membrane potential of algal cells: The schematic illustrates the typical trace for extracellular voltage (V_z), and membrane potential at the cortex and internodal cell as a function of distance and the inset represents a zoomed-in view of the V_z at the zone of extracellular voltage (ZEV). Artificial pond water (APW) was the reference solution for all measured voltages. The boxes within the schematic show measured values of extracellular voltage, membrane potential for cortex cells, and internodal (a: axial, b: branch, and c: non-corticated) cells (N = 25 each).

Effect of external and internal CO_2 on the extracellular voltage (V_z) and its influence on the membrane potential (V_m)

Effect of external CO_2

In our recent work, an interfacial zone, similar to the zone of extracellular voltage, but present near the charged hydrogel, was shown to be affected by CO_2 (Kowacz et al., 2023). When a gradient of CO_2 was imposed between the gel interior and its surrounding solution, the size and the voltage of this zone became larger and more negative respectively. The mechanism of CO_2 action on increasing the negative voltage near the gel surface is described in our previous work (Kowacz et al., 2023). In short, the voltage zone was enlarged due to charge separation (H^+ and HCO_3^- dissociated from CO_2) at the gel/water interface, driven by electrical and chemical forces that contribute to the directional movement of H^+ and HCO_3^- ions. H^+ ions are attracted to, while HCO_3^- ions are repelled from, the gel surface with its fixed negative charges. To verify this phenomenon in a living system, we introduced CO_2 into the bulk solution containing algal cells to manipulate the extracellular voltage (V_z). The goal was to explore the impact of changes in V_z on the cell's membrane potential, with the aim of understanding the correlation between them.

The increased CO_2 concentration in the bulk hyperpolarized the zone of extracellular voltage and depolarized the internodal cell. The changes in the extracellular voltage (ΔV_z) and membrane potential (ΔV_m) were (-15.91 ± 3.06) mV and (+16.84 ± 3.92) mV respectively (Fig. 2.2 a, b). Conversely, upon reducing external CO_2 concentration to the one in equilibrium with atmospheric CO_2, the V_z and V_m returned to the initial values as in the resting condition (Fig. 2.2 a, b). A lower magnitude of change in membrane potential of (+7.06 ± 3.08) mV, indicating less depolarization, was observed in cortex cells compared to internodal cells in response to an increase in external CO_2 concentration (Fig. 2.2 c). Similar to the reaction of internodal cells, cortex cells responded immediately to the elevated extracellular CO_2 concentration; however, they took a longer time to reach the steady membrane potential value compared to the response of internodal cells (Fig. 2.2 c). These measurements were performed for multiple cycles of increased and reduced concentration of external CO_2 (Fig. 2.S2 a, b). The magnitude of changes in V_z and V_m is approximately the same, while the direction of changes is opposite (indicated by purple arrows in Fig. 2.2 a and b). This suggests a

coupling effect between extracellular voltage and the cell membrane potential in response to our extracellular modifications. This implies that the modulation of extracellular voltage can alter the cell membrane potential indicating the importance of accounting for extracellular voltage in defining the membrane potential of a cell.

Based on our results, it can be concluded that the measured membrane potential of the cell (V_m) encompasses both its internal electrogenic (voltage generated within the cell) (V_i) and extracellular voltage (V_z) components, and alterations in their values contribute to the depolarization or hyperpolarization of the cell. Our results indicate that the internal voltage (V_i) of internodal cells remains constant in response to extracellular modifications (Fig. 2.3 red dashed line). On the other hand, by adjusting ion concentration inside the internodal cell through light and dark treatments, we change V_i without affecting V_z (within the timeframe of our experiments) (Fig. 2.3 gold dashed line). This indicates that internal voltage and the extracellular voltage can be independently modified, what is reflected in the overall membrane potential of a cell. Both V_i and V_z emerge as crucial components of the cell membrane potential, with alterations in their values resulting in hyperpolarization or depolarization of the cell. Thus, electric potential difference across the cell membrane (V_m), defining a degree of membrane's polarization, can be represented as $V_m = V_i - V_z$ (Fig. 2.3). In this context, the smaller change in V_m of the cortex cell than that in V_z (in response to elevated extracellular CO_2 concentration) implies a concomitant change in the intracellular component (V_i) leading to the opposite effect on the net membrane potential. In our case, it suggests an increase in the internal negativity of the cortex cells in response to increased extracellular CO_2 concentration. On the other hand, as observed in internodal cells, the same in magnitude (but opposite in sign) concurrent changes of V_z and V_m imply that intracellular component (V_i) remains virtually unchanged in response to extracellular CO_2 (Fig. 2.3). The changes in voltages of internodal cells, cortex cells, and the zone of extracellular voltage (ZEV) in response to internal and extracellular modifications are summarized in Table 2.S1.

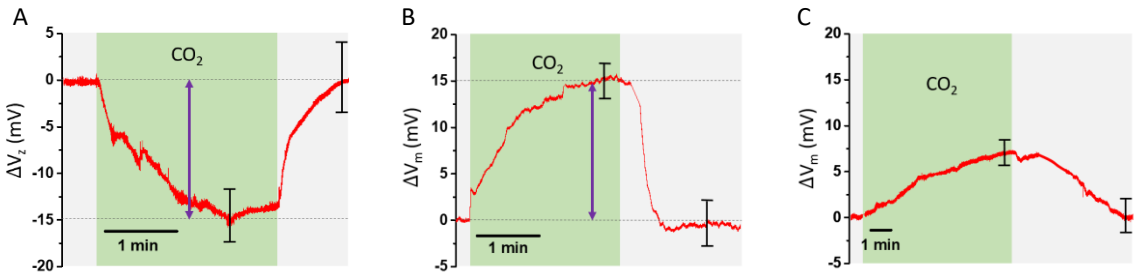

Fig. 2.2. Effect of extracellular CO_2 on extracellular voltage and membrane potential of algae: The graphs show the change in voltage (ΔV_z) and membrane potential (ΔV_m) in response to alternating increase (higher concentration than atmospheric CO_2) and reduced (in equilibrium with atmospheric CO_2) concentration of extracellular CO_2 for the zone of extracellular voltage (A), internodal (B), and cortex cells (C). The error bars in all the graphs represent the standard deviation of change in voltage values (N = 4).

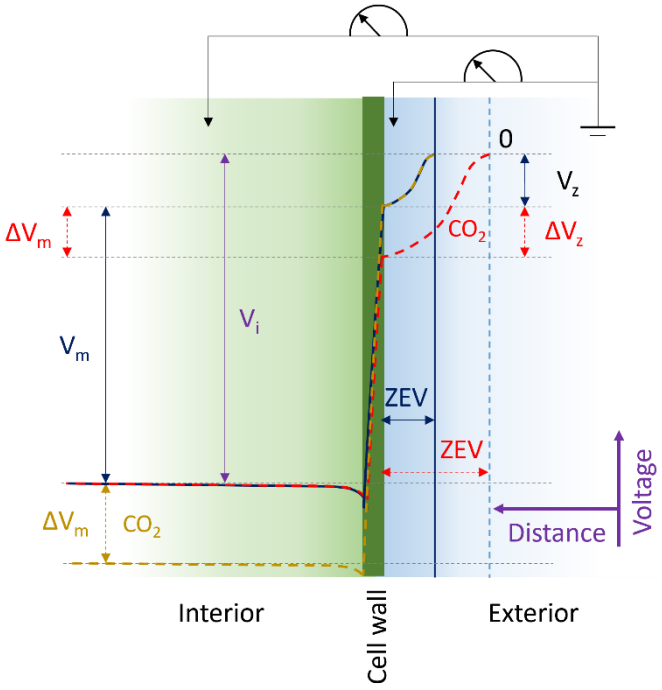

Fig. 2.3. Two-point concept of voltage measurement: Schematic representation of variation of the electrical potential difference (V_m) across the cell wall. $V_m = V_i - V_z$ represents the resting membrane potential (dark blue solid curve). The change in voltage (ΔV_z and ΔV_m) in response to elevated concentrations of extracellular CO_2 (red dashed curve) and intracellular CO_2 (gold dashed curve) are shown in exterior and interior of the cell, respectively. The zone of extracellular voltage (ZEV) is shown for the resting state (dark blue solid line) and in response to increased extracellular CO_2 concentration (blue dashed line).

Effect of internal CO_2

Cells were subjected to alternating periods of darkness and white light to explore their responses to changes in internal CO_2 concentration (Fig. 2.S3). During the dark treatment, the cells undergo metabolic activities such as dark respiration, which increases the internal CO_2 concentration (Bunce, 2021; Lautner et al., 2014; Pfanz et al., 2002), while photosynthesis in the light reduces it (Beer & Larkum, 2001; Villar et al., 1994). Both internodal and cortex cells were hyperpolarized in response to the dark treatment. The change in membrane potential was (-31.82 ± 5.72) mV for internodal cells and (-9.05 ± 2.54) mV for cortex cells. Conversely, the cells depolarized and returned to their initial values upon illumination (Fig. 2.4 a, b). Cortex cells took longer time to reach a steady membrane potential value in response to the dark and light treatments compared to the response of internodal cells (Fig. 2.4 b). The smaller change in membrane potential of cortex cells compared to internodal cells and the longer time to reach a steady state in response to dark and light treatments suggest a slower metabolic rate of the cortex cells.

The extracellular voltage remained unchanged in response to the dark and light treatments, suggesting that the extracellular space is not reacting to the changes induced by the cell's metabolic activities (photosynthesis and respiration) within the timeframe of the experiments. This indicates that changes in intracellular CO_2 concentration modulate cell membrane potential without affecting extracellular voltage. On the other hand, variations in the extracellular CO_2 concentration affect both, membrane (V_m) and extracellular potentials. Changes in extracellular environment should affect the measurement of V_z. At the same time, intracellular changes proceeding without immediate electrogenic ion exchange with the environment, will not affect the reading between the electrode external to the cell and the reference one located further in the bulk solution (Fig. 2.3). Regarding the mechanism of negativity increase by additional CO_2, as induced both internally and externally (Fig. 2.2 a, 4a), one has to consider the direction of the CO_2 concentration gradient and its interactions with barriers to cross: membrane and/or cell wall. Dark respiration increases the concentration of intracellular CO_2; prompting CO_2 outflow, while externally increased CO_2 concentration directs CO_2 inwardly to the cell. As explained in detail in our previous work (Kowacz et al., 2023), the movement of both H^+ and HCO_3^- ions in a specific direction (driven by chemical or electrical gradient), but at different diffusion rates, can lead to their separation near the

cell wall/membrane. The separation of charges within the solution result in the generation of voltage. This separation of charges is then further supported by their interactions with a selectively permeable barrier that accommodates cations (due to its fixed negative charges), but repels anions. Such charge separation near the cell wall is expected to cause the negative extracellular voltage to increase in reference to the bulk solution (in a manner alike to the one near gels (Kowacz et al., 2023)). In response to increased internal CO_2 (dark treatment), a similar mechanism may act within the cell to increase internal negativity. In fact, such approach to membrane potential generation is corroborated by other studies showing contribution of selective ion partitioning, occurring independently at either side of the membrane, to the outcome voltage (Heimburg, 2018; Tamagawa & Delalande, 2022). Selective, transient localization of protons, in particular, and its effect on induction of membrane polarization is also extensively discussed in a series of work by Lee (Lee, 2019, 2020, 2021, 2023).

Combined effect of both external and internal CO_2

Cells were further treated with dark and light conditions in the presence of a higher concentration of external CO_2 to understand the combined effect of both internal and external CO_2 on their membrane potential. The measurement began with an increased external CO_2 concentration, which depolarized the cell by (+16.33 ± 3.06) mV (Fig. 2.4 c). Subsequent treatment with the darkness hyperpolarized the cell by (-14.33 ± 3.51) mV, bringing its potential back to a more negative value (Fig. 2.4 c). Upon illuminating the cells, the membrane potential returned to a less negative value as it was induced by increased extracellular CO_2. The change in potential values resulting from the combined higher concentration of external CO_2 and the dark treatment was approximately half the value compared to the potential change by the dark treatment alone (in the absence of additional CO_2) (Fig. 2.4 a). This is because the changes in membrane potential caused by external and internal CO_2 act in opposite directions. Thus, the CO_2 in the beginning of the experiment had already depolarized the cell by (+16.33 ± 3.06) mV (Fig, 2.4 c), compensating for the change in membrane potential that was anticipated to be induced by the dark treatment alone. This indicates that the change in cell membrane potential occurs due to an additive effect of both external and internal changes in CO_2 concentrations. The same magnitude and sign of change in response to external CO_2 in

dark and in light indicates that the immediate effect of external CO_2 is not related to the metabolic activities of a cell.

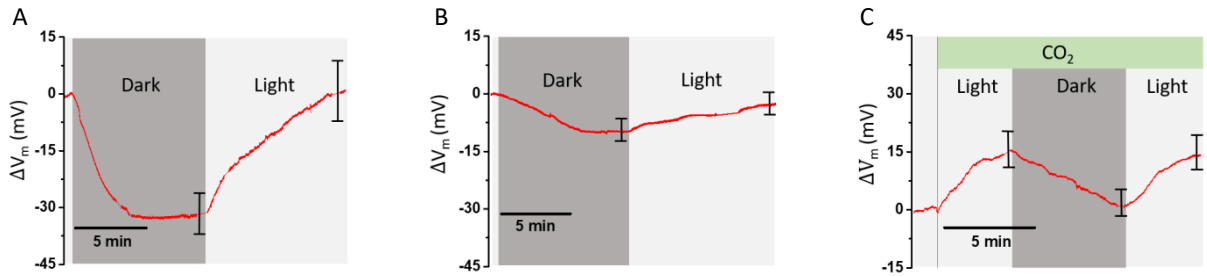

Fig. 2.4. Effect of intracellular and extracellular CO_2 on the membrane potential of algae: The graphs show the change in membrane potential (ΔV_m) in response to alternating dark and light treatments for internodal (A) and cortex cells (B) and in response to alternating dark and light treatments in the presence of increased concentration of extracellular CO_2 for internodal cells (C). The error bars in all the graphs represent the standard deviation of change in potential values (N = 5).

Effect of external stimuli on the zone of extracellular voltage

An increase in the concentration of CO_2 in the bulk solution altered the solution pH from 7.3 to 6.3. To verify whether the increase in negative extracellular voltage was simply due to the change in external solution pH or it is the effect of charge separation at the cell membrane/wall as a result of increased concentration of external CO_2, measurements of V_z were taken at pH 6.3, adjusted using HCl. The cell membrane potential did not change in response to altered solution pH and it was found that V_z was remaining unchanged (Fig. 2.5 a). This indicates that the increase in V_z was not the effect of a change in solution pH induced by CO_2 but as it was described previously in this study, the increase in negative voltage could be due to the charge separation at the zone/bulk interface generated by ions with distinct diffusion rates (H^+ and HCO_3^- from CO_2 in water (Kowacz et al., 2023)). At higher negative V_z, resulting from an increased concentration of external CO_2 the increase in the width of the zone of extracellular voltage (ZEV) was observed. Since the ZEV is known to exclude colloids (Kowacz et al., 2023; Zheng & Pollack, 2006), polymer microspheres were used to visualize the zone enlargement. Additional CO_2 raised a maximum negative extracellular voltage recorded near the cell wall to (-33.20 ± 1.30) mV and expanded the zone to a distance

of (54.17 ± 5.34) µm from the cell wall (Fig. 2.5 a, b, and c). To further confirm that the change in zone parameters (zone width and voltage) was due to an enhanced ion exchange across the cell membrane/wall, the cells were treated with another depolarizing agent, which is KCl. Increasing the concentration of KCl in the external solution always depolarizes algal cell (Keifer & Lucas, 1982; Shimmen, 2006). We verified that the addition of 0.3 mM KCl in APW induced the same degree of cell depolarization as that induced by external CO_2 in both light and dark conditions. However, the extracellular voltage increased in magnitude to (-25.75 ± 1.71) mV, and the zone extended up to (30.25 ± 2.22) µm in response to an additional 0.3 mM KCl (Fig. 2.5 a, c), the changes being lower than those induced by CO_2. The above results suggest that the charge separation at the cell membrane/wall interface (caused by induced ion concentration gradient near the cell) affects the extracellular voltage and the size of the ZEV. The development of different zone widths near the algal cell wall in response to external stimuli (CO_2 and KCl in our case) is the result of the separation of ionic charges with different diffusion rates across the zone of extracellular voltage (Kowacz et al., 2023). The linear dependence between extracellular voltage and width of the zone was observed (Fig. 2.5 d). The width of the zone and the extracellular voltage differ for various stimuli ((54.17 ± 5.34) µm for CO_2 and (30.25 ± 2.22) µm for KCl), even though they induce the same change in membrane potential of the cell ((+16.84 ± 3.92) mV for CO_2 and (+16.66 ± 1.53) mV for 0.3 mM KCl in this case). In reality, the external stimuli do not actually elicit the same intracellular changes; rather, it is the net effect that remains the same. What we measure as the cell's membrane potential is, in fact, combination of intracellular and extracellular voltages, which confirms our earlier assumptions (Fig. 2.3).

Additional experiments were conducted to visualize the zone of extracellular voltage near algal cell wall at resting condition using smaller microspheres (diameter: 0.5 µm). Microspheres were excluded to a distance of (5.40 ± 1.14) µm from the cell wall. At the same time, it was not possible to visualize this zone by large microspheres (diameter: 1.0 µm). This implies that the generated voltage was not strong enough to push larger microspheres away from the cell wall, although the voltage gradient could be detected up to (4.67 ± 1.21) µm from the cell wall (Fig. 2.1 inset). We observed that the smaller particles move to a longer distance than the larger particles for the same voltage change induced by 0.3 mM KCl (Fig. 2.S5). Similar phenomenon was also demonstrated in a

study, indicating that small ions can be excluded to a larger distance by a voltage of the same magnitude than charged objects (particles) of a larger mass (Nooryani et al., 2023).

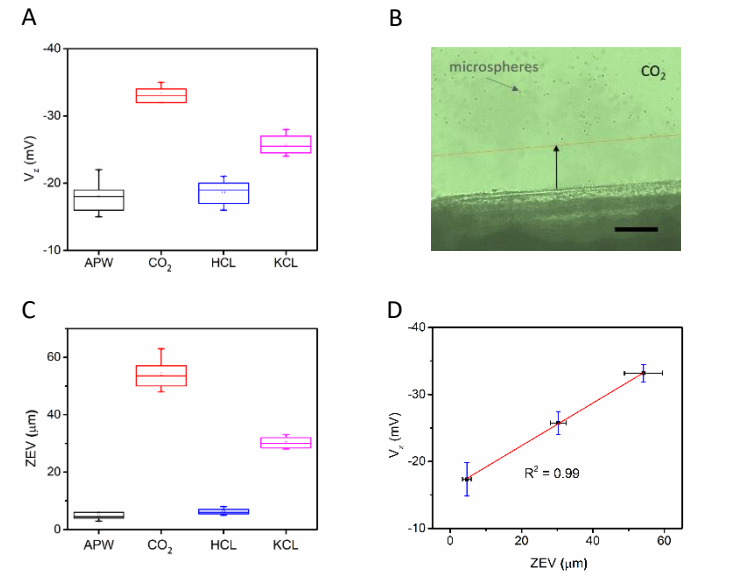

Fig. 2.5. Effect of external stimuli on the zone of extracellular voltage: A microscopic image shows the expanded zone of extracellular voltage (ZEV) upon influx of extracellular CO_2, observed with the help of microspheres (A). Box plots show the measured values of V_z (B) and the width of the zones (C) near the cell wall in APW (pH 7.3), APW + external CO_2 (pH 6.3), APW + 0.5 µM HCl (pH 6.3), and APW + 0.3 mM KCl (pH 7.3) respectively (B and C) (N = 5). Linear dependence of the size of the zone of extracellular voltage on V_Z (D). Scale bar in the image is 50 µm.

Comparison of V_m measured with microelectrodes and observed with voltage-sensitive dye: The importance of extracellular voltage

As outlined earlier, an increased concentration of both extracellular CO_2 and additional 0.3 mM KCl raised the extracellular voltage near the cell to a more negative value. However, the magnitude of change in extracellular voltage ((-33.20 ± 1.30) mV for extracellular CO_2 and (-25.75 ± 1.71) mV for 0.3 mM KCl) and the zone width ((54.17 ± 5.34) µm for extracellular CO_2 and (30.25 ± 2.22) µm 0.3 mM KCl) in response to additional CO_2 and 0.3 mM KCl were different (Fig. 2.5 a, c). The change in membrane potential in response to an additional 0.3 mM KCl was (+16.66 ± 1.53) mV, virtually the same as in response to increased concentration of CO_2 ((+16.84 ± 3.92) mV), when

measured using microelectrodes (indicated by purple arrows in Fig. 2.6 a and b). Yet, when observed by voltage-sensitive dye [$DiBAC_4(3)$] (Adams et al., 2016; Baxter et al., 2002; Yamada et al., 2001), respective changes were different for the two depolarizing agents. 0.3 mM KCl reduces internal negativity of the cells more than additional CO_2 (as evidenced by increased fluorescence in the former case, - Fig. 2.6 c and d). However, since the voltage-sensitive dye does not capture extracellular events, the observed net depolarization was likely incomplete. The membrane potential represents the electrical work required to transport ions across the cell membrane (Veech et al., 1995). When using electrodes, it becomes necessary to incorporate the extracellular voltage zone within the circuit (Fig. 2.3). This indicates that the net cell membrane potential measured with respect to the external solution includes the zone existing near the cell wall, suggesting the dependence of cell membrane potential on extracellular voltage. The overall cell depolarization can be shown when extracellular voltages (measured by microelectrodes) are considered in addition to the cell depolarization observed by voltage sensitive dye. That is, (i) additional 0.3 mM KCl induces a higher depolarization (as indicated by higher fluorescence) inside the cell (Fig. 2.6 d) and a lower hyperpolarization of the ZEV (as expressed in the zone width) (Figure 2.5 a), (ii) additional CO_2 induces a lower depolarization inside the cell (Fig. 2.6 c) and a higher hyperpolarization of the ZEV (Fig. 2.5 a). After considering the effect of extracellular voltage on cell membrane potential along with depolarization observed by fluorescent dye (for both 0.3 mM KCl and additional CO_2), the net depolarization may become equal as it was measured by microelectrode (coupling effect between V_z and V_m) (Fig. 6 a and b). This indicates that the extracellular voltage is an important additional component that needs to be taken into account in defining a cell's membrane potential.

Along with the increased fluorescence, a pattern of bright spots was observed in the cells with an additional 0.3 mM KCl, whereas a homogenous pattern of fluorescence with lower intensity was observed in the cells with additional CO_2 (Fig. 2.6 c and d). Additional CO_2 and dark respiration reduce the intracellular pH of the cell (Boron & De Weer, 1976; Bulychev & Krupenina, 2019; Coleman & Colman, 1981; Nimer et al., 1994). The cell's internal buffering system responds to changes in pH to maintain a stable pH level inside the cell. This system operates through the protonation and deprotonation of the protein components within the cell (Somero, 1985). At low intracellular pH, protonation results in the development of a positive charge on the

functional groups of proteins. This phenomenon may cause negatively charged dye molecules to bind to those positively charged protein residues (Bräuner et al., 1984; Sträuber & Müller, 2010), resulting in the generation of uniform fluorescence inside the cell. The bright spots observed upon the addition of KCl may possibly be the localized spots, resulting from salt treatment (Shimmen & Wakabayashi, 2008).

The results obtained from voltage-sensitive dye provide information only about intracellular changes. The potential values recorded by microelectrodes include the extracellular voltage and provide the net change in both intracellular and extracellular voltage in response to induced modifications. Alterations in the extracellular voltage component may affect cell physiology, as they can influence the exchange of charged metabolites or nutrients into and out of the cell.

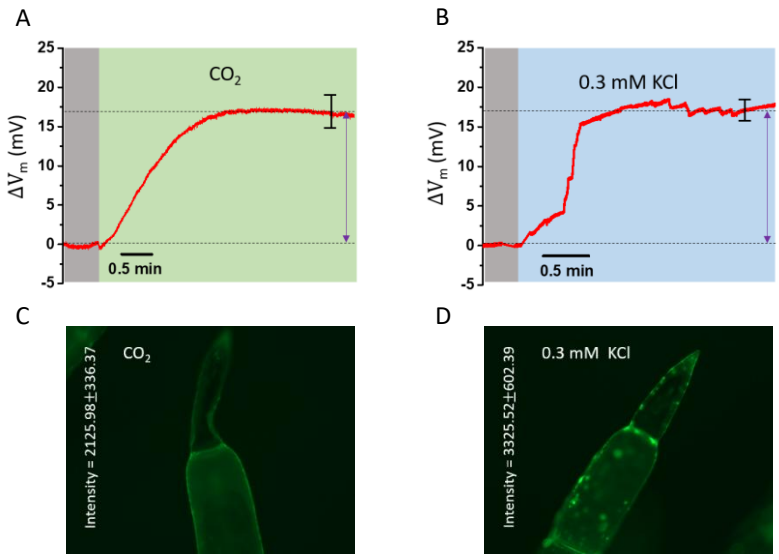

Fig. 2.6. Comparison of V_m measured with microelectrodes and observed with voltage-sensitive dye: Graphs show the same magnitude of change in membrane potential (ΔV_m) in response to additional 0.3 mM KCl (N = 3) and extracellular CO_2 (N = 4) in dark condition (A and B). Microscopic images show the change in fluorescence intensities upon addition of 0.3 mM KCl and extracellular CO_2 (C and D). An increase in fluorescence intensity from the dye indicates the cell depolarization. Conversely, hyperpolarization is indicated by decrease in fluorescence.

The evolution of the zone of extracellular voltage at the places where ion exchange is enhanced

Apart from the zone of extracellular voltage induced by means of the imposed concentration gradient (with additional CO_2 and KCl) prompting diffusional ion flow toward the cell, the zones were also observed next to the spine and naturally damaged cells (Fig. 2.7 a and b). Spine cells are elongated, finger-like projections that extend from the internodal cells of many species of algae, including *C. globularis*. These specialized structures may serve for the exchange of ions and nutrients required by the cell (Lambert, 2009). Similarly, there is an enhanced ion exchange next to damaged cells to support healing (Foissner & Wasteneys, 2011 Nov 28; Klima & Foissner, 2011; La Claire, 1982).

To verify the mechanism of ion exchange-induced zone formation, already established by us for gels (Kowacz et al., 2023), in living cells, algal cells were manually wounded at multiple sites on the cell surface to induce enhanced ion exchange. Within 10 minutes after wounding, zone enlargement was observed by the exclusion of colloidal particles (1.0 µm) near the wounded sites. The zones expanded to a maximum distance of (80.60 ± 8.02) µm from the cell wall measured with the help of micro electrodes (Fig. 2.7 c, d). An increased negative extracellular voltage of (-42.75 ± 1.71) mV was recorded near the cell wall within these zones (Fig. 2.7 e). These values follow the linear trend as shown earlier (Fig. 2.5 d). The evolved zones were diminished over time (approximately 4 hours after the cell was wounded). The wounded cells underwent depolarization from their resting potential value of (-184.52 ± 15.66) mV to (-151.40 ± 12.28) mV. Other studies have also reported a similar depolarization response of algal cells to wounding (Shimmen, 2001, 2002, 2008; Stahlberg & Cosgrove, 1992).

In our previous experiments, we enhanced directional ion diffusion toward the cell membrane/wall of algae by increasing the concentrations of extracellular CO_2 and KCl. This led to an increase in negative extracellular voltage and the zone width (Fig. 2.2 a, 2.5 a – c). The outcomes obtained from cell-wounding experiments also support the idea of zone expansion due to increased ion exchange at the injured sites. All of these results reinforce our expectation of ZEV expansion near surfaces with enhanced ion exchange. The extracellular voltage zone adjacent to wounded cells could potentially act as a protective barrier against pathogens, such as bacteria, viruses, or fungi, due to its ability

to exclude colloids and bacteria (Cheng & Moraru, 2018; Esplandiu et al., 2020; Spencer et al., 2018/06/25; Zheng & Pollack, 2006). This suggests an unrecognized strategy employed by algae to shield themselves from pathogen intrusion.

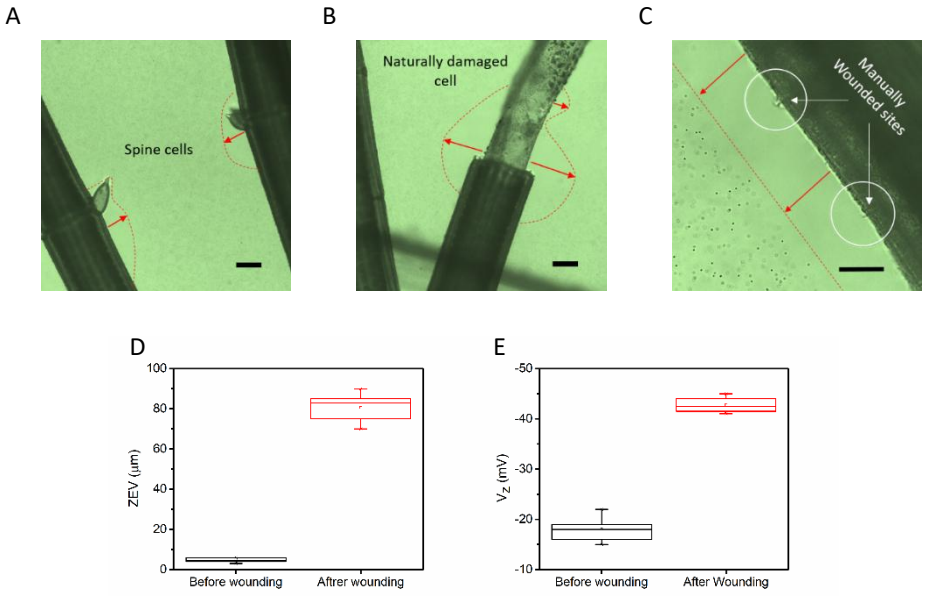

Fig. 2.7. Evolution of the zone of extracellular voltage near the spine and damaged cells of algae: microscopic images show the existence of the zones near spine, naturally damaged, and manually wounded cells (A, B, and C). The box plots show the width of the zone of extracellular voltage and V_z near the cells before and after wounding them (D and E) (N = 5). Scale bar in the image A and B is 100 µm and C is 50 µm.

2.3 Conclusions

The existence of extracellular voltage (V_z) adjacent to Chara cells, as demonstrated in this work, reveals the extension of a cell's membrane potential (V_m) beyond its membrane. To the best of our knowledge, this work provides the first experimental evidence for the presence of extracellular voltage near the algal cell. We successfully manipulated the extracellular voltage using CO_2 as a stimulant. Modulation of V_z altered V_m, and a coupling effect between them was observed in response to changes in the extracellular CO_2 concentration. Our results suggest that changes in the extracellular environment modifying V_z and resulting in a net change in membrane potential may proceed without affecting intracellular voltage (V_i). In this context, observed cell

depolarization, in response to augmented concentration of CO_2 in the extracellular environment, is ascribed to the increase in extracellular negativity that effectively diminishes voltage gradient across the membrane. On the other hand, an increase in intracellular CO_2 (induced by dark treatment) hyperpolarizes the cell by increasing internal negativity and without affecting V_z. These results suggest that the mechanism by which CO_2 increases the negativity of both extracellular and intracellular environments can be the same. A consistent degree of cell depolarization in response to increased extracellular CO_2 concentration in both dark- and light-treated cells further demonstrates that extracellular modifications in algae can influence the cell membrane potential independently of their metabolic activities.

Observations using a voltage-sensitive dye revealed alterations in intracellular voltage exclusively; nevertheless, the cell's membrane potential encompasses both intracellular and extracellular voltages. Therefore, the voltage measured by microelectrodes provides actual changes in membrane potential values that include changes in extracellular voltage in response to induced modifications. This indicates that extracellular voltage represents an essential additional component that contributes to defining the cell's membrane potential and may affect the selective exchange of ions across the cell membrane/wall. Enhanced ion exchange between the cell interior and exterior can increase the magnitude of extracellular voltage and expand the width of the zone of extracellular voltage (ZEV), as evidenced by the evolution of ZEV near the spines and wounded cells. The localized electrochemical environment near the cells may play a crucial role in various cellular processes, including signal transmission, nutrient uptake, and maintaining cellular homeostasis. Furthermore, the zone of extracellular voltage may act as a protective barrier against pathogens (bacteria, viruses, or fungi) because it has the ability to expel colloids.

2.4 Materials and methods

Sample Preparation

Freshwater green algae (*Chara globularis*) were cultivated in an aquarium. The soil used for algae cultivation was collected from a natural lake. Appropriate light conditions (1000-1450 lm, FLUVAL Plant 3.0) were provided in a 10:14 h (light: dark) cycle at room temperature (22°C). A healthy sample was obtained by cutting a portion of the

algae, including the cortex, and internodal (axial, branch, and non-corticated) cells (Fig. 2.S1). The extracted samples were rinsed two to three times with artificial pond water (APW, 0.1 mM NaCl, 0.1 mM KCl, and 0.1 mM $CaCl_2$, adjusted to pH 7.3 with 0.5 M $NaHCO_3$) to effectively remove contaminants. All chemicals used were purchased from Sigma Aldrich (Germany). KCl (Lot: K52082136 115), NaCl (Lot: K52782804 134), $CaCl_2$ *$2H_2O$ (Lot: A1756882 205), $NaHCO_3$ (Lot: K52580129 136). The cleaned algae sample was then immobilized on a glass bottom plastic Petri dish (35 mm, Ibidi GmbH, Germany) using thin plastic wires and curable silicone adhesive. The Petri dish containing the immobilized sample was filled with 3 mL of APW and allowed to stabilize at room temperature for two to three hours. This stabilization minimizes the stress on the sample caused by the extraction process. Following the stabilization phase, the sample was used for electrophysiological measurements.

Fabrication of glass microelectrode

Borosilicate glass capillaries with filaments (OD = 1.2 mm, ID = 0.68 mm, length = 75 mm) (World Precision Instruments (WPI), USA) were used for microelectrode fabrication. The process involved pulling clean glass capillaries using a micropipette puller (PUL - 1000, WPI, USA) in a looped program (heat index: 390, force: 250 g, distance: 0.60 mm, delay: 100). The diameter of the microelectrode tip was (1 to 2) µm. The pulled microelectrode was filled with 3 M KCl solution saturated with silver chloride (# 102545885, Source – BCCJ4878, Sigma Aldrich, Germany). The filled microelectrode was then carefully inserted into a microelectrode holder (PEL, WPI, USA) prefilled with 3 M KCl, ensuring the absence of air bubbles.

Measurement of cellular voltages

APW (pH 7.3) was used as the conducting medium for all experiments performed in this study. The immobilized, unstressed sample was positioned on the stage of an inverted microscope (Nikon ECLIPSE Ti), with an Ag/AgCl electrode immersed in the bulk solution serving as a reference electrode. An electrode holder containing a glass microelectrode filled with KCl was attached to a potential measurement probe connected to a low-noise dual-channel differential electrometer (model FD-223a, WPI, USA). The entire experimental setup was placed on an optical table within a Faraday cage to shield it from external mechanical vibrations and electrical interference. Prior to measuring the cell membrane potential, the potential difference (offset voltage) relative to the reference

electrode was set to zero. The measurement of the membrane potential of the algal cells was carried out under microscope light during the day at room temperature. To measure the extracellular voltage, the reference electrode was placed in the bulk solution while the microelectrode tip was carefully positioned near the cell surface with the help of the micromanipulator (Luigs & Neumann GmbH, Germany) (Fig. 2.S6 a). To assess the cell membrane potential, the microelectrode tip was carefully inserted into the cortex and internodal cells using the micromanipulator (Fig. 2.S6 b). LabScribe software (from iWorx, version 4.322) was used to display and record the potential values as waveforms (potential vs. time traces). Advanced Research software (NIS Elements, v 5.01) was used to visualize the microelectrode and live algal cells during potential recording. Glass microelectrodes may be sensitive to pH. Therefore, additional experiments were performed in the APW at pH 7.3 regulated by a pH buffer (5 mM HEPES (Lot: RNBK6522, Sigma Aldrich) (Kim et al., 2013)) in order to verify that the measurements made in the unbuffered APW were not affected by the possible pH sensitivity of the electrodes.

Effect of CO_2, HCl, and KCl

Experiments to verify the effect of metabolic activities (dark respiration and photosynthesis) on the membrane potential of algal cells were carried out in the light/dark conditions, using a microscope lamp as a light source. The darkness increases the concentration of intracellular CO_2 due to the dark respiration of the cell, while the light decreases the intracellular CO_2 due to photosynthesis. Experiments to verify the influence of extracellular CO_2 on cellular voltages of algae were carried out in both dark and light-treated cells by introducing CO_2 into the bulk solution containing immobilized samples. For this purpose, compressed CO_2 from a cylinder was supplied via a glass micro nozzle with a tip diameter of (10 to 15) µm at a pressure of (0.25 - 0.3) bar. The CO_2 concentration in the bulk solution was increased above its level in the APW in equilibrium with atmospheric CO_2. The concentration of dissolved CO_2 in the bulk solution was quantified by pH measurements (a change in pH from 7.3 to 6.3 indicated saturation of APW with CO_2). The effect of pH change, as the one induced in response to CO_2 influx, on cell membrane potential and extracellular voltage, was verified by reducing the pH of the solution from 7.3 to 6.3 using HCl. Further, to confirm that the change in measured extracellular voltage is not the effect of change in pH of the bulk solution by additional CO_2, the measurement of extracellular voltage and its alteration

by additional CO_2 was performed in the presence of a pH buffer in APW. While measuring the changes in extracellular voltage in response to additional CO_2, we placed an additional electrode away from the cell within the bulk, along with the one near the cell, and measured voltage with respect to the reference electrode (Fig. 2.S6 c). We observed a change in voltage upon an increase in extracellular CO_2 concentration from the electrode near the cell and no change in voltage from the other electrode, which was in the bulk. Experiments to verify the effect of KCl on the cellular voltages were conducted by dissolving (0.2, 0.3, 0.4, 0.5) mM KCl (data not shown) in APW containing the algal sample. 0.3 mM concentration of KCl was selected in this study because it has induced the same degree of depolarization as additional CO_2 in APW when measured with microelectrodes.

Measurement of the width of the extracellular voltage zone and its visualization

The width of the extracellular voltage zone was measured using microelectrodes and a micromanipulator. As the electrode was brought closer to the algal cell, the point at which the voltage drop occurred indicated the boundary of the zone. The zone width was determined by measuring the distance the electrode moved from the boundary of the zone until it made contact with the algal cell wall. The extension of the zone in the vicinity of healthy, naturally or manually damaged internodal and spine cells was visualized by exclusion of microspheres. For that purpose, a microsphere suspension was prepared by diluting 50 µl (equivalent to 1 drop) of uncharged, non-functionalized polystyrene microsphere solution (1.0 µm; analytical standard; 89904; Sigma Aldrich) in 15 ml APW. Algal samples immobilized on 35 mm glass-bottomed Petri dishes were immersed in 3 ml of the suspension, and formation of the zones void of microspheres adjacent to algal cells was observed under the microscope. Additionally, the zone of extracellular voltage near algal cells was observed with the use of smaller microspheres (0.5 µm; analytical standard; Cat# 19507-5; Polysciences, Inc., Germany). The reason for using smaller microspheres was that small ions can be excluded to a greater distance by the same magnitude of voltage near the surface compared to large charged particles (Nooryani et al., 2023). Therefore, smaller microspheres were employed to examine the particle exclusion ability of the extracellular voltage.

Membrane potential observation using voltage-sensitive dye

The voltage-sensitive dye $DiBAC_4(3)$ (bis-(1, 3-dibutylbarbituric acid) trimethine oxonol) (Lot: MKCQ7455, Sigma Aldrich, Germany) was used to observe the changes in membrane potential induced by CO_2 and KCl. An increase in fluorescence intensity compared to the control sample (not treated with CO_2 or KCl) indicates cell depolarization, while a decrease in fluorescence indicates hyperpolarization (Kim et al., 2013; Konrad & Hedrich, 2008). $DiBAC_4(3)$ powder was dissolved in 70% ethanol at a concentration of 1 mg/ml and then diluted (1:10) in deionized water to a concentration of 100 µg/ml. The resulting dye solution was further diluted (1:10) in APW (pH 7.3) to give a final dye concentration of 10 µg/ml. Effect of CO_2 was verified by incubating the samples with the dye for 30 minutes under 5% of CO_2 inside the incubator at room temperature in the dark. To observe the effect of KCl, the samples were incubated with the dye solution containing (0.1, 0.2, 0.3, 0.4, 0.5) mM KCl for 30 minutes at room temperature in the dark (Fig. 2.S4). Samples in the presence of CO_2 and also with 0.3 mM KCl were imaged using an inverted microscope (ZEISS, Germany) with the fluorescence imaging in the dark at room temperature. The intensity values of the fluorescence were estimated by plotting histograms for the selected area on algae cell's image using ZEN (V3.6) image analysis software. The area for plotting intensity histogram was selected as large as possible within the single cell using rectangular tool from the analysis software.

2.5 Acknowledgement

We thank Hydroidea Spółka z o.o. spółka Komandytowa Company for providing us the algae sample. We also thank Dr. Krzysztof Witek for supporting us with the fluorescence microscopy.

Author Contributions

M.K. conceptualized and supervised the project. M.M. conducted the laboratory work. M.M., M.K., and S.N. performed the data analysis and interpretations. S.N. supervised laboratory work. M.M., M.K., and S.N. wrote the original manuscript.

Funding

The National Science Centre of Poland under the grant number 2020/38/E/NZ3/00039 funded this work.

2.6 Supplementary Information

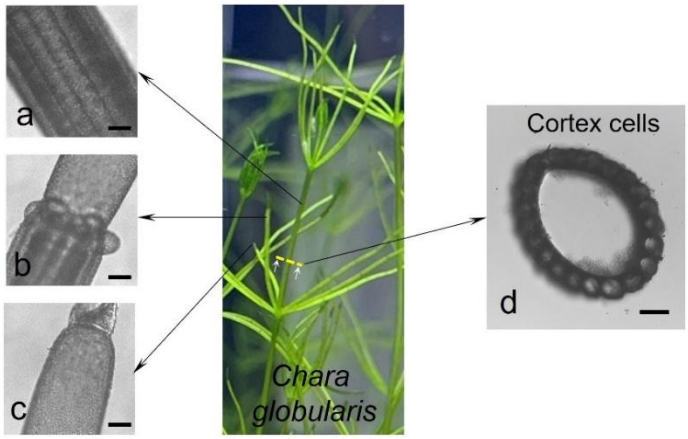

Fig. 2.S1. Images of different types of cells from freshwater green algae (*Chara globularis*): The figure shows the images of *Chara globularis* and its internodal axial (a), branch (b), non-corticated (c) cells and a cross sectional image of internodal cell with surrounding cortex cells. The scale bar in the image a, b, and c is 50 µm and d is 100 µm.

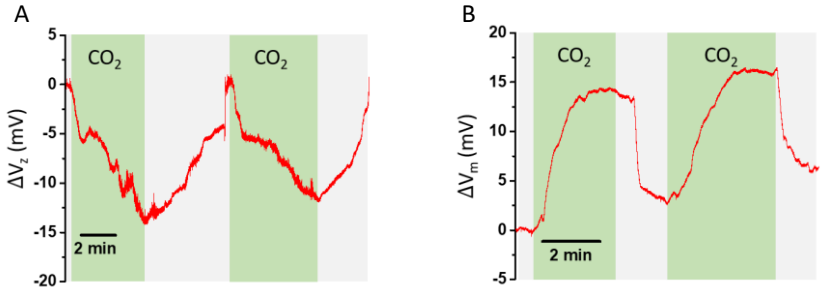

Fig. 2.S2. Effect of external CO_2 on extracellular voltage and membrane potential of algae: The graphs show the change in voltage (ΔV_z) and membrane potential (ΔV_m) in response to alternating increase (higher concentration than atmospheric CO_2) and reduced (in equilibrium with atmospheric CO_2) concentration of external CO_2 for the zone of extracellular voltage (A) and internodal cell (B).

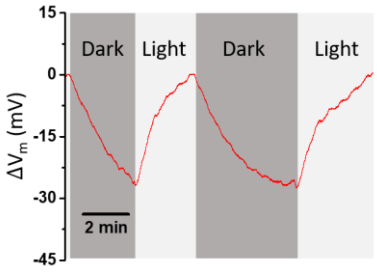

Fig. 2.S3. Effect of internal CO_2 on membrane potential of algae: The graph shows the change in membrane potential (ΔV_m) in response to alternating dark and light treatments for the internodal cell.

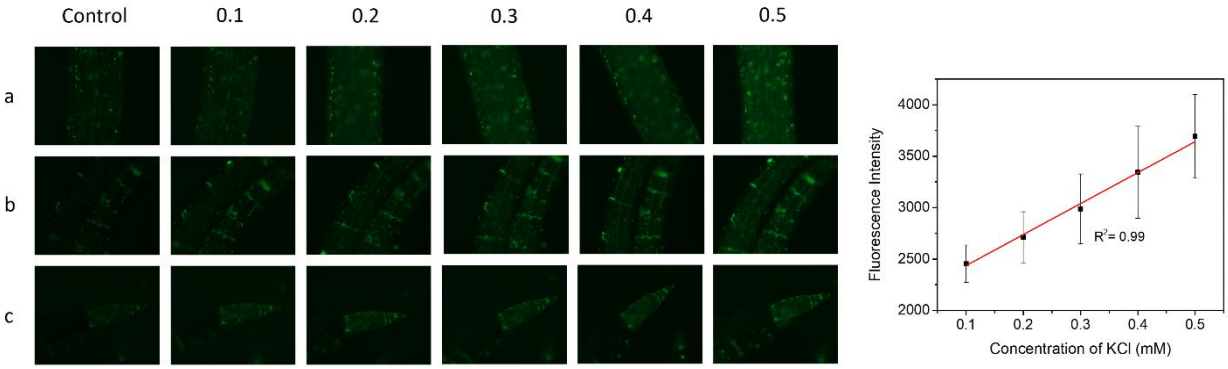

Fig. 2.S4. Effect of KCl on membrane potential of algae observed using voltage sensitive dye: The microscopic images show the change in intensity of the fluorescence (change in membrane potential) for algal internodal (a: axial, b: branch, and c: non-corticated) cells under control (untreated) and in response to additional KCl of (0.1, 0.2, 0.3, 0.4,0.5) mM observed using voltage sensitive dye. The graph shows linear dependence of fluorescence intensity of algal cells on the concentration of additional KCl (N = 3).

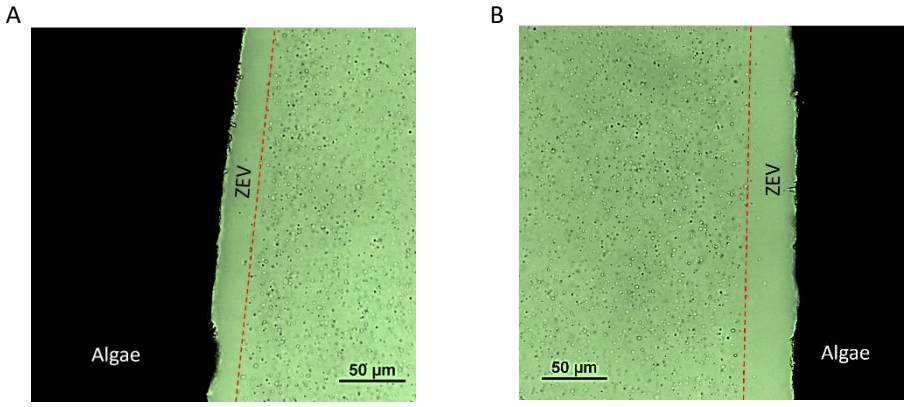

Fig. 2.S5. Visualization of the zone of extracellular voltage in response to additional KCl using microspheres of different diameters: Images show exclusion of the microspheres of diameters 1.0 µm (smaller zone) (A) and 0.5 µm (larger zone) near algal cell wall for the same magnitude of extracellular voltage induced by additional 0.3 mM KCl.

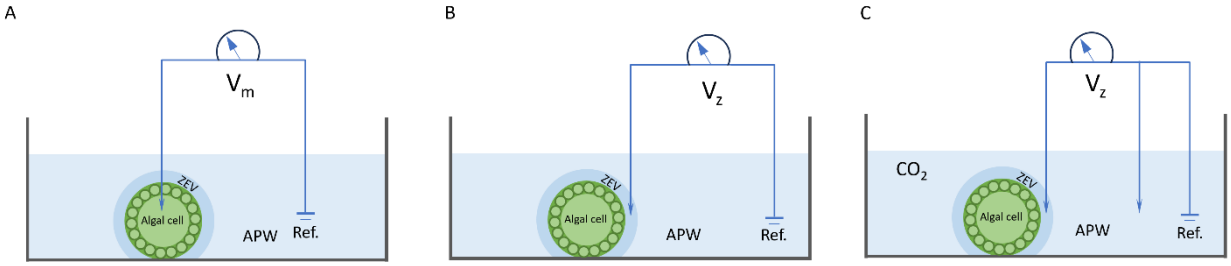

Fig. 2.S6. Schematic for measurement setup: The diagram illustrates the experimental setup for measuring the membrane potential inside the cell (A) and at the zone of extracellular voltage (ZEV) (B) in reference to the bulk solution (APW). The experimental arrangement shows the measurement of extracellular voltage and the voltage changes within the bulk (control) to verify the effect of change in solution pH in response to an increased concentration of extracellular CO_2 (C).

Table 2.S1. The table presents a summary of voltage changes for internodal cells (ΔV_m), cortex cells (ΔV_m), the zone of extracellular voltage (ZEV) (ΔV_z), and the width (D) change of the ZEV in response to external/internal stimulations. Positive and negative signs denote the depolarization and hyperpolarization, respectively. Blanks (-) in the table indicate that the membrane potentials for cortex cells in response to 0.3 mM KCl and wounding were not measured.

Stimuli	**Change in voltage (ΔV) (mV)**			**Width of the ZEV (µm)**
	Internodal cells (ΔV_m)	Cortex cells (ΔV_m)	ZEV (ΔV_z)	D
Extracellular CO_2	+16.84 ± 3.92	+7.06 ± 3.08	-15.91 ± 3.06	54.17 ± 5.34
Light → Dark	-31.82 ± 5.72	+9.05 ± 2.54	No alteration	No alteration
0.3 mM KCl	+16.66 ± 1.53	-	-9.50 ± 2.08	30.25 ± 2.22
Wounding	+28.25 ± 3.59	-	-26.25 ± 1.71	80.60 ± 8.02

Chapter 3

Modifying membrane potential synchronously controls the somite's formation periodicity and growth

Manohara Mahadeva[1], Sebastian Niestępski[1], Magdalena Kowacz[1]*

[1]Department of Reproductive Immunology & Pathology, Institute of Animal Reproduction and Food Research Polish Academy of Sciences, 10-748 Olsztyn, Poland

***Corresponding author**

Published in: Developmental Biology Volume 517, Pages 317-326 (2025),

DOI: 10.1016/j.ydbio.2024.11.002

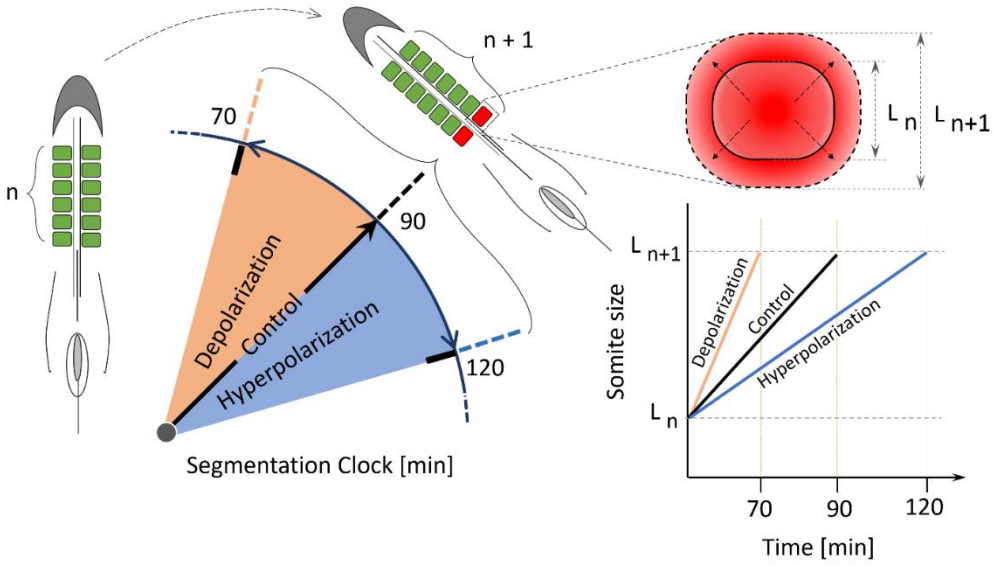

3.1 Introduction

Somitogenesis is the rhythmic segmentation of somites, where pairs of paraxial mesoderm blocks, originating from somite-forming cells or presomitic mesoderm (PSM), form on either side of the embryo's anterior-posterior axis (Pourquié, 2001). This process is characterized by tissue- and species-specific periodicity (Carraco et al., 2022). Somite formation occurs with temporal cyclicity accompanied by corresponding somite's growth, leading to development of defined spatial pattern with segment's size proportional to overall body length (Dale & Pourquié, 2000; Pourquié, 2003a). Temporal periodicity is regulated by gene oscillations known as the segmentation clock, driven by complex signaling pathways (Dequéant et al., 2006; Hubaud & Pourquié, 2014; Krol et al., 2011; Masamizu et al., 2006; Palmeirim et al., 1997). However, the mechanism setting the clock period and that synchronizes temporal periodicity with somite growth is not fully understood (Carraco et al., 2022; Ishimatsu et al., 2018). Studies have attempted to explain respective somite scaling and suggested that reduction in the somite formation interval should lead to larger somites with increasing the period having the reverse outcome (Juul et al., 2019; Lauschke et al., 2013). However, some experimental findings have shown the opposite effect: accelerating the timing of somite formation through genetic manipulation led to smaller somites, while slowing the segmentation resulted in larger segments (Harima et al., 2013; Schröter & Oates, 2010). Therefore, the question remains open: what precisely synchronizes periodicity of somite segmentation and somite growth rate to generate consistent early body pattern during embryonic development? To answer this question, it's crucial to understand the cellular processes involved in somitogenesis. A discrete number of cells from PSM need to migrate and self-assemble to form somite blocks, then proliferate to assure segment growth and differentiate to acquire structure-related function (Alvarez et al., 1989; Blomberg et al., 2008; Nakamura et al., 2007). All these fundamental processes must work in an orchestrated manner to generate somites with consistent size at precise time and space intervals. It has been demonstrated that the rate of cell proliferation and differentiation can be controlled by modifying the membrane potential of cells (Blackiston et al., 2009; Cone & Tongier, 1971). Also, cell migration and structure/pattern formation during tissue regeneration and embryo development were shown to be regulated by membrane potential (Fukumoto et al., 2005; Levin, 2012; Nishiyama et al., 2008; Ozkucur et al., 2011). However, the possibility to couple

proliferation with morphogenesis via bioelectric control of physiological processes is only beginning to be understood (Levin & Martyniuk, 2018). The membrane potential of different cell types has been measured and correlated with their preferability, revealing that proliferative cells are depolarized compared to differentiated ones (Binggeli & Weinstein, 1986). Generally, cells in embryos or tumors are highly proliferative, depolarized, and also share common characteristics of the microenvironment, enriched in CO_2 and K^+ compared to the one of quiescent cells (Chen et al., 2022; Kikuchi et al., 2019; Oginuma et al., 2017; Roblero et al., 1976; Roblero & Riffo, 1986). This suggests that the chemical composition of cells' surrounding may play a role in defining their membrane potential. Supporting this notion, we have recently demostrated for the first time that cells can in fact be depolarized by increasing the external CO_2, in addition to the known depolarizing effect of KCl (Mahadeva et al., 2024). We have experimentally demonstrated the existence of a negative extracellular voltage adjacent to the cell and its evolution in response to depolarization induced by either CO_2 or KCl (Mahadeva et al., 2024). Increased concentration of those components in the cell's environment prompted development of electric potential at the outer cell wall/membrane and caused corresponding changes in the overall transmembrane potential (TMP) value. By comparing the voltage measured using the direct microelectrode technique and observed using potential-sensitive dye, we have shown the importance of considering extracellular voltage in defining TMP of a cell. Increased concentration of intracellular CO_2 (from metabolic output of a cell) also resulted in negativity increase, but at the inner side of the membrane, thus having the opposite effect on TMP than environmental CO_2 (Mahadeva et al., 2024). These experimental findings are consistent with the previously defined concept that cell's TMP, as measured by microelectrodes and described by classical Nernst equation (Hopper et al., 2022), comprises both intracellular and extracellular negative components (Vodovnik et al., 1992), emergence of which is also consistent with Ling's theory (Tamagawa & Ikeda, 2018). Based on those considerations, it has been suggested that the overall transmembrane potential can be altered by affecting independently only extracellular voltage and that this can be responsible for the observed effect of externally applied electric field on cell proliferation (Vodovnik et al., 1992). It has been also recognized that endogenous extraembryonic electric fields contribute to embryo development by influencing cell migration (Hotary & Robinson, 1990). However, it is not yet known if the electric potential gradients can affect the timing of somite formation (cell migration

and self-assembly) and their synchronous growth (proliferation). Therefore, in this study, we aim to verify whether changes in membrane potential of somite-forming cells, induced by adjusting composition of their microenvironment, can control early body pattern formation by affecting elemental processes underlying somitogenesis. For this purpose, we use CO_2 and KCl to modify the membrane potential of chick embryonic cells and then assess the effect of the induced changes on somite segmentation rate and somite growth. Our data reveal that CO_2 and KCl, naturally enriched in the embryo's environment, contribute to depolarization of embryonic cells. The membrane potential (V_m), adjusted by those environmental stimuli to a given level, sets the new timing of somite appearance coordinated with its adequate spatial expansion. The somite formation periodicity (τ) depends linearly, while somite growth rate (L(t)) depends exponentially on V_m, with depolarization accelerating fundamental events of early somitogenesis.

3.2 Results and discussion

Mapping the voltage of somites in the chick embryo along its anterior-posterior axis

The membrane potential measured in this study, designates the electric potential difference between the somite interior and its surrounding medium. In chick embryo, the somite stages (SS) are represented by Roman numbers. The somite position along the axis, counted from most rostral to caudal one, is represented by Arabic numbers (Venters et al., 2008) (Fig. 3.1 a). In general, the somite stages reflect somite's intrinsic developmental time, while somite position along the axis (somite number) is related to its future fate in terms of giving rise to particular structures of vertebrate body. V_m was measured via microelectrode at control conditions of 5% CO_2 for all the somite stages (SS I - XIII) in embryos with 8 to 13 pairs of somites (Fig. 3.1 a). Rostral somites have consistently exhibited more negative V_m compared to that of caudal ones (Fig. 3.1 b). This indicates that somites become progressively hyperpolarized (acquiring more negative potential) with their maturation. This hyperpolarizing trend was also observed using a voltage-sensitive dye, showing that all the cells within the somites become hyperpolarized as they mature (Fig. 3.1 c). Embryonic cells have been previously shown to be hyperpolarized with progressing development (Arcangeli et al., 1997). Along with

the general hyperpolarizing trend we observed a step-like changes of V_m between specific groups of somites, specifically the youngest, most posterior ones (SS I – SS III), middle (SS IV – SS VIII), and most developmentally advanced, anterior somites (SS IX – SS XIII). We obtained the following V_m ranges for each somite group: (-8.49 ± 0.45 to -10.45 ± 0.47) mV for SS I – SS III, (-15.83 ± 0.98 to -19.28 ± 0.36) mV for SS IV – SS VIII, and (-22.82 ± 0.65 to -25.95 ± 0.25) mV for SS IX – SS XIII. Within each group, V_m exhibited a linear dependence on somite stage, with slopes of -0.95, -0.87, and -0.75 respectively for posterior, middle, and anterior somites, which shows that the developmental processes reflected in changes of V_m are more dynamic in caudal somites than in the rostral ones (Fig. 3.1 b). The most dynamical, youngest somites are structurally and functionally identical and still silent in terms of morphogen expression (Maschner et al., 2016). Therefore, observed changes in membrane potential are most probably related to their metabolic output, (Jakobsson, 1980; Mahadeva et al., 2024) what is in agreement with more posterior cells within the embryo showing the highest glycolytic activity (Oginuma et al., 2020). Intracellular anionic metabolites contribute to defining negative membrane potential of a cell (Jakobsson, 1980) , while metabolism in general provides both precursor molecules and energy necessary for gene expression that directs further development (Carthew, 2021). It is worth noting that membrane potential is not only a product of cell metabolism, but also regulates metabolic performance because membrane polarization directly affects the transport of all charged species (including nutrients and waste products) into and out of the cell. As we will discuss further in this work, induced membrane potential changes may control cell's behavior via this feedback loop with metabolism.

The embryos examined in our study are in their early-stages where occipital (1-5 from the rostral end) and cervical (following 5-19) somites are formed. During this stage of embryogenesis, the onset of expression of transcription factors (TFs) as well as the onset of the following morphological changes were shown to be delayed in comparison to later stages (Ibarra-Soria et al., 2023; Maschner et al., 2016). This means that for the same intrinsic developmental time (somite stage), occipital and cervical somites are less developmentally advanced than their counterparts formed later in the somitogenesis. Our potential-based classification of somites (into groups separated by abrupt potential changes) in fact reflects the previously recognized differences in somite development, already at the level of the expression of morphogenic TFs or, later on, at the level of

differentiation (Maschner et al., 2016). It has been shown that the expression of TFs in early embryogenesis starts only from the somite stage IV, what corresponds to the first step-like change in our V_m values. Then, differentiation begins from somite stage IX, thus corresponding exactly to the next step in otherwise linearly changing V_m. However, V_m is not specific for a given TF or a given morphological change. Expression of any TFs commences always at the same somite stage, but the identity of TFs being expressed differs for the same stage depending on somite position along the axis. Specifically, only Pax1 was detected in SS IV – SS XI in embryos with 8 to 11 pairs of somites, while both Pax1 and MyoD were expressed in those (and later) somite stages in embryos with 12 and 13 somite pairs. Yet, V_m values in those embryos are virtually constant for a given somite stage independently of its number along the axis. Morphological changes (manifested in the loosening of the epithelial integrity of occipital and cervical somites), on the other hand, begin always at SS IX, what is reflected in a step-like change of V_m. Nevertheless, then somites start to compartmentalize to form specific structures (here sclerotome), what is not mirrored by any abrupt change in V_m, that linearly increases within this (SS IX – SS XIII) morphologically nonuniform group. Therefore, the step-like changes of V_m, as reported in our study, closely reflect the onset (but not the identity) of either biochemical or structural changes within developing somites. In order to further verify this concept, we measured V_m in embryos having 4 to 7 pairs of somites, where all the somites are morphologically identical and do not show expression of any TFs (Maschner et al., 2016). In support of our conclusion, we observed no step-like change in V_m between SS III and SS IV, but linear hyperpolarizing trend (with the slope of -1.01) along anterior-posterior axis of the embryo (Fig. 3.2). Membrane potential marking the inception of different, non-specific changes again points toward the metabolism as the possible underlying factor. Once the level of energy and precursor materials is sufficient (and expressed in potential values), the processes can commence. In fact, it has been shown experimentally, that the rate of the whole embryo development is adjusted to the performance of its metabolism-limited slowest part (Carthew, 2021). The greater disparity in the step change of V_m values between the posterior and middle somite groups compared to that between the middle and anterior groups suggests that V_m is more sensitive to biochemical alterations than to structural ones (Fig. 3.1 b). To the best of our knowledge, this is the first report showing the pattern of V_m alterations along the body axis of vertebrate embryo and its correlation with the onset of developmental events. In the following section we show the possibilities of affecting the

V_m in order to later explore its ability to not only reflect, but also affect embryonic development, characterized by periodicity of somite formation and somite expansion rate.

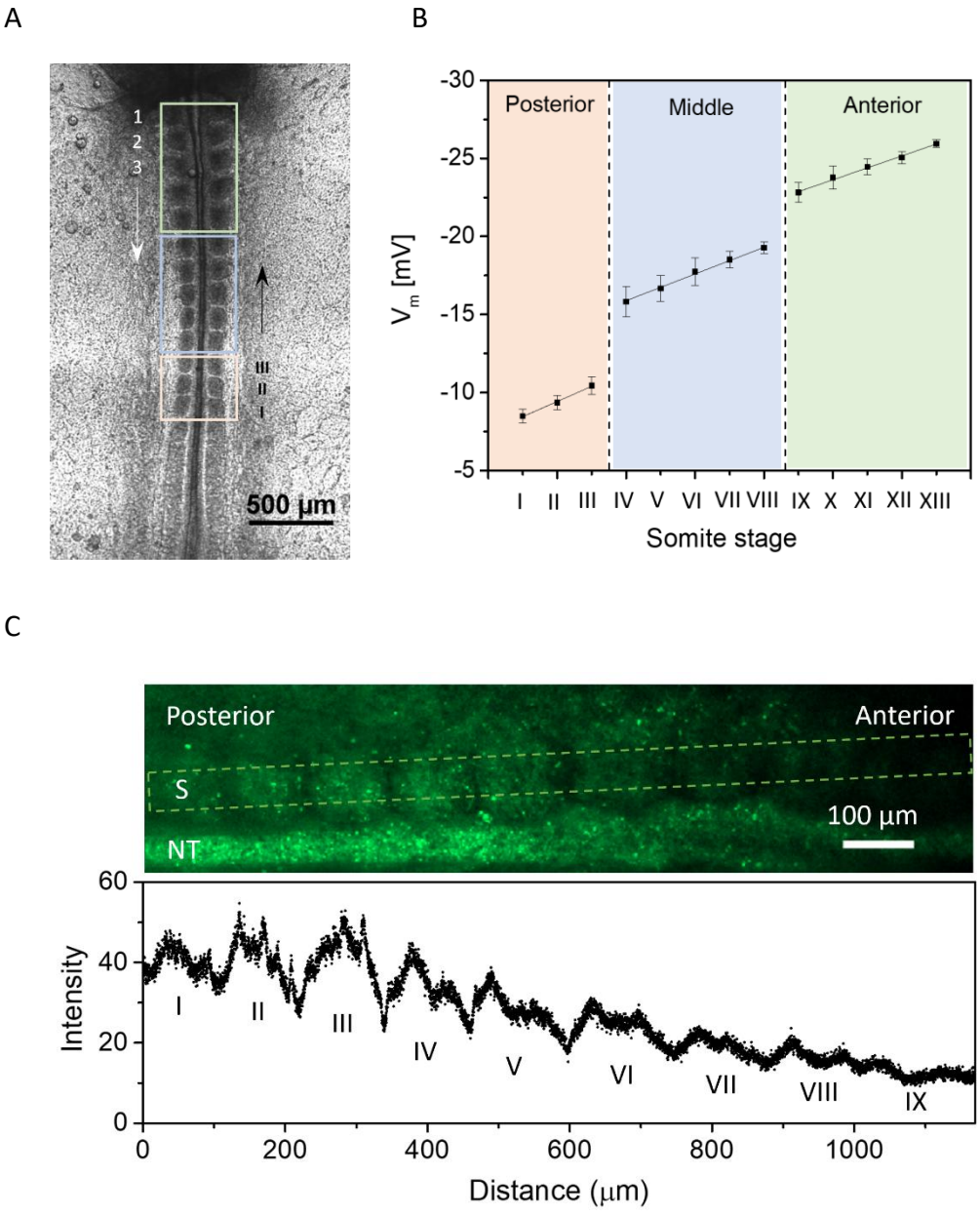

Fig. 3.1. Membrane potential (V_m) of somite-forming cells in chick embryo. A bright-field microscopy image shows embryo with 13 somite pairs, where somite stages are indicated by Roman numbers and somite positions are indicated by Arabic number. Posterior (SS I - III), middle, (SS IV - VIII) and anterior (SS IX – XIII) somite groups represented by orange, blue, and green boxes, respectively (A). Dependence of V_m on somite stages for embryos with 8 to 13 pairs of somites. The lines are linear fit for each somite group [$V_m = -0.95 \cdot SS - 7.4$, $R^2 = 0.99$

(posterior, orange), V_m = -0.88⋅SS – 12.35, R^2 = 0.99 (middle, blue), and V_m = -0.75⋅SS – 16.11, R^2 = 0.99 (anterior, green)] (N = 18) (B). Confocal microscopy image shows the change in fluorescence intensities of somites and fluorescence intensity versus distance graph shows the degree of hyperpolarization of somite-forming cells along anterior-posterior axis of chick embryo (9 somite pairs) (C) (N = 5). Decrease in fluorescence intensity of the dye indicates the cell hyperpolarization. S – somite, NT – neural tube.

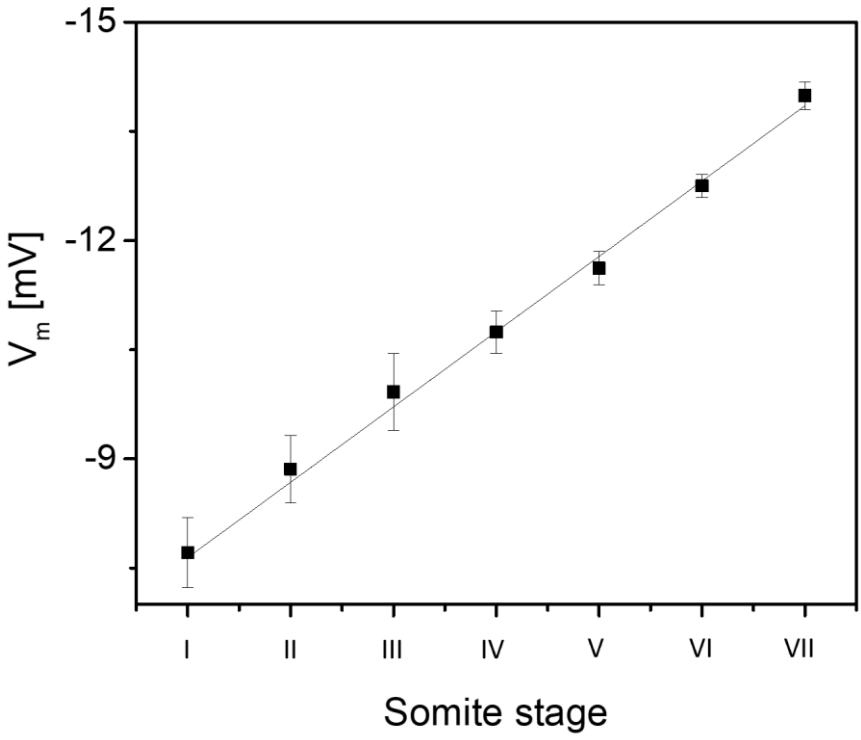

Fig. 3.2. Membrane potential (V_m) of somite-forming cells in early-stage chick embryos. Dependence of V_m on somite stages for the embryos with 4 to 7 pairs of somites. The line is the linear fit for the shown trend (V_m = -1.011⋅SS – 6.75, R^2 = 0.99) (N = 7).

The effect of external stimuli on the membrane potential of somite forming cells observed in the chick embryo

In this study, we have used CO_2 and KCl as the external stimuli to depolarize embryonic cells in early-stage chick embryos. Fertilized eggs were incubated (and analysed) at selected CO_2 levels (2%, 5%, and 7%) for a given experiment, while constant CO_2 (5%) level was maintained in experiments with additional (0.3 and 0.6) mM KCl to the medium (Pennett-Compton saline) containing 8.3 mM KCl (control). For the purpose of these experiments, somites were categorized, based on the Vm-bound groups along the

embryo's body axis, into: posterior (SS I – SS III), middle (SS IV – SS VIII), and anterior (SSIX – SS XIII). To compare the effect of different stimuli on a given group of somites, V_m of selected representative somites from each group was measured and averaged for any experimental conditions. At 2% CO_2, the V_m of posterior, middle, and anterior somites were (-14.63 ± 1.58) mV, (-22.27 ± 2.73) mV, and (-26.70 ± 2.32) mV, (Fig. 3.3 a). The somites in every group were depolarized by 42.78% to (-8.37 ± 1.31) mV, by 31.21% to (-15.32 ± 1.54) mV, and by 14.75% to (-22.76 ± 1.74) mV respectively, at 5% CO_2 (Fig. 3.3 a). Somites were further depolarized by 55.32% to (-3.74 ± 1.09) mV, by 43.79% to (-8.61 ± 1.37) mV, and by 41.08% to (-13.41 ± 1.65) mV in caudal to rostral direction, in embryos developing at 7% CO_2 (Fig. 3.3 a). The CO_2-induced depolarization was also shown by using potential-sensitive dye (Fig. 3.S1). An increased level of CO_2 acidifies the cell's microenvironment (Gatenby & Gillies, 2004; Parkins et al., 1997). To verify whether the induced depolarization of somites could be the effect of change in pH of the bulk solution, we have adjusted the bulk pH to 6.3 (maximum change in pH brought by 7% CO_2) using HCl. The V_m of somites remained unchanged in response to additional HCl (Table 3.S1). Therefore, the change in V_m in response to variations in CO_2 levels, as shown in our experiments, may not be attributed to changes in pH of the extracellular environment. Our results show that increasing levels of CO_2 in the embryo's surrounding always depolarize the somites. Next, the embryos grown at 5% CO_2 were treated with two different concentrations of KCl. Additional 0.3 mM KCl in the medium containing the embryo, has reduced (depolarized) V_m of posterior, middle, and anterior somites by 45.04% to (-4.60 ± 1.14) mV, by 34.73% to (-10.00 ± 1.58) mV, and by 23.55% to (-17.40 ± 1.82) mV, respectively, while, additional 0.6 mM KCl reduced V_m of corresponding somites by 80.88% to (-1.60 ± 0.55) mV, by 64.75% to (-5.40 ± 1.14) mV, and by 47.27% to (-12.00 ± 1.22) mV, compared to the control conditions (Fig. 3.3 b). From the above results it can be noted that not only the dynamics of V_m changes at constant environmental conditions was the highest in the youngest somites (Fig. 3.1 b), but also V_m response to the environmental stimuli is most expressed in this group (Fig. 3.3 a, b). Our results confirmed that CO_2 and potassium-enriched microenvironment of embryos may contribute to defining their V_m.

Our previous work has shown that cell depolarization induced by either CO_2 or KCl is accompanied by the emergence of a negative extracellular voltage (V_z) adjacent to the cell surface and that the overall membrane potential of a cell includes also V_z component

(Mahadeva et al., 2024). V_z has the ability to exclude colloidal particles, the property that can be employed for its visual detection. Therefore, we used microspheres to verify the possible emergence of V_z near the embryonic cells in response to their induced depolarization. The microspheres (diameter: 0.5 µm) could be observed in the immediate vicinity of the somite surface at conditions of 5% CO_2 (Fig. 4a), while they have moved to a distance of approximately (16.73 ± 2.86) µm from the surface at 7% of CO_2 (Fig. 3.4 b). The observed exclusion phenomenon could be either due to the anticipated electric field (V_z) developed in response to higher levels of CO_2 (Mahadeva et al., 2024), but possibly also due to an expansion of extracellular matrix (ECM). It has been recognized that microspheres (or other charged objects) of different sizes are excluded to different distances by the same magnitude of the interfacial voltage (Mahadeva et al., 2024; Nooryani et al., 2023). Therefore, to verify the mechanism behind the particle exclusion from the somite surface, we used smaller microspheres (diameter: 0.2 µm) and observed their exclusion to a larger distance of approximately (28.83 ± 2.79) µm (Fig. 3.4 c) at 7% of CO_2 (N = 5, each). If the particle movement resulted from an expansion of ECM, both smaller and larger microspheres would have been excluded to the same distance or the smaller ones could penetrate more into ECM network, due to possible increase in pore size of ECM caused by its expansion. Our observations therefore indicate the emergence of V_z near the somite surface in response its CO_2-induced depolarization. Previous studies have shown the existence of an endogenous extracellular electric fields along the anterior-posterior axis of chick embryo, with a more positive voltage gradient at the rostral end compared to caudal end (Hotary & Robinson, 1990; Nuccitelli, 2003). It has been suggested that the more positive charges are mainly due to Na^+ ions being pumped out by cells (Hotary & Robinson, 1990). When positive ions are moved from the cells, their membrane potential becomes more negative (hyperpolarization) (Gadsby & Cranefield, 1979), what is consistent with reported by us trend of changes in membrane potential of somite-forming cells along the body axis. The endogenous electric fields have been suggested to provide directional information for growing and migrating cells in chick embryo (Hotary & Robinson, 1990). It is important to note however, that the direction of an electric field related to the emergence of V_z, as suggested in our study, would be normal to the somite surface, thus affecting charge movement in/out of the somite. This is in contrast to the previously reported extraembryonic fields driving ionic current flow parallel to the somite surface. V_z, as defined by us (Mahadeva et al., 2024) and akin to the previously

recognized outer membrane potential (Vodovnik et al., 1992), is the component of transmembrane potential (Mahadeva et al., 2024) (here the electric potential difference measured across the somite surface), and as such may play yet unrecognized role in embryonic development.

A

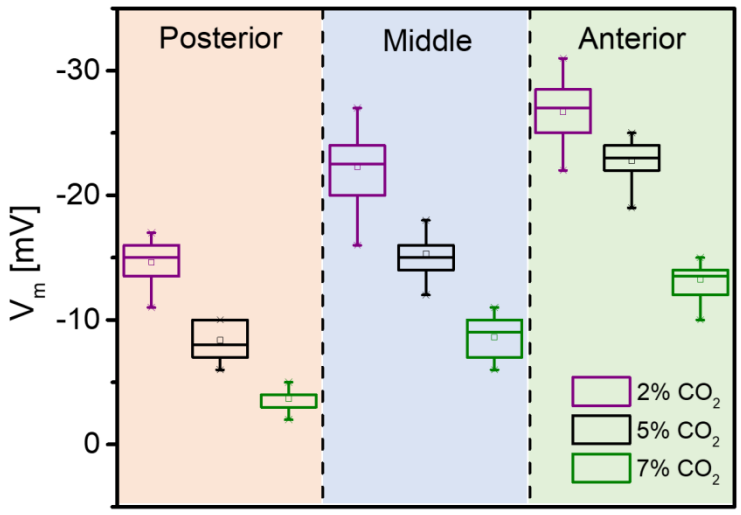

B

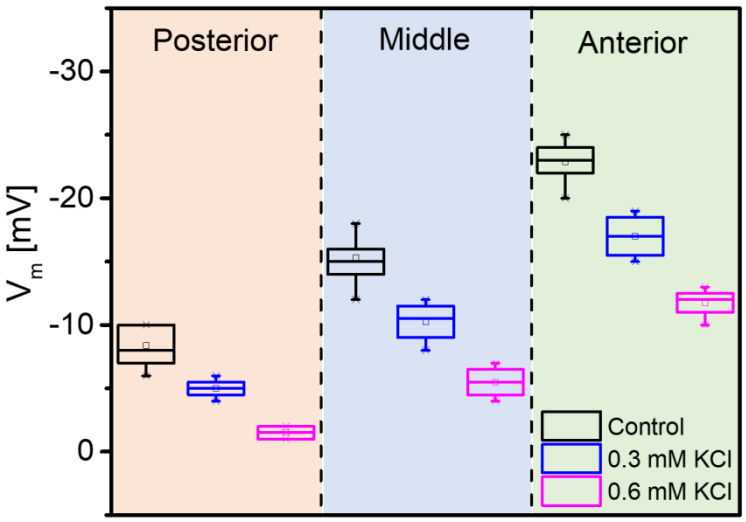

Fig. 3.3. Effect of CO_2 and KCl on the membrane potential (V_m) of somite-forming cells in chick embryo. Box plots show V_m for posterior (orange), middle (blue), and anterior (green) somites in response to change in concentrations of CO_2 and KCl. Depolarization and hyperpolarization of the somites were observed at 7% CO_2 (green) and 2% CO_2 (purple), respectively, compared to the control condition (5% CO_2) (black) (A) (N=20 each).

Depolarization of somites was observed at additional 0.3 mM KCl (blue) and additional 0.6 mM KCl (magenta), compared to the control condition (black) (B) (N=4 each).

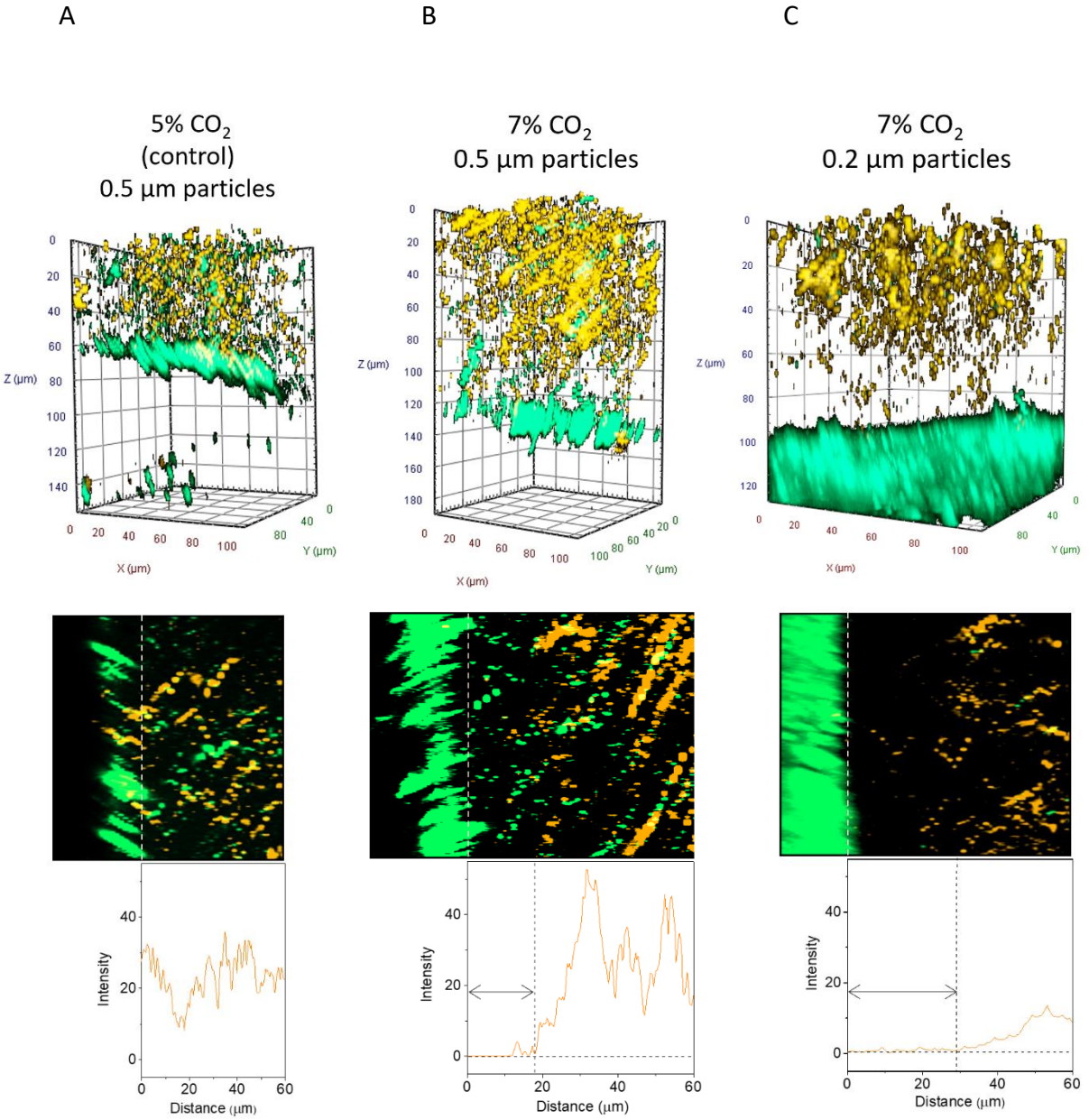

Fig. 3.4. Particle exclusion zone near somite's surface. Three dimensional graphs and two-dimensional confocal images show microspheres (0.5 µm, orange) attached to somite's surface (green) at control (5% CO_2) condition (A) and particle exclusion zones at 7% CO_2 for (0.5 and 0.2) µm, microspheres (orange) (B and C respectively). The line graphs show the intensity of the fluorescence of microspheres versus distance, where the arrows indicate the width of the zone largely devoid of microspheres.

Depolarization increases the pace of somite emergence and promotes its growth in the chick embryo

During somitogenesis, discrete clusters of cells organize and undergo segmentation to form somites. The segmentation of somites occurs at regular intervals of time. Studies have shown that the first five pairs of somites in chick embryo form approximately every 75 minutes, while somites of sixth pair onwards are formed at an average time of 90 minutes (measured at 5% CO_2) (Maia-Fernandes et al., 2024; Palmeirim et al., 1997). In our experiments, we have also observed the same temporal pattern, with somite formation occurring at a comparable periodicity of (89.80 ± 3.83) minutes across the examined embryo stages (7-13 pairs of somites) at control conditions (5% CO_2). In this study, to understand the contribution of Vm to the periodicity of the somite formation and its growth, we manipulated the membrane potential of early-stage chick embryos. As in the case of experiments examining the effect of specific stimuli on V_m, embryos were incubated and analysed at a given CO_2 concentration set to respective level for the whole experiment, or in the presence of a given concentration of KCl in the medium at constant 5% CO_2.

Modifications in V_m of somite forming cells prompted a shift in the pace of somite formation. At 2% of CO_2 level, the somite segmentation occurred in (121.60 ± 5.94) minutes. The somite segmentation time was reduced by 26% to (89.80 ± 3.83) minutes upon V_m depolarization induced in embryos developing at 5% CO_2. Somite segmentation time was accelerated by another 21% to (70.40 ± 3.84) minutes in response to further V_m depolarization in embryos growing at 7% CO_2. Depolarization induced in cells by KCl reduced the segmentation time by 12% to (79.00 ± 2.58) minutes and by subsequent 27% to (64.75 ± 4.04) minutes, in response to additional (0.3 and 0.6) mM KCl, respectively (Fig. 3.S2) (N = 5 for each CO_2, and N = 4 for each KCL treatment). In general, the time required for the segmentation of somites depends linearly on the membrane potential of somite-forming cells with less negative membrane potential setting the faster tempo (Fig. 3.5).

Alterations in V_m affected somite's expansion/growth rate (Fig. 3.5). At 2% of CO_2 level the rate of expansion of somites (changes in the width of the somite measured along anterior-posterior axis) was (2.58 ± 0.22) µm per hour. The expansion rate increased by 92% to (4.97 ± 0.84) µm per hour upon depolarization of V_m induced in embryos

exposed to 5% CO_2 (Fig. 3.5) and by further 103% to (10.11 ± 1.02) µm per hour as a result of even stronger depolarization experienced by embryos developing at 7% CO_2. Depolarization induced by additional 0.3 mM KCl has increased the somite expansion rate by 51% to (7.55 ± 0.45) µm per hour, whereas additional 0.6 mM KCl further accelerated it by 168% to (13.32 ± 0.60) µm per hour compared to control conditions (Fig. 3.5, 3.S2) (N = 7 for CO_2, and N = 4 for KCl treatments, respectively). The rate of somite growth, in terms of changes in somite's diameter (estimated based on previously reported data on changes of somite's volume by assuming that the somites are spherical in shape) (McColl et al., 2018), in later stages of embryogenesis is (3.31 ± 1.97) µm per hour (average growth rate of SS I – III) (McColl et al., 2018). In our case, the rate of increase in somite's diameter for SS II at control conditions is (4.97 ± 0.84) µm per hour. This discrepancy could be due to the fact that the previously reported growth rate of somites was calculated for more developed embryos (22 to 28 somite pairs) (McColl et al., 2018) compared to the ones used in our work (4 to 13 somite pairs). In fact, the developmental processes reflected in changes of V_m are more dynamic in early embryogenesis, as indicated by the slopes of V_m versus SS trends: -1.01 for embryos with 4 to 7 somite pairs, and -0.95 (for SS I – III) in embryos with 8 to 13 somite pairs, respectively (Fig. 3.1 b, 2). This may possibly translate into faster growth rate of somites in early embryogenesis. In general, our data show that the rate of somite expansion changes exponentially as a function of V_m (Fig. 3.5) and, as in the case of segmentation periodicity, depolarization speeds up the process.

The revealed dependencies of somite formation and growth on V_m follow their respective trend lines, independently of the stimuli used to alter V_m, thus confirming that the observed effects are not stimuli-specific, but rather potential-specific (Fig. 3.5). The different trends reflect the fact that the two processes are distinct in nature. The segmentation occurs as a result of cell migration and self-assembly, while volume expansion is governed by cell proliferation and growth. Earlier study has shown that increase in the size of somites of epithelial morphology (as the ones addressed in our work) is mainly due to the increase in the number of epithelial cells (Bagnall & Berdan, 1994). It has been also demonstrated that the number of cells within somites increases exponentially with somite stage (maturation) (Venters et al., 2008). Therefore, the exponential dependence of somite expansion on V_m (Fig. 3.5), suggests that V_m should affect cell proliferation rate. The rate of cell proliferation has been shown to be

accelerated by depolarizing the cells, and reduced by hyperpolarizing them (Blackiston et al., 2009; Cone & Tongier, 1971). Such observations are consistent with our findings showing increased and reduced somite expansion (cell proliferation) in response to induced depolarization and hyperpolarization respectively (Fig. 3.5). There are no preceding data on the effect of membrane potential changes on somite segmentation periodicity – a developmental process determined by cell migration and self-assembly (in the time course of our experiment, where all precursor cells are already present in the PSM). We are showing the possibility to shorten segmentation interval by unprecedented 27%, accompanied by a simultaneous increase in the somites' growth rate, thus maintaining their regular aspect ratio. Up to now the only way enabling somitogenesis acceleration was direct gene manipulation, which however resulted in only up to 9% increase in the respective tempo (Harima et al., 2013; Liao et al., 2016). Furthermore, faster segmentation periodicity led to narrower segments, as somite growth did not adjust to the newly established somite birth rate (Harima et al., 2013; Liao et al., 2016). In contrast, membrane potential alterations, as applied in our work, allow for the synchronous control of both somite formation and growth. This is expressed in the undisturbed body pattern formation at any given somitogenesis rate set by membrane potential. This conclusion is further strengthened by our observations that embryos incubated in ovo at different CO_2 conditions (related to differences in V_m) reach expected, more or less advanced development stage by the same time of incubation, yet they do not show any morphological abnormalities. It is generally recognized that somite size scales with the length of PSM (Ishimatsu et al., 2018; Lauschke et al., 2013). Recently it has been proposed that this is due to gene oscillation dynamics (underlying also periodicity of somite formation) scaling with the size of embryo axis (Juul et al., 2019; Lauschke et al., 2013). Those results therefore revealed tight coupling between segmentation rate and somite growth. Our findings, showing somite size scaling accordingly with somite formation period, support such interdependence. However, this was not the case for somitogenesis accelerated by direct manipulation of oscillatory genes, where smaller somites were generated (Harima et al., 2013). It might be due to the fact that alterations of V_m affect cell proliferation in the whole embryo, including the PSM (thus supporting its steady-state length), allowing somites to adjust to the new pace of segmentation without any size disruptions.

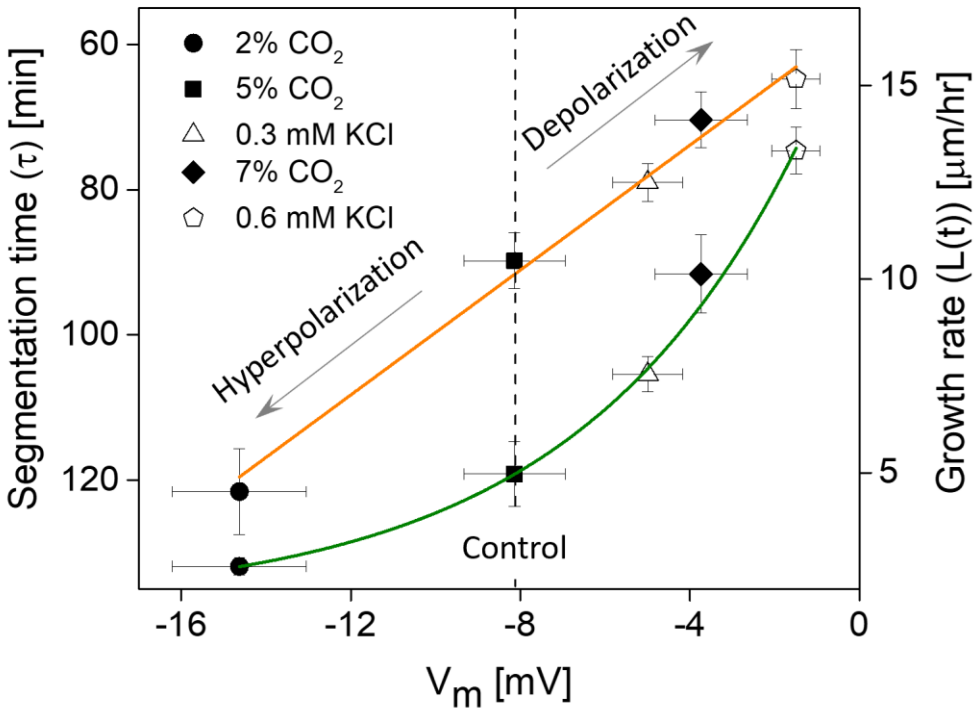

Fig. 3.5. Dependence of periodicity of somite formation (τ) and somite's growth rate (L(t)) on membrane potential (V_m) of somite-forming cells. The linear fit, $\tau = -4.30 \cdot Vm + 56.64$, $R^2 = 0.98$, (N = 5 for each point) corresponds to the periodicity of somite formation (orange), whereas the exponential fit, $L(t) = 1.58 + 15.65 \cdot e^{0.18 \cdot Vm}$, $R^2 = 0.99$ (N = 4 for each point) corresponds to the rate of individual somite expansion (green). Individual data points represent the values at 2% CO_2 (solid circle), 5% CO_2 (solid square), additional 0.3 mM KCl (empty triangle), 7% CO_2 (solid diamond), and additional 0.6 mM KCl (empty pentagon).

Cell proliferation and migration/self-assembly are the processes that are known to be regulated by β-catenin/Wnt signalling pathway that controls somitogenesis, but also tumorigenesis and tissue regeneration (Qin et al., 2007; Sharma et al., 2021). In this study, we have shown that cell proliferation (in terms of change in the rate of somite expansion) and migration/self-assembly (in terms of change in periodicity of somite formation) could be synchronously altered by modifying V_m using external stimuli (Fig. 3.5). Our results show that the step-like changes in V_m reflect the onset of transcription factors expression and the onset of cells differentiation. This suggests that V_m might control the expression of genes that drive somitogenesis. In support of this, it has been previously shown that induced depolarization in cells results in the translocation of β-catenin (a protein molecule that transduces signal in Wnt signalling pathway) from the cytoplasm into the nucleus, prompting the onset of expression of TFs that lead to cell

proliferation and differentiation (Rapetti-Mauss et al., 2017). β-catenin was also shown to be activated by increase in intracellular pH resulting from aerobic glycolysis (the prevalent metabolic pathway in early embryos). This process releases lactic acid, which carries its counterions (protons) out of the cells, thereby increasing intracellular pH (Oginuma et al., 2020). In our case, the induced depolarization of somite-forming cells, should facilitate the outward movement of protons due to lower electric force (less intracellular negativity) counteracting their expulsion. Simultaneously, the negative V_z near the depolarized cells should also aid proton removal, by providing electric force attracting positive charges into extracellular space. This possibility is supported by previous studies, arguing that application of an external electric field causes the cell membrane facing the negative electrode, analogous to our V_z, to become depolarized (Jaffe & Nuccitelli, 1977; Robinson, 1985; Vodovnik et al., 1992). The induced depolarization, in turn, reduces resistance of the membrane and increases transmembrane ionic current, thus supporting e.g., proton efflux (Vodovnik et al., 1992). Proton export, the predicted effect of lower membrane polarization, upregulates aerobic glycolysis (Man et al., 2022; Russell et al., 2022) pointing toward membrane potential acting upstream of metabolism. Therefore, modifications of the electric field running across the somite boundary shown in our study might support pH changes leading to activation of β-catenin/Wnt signalling pathway and thereby accelerating the periodicity of somite formation and growth. Thus, alterations in membrane potential of embryonic cells could potentially control the somitogenesis via β-catenin/Wnt signalling pathway.

Apart from biochemical factors, modulations in the softness of cells and the stiffness of the substrate can affect the developmental processes such as cell proliferation, migration, and differentiation (Kim et al., 2017; Kim et al., 2020; Wang et al., 2012). Achieving an optimal ratio of stiffness between the cells and extracellular matrix is crucial for supporting those processes (Marchant et al., 2022). Highly proliferative cells, such as those of embryos or tumors are more deformable or softer than differentiated cells (Chowdhury et al., 2010) and also relatively depolarized (Chen et al., 2022). Further to this end, it has been shown that induced depolarization of cells makes them softer (Callies et al., 2011). In our preliminary experiments, we have also observed an enhanced deformability of somites in chick embryo upon depolarizing them (data not shown). Cells may become softer as a result of depolarization-induced depolymerization of actin filaments in cytoskeleton of cells (Chifflet et al., 2003; Nin et al., 2009).

Depolymerized actin facilitates the translocation of β-catenin into the nucleus, activating the Wnt signalling pathway, which in turn regulates cell proliferation, migration, and differentiation (Sen et al., 2022; Torres & Nelson, 2000). Also, the stiffness of extracellular matrix guides cell migration (durotaxis) and increases the rate of cell proliferation and differentiation (Jacob et al., 1991; Li et al., 2013; Pek et al., 2010; Peyton et al., 2006; Wang et al., 2012; Winer et al., 2009). It might be possible to alter the stiffness of ECM by modifying the extracellular voltage. Such possibility is corroborated by our previous findings showing that the voltage that runs through a hydrogel (a material which resembles the extracellular matrix by its porous structure and surface charge), makes the hydrogel resistant to hydrostatic and osmotic pressure (characteristic of a stiff material) (Kowacz & Pollack, 2020). Therefore, an increase in negative voltage (V_z) near the embryonic cells, as inferred from our experiments (Fig. 3.4), might enhance the stiffness of the ECM and thereby contribute to embryo development. Therefore, increase in cell migration/self-assembly (shift in periodicity of somite formation) and cell proliferation and growth (somite expansion) shown in our study could also be correlated to electric potential-induced changes in mechanics of cells and ECM.

The above considerations suggest that changes in the pace of somite segmentation and growth in response to induced alterations of V_m may be related to: i) the indirect modifications in gene expression, via β-catenin/Wnt signalling pathway triggered by supporting metabolic outcome of glycolysis and/or to ii) changes in tissue mechanics in the direction characteristic for morphing and spreading tissues.

3.3 Conclusions

In this study, we present for the first time the electric potential pattern of somites along the rostro-caudal axis of the chick embryo. We demonstrate that the changes in V_m reflect somites' maturation state as well as the reported onset of expression of morphogenic transcription factors and the onset of differentiation. V_m not only reflects these developmental transitions but also regulates the underlying processes. This is manifested in the fact that modifying V_m, via physiologically relevant environmental stimuli, establishes a new tempo of somitogenesis. To the best of our knowledge, this study is the first to show that V_m can synchronize both periodicity of somite formation

(cell migration and self-assembly) and somite growth (cell proliferation), thereby producing a consistent body pattern during early embryogenesis. Our results, therefore, provide a new perspective for understanding the regulatory mechanisms involved in somitogenesis. Furthermore, characteristics such as cell proliferation, motility, depolarized membrane potentials, CO_2- and K^+-enriched microenvironment, tissue softening, as well as specific signalling pathways and genetic factors, are common to embryogenesis, tumorigenesis and tissue regeneration. Therefore, the unraveled correlations between V_m, microenvironment and early development, may help to understand also those other physiological and pathological processes.

3.4 Materials and methods

Embryo culture and extraction

Fertilized chicken eggs (Ross 308) from a farm were incubated in a humidified incubation chamber at 37.5 °C with 2%, 5% (control) and 7% CO_2 until they reached Hamburger-Hamiltonstages 7 to 11 (4 to 13 pairs of somites) (Hamburger & Hamilton, 1992). When the embryos reached the required stage, they were extracted using filter paper and placed on the prepared albumin agar medium as previously described by Chapman (Chapman et al., 2001). The embryos were oriented with the ventral side facing up to avoid the vitelline membrane interference while approaching the somite with the microelectrode during the membrane potential measurement. The filter paper holding the embryo was immobilized with a metal ring, and the Petri dish was filled with Pennett-Compton (PC) saline, serving as the conducting medium for measuring the membrane potential of embryonic cells. PC saline is a mixture consisting of two aqueous solutions: 4% of Solution A (2.07 M NaCl, 207.91 mM KCl, 70.88 mM $CaCl_2 \cdot H_2O$, and 62.47 mM $MgCl_2 \cdot 6H_2O$), and 6% of Solution B (13.29 mM $Na_2HPO_4 \cdot 2H_2O$ and 1.21 mM $NaH_2PO_4 \cdot 2H_2O$), mixed with deionized water (Schmitz et al., 2016). Experiments to verify the effect of KCl on V_m were conducted on embryos grown at 5% CO_2 by adding (0.3 and 0.6) mM KCl to the PC saline. All chemicals were purchased from Sigma Aldrich (Germany). The prepared samples were then used for V_m measurement.

Preparation of glass microelectrodes

Microelectrodes were prepared using borosilicate glass capillaries (OD = 1.2 mm, ID = 0.68 mm, length = 75 mm) (World Precision Instruments (WPI), USA). The capillaries were pulled using a micropipette puller (Model P-1000, Sutter Instruments, USA) with the following set parameters: heat index: 480, pull: 250, velocity: 420, delay: 70, pressure: 500. The pulled microelectrode was filled with 3 M KCl solution and inserted into a microelectrode holder (PEL, WPI, USA), without introducing air bubbles.

Measurement of membrane potential of somite-forming cells

The Petri dish containing the embryo and PC saline was positioned on a heating unit with an aperture (Bioscience Tools, USA), placed on the stage of an inverted microscope (Nikon ECLIPSE Ti, Japan), allowing visualization of the embryo. An Ag/AgCl electrode (WIP, USA) was immersed in the PC saline, serving as a reference electrode. The entire setup was placed on an optical table (MCI Air, NeuroGig Limited, UK) equipped with a Faraday cage (NG-FC-Custom-104, NeuroGig Limited, UK) to prevent external mechanical vibrations and electrical interference during the voltage measurement. A low-noise dual-channel differential electrometer (FD-223a, WPI, USA) was used to measure the membrane potential of somite-forming cells. During the measurement, the temperature of the medium containing the embryo was set to 37.5 °C, and the condition of PC solution was maintained by continuously replacing it with PC solution equilibrated with the atmosphere of the required levels of CO_2 (2%, 5%, and 7%), using a peristaltic pump. An electrode holder with a KCl-filled glass microelectrode was attached to a voltage measuring probe connected to the electrometer. V_m was measured by carefully inserting the glass microelectrode into the somite with the help of a micromanipulator (Luigs & Neumann GmbH, Germany). Voltage vs. time trace was recorded and analysed using LabScribe software (iWorx, version 4.322). Advanced Research software (NIS Elements, v 5.01) was used to visualize the glass microelectrode and the embryo during V_m recording.

Determination of periodicity of somite formation, and somite growth

To define the periodicity of somite formation (τ), the time between the appearance of two new pairs of somites of embryos cultured under appropriate experimental conditions was measured. The new segment formation was examined in embryos with initial 7 or more somite pairs. The rate of somite growth (L(t)) was determined by measuring the

change in width (L) of the somite, along the anterior-posterior axis of the embryo, over time (t). For that purpose, the somite in SS II was tracked over the period of 2 hours (therefore transitioning into SS III during the measurement) under the given incubation conditions.

Membrane potential of somite-forming cells observed using potential-sensitive dye

The potential-sensitive dye $DiBAC_4(3)$ (bis-(1, 3-dibutylbarbituric acid) trimethine oxonol) (Lot: MKCQ7455, Sigma Aldrich, Germany) was used to observe the membrane potential of somite-forming cells along the anterior-posterior axis of chick embryo. As the intensity of fluorescence increases, the cell becomes more hyperpolarized (Kim et al., 2013; Konrad & Hedrich, 2008). The dye solution was prepared by dissolving $DiBAC_4(3)$ in 70% ethanol to a concentration of 1 mg/ml. This stock solution was diluted (1:10) in deionized water to achieve a concentration of 100 µg/ml. This solution was then further diluted (1:10) in PC saline to reach a final concentration of 10 µg/ml. To observe V_m, eggs were initially incubated under given conditions (37.5 °C, 5% and 7% of CO_2). The embryos were then extracted into a Petri dish (without culture medium) using filter paper and immersed in the PC-dye solution for 30 minutes under the same CO_2 conditions. Following incubation, the embryos were washed with PC saline and imaged using confocal microscopy on an inverted microscope (ZEISS, Germany). Imaging was conducted by placing the embryos inside an incubator chamber set at 37.5 °C with 5% or 7% of CO_2 on the microscope stage. All images were captured at the same acquisition settings and all calculations were performed at raw source images. The image editing, in the form of adjusting intensity threshold, was employed solely for the better visualization of the representative image shown in the Supplementary Information (Fig 3.S1 $_A$), where relatively low sample fluorescence (as expected due to cells hyperpolarization) was obscured by normal background fluorescence. The fluorescence intensity values for somites were estimated from an intensity profile graph based on the intensities collected from the rectangular area encompassing somites along the anterior-posterior axis of the embryo (Fig. 3.1 c) or encompassing a single somite area (Fig 3.S1), using ZEN (V3.6) image analysis software. It should be noted that advanced state-of-the-art systems employing voltage-sensitive dyes could also be used to obtain absolute membrane potential values (Brinks et al., 2015; Gest et al., 2024; Lazzari-Dean et al., 2019; Lazzari-Dean & Miller, 2021; McMillen & Levin, 2024) that in this work were measured using direct microelectrode

method. The dyes have the advantage of additionally providing spatial information and $DiBAC_4(3)$ was used for such purpose in this work.

To observe the zone of extracellular voltage adjacent to the somite's surface, as demonstrated in our previous study using algal cells (Mahadeva et al., 2024), embryos were grown, extracted, and stained as mentioned above. Subsequently, the embryos were washed with PC saline and transferred into a new Petri dish with 2 ml PC saline. The evolution of the zone in the vicinity of the somite surface was visualized by exclusion of microspheres. For this purpose, suspensions of particles of two different sizes (0.5 µm and 0.2 µm) were prepared by diluting 100 µl of uncharged, non-functionalized polystyrene microspheres solutions (analytical standard; cat# 19507-5; Cat# 24050-5; Polyscience, Inc.)] in 5 ml PC saline. The Petri dish containing embryo was kept inside the incubation chamber (set to 37.5 °C and 5% or 7% CO_2) positioned on the microscope stage and filled with microsphere suspension (0.5 µm or 0.2 µm). Confocal images were captured using an inverted microscope (ZEISS, Germany). Additional experiments were performed with 0.5 µm particles to track dynamic exclusion of microspheres by changing the atmosphere in the chamber from initial 5% CO_2 to 7% CO_2 and observing the movement of particles away from the surface. The width of the particle exclusion zone was estimated by plotting the fluorescence intensity of microspheres versus distance from the somite surface using ZEN (V3.6) image analysis software. The exclusion distance was determined by the deflection point of the intensity curve, after which the intensity (indicating microsphere concentration) started to increase from the near-zero value adjacent to the surface.

3.5 Acknowledgement

We thank Prof. Jan Jankowski and AWB Spółka Fermowa sp. z o.o. Wola Szydłowska 44, 06-561 Stupsk, Ferma Drobiu Trzcianka Kolonia 39 and Turza Mała 45a for providing fertilized chicken eggs, Prof. Raquel P. Andrade for training us in chick embryo culture and extraction techniques. We also thank Cell and Tissue Analysis and Imaging Laboratory, especially Dr. Krzysztof Witek for his support with fluorescence microscopy.

Author Contributions

M.K. conceptualized and supervised the project. M.M. conducted the laboratory work. M.M., M.K., and S.N. performed the data analysis and interpretations. S.N. supervised laboratory work. M.M., M.K., and S.N. wrote the original manuscript.

Funding

The National Science Centre of Poland under the grant number 2020/38/E/NZ3/00039 funded this work.

Supplementary Information

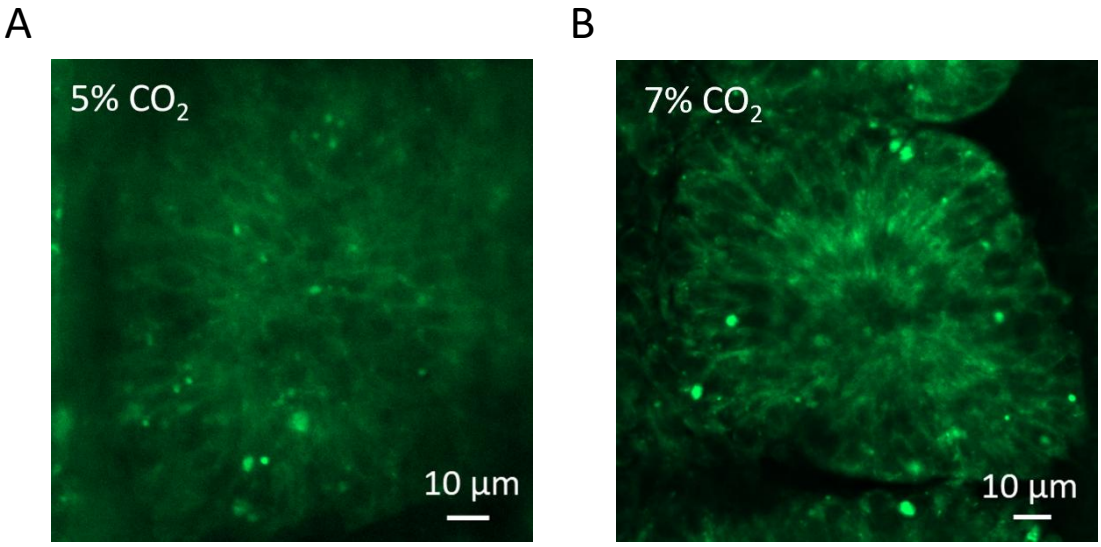

Figure. 3.S1. Membrane potential observed using potential-sensitive dye. Confocal microscopy images show single somites (somite stage II from embryos with 9 pairs of somites) from embryos grown at 5% (A) and 7% (B) CO_2. Increase in fluorescence intensity of cells in somite at 7% CO_2 (Intensity: 113.13 ± 6.32) indicates that those cells are depolarized more compared to the cells of embryo developed at 5% CO_2 (Intensity: 44.90 ± 5.81). (N = 5, each)

Table. 3.S1. Membrane potential values for somite-forming cells at conditions of varying composition and pH of the embryo environment. Table shows the average membrane potential values for posterior, middle, and anterior somites (obtained as described in the results section) at 7% CO_2 (blue) (N = 20), additional HCl (blue) (N = 5), 5% CO_2 (orange) (N = 20), additional (0.3 and 0.6) mM KCl (orange) (N = 5), and 2% CO_2 (green) (N = 20).

Note: No correlation between pH of the embryo environment and membrane potential values. Somite-forming cells in solution with the same pH show different membrane potential values. Therefore, pH of the embryo environment does not affect the membrane potential of somite-forming cells.

Somites	pH 6.3 (7% CO_2)	pH 6.3 (HCl)	pH 7 (5% CO_2)	pH 7 (0.3 mM KCl)	pH 7 (0.6 mM KCl)	pH 7.2 (2% CO_2)
Posterior	-3.74±1.09	-8.20±1.64	-8.37±1.31	-4.60±1.14	-1.60±0.55	-14.63±1.58
Middle	-8.61±1.37	-15.40±1.41	-15.32±1.54	-10.00±1.58	-5.40±1.14	-22.27±2.73
Anterior	-13.41±1.65	-23.00±1.23	-22.76±1.74	-17.40±1.82	-12.00±1.22	-26.70±2.32

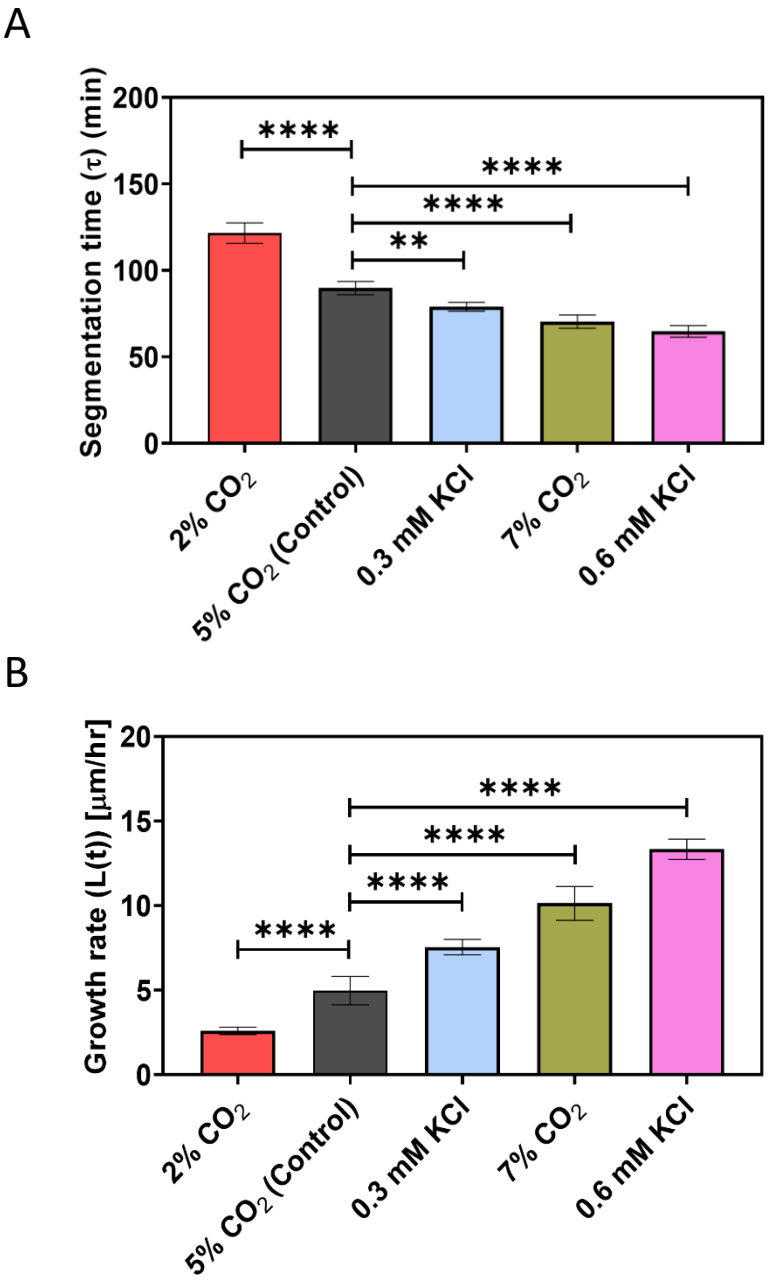

Figure. 3.S2. Effect of stimuli on somite segmentation time and somite growth rate. Graphs show statistically significant differences in somite segmentation time (A) and somite growth rate (B) in response to 2% CO_2 (red), 0.3 mM KCl (blue), 7% CO_2 (green), and 0.6 mM KCl (magenta) compared to 5% CO_2 (control) (black). ** $P \leq 0.01$, **** $P \leq 0.0001$.

Chapter 4

Bioelectric control of tissue mechanics: Effect of membrane potential on somite deformability in chick embryos

Manohara Mahadeva[1], Sebastian Niestępski[1], Magdalena Kowacz[1]*

[1]Department of Reproductive Immunology & Pathology, Institute of Animal Reproduction and Food Research Polish Academy of Sciences, 10-748 Olsztyn, Poland

***Corresponding author**

Status: Submitted (Developmental Biology)

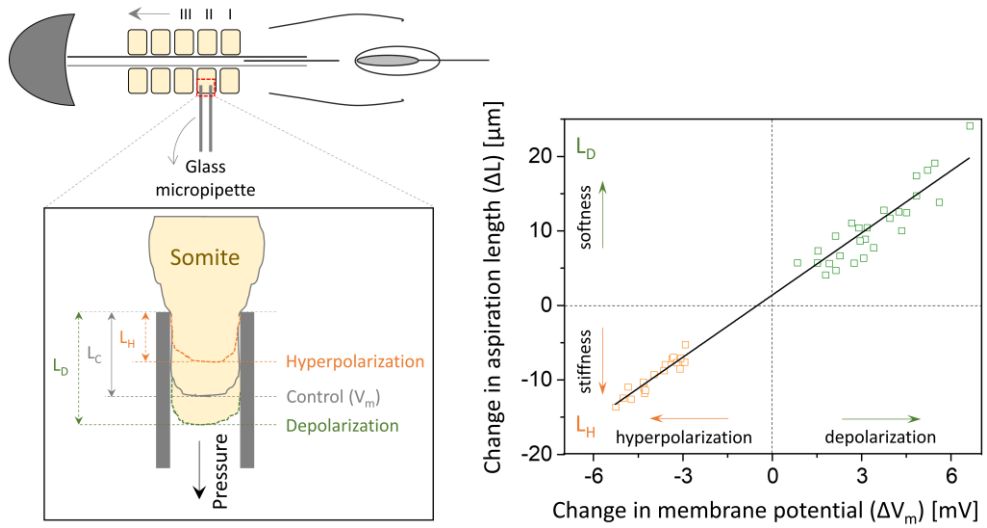

4.1 Introduction

Somitogenesis is a rhythmic process characterized by the segmentation of tissue blocks, known as somites, occurring with a specific periodicity that varies across different tissues and species (Carraco et al., 2022). To maintain proportionality with overall body size, somite segmentation must be precisely coordinated with the corresponding somite growth (Dale & Pourquié, 2000; Pourquié, 2003b). This tightly regulated developmental process involves cell migration, self-assembly, proliferation, and differentiation. The cell migration and pattern formation during embryonic development and tissue regeneration have been shown to be controlled by membrane potential (V_m) (Fukumoto et al., 2005; Levin, 2012; Nishiyama et al., 2008; Ozkucur et al., 2011). Additionally, changes in V_m can also modify the rate of cell proliferation and differentiation (Blackiston et al., 2009; Cone & Tongier, 1971). In our recent study, we demonstrated that modifications in membrane potential of somite-forming cells can synchronously alter the pace of somite formation (cell migration/self-assembly) and the rate of somite growth (cell proliferation) with induced depolarization accelerating the rate of these processes, and hyperpolarization slowing them down (Mahadeva et al., 2025). Yet, the mechanism by which V_m controls cell migration/self-assembly, and proliferation is not fully understood. It is well-established that highly proliferative cells, such as embryonic and tumor cells, tend to be more depolarized compared to quiescent cells (Binggeli & Weinstein, 1986; Yang & Brackenbury, 2013). Apart from being depolarized, proliferative cells exhibit greater softness than differentiated cells (Chowdhury et al., 2010). Cell stiffness is an important factor in embryonic development, as it regulates cell division (Fujii et al., 2021), drives tissue morphogenesis (Huang et al., 2024), and contributes to organ formation (Majkut et al., 2013; Thompson et al., 2019). The cell stiffness is mainly regulated by the cytoskeleton, a dynamic network of protein filaments that provides structural support and mechanical integrity to the cell. The cytoskeleton consists three primary intracellular filaments: actin filaments, microtubules, and intermediate filaments. Among these, actin filaments are more dynamic and play a key role in determining cell stiffness (Jalilian et al., 2015). Studies have demonstrated that alterations in the polymerization state of actin filaments can modulate cell stiffness (Kasas et al., 2005; Oberleithner et al., 2009; Rotsch & Radmacher, 2000; Salker et al., 2016). Interestingly, V_m has been implicated in actin cytoskeleton regulation, with changes in V_m leading to actin filament reorganization, which influences cell stiffness

(Callies et al., 2011; Chifflet et al., 2004; Chifflet et al., 2003). An increase in V_m has also been correlated with elevated tissue density (Mukherjee et al., 2024), which together with the cytoskeleton that acts at the cellular level, modulates tissue stiffness (Koser et al., 2015; Koser et al., 2016; Shyer et al., 2017). The raise in V_m can be driven by an increase in intracellular biomass concentration (Kay, 2017; Mukherjee et al., 2024) on tissue compaction or as a result of the synthesis of cytoplasmic components during development, which would also lead to increase in cell stiffness (Guo et al., 2017). V_m not only reflects the changes in tissue density but also regulates it, with hyperpolarization inhibiting cell proliferation and stabilizing tissue structure, while depolarization promoting proliferation and tissue expansion (Mahadeva et al., 2025; Mukherjee et al., 2024). Furthermore, embryonic cell migration, indicated in our study to be controlled by V_m, was also shown to be regulated by cell stiffness changes (Marchant et al., 2022). Therefore, in this work, we aim to determine whether V_m affects somite deformability during early embryonic development and by this mean controls fundamental events of early body pattern formation, as revealed recently by our findings (Mahadeva et al., 2025). For this purpose, we measured the deformability of somite-forming cells, after modifying their V_m, along the anterior-posterior axis of chick embryo using micropipette aspiration technique. CO_2 and KCl were used as external stimuli to modify V_m of somite-forming cells, thereby altering the timing of somite appearance and somite growth (Mahadeva et al., 2025). Our findings show that induced depolarization causes somite-forming cells to become softer, while hyperpolarization increases their stiffness. Furthermore, our results reveal that the changes in somite deformability are directly related to the induced changes in V_m, suggesting that V_m may play a key role in regulating somitogenesis by altering the mechanical properties of somite-forming cells.

4.2 Results and discussion

Membrane potential of somite-forming cells in chick embryo changes in response to external stimulations

To investigate whether V_m influences somite mechanics in embryonic cells, we modified the V_m of somite-forming cells using external stimuli: CO_2 and KCl, and measured the somite deformability. In this section, we show the measured V_m for all somite stages (SS) in response to external stimuli (methods, Fig. 4.1). We found V_m negativity to

progressively increase with somites' maturation. Apart from this general hyperpolarization trend we observed step-like changes in V_m between specific somite stages (Fig. 4.1). In our recent study (Mahadeva et al., 2025), we suggested that these step-like changes may reflect previously reported differences during somite development, as indicated in the expression of morphogenic transcription factors (starting from SSIV) and structural alterations (in early embryogenesis beginning from SSIX) (Maschner et al., 2016). In our current work, we grouped somites, based on V_m-bound classification along the embryo's body axis, into: posterior (SSI – SSIII), middle (SSIV – SSVIII), and anterior (SSIX – SS XIII) groups. The following are the ranges of V_m values for each somite group obtained under control conditions (5% CO_2): (-8.12 ± 0.34 to -10.11 ± 0.49) mV for posterior, (-15.11 ± 0.81 to -18.62 ± 0.57) mV for middle, and (-22.88 ± 0.42 to -25.92 ± 0.05) mV for anterior somites. Somites were depolarized, with respect to the control conditions, by increasing the concentration of CO_2 or KCl in their microenvironment. The obtained ranges of V_m values (ordered from the most to least depolarizing conditions) were as follows: at additional 0.6 mM KCl, (-1.51 ± 0.41 to -4.92 ± 0.34) mV for SSI-SSIII, (-10.30 ± 0.36 to -14.90 ± 0.78) mV for SSIV-SSVIII, and (-17.30 ± 0.56 to -22.03 ± 0.07) mV for SSIX-SSXIII; at 7% CO_2, (-3.64 ± 0.31 to -6.95 ± 0.67) mV, (-12.23 ± 0.52 to -16.52 ± 0.77) mV, and (-20.24 ± 0.66 to -23.98 ± 1.21) mV; and at additional 0.3 mM KCL, (-5.08 ± 0.36 to -7.86 ± 0.26) mV, (-13.62 ± 0.38 to -17.80 ± 0.53), and (-21.37 ± 0.82 to -24.69 ± 0.25) mV, for posterior, middle and anterior somite groups, respectively. On the contrary, somites were hyperpolarized, with respect to control potential values, by reducing the concentration of CO_2 or KCl in the environment of the developing embryo, and the V_m ranges were: (-13.15 ± 0.27 to -14.87 ± 0.48) mV, (-19.97 ± 0.32 to -22.97 ± 0.38), and (-26.87 ± 0.54 to -29.69 ± 0.17) mV at 2% CO_2; (-11.74 ± 0.24 to -13.49 ± 0.41) mV, (-18.45 ± 0.56 to -21.71 ± 0.55) mV, and (-25.82 ± 0.64 to -28.82 ± 0.14) mV at reduced 0.3 mM KCl for each somite group, respectively (Fig. 4.1). Despite these alterations in V_m, the step-like changes between specific somite groups were preserved across all experimental conditions (Fig. 4.1). Also, the V_m shift between SSIII and SSIV was greater than that between SSVIII and SSIX under control as well as modified conditions (Table 4.S1). This suggests that membrane potential is more sensitive to the onset of expression of transcription factors between SSIII and SSIV than to the onset of morphological changes between SSVIII and SSIX, as previously proposed (Mahadeva et al., 2025). The dynamics of change in V_m within the somite groups (as expressed in the slope values of V_m versus somite stage

trends), was always higher in the posterior somites, which are depolarized compared to middle and anterior somites. (Table 4.S2). Furthermore, within each somite group, the slopes of V_m versus somite stage were steeper when somite-forming cells were depolarized compared to when they were hyperpolarized (Fig. 4.1). This suggests that changes in developmental processes, as reflected in membrane potential alterations, can proceed at faster rate upon depolarization. Such conclusion is corroborated by our previous data showing depolarization-induced acceleration of the rate of somite formation (cell migration/self-assembly) and growth (proliferation) with hyperpolarization having the opposite effect and slowing down the tempo (Mahadeva et al., 2025). V_m depends on the concentration of intracellular negatively charged components, including proteins synthesised during development (Kay, 2017; Veech et al., 1995). Therefore, the higher dynamics of V_m changes, related to faster rate of somitogenesis, might reflect upregulation of glycolytic metabolism that supports biomass production necessary for cell proliferation (Vander Heiden et al., 2009). Moreover, both, V_m and stiffness are sensitive to the concentration of cytoplasmic proteins (Guo et al., 2017; Kay, 2017). This common underlying factor further supports our aim to explore the correlation between V_m and mechanical properties of cells during embryonic development. Therefore, in the following section, we show the response of somite-forming cell's deformability to induced modifications in their membrane potential.

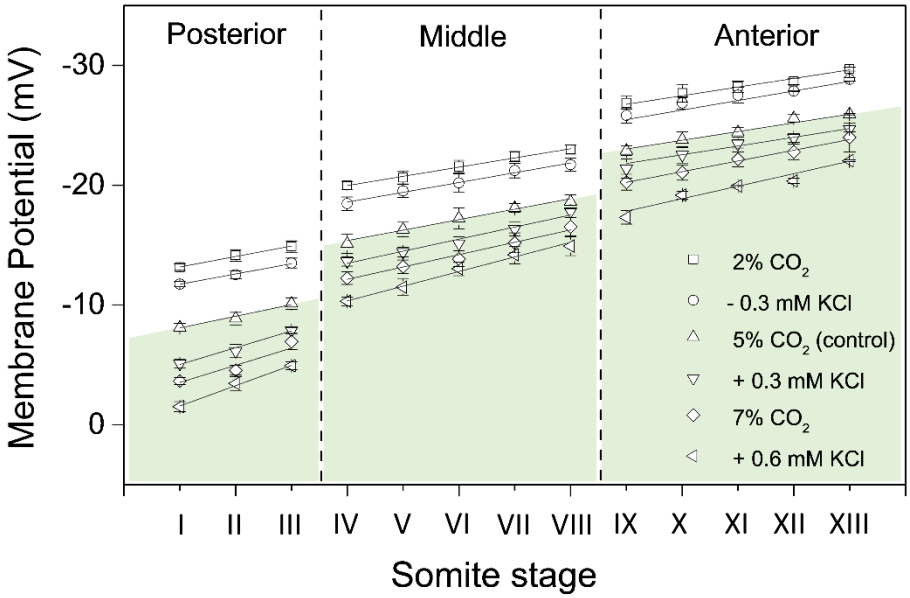

Fig. 4.1. Effect of CO_2 and KCl on membrane potential (V_m) of somite-forming cells along the body axis of chick embryo. Graph shows V_m for posterior, middle, and anterior somites in response to change in concentrations of CO_2 and KCl in the microenvironment embryos having 8 to 13 pairs of somites, where somite stages (SS) are indicated by Roman numbers. All the lines are linear fit for each somite group. Depolarization (green shade) of somites was observed at additional 0.3 mM KCl (open inverted triangle) (N=5), additional 0.6 mM KCl (open triangle pointing left side) (N=6), and 7% CO_2 (open diamond) (N=9) and hyperpolarization (no shade) of somites was observed at 2% CO_2 (open square) (N=6) and reduced 0.3 mM KCl (open circle) (N=5) concentration from control solution (PC having 8.3 mM KCl), respectively, compared to control condition (open triangle) (5% CO_2) (N=7).

Alterations in deformability of somite-forming cells along the anterior-posterior axis of chick embryo in response to induced modifications of V_m

We measured the deformability of somite-forming cells along the caudal-to-rostral axis in early-stage embryos at two different pressures (see in the method section). In this study, the somite deformability was expressed as aspiration length (L) with longer L indicating softer (easier to deform) and shorter L stiffer (more resistant to deformation) somites. The ranges of aspiration lengths at control conditions were (81.29 ± 4.20) µm to (51.34 ± 1.88) µm, with the first value corresponding to SSI and the second to SSIX within a given embryo at 10 mbar and (96.20 ± 2.25) µm to (65.83 ± 1.58) µm at 15 mbar. The deformability of somite-forming cells decreased exponentially with somite

stage along the body axis of embryo (Fig. 4.2), by (38.09 ± 4.22) % at 10 mbar and (32.16 ± 3.24) % at 15 mbar from SSI to SSIX.

When embryos were depolarized by increasing the concentrations of CO_2 or KCl in their environment, with respect to control conditions, the deformability of all somites increased, as indicated by higher aspiration lengths (Fig. 4.2). The percentage increase in the aspiration lengths for posterior most (SSI) and anterior most (SSIX) somites, listed in the order from the most to least depolarizing conditions, were as follows: by (26.71 ± 4.92) % to (105.38 ± 3.13) µm and by (26.12 ± 2.19) % to (65.18 ± 0.03) µm at 10 mbar and by (22.93 ± 1.74) % to (118.20 ± 3.56) µm and (13.63 ± 2.89) % to (74.00 ± 2.46) µm at 15 mbar for additional 0.6 mM KCl; by (13.78 ± 4.03) % to (93.72 ± 0.99) µm and by (22.75 ± 3.38) % to (62.38 ± 0.74) µm at 10 mbar and by (17.17 ± 2.78) % to (113.35 ± 0.80) µm and by (10.47 ± 0.56) % to (72.68 ± 1.83) µm at 15 mbar for 7% CO_2; and by (6.31 ± 0.37) % to (87.61 ± 0.91) µm and by (14.23 ± 1.59) % to (58.65 ± 4.56) µm at 10 mbar and by (8.89 ± 3.03) % to (105.19 ± 1.15) µm and by (4.48 ± 1.55) % to (68.72 ± 5.19) µm at 15 mbar for 0.3 mM KCl (Fig. 4.2 a, b).

Conversely, deformability decreased in response to hyperpolarization induced by reducing the concentration of CO_2 or KCl in the environment of the embryos, with respect to control conditions (Fig. 4.2). The percentage decrease in the aspiration lengths for SSI and SSIX, were as follows: by (16.51 ± 1.72) % to (68.82 ± 1.09) µm and (17.92 ± 1.54) % to (42.05 ± 1.83) µm at 10 mbar and by (13.98 ± 2.81) % to (83.49 ± 2.07) µm and (17.89 ± 4.74) % to (53.97 ± 2.78) µm at 15 mbar for 2% CO_2; and by (10.04 ± 3.15) % to (73.34 ± 1.32) µm and (12.32 ± 2.72) % to (46.07 ± 0.36) µm at 10 mbar and by (7.66 ± 3.27) % to (88.51 ± 1.14) µm and (10.96 ± 3.39) % to (57.95 ± 1.37) µm at 15 mbar for reduced 0.3 mM KCl (Fig. 4.2 a, b). Under all experimental conditions, at both pressures, somite deformability followed an exponential dependence on somite stage (Fig. 4.2 a, b). The increasing resistance to deformation was accompanied by progressive hyperpolarization of somites as they reach developmentally more advanced stages (Fig. 4.1). This parallel rise in negativity of membrane potential and cell stiffness can result from increasing intracellular biomass concentration that affects both, mechanical and electrical properties (Barriga et al., 2018; Guo et al., 2017; Kay, 2017; Mukherjee et al., 2024; Schaeffer et al., 2022).

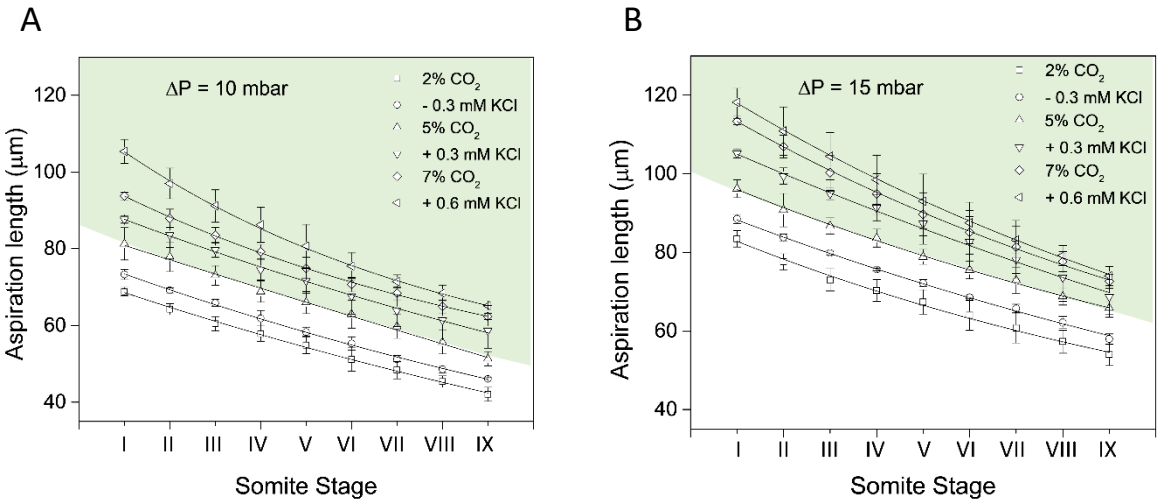

Fig. 4.2. Deformability of somite-forming cells observed in chick embryo. Graphs show measured aspiration lengths for SSI-SSIX along the rostral-caudal axis of chick embryo at 10 mbar (A) and at 15 mbar (B) aspiration pressures under depolarized [green shade, additional (0.3 and 0.6) mM KCl and 7% CO_2] and hyperpolarized (no shade, 2% CO_2 and reduced 0.3 mM KCl) conditions compared to control (5% CO_2) (N=5 each). The lines are exponential fit for aspiration length versus somites stage at each experimental condition.

To understand the correlation between induced changes in somite deformability in response to modified V_m, we further analysed L as a function of V_m after somite-forming cells were subjected to depolarization and hyperpolarization (Fig. 4.3). Each somite group exhibited a distinct pattern of exponential dependence of somite deformability on modified V_m values. Posterior somites showed a steeper, middle somites exhibited a shallower, and anterior somites displayed a gradual decay in exponential increase of deformability with depolarization (Fig. 4.3, Table 4.S3). These trends remained consistent at both 10 mbar and 15 mbar aspiration pressures (Fig. 4.3 a, b). Differences in somites response depending on their developmental stage, may reflect contribution of the factor other than V_m that will define mechanical properties of a tissue and will change with its maturation. The possible candidate is extracellular matrix (ECM), which is recognized to contribute significantly in enhancing somite stiffness (Schaeffer et al., 2022), and which thickness increases from posterior to anterior direction along embryo body axis (Rifes & Thorsteinsdóttir, 2012). Any softening impact of depolarization will then be contradicted by stiffness-promoting ECM, which deposition increases with

advancing somite stage. Thus, anterior-posterior ECM thickness gradient in the embryo may contribute to a reduced sensitivity of somite deformability to V_m depolarization as somites mature, reflected in progressively shallower or decaying exponential L vs V_m trend (Fig. 4.3). Interestingly, the ECM gradient, suggested here to oppose the cell-softening effects of depolarization, was also indicated to play an inhibitory role on somitogenic oscillations in chick embryos (Hubaud et al., 2017), that were shown by us to be accelerated by V_m depolarization (Mahadeva et al., 2025). Despite of the differences in the correlation between overall somite deformability and V_m values, the change in somite aspiration length (ΔL) for a given somite stage was linearly dependent on the change in membrane potential (ΔV_m) (invoked by altered environmental conditions), regardless of the somite position along the body axis (Fig. 4.4 a, b). This shows that somite deformability is directly influenced by the induced modifications in V_m. The triggered response is not affected by the ECM gradient (correlating with somite position along the axis), indicating that V_m modifies somite stiffness by acting at a cellular level. The induced biomechanical changes depend linearly on V_m shift, irrespective of the stimuli used to promote the latter. The slopes of the linear trends of ΔL vs ΔV_m were statistically similar at both aspiration pressures (2.77 ± 0.06 at 10 mbar and 2.82 ± 0.08 at 15 mbar, $p = 0.587 > 0.05$) (Fig. 4.4 a, b), indicating that the observed changes in somite deformability in response to V_m modifications are independent of the applied pressure. In summary, our results demonstrate that induced depolarization always softens somites, whereas induced hyperpolarization stiffens them. Apart from the induced V_m alterations, progressive V_m hyperpolarization with somite maturation should be a direct consequence of biomass synthesis during the developmental process (Kay, 2017; Mukherjee et al., 2024). Both, synthesis of structural components within a single cell (that at physiological pH are mostly negatively charged) and simple tissue compaction due to cell number increase within the somite, result in higher cytoplasmic density. The latter, with its negative charges, is a source of Donnan potential that contributes to the establishment of a resting membrane potential of a cell (Veech et al., 2002; Veech et al., 1995). The same process of increasing biomass density will lead to physiological somite stiffening with maturation (Guo et al., 2017). On the contrary, changes in somite stiffness induced by V_m modifications, are not governed by biomass synthesis, as depolarization leading to faster cell proliferation (Mahadeva et al., 2025) promotes somite softening, and hyperpolarization, hampering cell proliferation, results in somite stiffening (Fig 4.2, 4.3 and 4.4). Therefore, we suggest that it might be

modification of cytoskeleton structure that underlines this acute response of cell mechanical properties to V_m changes, which is consistent with the mechanism previously proposed (Callies et al., 2011). However, due to depolarization-supported cell proliferation, depolarized and therefore softer somites, stiffen and become hyperpolarized at a faster rate than those made stiffer and less proliferative by hyperpolarization. This is expressed in the dynamics of respective changes with increasing somite stage at conditions of altered V_m (Fig. 4.1 and 4.2; Table 4.S2) Therefore, somite hyperpolarization and stiffening are physiological consequences of their maturation, yet the rates of progression of those electrical and biomechanical changes during development can be adjusted by setting new V_m values.

We calculated somite stiffness by quantifying Young's modulus (E) for all somite stages. (Table S4). The range of Young's modulus (E) for somites along the body axis (SSI-SSIX) at control condition is (380.29 ± 17.11) Pa to (604 ± 29.45) Pa, showing a gradual increase from the posterior (SSI) to the anterior (SSIX) somites. The stiffness values (E) were higher at 15 mbar than at 10 mbar (Table 4.S4). This kind of mechanical response to the applied stretching force is consistent with previous findings showing that when cell aggregates are aspirated using a micropipette, their surface tension increases with increase in aspiration pressure (Guevorkian et al., 2010). This behavior was not observed in the classical parallel-plate compression method, where the aggregate is allowed to relax to equilibrium (Forgacs et al., 1998). In contrast, micropipette aspiration exerts a continuous traction force generated by applied suction pressure. This mechanical force can enhance tissue contractility and induce cytoskeletal remodeling, which in turn modifies the tissue mechanical characteristics (Gonzalez-Rodriguez et al., 2012; Hochmuth, 2000). In our study, increased aspiration pressure from 10 mbar to 15 mbar amplifies the traction force, possibly promoting actin cytoskeletal remodeling and contributing to increased tissue stiffness. A study on chick embryo at similar developmental stages to those used in our work reported that the segmented somites are stiffer than presomitic mesoderm and that SSV is slightly stiffer than SSIII (Marrese et al., 2020). This finding supports our observations of increasing somite stiffness with its maturation. Another study estimated the Young's modulus of different regions in the chick embryo as follows: (2.4 ± 0.1) kPa at midline structure (notochord, neural tube, and somites); (2.1 ± 0.1) kPa at area pellucida, and (11.9 ± 0.8) kPa at area opaca (Agero et al., 2010). Mechanical properties of discrete structures – the somites, as assessed in

our study, and averaged stiffness of the large regions encompassing different embryonic structures, as measured by Agero, et al., cannot be directly compared. However, our calculated somite stiffness values (E) at control conditions (Table 4.S4) lie between the typical stiffness of mesenchymal cells, reported to fall in the order of 500 Pa (Tan et al., 2008) and that of epithelial cells, measured to yield approximately 700 Pa (Guevorkian et al., 2010). Epithelial and mesenchymal are the type of cells that somites are composed of. Apart from assessing the overall deformability, we observed that while middle and anterior somites (from SSIV to SSIX) fully retracted from the micropipette after the suction pressure was released, the youngest posterior somites (SSI to SSIII) did not. This kind of behavior has been reported as tissue mechanical plasticity (Molnar & Labouesse, 2021). The plasticity of tissue refers to its ability to undergo permanent structural deformations, which may support tissues in adapting their shape necessary for morphogenic changes during development. Notably, under depolarized conditions, plasticity of somites was shown up to SSIV, whereas under hyperpolarized conditions, it was restricted to SSI and SSII. Additionally, we observed that the older somites (SSX and SSXI) also did not completely retract from the pipette upon pressure release (deformability of these somites was measured with limited success, data not shown), displaying a shift toward plastic-like behavior. This behavior of developmentally advanced somites may be attributed to a loss of tissue integrity that occurs during the structural changes. Supporting this, it has been shown that the stiffness of advanced somites (SSX-XIII) is lower compared to that of SSVII-SSIX (Schaeffer et al., 2022), potentially indicating their structural alterations. In the next part of this section, we explore the dynamics of somite deformability across different stages and conditions.

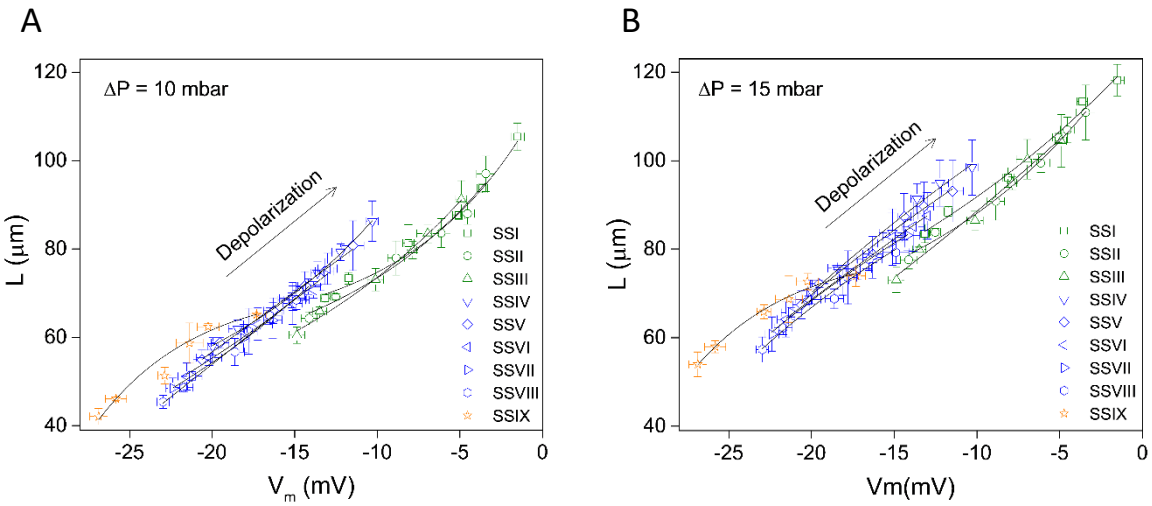

Fig. 4.3. Dependence of somite deformability on its membrane potential. Graphs show dependence of aspiration lengths (L) of somites (SSI-SSIX) on modified membrane potentials (V_m) (by CO_2 and KCl) at 10 mbar (A) and 15 mbar (B) applied suction pressures (N=5 each). The lines are exponential fit of L versus V_m for posterior (olive green), middle (blue), and anterior (orange) somite groups. Deformability increased exponentially with depolarization, showing a steeper rise in posterior somites, a shallower increase in middle somites, and a gradual decay in anterior somites.

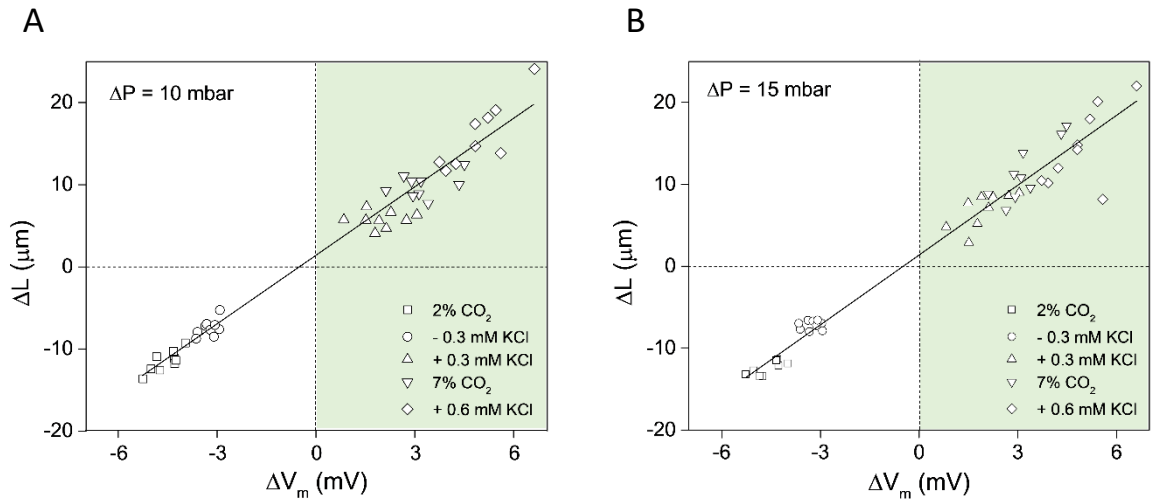

Fig. 4.4. Dependence of changes in somite deformability on the changes in membrane potential. Linear dependence of change in aspiration lengths on the change in membrane potential [induced depolarization (green shade) by additional (0.3 and 0.6) mM KCl and 7% CO_2, and induced hyperpolarization (no shade) by 2% CO_2 and reduced 0.3 mM KCl compared to control condition (5% CO_2)] was observed at both 10 mbar (A) and 15 mbar (B) applied pressures. The lines are linear fit for ΔL Vs. ΔV_m at 10 mbar [$\Delta L = 2.77 \cdot \Delta V_m - 1.14$, $R^2 = 0.97$] and at 15 mbar [$\Delta L = 2.83 \cdot \Delta V_m - 1.33$, $R^2 = 0.96$].

Deformability dynamics of somite-forming cells in response to induced depolarization and hyperpolarization

When somites were subjected to micropipette aspiration at 10 mbar, they initially exhibited a rapid increase in aspiration length, followed by a gradual rise over time until reaching an equilibrium state. When the pressure was increased to 15 mbar, somites showed further gradual increase in aspiration length, eventually stabilizing at a higher value (Fig. 4.5a). This deformation profile is a characteristic of viscoelastic solid material and is aligns with previously observed deformation behaviour in mesenchymal (Tan et al., 2008) and endothelial cells (Hochmuth, 2000). In our study, posterior somites, being more depolarized and softer than their anterior counterparts, reached equilibrium states at a faster rate and exhibited greater aspiration lengths at both the pressures under control conditions (5% CO_2) (Fig. 4.5a), indicating their lower resistance to deformation and lesser viscoelasticity compared to middle and anterior somites. This suggests that somites become progressively more viscoelastic as they mature (somite's transition from a depolarized to a hyperpolarized state) along the body axis of the embryo. Furthermore, induced depolarization decreased viscoelastic response of a given somite (of any given stage), while hyperpolarization enhanced it (Fig. 4.5b). Similar responses were observed for all somite stages under their modified V_m values (Fig. 4.S1). These observations are in line with previous findings showing that tumor cells (which are depolarized relative to normal cells (Binggeli & Weinstein, 1986)), exhibit reduced viscoelasticity compared to healthy cells (Xie et al., 2019). Depolarized V_m is often associated with enhanced cell motility and invasiveness (Yang & Brackenbury, 2013), and invasive cancer cells have been reported to exhibit lower viscoelasticity than non-invasive ones, mediated by altered actin filament organization within the cytoskeleton (Tabatabaei et al., 2021). Likewise, in our study, depolarization-induced reduction in somite viscoelasticity, might be related to structural changes in the cytoskeleton network. Such changes could support cell motility, what is in fact in agreement with our observations showing accelerated rate of somite formation, the process governed by cell migration and self-assembly, in response to depolarization (Mahadeva et al., 2025). Therefore, our results suggest that V_m-dependent biomechanical alterations of somites are closely linked to structural changes in cellular components.

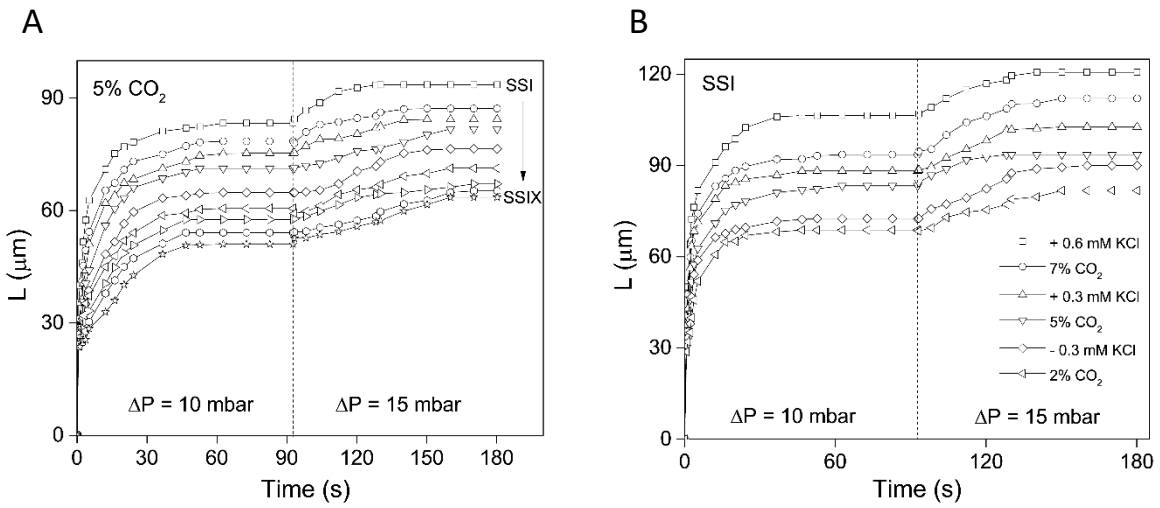

Fig. 4.5. Dynamics of somite deformability. Aspiration length-time curves show the viscoelastic behavior of somite stages SSI-SSIX along the body axis of a chick embryo (A), and of SSI from a given embryo under depolarized [additional (0.3 and 0.6) mM KCl and 7% CO_2] and hyperpolarized (2% CO_2 and reduced 0.3 mM KCl) conditions compared to control (5% CO_2) (B), the aspiration lengths were measured at an initial pressure of 10 mbar for up to 90 seconds, followed by an increased pressure of 15 mbar for an additional 90 seconds. Depolarized somites exhibited slightly lower viscoelasticity (less viscus creep) and higher deformability compared to hyperpolarized somites.

Possible mechanism through which V_m alters the stiffness of somites in chick embryo – a hypothesis

In support of our findings, induced depolarization has been shown to reduce stiffness in various cell types, such as vascular endothelial cells (Callies et al., 2011) and epithelial outer hair cells (He & Dallos, 1999, 2000), whereas hyperpolarization was recognized to increase cell stiffness (He & Dallos, 1999, 2000). The mechanical alterations enable cells to adapt to external cues during functional responses. In embryonic development, epithelial cells have been reported to dynamically regulate stiffness by remodeling their cytoskeleton and junctions in response to external stimuli (Molnar & Labouesse, 2021). The cytoskeleton-dependent alterations in stiffness were also observed in tumor cells (Chen et al., 2023). It has been shown that the cells can alter their stiffness also through volume changes (Guo et al., 2017). However, in our study, we did not observe any noticeable alterations in overall somite volume in response to induced modifications of

V_m but clear changes in somite stiffness were observed (Fig. 4.2). Therefore, we hypothesize in this study that changes in V_m may affect the cell stiffness through the alterations of cytoskeleton structure. In support of this, a previous study has experimentally shown that the disrupted cytoskeleton in cells eliminates the effect of V_m on stiffness, emphasizing the cytoskeleton's central role in mediating V_m-dependent stiffness changes. Additionally, the same study found no correlation between changes in cell volume and stiffness, suggesting that V_m-induced stiffness alterations are primarily cytoskeleton-driven (Callies et al., 2011). The V_m-dependent mechanical changes in cells were also shown to be associated with cell elongation and contraction (He & Dallos, 2000), likely driven by structural alterations in the cytoskeletal network. This raises the question: by what mechanism does V_m affect cytoskeleton network in order to modulate cell stiffness? It was speculated that electric field generated by membrane potential across the cell membrane can directly influence polymerization state of actin cortex, by interacting with polar filaments of the cytoskeleton (Callies et al., 2011; Cantiello et al., 1991). During the development, actin polymerization enhances cell stiffness, while actin depolymerization leads to cell softening (Bai et al., 2023). Apart from being possibly sensitive to the electric field (Callies et al., 2011; Cantiello et al., 1991), actin polymerization is also pH-dependent, with alkaline pH preventing and acidic pH promoting polymerization (Wang et al., 1989; Yonezawa et al., 1985). Further in this context, it has been shown that depolarization and increase in intracellular pH (pH_i) of cells can lead to the disintegration of cytoskeletal structures, while hyperpolarization and decrease in pH_i promotes a more stabilized and organized cytoskeletal architecture during development (Weiß & Bohrmann, 2019a, 2019b). V_m and pH_i are correlated due to the fact that V_m is one of the key components defining proton motive force that drives proton flux between the cytosol and the extracellular space (Casey et al., 2010). It has been shown specifically, that induced depolarization may cause an increase in pH_i by supporting proton efflux through proton channels (Cheng et al., 2008). Therefore, it is possible, that also in our experiments the depolarization of somite-forming cells may lead to increase in their pH_i. The proton removal from the cell should be facilitated by the reduced intracellular electric force, otherwise holding cytosolic protons, and possible attractive force of negative extracellular voltage (V_z) that can develop near the depolarized cells and drive protons into the extracellular space (Mahadeva et al., 2024, 2025). Outward proton transport is a natural consequence of aerobic glycolysis, a metabolic pathway active in early

embryos, which leads to an increase in pH_i (Oginuma et al., 2020). By inducing depolarization in embryonic cells, we may support this natural proton extrusion, thereby upregulating the rate of glycolysis in cells. In fact, it has been shown that proton export can upregulate glycolysis (Man et al., 2022; Russell et al., 2022). Therefore, depolarization-induced acceleration in somite formation and growth rate during early embryogenesis, as shown in our recent study (Mahadeva et al., 2025), may be facilitated by pH-dependent enhanced glycolysis. Furthermore, the stimuli (CO_2 and KCl) used in our study to depolarize V_m have been shown to increase pH_i, leading to enhanced glycolysis rate in cells (Theparambil et al., 2016). Although an increase in extracellular CO_2 concentration was expected to cause intracellular acidification due to CO_2 diffusion into the cells, it instead resulted in intracellular alkalinization. This has been attributed to electrogenic bicarbonate uptake, which may dominate over CO_2 diffusion in driving intracellular alkalinization (Theparambil et al., 2016). However, in our study, we would expect pH_i to increase in response to elevated extracellular CO_2 and KCl concentration, because both CO_2 and KCl induce depolarization in cells (Mahadeva et al., 2024, 2025), which should facilitate proton expulsion. Therefore, induced depolarization may promote cell softening by increasing pH_i that causes pH-dependent actin depolymerization (Wang et al., 1989; Weiß & Bohrmann, 2019a, 2019b; Yonezawa et al., 1985). Conversely, induced hyperpolarization may reduce pH_i and aid actin polymerization, thereby increasing cell stiffness. Notably, the stiffness-modifying polymerization state of the cytoskeleton can affect also signaling pathways, such as Wnt and Notch, that are known to regulate somitogenesis (involving cell migration, self-assembly and proliferation) (Gibb et al., 2009; Wang et al., 2013; Wang et al., 2015), and can be both activated by pH_i alkalinization (Oginuma et al., 2020; Romero-Moreno et al., 2024). In particular, depolymerization of actin cytoskeleton, which can be influenced by depolarization-induced intracellular pH alterations, facilitates nuclear transport of β-catenin (a key transducer molecule in the Wnt signalling pathway) (Torres & Nelson, 2000) and promotes YAP (yes-associated protein) exit from the nucleus (Sen et al., 2022). Via these intracellular translocations, β-catenin initiates transcription of the Wnt-target genes, while YAP activates the Notch pathway (Passier et al., 2024). The YAP and Notch, specifically, act together to orchestrate segmentation clock, with lower YAP nuclear presence serving as a threshold signal to activate the Notch that further triggers oscillations (Hubaud et al., 2017). The periodicity of those oscillations was shown in our previous work to be controlled by V_m and specifically accelerated by

depolarization (Mahadeva et al., 2025). Therefore, alterations in the cytoskeletal network structure, driven by intracellular pH variations and resulting in changes in cell stiffness, may serve as a key mechanism through which membrane potential modulates developmental processes during early embryogenesis.

4.3 Conclusions

This study demonstrates a progressive increase in somite stiffness along the anterior-posterior axis of chick embryos, which correlates with increasing negativity of V_m. V_m not only reflects changes in somite stiffness but also regulates it. By adjusting the chemical compositions of embryonic cell's microenvironment, we were able to modulate somite stiffness through V_m manipulations: induced depolarization led to softening of somites, whereas hyperpolarization resulted in increased stiffness. Although V_m is not the sole factor determining the overall stiffness of the somite, the observed linear correlation between changes in somite deformability and V_m alterations shows a direct influence of V_m on somite mechanics. Moreover, V_m depolarization accelerates the pace of somite formation (cell migration/self-assembly) and rate of somite growth (cell proliferation), while hyperpolarization slows them down in a synchronized manner, contributing to the establishment of regular body patterning, as shown in our recent findings. Our current results suggest that depolarization-induced cell softening may promote an increased rate of somitogenesis, whereas hyperpolarization-associated increase in stiffness may result in a deceleration of this developmental process. In conclusion, our findings reveal that the membrane potential modifications can regulate key developmental processes such as cell proliferation, migration, and self-assembly by altering the mechanical properties of embryonic cells during early embryogenesis. Since these processes are also fundamental to tumorigenesis and tissue regeneration, our findings may provide valuable insights into the mechanism underlying both normal development and disease.

4.4 Materials and methods

Embryo culture and sample preparation

Fertilized chicken eggs (Ross 308) were incubated at 37.5 °C in a humidified atmosphere with 2%, 5% (control) and 7% CO_2 until they reach required developmental stage, corresponding to Hamburger-Hamilton stages 9 to 11 (8 to 13 pairs of somites) (Hamburger & Hamilton, 1992). Somites were counted and staged according to the method described by Venters (Venters et al., 2008), in which somite stages (SS) are designated using Roman numbers. The newly segmented somite pair is labeled as SSI, followed by SSII for the next oldest pair, continuing sequentially in the order of somite formation along the anterior-posterior axis of the embryo. The embryos were extracted using a filter paper as previously shown by Chapman (Chapman et al., 2001). The extracted embryos were then submerged into Pennett-Compton (PC) saline, which served as a conducting medium for measuring the V_m of somite-forming cells, by orienting ventral side facing up and the papers holding the embryos were immobilized by placing a metal ring on it. For aspiration experiments, to ensure we are aspiring only the somites, the endoderm layer was removed using glass micropipette. Any remaining endoderm fragments in the PC saline were eliminated by replacing the solution with fresh PC. The PC saline was prepared by mixing two aqueous solutions: 4% of Solution A (2.07 M NaCl, 207.91 mM KCl, 70.88 mM $CaCl_2 \cdot H_2O$, and 62.47 mM $MgCl_2 \cdot 6H_2O$), and 6% of Solution B (13.29 mM $Na_2HPO_4 \cdot 2H_2O$ and 1.21 mM $NaH_2PO_4 \cdot 2H_2O$), added in deionized water (Schmitz et al., 2016). All chemicals used in this study were purchased from Sigma Aldrich (Germany). All experimental conditions used in this work are listed in the table below (Table 4.1).

Table. 4.1. Shows the list of experimental conditions used to modify the membrane potential of somite-forming cells in chick embryos.

Experimental conditions	Chemical compositions
Control	PC + 5% CO_2
Additional CO_2 (depolarization)	PC + 7% CO_2
Reduced CO_2 from control (hyperpolarization)	PC + 2% CO_2
Additional KCl (depolarization)	PC (with 8.3 mM KCl) + 0.3 mM KCl + 5% CO_2, PC (with 8.3 mM KCl) + 0.6 mM KCL + CO_2
Reduced KCl (hyperpolarization)	PC (with 8.0 mM KCl) + 5% CO_2

Preparation of glass microelectrode and micropipette

Microelectrodes and micropipettes were prepared using borosilicate glass capillaries (OD = 1.2 mm, ID = 0.68 mm, length = 75 mm) (World Precision Instruments (WPI), USA). The following parameter were set for pulling the capillaries using a micropipette puller (Model P-1000, Sutter Instruments, USA): heat index: 480, pull: 250, velocity: 420, delay: 70, pressure: 500. The pulled microelectrode was filled with 3 M KCl solution, carefully inserted into a microelectrode holder (PEL, WPI, USA) without introducing air bubbles, and used for V_m measurements. The capillaries pulled using the same set of pulling parameters were further processed using a micro forge instrument (MF-900, NARISHIGE, Japan) to fabricate micropipettes with an inner diameter of approximately 60 µm. The prepared micropipettes were silanized using bis(dimethylamino)dimethylsilane as described previously by Raif Musa-Aziz (Musa-Aziz et al., 2010), to render the inner surface hydrophobic and prevent somite-forming cells from sticking during aspiration.

Measurement of membrane potential of somite-forming cells

Petri dish containing the prepared embryo sample was placed on a heating unit, set to 37.5 °C, with an aperture (enables embryo visualization) (Bioscience Tools, USA) and positioned on a motorized stage of an inverted microscope (Nikon ECLIPSE Ti, Japan). To minimize external mechanical vibrations and electrical interference during voltage measurements, the entire setup was mounted on an optical table (MCI Air, NeuroGig

Limited, UK) and enclosed within a Faraday cage (NG-FC-Custom-104, NeuroGig Limited, UK). Membrane potential measurements of somite-forming cells were conducted using a low-noise dual-channel differential electrometer (FD-223a, WPI, USA). An Ag/AgCl electrode (WIP, USA) was immersed in bulk solution (PC), serving as a reference electrode. A glass microelectrode filled with KCl, connected to the electrometer through a voltage measuring probe, was carefully inserted into the somite using a micromanipulator (Luigs & Neumann GmbH, Germany) to measure V_m. During voltage recording, the solution temperature was consistently maintained at 37.5 °C, and the PC solution was continuously replenished using a peristaltic pump to sustain its composition under specific experimental conditions, including varying CO_2 levels and KCl concentrations (CO_2 levels of 2%, 5%, 7%, as well as 5% CO_2 with the addition of 0.3 mM KCl, 0.6 mM KCl, and 0.3 mM KCl reduction from the control PC). Voltage traces over time were recorded for all somites in a given embryo and analysed using LabScribe software (iWorx, version 4.322), while Advanced Research software (NIS Elements, v 5.01) was used to visualize the microelectrode and the embryo simultaneously during V_m measurements.

Measurement of somite's deformability

The standard micropipette aspiration technique was used to assess the deformability of somite-forming cells. This unique technique has been previously used to evaluate the elasticity of embryonic tissue (von Dassow & Davidson, 2009), and mechanics of soft tissues as well as cell aggregates (Guevorkian et al., 2010; Guevorkian & Maître, 2017). Deformability measurements were taken for all somite stages along the rostral-caudal axis of chick embryos under specific experimental conditions. A silanized micropipette was positioned near a selected somite, and a seal was established between the pipette opening and the somite using an initial aspiration pressure of 3 mbar. The somite was then aspirated at 10 mbar for 90 seconds, followed by an increased pressure of 15 mbar for an additional 90 seconds. Although embryos with up to SSXIII were used in this study, we were able to measure the deformability of somite stage SSI to SSIX only, due to the difficulty in assessing older somites (SSX to SSXIII). This limitation arose from the presence of extraembryonic tissue near the anterior region as the embryo develops. Nevertheless, attempts were made to measure the deformability of older somites with limited success. Time-lapse images were captured every 0.5 second during the first 30 seconds of aspiration to observe rapid changes in somite deformability, and every 2

seconds thereafter throughout the aspiration process. The maximum extent to which the somite was aspirated into the micropipette at each pressure level was tracked from the time-lapse images using Advanced Research software (NIS Elements, v 5.01).

Previous studies have utilized aspiration length measured using micropipette aspiration technique to calculate stiffness or Young's modulus of embryonic tissue (Khalilian et al., 2010; von Dassow et al., 2010). Therefore, to calculate the stiffness of somites from their deformability, in this study, we used a well-established correlation between Young's modulus and aspiration length (Argatov & Mishuris, 2016; Lee & Liu, 2014). $E = (3*\Delta P*\varphi(\eta)*R)/2\pi*L$, an equation based on the elastic half-space model, where E is Young's modulus, ΔP is the applied pressure, $\varphi(\eta)$ is a dimensionless factor, defined as pipette wall function, η is the ratio of thickness and inner radius of pipette, $\varphi(\eta)$ was considered as 2.1 for a practical range of values of η used by previous studies, R is the inner radius of the micropipette, and L is the aspiration length (Argatov & Mishuris, 2016; Jones et al., 1999; Lee & Liu, 2014). However, as the primary objective of this study was to compare the deformability of somite-forming cells when their V_m values were modified rather than to determine absolute stiffness values, we opted to analyze aspiration length values directly. Calculated Young's modulus values were used only for comparison purposes. The dynamics of somite deformability were analyzed by tracking the changes in aspiration length over time until a stable value was reached at each applied pressure. In the aspiration length versus time curve, the initial rapid deformation of aspired cell/tissue is related to its elastic properties. Further the aspiration length reaching a maximum value and staying constant with time at a given pressure is a characteristic of solid materials (Jones et al., 1999; Lee & Liu, 2014). This dynamic viscoelastic behavior has been shown for mesenchymal (Tan et al., 2008) and endothelial cells (Hochmuth, 2000), the type of cells present in somites.

Statistical analysis

To compare the relationship between change in aspiration length (ΔL) and change in membrane potential (ΔV_m) at aspiration pressures of 10 mbar and 15 mbar, linear regression analyses were performed. The slopes of the regression lines were compared using analysis of covariance (ANCOVA).

4.5 Acknowledgement

We thank Prof. Jan Jankowski and AWB Spółka Fermowa sp. z o.o. Wola Szydłowska 44, 06-561 Stupsk, Ferma Drobiu Trzcianka Kolonia 39 and Turza Mała 45a for providing fertilized chicken eggs, Prof. Raquel P. Andrade for training us in chick embryo culture and extraction techniques. We also thank the Embryology Team, especially Prof. Izabela Wocławek–Potocka for allowing us to use the micropipette puller and micro forge instruments.

Author Contributions

M.K. conceptualized and supervised the project. M.M. conducted the laboratory work. M.M., M.K., and S.N. performed the data analysis and interpretations. S.N. supervised laboratory work. M.M., M.K., and S.N. wrote the original manuscript.

Funding

The National Science Centre of Poland under the grant number 2020/38/E/NZ3/00039 funded this work.

Supplementary Information

Table. 4.S1. Shows the difference in the membrane potential values between the posterior and middle, middle and anterior somite groups after somites were depolarized [by additional 0.3 mM KCl (N=5), additional 0.6 mM KCl (N=6) and 7% CO_2(N=8)] and hyperpolarized [by 2% CO_2 (N=6) and reduced 0.3 mM KCl (N=3) from the control PC solution] compared to control condition (5% CO_2) (N=5).

Experimental conditions	SSIII – SSIV Posterior-Middle	SSVIII – SSIX Middle-anterior
2% CO_2	5.09 ± 0.61	3.89 ± 0.51
Reduced 0.3 mM KCl from control PC solution	4.88 ± 0.11	4.11 ± 0.69
5% CO_2 (control)	5.05 ± 0.55	4.26 ± 0.59
Additional 0.3 mM KCl	5.76 ± 0.35	3.62 ± 0.91
7% CO_2	5.28 ± 0.96	3.65 ± 1.30
Additional 0.6 mM KCl	5.38 ± 0.42	3.41 ± 0.68

Table. 4.S2. Shows the slope values of membrane potential versus somite stages trends for a given embryo, in posterior, middle, and anterior somite groups when somites were depolarized [by additional (0.3 and 0.6) mM KCl and 7% CO_2] and hyperpolarized (by 2% CO_2 and reduced 0.3 mM KCl from the control PC solution) compared to control condition.

Experimental conditions	Posterior	middle	anterior
2% CO_2	0.86	0.77	0.65
Reduced 0.3 mM KCl from control PC solution	0.87	0.82	0.69
5% CO_2 (control)	0.99	0.88	0.78
Additional 0.3 mM KCl	1.39	1.02	0.81
7% CO_2	1.65	1.05	0.92
Additional 0.6 mM KCl	1.70	1.19	1.06

Table. 4.S3. Tables show the equations for exponential fits for somite aspiration length (L) versus modified membrane potentials (V_m) trends for all somite stages (SS).

SS (at 10 mbar)	Exponential fitting equations for L vs V_m trends $\boldsymbol{L = L_o + A * e^{R_o * V_m}}$	R^2
I	L = 59.75 + 54.16*$e^{0.13*V_m}$	0.99
II	L = 49.21 + 63.93*$e^{0.09*V_m}$	0.99
III	L = 28.76 + 85.67*$e^{0.06*V_m}$	0.98
IV	L = 33.58 + 119.39*$e^{0.07*V_m}$	0.99
V	L = 356.58 – 250.17*$e^{-0.01*V_m}$	0.99
VI	L = 427.7 – 352.18*$e^{-0.01*V_m}$	0.99
VII	L = 148.92 – 39.81*$e^{-0.03*V_m}$	0.99
VIII	L = 251.43 – 145.40*$e^{-0.02*V_m}$	0.98
IX	L = 71.51 – 0.38*$e^{-0.16*V_m}$	0.99

SS (at 15 mbar)	Exponential fitting equations for L vs V_m trends $\boldsymbol{L = L_o + A * e^{R_o * V_m}}$	R^2
I	L = 54.86 + 73.85*$e^{0.08*V_m}$	0.99
II	L = 29.22 + 95.63*$e^{0.04*V_m}$	0.98
III	L = 35.02 + 90.47*$e^{0.05*V_m}$	0.98
IV	L = 206.16 – 82.95*$e^{-0.02*V_m}$	0.99
V	L = 199.66 – 80.62*$e^{-0.02*V_m}$	0.99
VI	L = 472.70 – 352.18*$e^{-0.01*V_m}$	0.99
VII	L = 148.92 – 39.81*$e^{-0.04*V_m}$	0.99
VIII	L = 126.71 – 22.63*$e^{-0.05*V_m}$	0.99
IX	L = 80.19 – 0.35*$e^{-0.16*V_m}$	0.99

Table. 4.S4. Shows the stiffness values in micrometres for all somite stages (SSI-SSIX) for embryos at given experimental conditions at both (10 and 15) mbar aspiration pressures. The stiffness values were calculated using the equation $E = (3*\Delta P*\varphi*R)/2\pi*L$ from the elastic half-space model, where E is Young's modulus, ΔP is applied suction pressure, φ is a dimensionless factor determined by the geometry of the micropipette, which was taken as 2.1, R is inner radius of the micropipette, and L is the aspiration length. (N = 5 each)

SS (at 10 mbar)	2% CO_2	reduced 0.3 mM KCl	5% CO_2	0.3 mM KCl	7% CO_2	0.6 mM KCl
I	446.08±6.56	415.93±8.73	380.29±17.11	355.27±9.18	328.10±7.12	295.40±3.93
II	476.41±19.56	443.82±11.02	396.53±15.47	370.08±15.89	347.00±11.99	318.78±11.07
III	506.26±21.72	466.02±10.89	422.54±11.89	387.79±14.21	365.56±12.85	339.05±10.79
IV	528.77±28.47	498.50±15.38	448.46±11.34	415.02±20.97	385.04±11.64	358.76±15.67
V	557.93±28.47	522.73±15.56	467.80±12.54	432.22±26.15	407.62±14.47	383.91±23.03
VI	600.17±41.35	555.22±20.39	491.17±20.46	458.92±38.87	431.79±15.77	409.74±15.10
VII	632.30±35.84	599.39±16.84	519.55±19.72	485.65±36.93	446.28±16.39	432.53±10.28
VIII	674.75±28.95	632.12±17.74	547.83±20.11	506.35±46.52	471.41±19.69	451.67±8.48
IX	732.08±29.51	669.32±14.71	604.56±29.45	524.86±48.61	488.90±6.26	467.91±10.57

SS (at 15 mbar)	2% CO_2	reduced 0.3 mM KCl	5% CO_2	0.3 mM KCl	7% CO_2	0.6 mM KCl
I	551.73±11.21	516.91±9.58	480.51±16.72	438.55±11.43	410.29±9.46	395.04±4.49
II	591.88±22.19	550.29±14.35	512.88±22.15	463.96±9.91	428.09±14.08	418.66±18.35
III	628.89±28.07	576.71±12.97	532.15±14.15	485.93±9.80	456.68±17.35	444.51±19.84
IV	653.38±27.91	611.23±16.23	550.07±15.95	505.17±16.40	484.50±19.95	471.94±24.55
V	682.19±37.84	635.85±6.76	583.44±16.17	529.33±28.85	511.68±32.15	499.66±31.65
VI	717.75±53.38	671.77±17.92	609.38±23.18	559.89±39.77	539.44±37.65	530.75±29.28
VII	757.53±58.32	703.51±25.45	634.40±29.48	591.65±31.26	565.34±47.33	558.12±22.87
VIII	802.21±46.54	743.44±32.80	672.06±24.98	629.38±46.17	598.71±30.12	589.48±22.87
IX	856.19±46.96	789.46±23.74	702.65±16.95	673.76±45.33	629.61±5.61	625.09±7.15

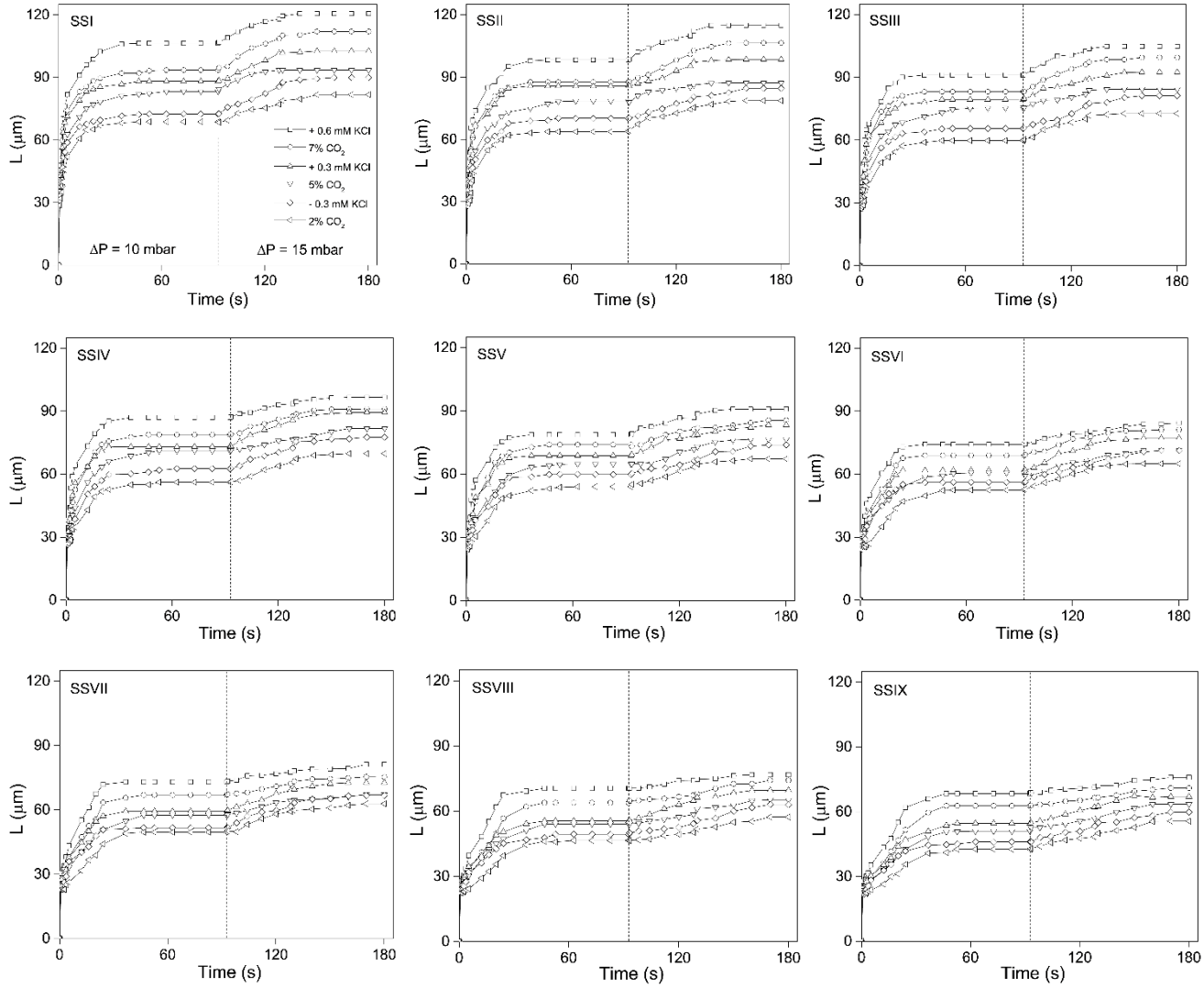

Fig. 4.S1. Dynamics of somite deformability. Aspiration length-time graphs show the viscoelastic behavior of all somite stages (SSI-SSIX) in a given embryo when they were depolarized [by additional (0.3 and 0.6) mM KCl and 7% CO_2] and hyperpolarized (by 2% CO_2 and reduced 0.3 mM KCl from the control PC solution), compared to control condition (5% CO_2). Aspiration lengths were measured at an initial pressure of 10 mbar for up to 90 seconds, followed by an increased pressure of 15 mbar for an additional 90 seconds.

Chapter 5

General discussion

The role of V_m and cell mechanics in somitogenesis, in which the cellular processes such as cell migration, self-assembly, and proliferation must work in an orchestrated manner to produce somites of specified sizes at precise time intervals, was examined in this work. V_m and stiffness of somites were mapped along the anterior-posterior axis of chick embryos. An increase in hyperpolarization and stiffness of somites with their maturation and step like changes of V_m between specific groups of somites were observed along the body axis of embryos (Chapter 3, 4). The abrupt changes in V_m between specific somite stages, in fact mirror previously discovered timing of biochemical (expression of transcription factors) and morphological (structural transitions) changes occurrence during embryo development (Maschner et al., 2016). The dynamics of V_m changes within posterior somite group was higher compared to middle and anterior ones (Chapter 3). This suggests that the changes in the rate of developmental processes might be reflected in the V_m alterations. V_m in general depends on the concentration of intracellular negatively charged elements, including synthesized metabolites (Kay, 2017; Veech et al., 1995). Therefore, higher dynamics of V_m at the caudal end might be attributed to increased glycolytic metabolism that aids biomass production required for growth (Vander Heiden et al., 2009). Additionally, both V_m and stiffness are sensitive to the concentration of cytoplasmic proteins (Guo et al., 2017; Kay, 2017), which explains why the increased hyperpolarization and stiffness of somites were observed with their advancement in development.

In this study, it was necessary to modify the V_m in order to explore its effect on somitogenesis rate. Therefore, freshwater green algae were utilized to examine the possibilities of affecting V_m. The reason for using this model was to verify whether the cell's response to induced changes is the same irrespective of the cell type. CO_2 and KCl - physiologically relevant stimuli, were used to adjust the chemical compositions of cells environment to modify V_m. Increase in concentration of both CO_2 and KCl in the extracellular space has depolarized the cells (Chapter 2). Modifications in ionic concentrations in cell's surrounding not only affected V_m, but also shown enhancement of negative voltage gradient in the vicinity of algal cell wall. This was the first report to show the existence of a gradient of negative voltage, extracellular voltage (V_z), adjacent to algal cell wall, extending for up to a few tens of micrometers (Chapter 2). Similar region of extracellular voltage gradient near the gel (polymer material resembling cell wall of plant or cytoskeletal network of an animal cell from its porous structure and

negative surface charge) was shown as an interfacial zone generated due to charge separation at the zone/bulk interface as a result of different diffusion rates of ions (Kowacz et al., 2023). Elevated concentration of CO_2 outside of algal cells increases the magnitude of V_z and corresponding width of the zone of extracellular voltage (ZEV) (Chapter 2). Supporting this physical phenomenon, the voltage zone similar to ZEV present near charged hydrogel has been shown to be affected by modifying the concentration of CO_2 within the solution (Kowacz et al., 2023). Along with increasing the value of V_z, augmentation in CO_2 level decreased overall V_m by the same magnitude, indicating a coupling effect between them. The same effect was shown by treating algal cells with KCl, known to depolarize cells, where the algal cells were depolarized and the ZEV was enlarged. This indicates that there is an evolution of ZEV adjacent to depolarized cells. Such conclusions were drawn based on the observed enhanced width of ZEV near naturally damaged and manually wounded cells (Chapter 2), which have been shown to be depolarized (Shimmen, 2002, 2008). A large ZEV up to a few tens of micrometers was observed also near spine cells, that are specialized structures in many species of algae that may serve for the exchange of nutrients and ions (Lambert, 2009). These results indicate that the ZEV may enlarge near depolarized and/or developing cells, where there is an enhanced rate of ion exchange between the cytoplasm and extracellular environment (Chapter 2). Supporting this suggestion, an evolution of ZEV was witnessed near early embryonic cells in response to elevated CO_2 level in their microenvironment, which depolarizes the cells (Chapter 3). This indicates that there might be an existence of V_z near embryonic cells, similar to what we observed near algal cells. Akin to V_z, an externally applied electric field near the cells has been shown to affect their proliferation (Vodovnik et al., 1992). Therefore, V_z being a component of overall membrane potential may play role in embryonic development.

Modulations of V_m of somite-forming cells alter the timing of somite segmentation and adjust the somite size to the newly set tempo, resulting therefore in development of undisturbed body pattern of embryos (Chapter 3). Induced depolarization speeds up the somite segmentation clock and the somite's growth rate in a synchronized manner, while hyperpolarization slows them down (Chapter 3). A previous study has shown that the species-specific developmental timing is related to metabolic activity. In particular, increasing metabolic rate accelerates the segmentation time, while diminishing the metabolic rate slows down the process (Diaz-Cuadros et al., 2023). Alterations in V_m

and resulting modifications in the pace of somitogenesis shown in this study could be possibly changing the rate of cell metabolism. However, the question of how V_m coordinates both timing of somite formation and somite growth remains unanswered. The observed changes in stiffness of somite-forming cells in response to induced modifications in V_m provide a hint that alterations in somitogenesis rate may be connected to V_m-driven changes in cell mechanics. Induced depolarization softened somites, whereas hyperpolarization increased their stiffness. A direct correlation between changes in somite's deformability and induced changes in V_m was observed. This suggests that V_m might be controlling somitogenesis rate via biomechanical alterations of somite-forming cells, but how the cell stiffness could be altered by V_m modifications remains a question. The cell's stiffness has earlier been shown to be altered by modulating V_m (He & Dallos, 1999, 2000). In fact, epithelial cells have been shown to dynamically regulate their stiffness in response to external stimuli, by remodeling their cytoskeleton network during embryonic development (Molnar & Labouesse, 2021). A study has shown that the cytoskeleton-dependent alterations in cell stiffness are related to V_m (Callies et al., 2011), which also stresses that cell's cytoskeleton network, especially actin filaments, paly crucial role in mediating V_m-associated stiffness changes. However, the mechanism through which V_m affects cytoskeleton in the course of altering cell's stiffness is elusive. Previous studies have speculated that electric field produced by V_m can directly interact with actin filaments and alter their polymerization state (Callies et al., 2011; Cantiello et al., 1991), thereby affecting cell stiffness. In general, actin polymerization increases cell stiffness, whereas actin depolymerization makes cell softer in developing vertebrates (Bai et al., 2023). The polymerization state of actin has also been shown to be related to cellular pH: acidification promotes actin polymerization and alkalinization prevents it (Wang et al., 1989; Yonezawa et al., 1985). Moreover, a correlation between intracellular pH (pH_i), cytoskeletal architecture, and V_m has been observed during the development (Weiß & Bohrmann, 2019a, 2019b). The depolarization and increase in pH_i of cells can result in disintegration of cytoskeleton structure, while hyperpolarization and decreases in pH_i leads to more stabilized cytoskeleton network (Weiß & Bohrmann, 2019a, 2019b). Similarly, induced depolarization in somite-forming cells as shown in this study may cause increased pH_i and affect cytoskeletal structure leading to their softness, while induced hyperpolarization may have the opposite effect. The claim of depolarization-induced increase in pH_i could be explained by the fact that, when cells were depolarized,

there is reduced intracellular electric force (less negative V_m) and it is easier for cells to export cations, specifically protons. This process might also be promoted by probable attractive force generated by negative V_z that has been shown to be developed adjacent to depolarized cells (Chapter 2 and 3). Therefore, it is possible that the induced depolarization of somite-forming cells may results in increased pH_i by supporting proton expulsion out of the cells. This is corroborated by a previous study showing the increase in pH_i as a result of protons moving out through the channels when the cells are subjected to depolarization (Cheng et al., 2008). Therefore, V_m-induced changes in the pace of somite formation and growth rate, as shown in this study, may be attributed to V_m-induced alterations in cells stiffness, possibly related to pH-dependent alterations in cytoskeleton structure. It is worth to note that the polymerization state of cytoskeleton also influences signaling pathways such as Wnt and Notch that regulate somitogenesis, which includes cell migration, self-assembly, and proliferation (Gibb et al., 2009; Wang et al., 2013; Wang et al., 2015). These signaling pathways can be initiated by increase in intracellular pH (Oginuma et al., 2020; Romero-Moreno et al., 2024). Specifically, actin depolymerization, which can be promoted by depolarization-induced pH_i alterations, enables translocation of β-catenin into the nucleus, a crucial molecule that contributes to Wnt pathway (Torres & Nelson, 2000), and at the same time causes export of YAP (Yes-associated protein) out of the nucleus (Sen et al., 2022). These translocations that occur within the cell facilitate β-catenin to trigger transcription of target genes for the initiation of Wnt and allow YAP to activate the Notch pathway (Passier et al., 2024). Both YAP and Notch have been shown to take part in somite segmentation, with diminished nuclear YAP serving as a threshold signal to initiate Notch activity and oscillations (Hubaud et al., 2017). The periodicity of those oscillations in this study was demonstrated to be directly controlled by modifying V_m of somite-forming cells (Chapter 3). Therefore, cell mechanics altered by V_m, possibly via cytoskeleton reorganization indued by V_m-related intracellular pH variations, may serve as a key mechanism through which membrane potential governs developmental processes during early embryogenesis.

Chapter 6

Conclusions

The presented results show V_m as a dynamic regulator of developmental process in chick embryos. By modifying V_m it has been demonstrated experimentally that V_m is not limited to intracellular voltage but also encompasses extracellular component, V_z, which extends beyond the cell wall/membrane. Induced changes in V_z, on the other hand altered V_m, suggesting a coupling effect between V_m and V_z. It has been shown that both intracellular voltage component, V_i, and V_z can be independently modified, which is then reflected in the overall V_m of a cell. Furthermore, an increase in V_z was observed when the cells were depolarized and near naturally damaged or manually wounded ones, which are also depolarized, and spine cells, where there is an increased ion exchange to uptake the nutrients. Similar phenomenon was recognized near depolarized embryonic cells what suggested that it might contribute to developmental processes. To explore its role on the rate of somitogenesis, V_m was measured for all somite-stages in given embryos. The patterns of V_m of somite-forming cells along the rostro-caudal axis were shown to be associated with somite maturation, and reflect the previously reported initiation of transcription factors expression, and structural changes of cells within the somites. It is important to note that V_m is not a passive marker, instead, it actively regulates the rate of somitogenesis by synchronously controlling both the timing of somite segmentation (cell migration and self-assembly) and somite growth rate (cell proliferation). V_m has a direct effect on the tissue mechanics: induced-depolarization makes the cells softer and speeds up somitogenesis, while hyperpolarization makes them stiffer and slows down the process. Therefore, V_m might possibly bring the link among bioelectrical, biomechanical, and biochemical signals in producing a coherent body pattern.

The findings reported in this study suggest that V_m serves as a master regulator connecting the extracellular milieu, intracellular physiology, and developmental processes during embryogenesis. Modifications in V_m affect fundamental processes such as proliferation, migration, self-assembly, and tissue stiffness. These processes are also hallmarks of tumorigenesis and tissue regeneration, where similar features of depolarized V_m and alterations in the microenvironmental conditions, as those in embryonic cells, can be also observed. Overall, the presented studies illustrate the

interactions among membrane potential, extracellular voltage, and cellular mechanics in living systems, highlighting the broad significance of bioelectricity in developmental biology.

Chapter 7

Implications and future perspective

V_m is recognized in this study as an indicator and also a regulator of biological processes. By identifying the existence of electric voltage beyond the cell membrane, V_z, and its contribution to defining overall V_m, the classical understanding of the mechanism behind V_m generation has been enhanced. This reveals that V_z influences cellular physiology, ion exchange, and local electrochemical environment of cells, which may help with processes such as nutrient uptake, signaling, and even the defense against pathogens. Similar V_z observed in the vicinity of embryonic cells might imply its contributing role in embryonic development. V_m serves as a driving factor for morphogenesis as well as an indicator of developmental progression. This study uncovers the role of V_m in orchestrating cellular processes such as cell migration, self-assembly and proliferation as shown by its ability to synchronously control the rate of somite growth and the timing of somite segmentation. A direct correlation between changes in deformability of somites and induced changes in V_m was shown and suggested that biomechanics might be involved in the processes of V_m-dependent regulation of temporal and spatial information during development. Obtained results indicate that V_m might regulate the segmentation clock and body patterning in conjunction with well-known molecular pathways such as Wnt and Notch. The same pathways are involved during tumorigenesis and tissue regeneration, suggesting that the presented data provide valuable insights into fundamental mechanisms underlying both normal development and disease.

Future studies must focus on acquiring experimental data to understand the possible molecular mechanisms through which V_m regulates development processes. As a preliminary study, an attempt was made to verify the gene oscillation pattern of *hairy 2*, a gene shown to be responsible for somite segmentation clock in chick embryos, in response to induced changes in V_m. In situ hybridization technique was employed to observe *hairy 2* expression pattern. Embryos were incubated at 5% CO_2 environmental condition, after they have been extracted, we dissected them into two halves (explants) along central axis (neural tube). One half was grown at 5% CO_2 (control) and the other at 7% CO_2 (depolarized condition). Newly formed somites were observed after the explants were grown for 90 minutes. Same number of somites and the same pattern of hairy 2 expression were exhibited in both the explants at control condition (Fig. 7.1 a,

b). In contrast, depolarized explants exhibited faster somite segmentation rate compared to explants grown at control condition (Fig. 7.1 c), as it was shown in this study. Interestingly, variations in *hairy 2* expression patterns were observed in depolarized explants compared to the ones grown at control condition (Figure 7.1 d). This suggests that induced changes in V_m might be affecting the clock gene expression pattern in the course of altering somite segmentation timing. Further, extensive studies are required to confirm how clock genes are regulated by V_m.

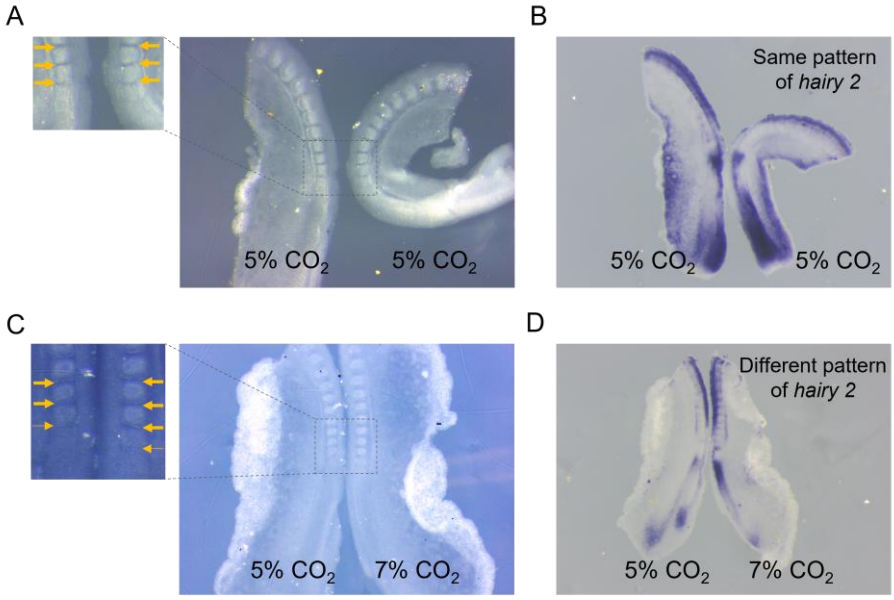

Fig. 7.1 Effect of membrane potential on clock gene (*hairy 2*) expression pattern: microscopic images show number of somites and the *hairy 2* expression patterns for both the explants grown at control (5% CO_2) (A, B) and one half at control and the other at depolarized conditions (7% CO_2) (C, D), extracted from a given embryo.

References

Abdul Kadir, L., Stacey, M., & Barrett-Jolley, R. (2018). Emerging Roles of the Membrane Potential: Action Beyond the Action Potential. *Front Physiol*, *9*, 1661. https://doi.org/10.3389/fphys.2018.01661

Adams, D. S., Uzel, S. G., Akagi, J., Wlodkowic, D., Andreeva, V., Yelick, P. C.,…Levin, M. (2016). Bioelectric signalling via potassium channels: a mechanism for craniofacial dysmorphogenesis in KCNJ2-associated Andersen-Tawil Syndrome. *J Physiol*, *594*(12), 3245-3270. https://doi.org/10.1113/JP271930

Agero, U., Glazier, J. A., & Hosek, M. (2010). Bulk elastic properties of chicken embryos during somitogenesis. *Biomed Eng Online*, *9*, 19. https://doi.org/10.1186/1475-925X-9-19

Alvarez, I. S., Martín-Partido, G., Rodríguez-Gallardo, L., González-Ramos, C., & Navascués, J. (1989). Cell proliferation during early development of the chick embryo otic anlage: quantitative comparison of migratory and nonmigratory regions of the otic epithelium. *J Comp Neurol*, *290*(2), 278-288. https://doi.org/10.1002/cne.902900208

Arcangeli, A., Rosati, B., Cherubini, A., Crociani, O., Fontana, L., Ziller, C.,…Olivotto, M. (1997). HERG- and IRK-like inward rectifier currents are sequentially expressed during neuronal development of neural crest cells and their derivatives. *Eur J Neurosci*, *9*(12), 2596-2604. https://doi.org/10.1111/j.1460-9568.1997.tb01689.x

Argatov, I., & Mishuris, G. (2016). Pipette aspiration testing of soft tissues: the elastic half-space model revisited. *Proc Math Phys Eng Sci*, *472*(2193), 20160559. https://doi.org/10.1098/rspa.2016.0559

Bagnall, K. M., & Berdan, R. C. (1994). Increases in the number of cells in different areas of epithelial somites related to changes in morphology and development. *Anat Embryol (Berl)*, *190*(5), 495-500. https://doi.org/10.1007/BF00235497

Bai, Y., Zhao, F., Wu, T., Chen, F., & Pang, X. (2023). Actin polymerization and depolymerization in developing vertebrates. *Front Physiol*, *14*, 1213668. https://doi.org/10.3389/fphys.2023.1213668

Bard, J. B. (1990). Traction and the formation of mesenchymal condensations in vivo. *Bioessays*, *12*(8), 389-395. https://doi.org/10.1002/bies.950120809

Barriga, E. H., Franze, K., Charras, G., & Mayor, R. (2018). Tissue stiffening coordinates morphogenesis by triggering collective cell migration in vivo. *Nature*, *554*(7693), 523-527. https://doi.org/10.1038/nature25742

Baudenbacher, F., Fong, L. E., Thiel, G., Wacke, M., Jazbinsek, V., Holzer, J. R.,…Trontelj, Z. (2005). Intracellular axial current in Chara corallina reflects the altered kinetics of ions in cytoplasm under the influence of light. *Biophys J*, *88*(1), 690-697. https://doi.org/10.1529/biophysj.104.044974

Baxter, D. F., Kirk, M., Garcia, A. F., Raimondi, A., Holmqvist, M. H., Flint, K. K.,…Xie, Y. (2002). A novel membrane potential-sensitive fluorescent dye improves cell-based assays for ion channels. *J Biomol Screen*, *7*(1), 79-85. https://doi.org/10.1177/108705710200700110

Beer, D. D., & Larkum, A. W. D. (2001). Photosynthesis and calcification in the calcifying algae Halimeda discoidea studied with microsensors. *Plant, Cell & Environment*, *24*(11). https://doi.org/10.1046/j.1365-3040.2001.00772.x

Beilby, M. J. (2016). Multi-Scale Characean Experimental System: From Electrophysiology of Membrane Transporters to Cell-to-Cell Connectivity, Cytoplasmic Streaming and Auxin Metabolism. *Front Plant Sci*, *7*, 1052. https://doi.org/10.3389/fpls.2016.01052

Beilby, M. J., Bisson, M. A., & Schneider, S. C. (2022). How Characean algae take up needed and excrete unwanted ions – An overview explaining how insights from electrophysiology are useful to understand the ecology of aquatic macrophytes. *Aquatic Botany*, *181*. https://doi.org/10.1016/j.aquabot.2022.103542

Binggeli, R., & Weinstein, R. C. (1986). Membrane potentials and sodium channels: hypotheses for growth regulation and cancer formation based on changes in sodium

channels and gap junctions. *J Theor Biol*, *123*(4), 377-401. https://doi.org/10.1016/s0022-5193(86)80209-0
Blackiston, D. J., McLaughlin, K. A., & Levin, M. (2009). Bioelectric controls of cell proliferation: ion channels, membrane voltage and the cell cycle. *Cell Cycle*, *8*(21), 3527-3536. https://doi.org/10.4161/cc.8.21.9888
Blomberg, L., Hashizume, K., & Viebahn, C. (2008). Blastocyst elongation, trophoblastic differentiation, and embryonic pattern formation. *Reproduction*, *135*(2), 181-195. https://doi.org/10.1530/REP-07-0355
Boron, W. F., & De Weer, P. (1976). Intracellular pH transients in squid giant axons caused by CO2, NH3, and metabolic inhibitors. *J Gen Physiol*, *67*(1), 91-112. https://doi.org/10.1085/jgp.67.1.91
Brinks, D., Klein, A. J., & Cohen, A. E. (2015). Two-Photon Lifetime Imaging of Voltage Indicating Proteins as a Probe of Absolute Membrane Voltage. *Biophys J*, *109*(5), 914-921. https://doi.org/10.1016/j.bpj.2015.07.038
Bräuner, T., Hülser, D. F., & Strasser, R. J. (1984). Comparative measurements of membrane potentials with microelectrodes and voltage-sensitive dyes. *Biochim Biophys Acta*, *771*(2), 208-216. https://doi.org/10.1016/0005-2736(84)90535-2
Bulychev, A. A., & Kamzolkina, N. A. (2006). Differential effects of plasma membrane electric excitation on H+ fluxes and photosynthesis in characean cells. *Bioelectrochemistry*, *69*(2), 209-215. https://doi.org/10.1016/j.bioelechem.2006.03.001
Bulychev, A. A., & Krupenina, N. A. (2019). Interchloroplast communications in Chara are suppressed under the alkaline bands and are relieved after the plasma membrane excitation. *Bioelectrochemistry*, *129*, 62-69. https://doi.org/10.1016/j.bioelechem.2019.05.006
Bunce, J. A. (2021). Three new methods indicate that CO. *AoB Plants*, *13*(1), plab004. https://doi.org/10.1093/aobpla/plab004
Callies, C., Fels, J., Liashkovich, I., Kliche, K., Jeggle, P., Kusche-Vihrog, K., & Oberleithner, H. (2011). Membrane potential depolarization decreases the stiffness of vascular endothelial cells. *J Cell Sci*, *124*(Pt 11), 1936-1942. https://doi.org/10.1242/jcs.084657
Campetelli, A., Bonazzi, D., & Minc, N. (2012). Electrochemical regulation of cell polarity and the cytoskeleton. *Cytoskeleton (Hoboken)*, *69*(9), 601-612. https://doi.org/10.1002/cm.21047
Cantiello, H. F., Patenaude, C., & Zaner, K. (1991). Osmotically induced electrical signals from actin filaments. *Biophys J*, *59*(6), 1284-1289. https://doi.org/10.1016/S0006-3495(91)82343-8
Carraco, G., Martins-Jesus, A. P., & Andrade, R. P. (2022). The vertebrate Embryo Clock: Common players dancing to a different beat. *Front Cell Dev Biol*, *10*, 944016. https://doi.org/10.3389/fcell.2022.944016
Carthew, R. W. (2021). Gene Regulation and Cellular Metabolism: An Essential Partnership. *Trends Genet*, *37*(4), 389-400. https://doi.org/10.1016/j.tig.2020.09.018
Casey, J. R., Grinstein, S., & Orlowski, J. (2010). Sensors and regulators of intracellular pH. *Nat Rev Mol Cell Biol*, *11*(1), 50-61. https://doi.org/10.1038/nrm2820
Chai, B., Yoo, H., & Pollack, G. H. (2009). Effect of radiant energy on near-surface water. *J Phys Chem B*, *113*(42), 13953-13958. https://doi.org/10.1021/jp908163w
Chapman, S. C., Collignon, J., Schoenwolf, G. C., & Lumsden, A. (2001). Improved method for chick whole-embryo culture using a filter paper carrier. *Dev Dyn*, *220*(3), 284-289. https://doi.org/10.1002/1097-0177(20010301)220:3<284::AID-DVDY1102>3.0.CO;2-5
Chen, S., Cui, W., Chi, Z., Xiao, Q., Hu, T., Ye, Q.,…Wang, D. (2022). Tumor-associated macrophages are shaped by intratumoral high potassium via Kir2.1. *Cell Metab*, *34*(11), 1843-1859.e1811. https://doi.org/10.1016/j.cmet.2022.08.016
Chen, X., Xu, Z., Tang, K., Hu, G., Du, P., Wang, J.,…Tan, Y. (2023). The Mechanics of Tumor Cells Dictate Malignancy via Cytoskeleton-Mediated APC/Wnt/β-Catenin Signaling. *Research (Wash D C)*, *6*, 0224. https://doi.org/10.34133/research.0224

Cheng, Y., & Moraru, C. I. (2018). Long-range interactions keep bacterial cells from liquid-solid interfaces: Evidence of a bacteria exclusion zone near Nafion surfaces and possible implications for bacterial attachment. *Colloids Surf B Biointerfaces*, *162*, 16-24. https://doi.org/10.1016/j.colsurfb.2017.11.016

Cheng, Y. M., Kelly, T., & Church, J. (2008). Potential contribution of a voltage-activated proton conductance to acid extrusion from rat hippocampal neurons. *Neuroscience*, *151*(4), 1084-1098. https://doi.org/10.1016/j.neuroscience.2007.12.007

Chifflet, S., Correa, V., Nin, V., Justet, C., & Hernández, J. A. (2004). Effect of membrane potential depolarization on the organization of the actin cytoskeleton of eye epithelia. The role of adherens junctions. *Exp Eye Res*, *79*(6), 769-777. https://doi.org/10.1016/j.exer.2004.08.031

Chifflet, S., Hernández, J. A., Grasso, S., & Cirillo, A. (2003). Nonspecific depolarization of the plasma membrane potential induces cytoskeletal modifications of bovine corneal endothelial cells in culture. *Exp Cell Res*, *282*(1), 1-13. https://doi.org/10.1006/excr.2002.5664

Chowdhury, F., Na, S., Li, D., Poh, Y. C., Tanaka, T. S., Wang, F., & Wang, N. (2010). Material properties of the cell dictate stress-induced spreading and differentiation in embryonic stem cells. *Nat Mater*, *9*(1), 82-88. https://doi.org/10.1038/nmat2563

Coleman, J. R., & Colman, B. (1981). Photosynthetic carbon assimilation in the blue-green alga Coccochloris peniocystis. *Plant, Cell & Environment*, *4*(4). https://doi.org/10.1111/1365-3040.ep11604546

Cone, C. D., & Cone, C. M. (1976). Induction of mitosis in mature neurons in central nervous system by sustained depolarization. *Science*, *192*(4235), 155-158. https://doi.org/10.1126/science.56781

Cone, C. D., & Tongier, M. (1971). Control of somatic cell mitosis by simulated changes in the transmembrane potential level. *Oncology*, *25*(2), 168-182. https://doi.org/10.1159/000224567

Cooke, J., & Zeeman, E. C. (1976). A clock and wavefront model for control of the number of repeated structures during animal morphogenesis. *J Theor Biol*, *58*(2), 455-476. https://doi.org/10.1016/s0022-5193(76)80131-2

Dale, K. J., & Pourquié, O. (2000). A clock-work somite. *Bioessays*, *22*(1), 72-83. https://doi.org/10.1002/(SICI)1521-1878(200001)22:1<72::AID-BIES12>3.0.CO;2-S

Dequéant, M. L., Glynn, E., Gaudenz, K., Wahl, M., Chen, J., Mushegian, A., & Pourquié, O. (2006). A complex oscillating network of signaling genes underlies the mouse segmentation clock. *Science*, *314*(5805), 1595-1598. https://doi.org/10.1126/science.1133141

Diaz-Cuadros, M., Miettinen, T. P., Skinner, O. S., Sheedy, D., Díaz-García, C. M., Gapon, S.,…Pourquié, O. (2023). Metabolic regulation of species-specific developmental rates. *Nature*, *613*(7944), 550-557. https://doi.org/10.1038/s41586-022-05574-4

Esplandiu, M. J., Reguera, D., & Fraxedas, J. (2020). Electrophoretic origin of long-range repulsion of colloids near water/Nafion interfaces. *Soft Matter*, *16*(15), 3717-3726. https://doi.org/10.1039/d0sm00170h

Fels, J., Orlov, S. N., & Grygorczyk, R. (2009). The hydrogel nature of mammalian cytoplasm contributes to osmosensing and extracellular pH sensing. *Biophys J*, *96*(10), 4276-4285. https://doi.org/10.1016/j.bpj.2009.02.038

Florea, D., Musa, S., Huyghe, J. M., & Wyss, H. M. (2014). Long-range repulsion of colloids driven by ion exchange and diffusiophoresis. *Proc Natl Acad Sci U S A*, *111*(18), 6554-6559. https://doi.org/10.1073/pnas.1322857111

Foissner, I., & Wasteneys, G. (2011 Nov 28). The characean internodal cell as a model system for studying wound healing. *Journal of microscopy*, *247*(1). https://doi.org/10.1111/j.1365-2818.2011.03572.x

Forgacs, G., Foty, R. A., Shafrir, Y., & Steinberg, M. S. (1998). Viscoelastic properties of living embryonic tissues: a quantitative study. *Biophys J*, *74*(5), 2227-2234. https://doi.org/10.1016/S0006-3495(98)77932-9

Fujii, Y., Koizumi, W. C., Imai, T., Yokobori, M., Matsuo, T., Oka, K.,…Okajima, T. (2021). Spatiotemporal dynamics of single cell stiffness in the early developing ascidian chordate embryo. *Commun Biol*, *4*(1), 341. https://doi.org/10.1038/s42003-021-01869-w

Fukumoto, T., Blakely, R., & Levin, M. (2005). Serotonin transporter function is an early step in left-right patterning in chick and frog embryos. *Dev Neurosci*, *27*(6), 349-363. https://doi.org/10.1159/000088451

Gadsby, D. C., & Cranefield, P. F. (1979). Electrogenic sodium extrusion in cardiac Purkinje fibers. *J Gen Physiol*, *73*(6), 819-837. https://doi.org/10.1085/jgp.73.6.819

Gatenby, R. A., & Gillies, R. J. (2004). Why do cancers have high aerobic glycolysis? *Nat Rev Cancer*, *4*(11), 891-899. https://doi.org/10.1038/nrc1478

George, L. F., & Bates, E. A. (2022). Mechanisms Underlying Influence of Bioelectricity in Development. *Front Cell Dev Biol*, *10*, 772230. https://doi.org/10.3389/fcell.2022.772230

Gest, A. M. M., Grenier, V., & Miller, E. W. (2024). Optical Estimation of Membrane Potential Values Using Fluorescence Lifetime Imaging Microscopy and Hybrid Chemical-Genetic Voltage Indicators. *Bioelectricity*, *6*(1), 34-41. https://doi.org/10.1089/bioe.2023.0027

Gibb, S., Zagorska, A., Melton, K., Tenin, G., Vacca, I., Trainor, P.,…Dale, J. K. (2009). Interfering with Wnt signalling alters the periodicity of the segmentation clock. *Dev Biol*, *330*(1), 21-31. https://doi.org/10.1016/j.ydbio.2009.02.035

Gonzalez-Rodriguez, D., Guevorkian, K., Douezan, S., & Brochard-Wyart, F. (2012). Soft matter models of developing tissues and tumors. *Science*, *338*(6109), 910-917. https://doi.org/10.1126/science.1226418

Guevorkian, K., Colbert, M. J., Durth, M., Dufour, S., & Brochard-Wyart, F. (2010). Aspiration of biological viscoelastic drops. *Phys Rev Lett*, *104*(21), 218101. https://doi.org/10.1103/PhysRevLett.104.218101

Guevorkian, K., & Maître, J. L. (2017). Micropipette aspiration: A unique tool for exploring cell and tissue mechanics in vivo. *Methods Cell Biol*, *139*, 187-201. https://doi.org/10.1016/bs.mcb.2016.11.012

Guo, M., Pegoraro, A. F., Mao, A., Zhou, E. H., Arany, P. R., Han, Y.,…Weitz, D. A. (2017). Cell volume change through water efflux impacts cell stiffness and stem cell fate. *Proc Natl Acad Sci U S A*, *114*(41), E8618-E8627. https://doi.org/10.1073/pnas.1705179114

Hamburger, V., & Hamilton, H. L. (1992). A series of normal stages in the development of the chick embryo. 1951. *Dev Dyn*, *195*(4), 231-272. https://doi.org/10.1002/aja.1001950404

Harima, Y., Takashima, Y., Ueda, Y., Ohtsuka, T., & Kageyama, R. (2013). Accelerating the tempo of the segmentation clock by reducing the number of introns in the Hes7 gene. *Cell Rep*, *3*(1), 1-7. https://doi.org/10.1016/j.celrep.2012.11.012

Harris, M. P. (2021). Bioelectric signaling as a unique regulator of development and regeneration. *Development*, *148*(10). https://doi.org/10.1242/dev.180794

Hatsuki, R., Yujiro, F., & Yamamoto, T. (2013). Direct measurement of electric double layer in a nanochannel by electrical impedance spectroscopy. *Microfluidics and Nanofluidics*, *14*(6), 983-988. https://doi.org/10.1007/s10404-012-1105-5

He, D. Z., & Dallos, P. (1999). Somatic stiffness of cochlear outer hair cells is voltage-dependent. *Proc Natl Acad Sci U S A*, *96*(14), 8223-8228. https://doi.org/10.1073/pnas.96.14.8223

He, D. Z., & Dallos, P. (2000). Properties of voltage-dependent somatic stiffness of cochlear outer hair cells. *J Assoc Res Otolaryngol*, *1*(1), 64-81. https://doi.org/10.1007/s101620010006

Heimburg, T. (2018). Comment on Tamagawa and Ikeda's reinterpretation of the Goldman-Hodgkin-Katz equation : Are transmembrane potentials caused by polarization? *Eur Biophys J*, *47*(8), 865-867. https://doi.org/10.1007/s00249-018-1335-x

Hochmuth, R. M. (2000). Micropipette aspiration of living cells. *J Biomech*, *33*(1), 15-22. https://doi.org/10.1016/s0021-9290(99)00175-x

Hodgkin, A. L., & horowicz, P. (1959). The influence of potassium and chloride ions on the membrane potential of single muscle fibres. *J Physiol*, *148*(1), 127-160. https://doi.org/10.1113/jphysiol.1959.sp006278
Hope, A. (1965). Ionic Relations of Cells of Chara Australls X. Effects of Bicarbonate Ions on Electrical Properties. *Australian Journal of Biological Sciences*, *18*(4). https://doi.org/10.1071/bi9650789
Hopper, A., Beswick-Jones, H., & Brown, A. M. (2022). The Nernst equation: using physico-chemical laws to steer novel experimental design. *Adv Physiol Educ*, *46*(1), 206-210. https://doi.org/10.1152/advan.00191.2021
Hotary, K. B., & Robinson, K. R. (1990). Endogenous electrical currents and the resultant voltage gradients in the chick embryo. *Dev Biol*, *140*(1), 149-160. https://doi.org/10.1016/0012-1606(90)90062-n
Huang, H., Gao, S., & Bao, M. (2024). Exploring Mechanical Forces Shaping Self-Organization and Morphogenesis During Early Embryo Development. *Annu Rev Cell Dev Biol*, *40*(1), 75-96. https://doi.org/10.1146/annurev-cellbio-120123-105748
Hubaud, A., & Pourquié, O. (2014). Signalling dynamics in vertebrate segmentation. *Nat Rev Mol Cell Biol*, *15*(11), 709-721. https://doi.org/10.1038/nrm3891
Hubaud, A., Regev, I., Mahadevan, L., & Pourquié, O. (2017). Excitable Dynamics and Yap-Dependent Mechanical Cues Drive the Segmentation Clock. *Cell*, *171*(3), 668-682.e611. https://doi.org/10.1016/j.cell.2017.08.043
Hughes, M. P., Fry, C. H., & Labeed, F. H. (2022). Cytoplasmic anion/cation imbalances applied across the membrane capacitance may form a significant component of the resting membrane potential of red blood cells. *Sci Rep*, *12*(1), 15005. https://doi.org/10.1038/s41598-022-19316-z
Hughes, M. P., Kruchek, E. J., Beale, A. D., Kitcatt, S. J., Qureshi, S., Trott, Z. P.,…Labeed, F. H. (2021). V. *Sci Rep*, *11*(1), 19446. https://doi.org/10.1038/s41598-021-98102-9
Ibarra-Soria, X., Thierion, E., Mok, G. F., Münsterberg, A. E., Odom, D. T., & Marioni, J. C. (2023). A transcriptional and regulatory map of mouse somite maturation. *Dev Cell*, *58*(19), 1983-1995.e1987. https://doi.org/10.1016/j.devcel.2023.07.003
Ishimatsu, K., Hiscock, T. W., Collins, Z. M., Sari, D. W. K., Lischer, K., Richmond, D. L.,…Megason, S. G. (2018). Size-reduced embryos reveal a gradient scaling-based mechanism for zebrafish somite formation. *Development*, *145*(11). https://doi.org/10.1242/dev.161257
Jacob, M., Christ, B., Jacob, H. J., & Poelmann, R. E. (1991). The role of fibronectin and laminin in development and migration of the avian Wolffian duct with reference to somitogenesis. *Anat Embryol (Berl)*, *183*(4), 385-395. https://doi.org/10.1007/BF00196840
Jaffe, L. F., & Nuccitelli, R. (1977). Electrical controls of development. *Annu Rev Biophys Bioeng*, *6*, 445-476. https://doi.org/10.1146/annurev.bb.06.060177.002305
Jakobsson, E. (1980). Interactions of cell volume, membrane potential, and membrane transport parameters. *Am J Physiol*, *238*(5), C196-206. https://doi.org/10.1152/ajpcell.1980.238.5.C196
Jalilian, I., Heu, C., Cheng, H., Freittag, H., Desouza, M., Stehn, J. R.,…Gunning, P. W. (2015). Cell elasticity is regulated by the tropomyosin isoform composition of the actin cytoskeleton. *PLoS One*, *10*(5), e0126214. https://doi.org/10.1371/journal.pone.0126214
Johnson, B. R., Wyttenbach, R. A., Wayne, R., & Hoy, R. R. (2002). Action potentials in a giant algal cell: a comparative approach to mechanisms and evolution of excitability. *J Undergrad Neurosci Educ*, *1*(1), A23-27.
Jones, W. R., Ting-Beall, H. P., Lee, G. M., Kelley, S. S., Hochmuth, R. M., & Guilak, F. (1999). Alterations in the Young's modulus and volumetric properties of chondrocytes isolated from normal and osteoarthritic human cartilage. *J Biomech*, *32*(2), 119-127. https://doi.org/10.1016/s0021-9290(98)00166-3
Juul, J. S., Jensen, M. H., & Krishna, S. (2019). Constraints on somite formation in developing embryos. *J R Soc Interface*, *16*(158), 20190451. https://doi.org/10.1098/rsif.2019.0451

Kamiya, N. (1986). Cytoplasmic streaming in giant algal cells: A historical survey of experimental approaches. *The Botanical Magazine Tokyo*, *99*(4), 441-467. https://doi.org/10.1007/bf02488723

Kamiya, N., & Kamiya, N. (1981). Physical and Chemical Basis of Cytoplasmic Streaming. *Annual Review of Plant Biology*, *32*. https://doi.org/10.1146/annurev.pp.32.060181.001225

Kasas, S., Wang, X., Hirling, H., Marsault, R., Huni, B., Yersin, A.,…Catsicas, S. (2005). Superficial and deep changes of cellular mechanical properties following cytoskeleton disassembly. *Cell Motil Cytoskeleton*, *62*(2), 124-132. https://doi.org/10.1002/cm.20086

Kay, A. R. (2017). How Cells Can Control Their Size by Pumping Ions. *Front Cell Dev Biol*, *5*, 41. https://doi.org/10.3389/fcell.2017.00041

Kay, A. R., & Blaustein, M. P. (2019). Evolution of our understanding of cell volume regulation by the pump-leak mechanism. *J Gen Physiol*, *151*(4), 407-416. https://doi.org/10.1085/jgp.201812274

Keifer, D. W., & Lucas, W. J. (1982). Potassium Channels in Chara corallina: control and interaction with the electrogenic h pump. *Plant Physiol*, *69*(4), 781-788. https://doi.org/10.1104/pp.69.4.781

Kempson, S. A. (2012). The Plasma Membrane, Membrane Transport, and the Resting Membrane Potential. In (pp. 19-36). https://faculty.ksu.edu.sa/sites/default/files/smch2.pdf

Kerszberg, M., & Wolpert, L. (2000). A clock and trail model for somite formation, specialization and polarization. *J Theor Biol*, *205*(3), 505-510. https://doi.org/10.1006/jtbi.2000.2085

Khalilian, M., Navidbakhsh, M., Valojerdi, M. R., Chizari, M., & Yazdi, P. E. (2010). Estimating Young's modulus of zona pellucida by micropipette aspiration in combination with theoretical models of ovum. *J R Soc Interface*, *7*(45), 687-694. https://doi.org/10.1098/rsif.2009.0380

Kikuchi, R., Iwai, Y., Tsuji, T., Watanabe, Y., Koyama, N., Yamaguchi, K.,…Aoshiba, K. (2019). Hypercapnic tumor microenvironment confers chemoresistance to lung cancer cells by reprogramming mitochondrial metabolism in vitro. *Free Radic Biol Med*, *134*, 200-214. https://doi.org/10.1016/j.freeradbiomed.2019.01.014

Kim, H. Y., Jackson, T. R., & Davidson, L. A. (2017). On the role of mechanics in driving mesenchymal-to-epithelial transitions. *Semin Cell Dev Biol*, *67*, 113-122. https://doi.org/10.1016/j.semcdb.2016.05.011

Kim, H. Y., Jackson, T. R., Stuckenholz, C., & Davidson, L. A. (2020). Tissue mechanics drives regeneration of a mucociliated epidermis on the surface of Xenopus embryonic aggregates. *Nat Commun*, *11*(1), 665. https://doi.org/10.1038/s41467-020-14385-y

Kim, J., Sasaki, Y., Yoshida, W., Kobayashi, N., Veloso, A. J., Kerman, K.,…Sode, K. (2013). Rapid cytotoxicity screening platform for amyloid inhibitors using a membrane-potential sensitive fluorescent probe. *Anal Chem*, *85*(1), 185-192. https://doi.org/10.1021/ac302442q

Kirkegaard, K., Hindkjaer, J. J., & Ingerslev, H. J. (2013). Effect of oxygen concentration on human embryo development evaluated by time-lapse monitoring. *Fertil Steril*, *99*(3), 738-744.e734. https://doi.org/10.1016/j.fertnstert.2012.11.028

Klima, A., & Foissner, I. (2011). Actin-dependent deposition of putative endosomes and endoplasmic reticulum during early stages of wound healing in characean internodal cells. *Plant Biol (Stuttg)*, *13*(4), 590-601. https://doi.org/10.1111/j.1438-8677.2010.00413.x

Konrad, K. R., & Hedrich, R. (2008). The use of voltage-sensitive dyes to monitor signal-induced changes in membrane potential-ABA triggered membrane depolarization in guard cells. *Plant J*, *55*(1), 161-173. https://doi.org/10.1111/j.1365-313X.2008.03498.x

Koser, D. E., Moeendarbary, E., Hanne, J., Kuerten, S., & Franze, K. (2015). CNS cell distribution and axon orientation determine local spinal cord mechanical properties. *Biophys J*, *108*(9), 2137-2147. https://doi.org/10.1016/j.bpj.2015.03.039

Koser, D. E., Thompson, A. J., Foster, S. K., Dwivedy, A., Pillai, E. K., Sheridan, G. K.,…Franze, K. (2016). Mechanosensing is critical for axon growth in the developing brain. *Nat Neurosci*, *19*(12), 1592-1598. https://doi.org/10.1038/nn.4394

Kowacz, M., & Pollack, G. H. (2020). Cells in New Light: Ion Concentration, Voltage, and Pressure Gradients across a Hydrogel Membrane. *ACS Omega*, *5*(33), 21024-21031. https://doi.org/10.1021/acsomega.0c02595

Kowacz, M., Withanage, S., & Niestępski, S. (2023). Voltage and concentration gradients across membraneless interface generated next to hydrogels: relation to glycocalyx. *Soft Matter*, *19*(39), 7528-7540. https://doi.org/10.1039/d3sm00889d

Krol, A. J., Roellig, D., Dequéant, M. L., Tassy, O., Glynn, E., Hattem, G.,…Pourquié, O. (2011). Evolutionary plasticity of segmentation clock networks. *Development*, *138*(13), 2783-2792. https://doi.org/10.1242/dev.063834

La Claire, J. W. (1982). Wound-healing motility in the green alga Ernodesmis: calcium ions and metabolic energy are required. *Planta*, *156*(5), 466-474. https://doi.org/10.1007/BF00393319

Lambert, D. S. (2009). *Stoneworts : their habitats ,ecological requirements and conservation* T. E. Agency. https://assets.publishing.service.gov.uk/media/5a7ba34140f0b645ba3c59a5/scho0309bpsd-e-e.pdf

Lauschke, V. M., Tsiairis, C. D., François, P., & Aulehla, A. (2013). Scaling of embryonic patterning based on phase-gradient encoding. *Nature*, *493*(7430), 101-105. https://doi.org/10.1038/nature11804

Lautner, S., Stummer, M., Matyssek, R., Fromm, J., & Grams, T. E. (2014). Involvement of respiratory processes in the transient knockout of net CO2 uptake in Mimosa pudica upon heat stimulation. *Plant Cell Environ*, *37*(1), 254-260. https://doi.org/10.1111/pce.12150

Lazzari-Dean, J. R., Gest, A. M., & Miller, E. W. (2019). Optical estimation of absolute membrane potential using fluorescence lifetime imaging. *Elife*, *8*. https://doi.org/10.7554/eLife.44522

Lazzari-Dean, J. R., & Miller, E. W. (2021). Optical Estimation of Absolute Membrane Potential Using One- and Two-Photon Fluorescence Lifetime Imaging Microscopy. *Bioelectricity*, *3*(3), 197-203. https://doi.org/10.1089/bioe.2021.0007

Lee, J. W. (2019). Electrostatically localized proton bioenergetics: better understanding membrane potential. *Heliyon*, *5*(7), e01961. https://doi.org/10.1016/j.heliyon.2019.e01961

Lee, J. W. (2020). Protonic conductor: better understanding neural resting and action potential. *J Neurophysiol*, *124*(4), 1029-1044. https://doi.org/10.1152/jn.00281.2020

Lee, J. W. (2021). Mitochondrial energetics with transmembrane electrostatically localized protons: do we have a thermotrophic feature? *Sci Rep*, *11*(1), 14575. https://doi.org/10.1038/s41598-021-93853-x

Lee, J. W. (2023). Transient protonic capacitor: Explaining the bacteriorhodopsin membrane experiment of Heberle et al. 1994. *Biophys Chem*, *300*, 107072. https://doi.org/10.1016/j.bpc.2023.107072

Lee, L. M., & Liu, A. P. (2014). The Application of Micropipette Aspiration in Molecular Mechanics of Single Cells. *J Nanotechnol Eng Med*, *5*(4), 0408011-0408016. https://doi.org/10.1115/1.4029936

Levin, M. (2012). Molecular bioelectricity in developmental biology: new tools and recent discoveries: control of cell behavior and pattern formation by transmembrane potential gradients. *Bioessays*, *34*(3), 205-217. https://doi.org/10.1002/bies.201100136

Levin, M. (2014). Molecular bioelectricity: how endogenous voltage potentials control cell behavior and instruct pattern regulation in vivo. *Mol Biol Cell*, *25*(24), 3835-3850. https://doi.org/10.1091/mbc.E13-12-0708

Levin, M. (2021). Bioelectric signaling: Reprogrammable circuits underlying embryogenesis, regeneration, and cancer. *Cell*, *184*(8), 1971-1989. https://doi.org/10.1016/j.cell.2021.02.034

Levin, M., & Martyniuk, C. J. (2018). The bioelectric code: An ancient computational medium for dynamic control of growth and form. *Biosystems*, *164*, 76-93. https://doi.org/10.1016/j.biosystems.2017.08.009

Li, Z., Gong, Y., Sun, S., Du, Y., Lü, D., Liu, X., & Long, M. (2013). Differential regulation of stiffness, topography, and dimension of substrates in rat mesenchymal stem cells. *Biomaterials*, *34*(31), 7616-7625. https://doi.org/10.1016/j.biomaterials.2013.06.059

Li, Z., & Pollack, G. H. (2020). Surface-induced flow: A natural microscopic engine using infrared energy as fuel. *Sci Adv*, *6*(19), eaba0941. https://doi.org/10.1126/sciadv.aba0941

Liao, B. K., Jörg, D. J., & Oates, A. C. (2016). Faster embryonic segmentation through elevated Delta-Notch signalling. *Nat Commun*, *7*, 11861. https://doi.org/10.1038/ncomms11861

Lucas, W. J. (1982). Mechanism of acquisition of exogenous bicarbonate by internodal cells of Chara corallina. *Planta*, *156*(2), 181-192. https://doi.org/10.1007/BF00395434

Lucas, W. J., & Ogata, K. (1985). Hydroxyl– and Bicarbonate-Associated Transport Processes in Chara corallina: Studies on the Light-Dark Regulation Mechanism. *Journal of Experimental Botany*, *36*(12). https://doi.org/10.1093/jxb/36.12.1947

Mahadeva, M., Niestępski, S., & Kowacz, M. (2024). Dependence of cell's membrane potential on extracellular voltage observed in Chara globularis. *Biophys Chem*, *307*, 107199. https://doi.org/10.1016/j.bpc.2024.107199

Mahadeva, M., Niestępski, S., & Kowacz, M. (2025). Modifying membrane potential synchronously controls the somite's formation periodicity and growth. *Dev Biol*, *517*, 317-326. https://doi.org/10.1016/j.ydbio.2024.11.002

Maia-Fernandes, A. C., Martins-Jesus, A., Borralho-Martins, N., Pais-de-Azevedo, T., Magno, R., Duarte, I., & Andrade, R. P. (2024). Spatio-temporal dynamics of early somite segmentation in the chicken embryo. *PLoS One*, *19*(4), e0297853. https://doi.org/10.1371/journal.pone.0297853

Majkut, S., Idema, T., Swift, J., Krieger, C., Liu, A., & Discher, D. E. (2013). Heart-specific stiffening in early embryos parallels matrix and myosin expression to optimize beating. *Curr Biol*, *23*(23), 2434-2439. https://doi.org/10.1016/j.cub.2013.10.057

Man, C. H., Mercier, F. E., Liu, N., Dong, W., Stephanopoulos, G., Jiang, L.,…Scadden, D. T. (2022). Proton export alkalinizes intracellular pH and reprograms carbon metabolism to drive normal and malignant cell growth. *Blood*, *139*(4), 502-522. https://doi.org/10.1182/blood.2021011563

Marchant, C. L., Malmi-Kakkada, A. N., Espina, J. A., & Barriga, E. H. (2022). Cell clusters softening triggers collective cell migration in vivo. *Nat Mater*, *21*(11), 1314-1323. https://doi.org/10.1038/s41563-022-01323-0

Marrese, M., Antonovaité, N., Nelemans, B. K. A., Ahmadzada, A., Iannuzzi, D., & Smit, T. H. (2020). In vivo characterization of chick embryo mesoderm by optical coherence tomography-assisted microindentation. *FASEB J*, *34*(9), 12269-12277. https://doi.org/10.1096/fj.202000896R

Masamizu, Y., Ohtsuka, T., Takashima, Y., Nagahara, H., Takenaka, Y., Yoshikawa, K.,…Kageyama, R. (2006). Real-time imaging of the somite segmentation clock: revelation of unstable oscillators in the individual presomitic mesoderm cells. *Proc Natl Acad Sci U S A*, *103*(5), 1313-1318. https://doi.org/10.1073/pnas.0508658103

Maschner, A., Krück, S., Draga, M., Pröls, F., & Scaal, M. (2016). Developmental dynamics of occipital and cervical somites. *J Anat*, *229*(5), 601-609. https://doi.org/10.1111/joa.12516

Matsuda, M., Hayashi, H., Garcia-Ojalvo, J., Yoshioka-Kobayashi, K., Kageyama, R., Yamanaka, Y.,…Ebisuya, M. (2020). Species-specific segmentation clock periods are due to differential biochemical reaction speeds. *Science*, *369*(6510), 1450-1455. https://doi.org/10.1126/science.aba7668

McColl, J., Mok, G. F., Lippert, A. H., Ponjavic, A., Muresan, L., & Münsterberg, A. (2018). 4D imaging reveals stage dependent random and directed cell motion during somite morphogenesis. *Sci Rep*, *8*(1), 12644. https://doi.org/10.1038/s41598-018-31014-3

McCormick, D. A. (2014). Membrane Potential and Action Potential. In *An Introduction to Cellular and Molecular Neuroscience* (Third edition ed., pp. 351-376). Academic press. https://doi.org/https://doi.org/10.1016/B978-0-12-397179-1.00012-9

McLaughlin, K. A., & Levin, M. (2018). Bioelectric signaling in regeneration: Mechanisms of ionic controls of growth and form. *Dev Biol*, *433*(2), 177-189. https://doi.org/10.1016/j.ydbio.2017.08.032

McMillen, P., & Levin, M. (2024). Optical Estimation of Bioelectric Patterns in Living Embryos. *Methods Mol Biol*, *2745*, 91-102. https://doi.org/10.1007/978-1-0716-3577-3_6

Michel, G., Tonon, T., Scornet, D., Cock, J. M., & Kloareg, B. (2010). The cell wall polysaccharide metabolism of the brown alga Ectocarpus siliculosus. Insights into the evolution of extracellular matrix polysaccharides in Eukaryotes. *New Phytol*, *188*(1), 82-97. https://doi.org/10.1111/j.1469-8137.2010.03374.x

Molnar, K., & Labouesse, M. (2021). The plastic cell: mechanical deformation of cells and tissues. *Open Biol*, *11*(2), 210006. https://doi.org/10.1098/rsob.210006

Morelli, L. G., Ares, S., Herrgen, L., Schröter, C., Jülicher, F., & Oates, A. C. (2009). Delayed coupling theory of vertebrate segmentation. *HFSP J*, *3*(1), 55-66. https://doi.org/10.2976/1.3027088

Mukherjee, A., Huang, Y., Elgeti, J., Oh, S., Abreu, J. G., Neliat, A. R.,…Basan, M. (2024). Membrane potential mediates the cellular response to mechanical pressure. *bioRxiv*. https://doi.org/10.1101/2023.11.02.565386

Musa-Aziz, R., Boron, W. F., & Parker, M. D. (2010). Using fluorometry and ion-sensitive microelectrodes to study the functional expression of heterologously-expressed ion channels and transporters in Xenopus oocytes. *Methods*, *51*(1), 134-145. https://doi.org/10.1016/j.ymeth.2009.12.012

Nakamura, Y., Yamamoto, Y., Usui, F., Mushika, T., Ono, T., Setioko, A. R.,…Tagami, T. (2007). Migration and proliferation of primordial germ cells in the early chicken embryo. *Poult Sci*, *86*(10), 2182-2193. https://doi.org/10.1093/ps/86.10.2182

Naoki, H., & Matsui, T. (2020). Somite boundary determination in normal and clock-less vertebrate embryos. *Dev Growth Differ*, *62*(3), 177-187. https://doi.org/10.1111/dgd.12655

Nimer, N. A., Brownlee, C., & Merrett, M. J. (1994). Carbon dioxide availability, intracellular pH and growth rate of the coccolithophore Emiliania huxleyi. *Marine Ecology Progress Series*, *109*. https://doi.org/10.3354/meps109257

Nin, V., Hernández, J. A., & Chifflet, S. (2009). Hyperpolarization of the plasma membrane potential provokes reorganization of the actin cytoskeleton and increases the stability of adherens junctions in bovine corneal endothelial cells in culture. *Cell Motil Cytoskeleton*, *66*(12), 1087-1099. https://doi.org/10.1002/cm.20416

Nishiyama, M., von Schimmelmann, M. J., Togashi, K., Findley, W. M., & Hong, K. (2008). Membrane potential shifts caused by diffusible guidance signals direct growth-cone turning. *Nat Neurosci*, *11*(7), 762-771. https://doi.org/10.1038/nn.2130

Nooryani, M., Benneker, A. M., & Natale, G. (2023). Self-generated exclusion zone in a dead-end pore microfluidic channel. *Lab Chip*, *23*(8), 2122-2130. https://doi.org/10.1039/d2lc01130a

Nuccitelli, R. (2003). Endogenous electric fields in embryos during development, regeneration and wound healing. *Radiat Prot Dosimetry*, *106*(4), 375-383. https://doi.org/10.1093/oxfordjournals.rpd.a006375

Oberleithner, H., Callies, C., Kusche-Vihrog, K., Schillers, H., Shahin, V., Riethmüller, C.,…de Wardener, H. E. (2009). Potassium softens vascular endothelium and increases nitric oxide release. *Proc Natl Acad Sci U S A*, *106*(8), 2829-2834. https://doi.org/10.1073/pnas.0813069106

Oginuma, M., Harima, Y., Tarazona, O. A., Diaz-Cuadros, M., Michaut, A., Ishitani, T.,…Pourquié, O. (2020). Intracellular pH controls WNT downstream of glycolysis in amniote embryos. *Nature*, *584*(7819), 98-101. https://doi.org/10.1038/s41586-020-2428-0

Oginuma, M., Moncuquet, P., Xiong, F., Karoly, E., Chal, J., Guevorkian, K., & Pourquié, O. (2017). A Gradient of Glycolytic Activity Coordinates FGF and Wnt Signaling during Elongation of the Body Axis in Amniote Embryos. *Dev Cell*, *40*(4), 342-353.e310. https://doi.org/10.1016/j.devcel.2017.02.001

Ozkucur, N., Perike, S., Sharma, P., & Funk, R. H. (2011). Persistent directional cell migration requires ion transport proteins as direction sensors and membrane potential differences in order to maintain directedness. *BMC Cell Biol*, *12*, 4. https://doi.org/10.1186/1471-2121-12-4

Palmeirim, I., Henrique, D., Ish-Horowicz, D., & Pourquié, O. (1997). Avian hairy gene expression identifies a molecular clock linked to vertebrate segmentation and somitogenesis. *Cell*, *91*(5), 639-648. https://doi.org/10.1016/s0092-8674(00)80451-1

Parkins, C. S., Stratford, M. R., Dennis, M. F., Stubbs, M., & Chaplin, D. J. (1997). The relationship between extracellular lactate and tumour pH in a murine tumour model of ischaemia-reperfusion. *Br J Cancer*, *75*(3), 319-323. https://doi.org/10.1038/bjc.1997.53

Passier, M., Bentley, K., Loerakker, S., & Ristori, T. (2024). YAP/TAZ drives Notch and angiogenesis mechanoregulation in silico. *NPJ Syst Biol Appl*, *10*(1), 116. https://doi.org/10.1038/s41540-024-00444-3

Pedregal-Cortés, R., Toriz, G., Delgado, E., & Pollack, G. H. (2019). Interfacial water and its potential role in the function of sericin against biofouling. *Biofouling*, *35*(7), 732-741. https://doi.org/10.1080/08927014.2019.1653863

Pek, Y. S., Wan, A. C., & Ying, J. Y. (2010). The effect of matrix stiffness on mesenchymal stem cell differentiation in a 3D thixotropic gel. *Biomaterials*, *31*(3), 385-391. https://doi.org/10.1016/j.biomaterials.2009.09.057

Peyton, S. R., Raub, C. B., Keschrumrus, V. P., & Putnam, A. J. (2006). The use of poly(ethylene glycol) hydrogels to investigate the impact of ECM chemistry and mechanics on smooth muscle cells. *Biomaterials*, *27*(28), 4881-4893. https://doi.org/10.1016/j.biomaterials.2006.05.012

Pfanz, H., Aschan, G., Langenfeld-Heyser, R., Wittmann, C., & Loose, M. (2002). Ecology and ecophysiology of tree stems: corticular and wood photosynthesis. *Naturwissenschaften*, *89*(4), 147-162. https://doi.org/10.1007/s00114-002-0309-z

Pourquié, O. (2001). Vertebrate somitogenesis. *Annu Rev Cell Dev Biol*, *17*, 311-350. https://doi.org/10.1146/annurev.cellbio.17.1.311

Pourquié, O. (2003a). The segmentation clock: converting embryonic time into spatial pattern. *Science*, *301*(5631), 328-330. https://doi.org/10.1126/science.1085887

Pourquié, O. (2003b). Vertebrate somitogenesis: a novel paradigm for animal segmentation? *Int J Dev Biol*, *47*(7-8), 597-603.

Primmett, D. R., Norris, W. E., Carlson, G. J., Keynes, R. J., & Stern, C. D. (1989). Periodic segmental anomalies induced by heat shock in the chick embryo are associated with the cell cycle. *Development*, *105*(1), 119-130. https://doi.org/10.1242/dev.105.1.119

Qin, X., Zhang, H., Zhou, X., Wang, C., Zhang, X., & Ye, L. (2007). Proliferation and migration mediated by Dkk-1/Wnt/beta-catenin cascade in a model of hepatocellular carcinoma cells. *Transl Res*, *150*(5), 281-294. https://doi.org/10.1016/j.trsl.2007.06.005

Rapetti-Mauss, R., Bustos, V., Thomas, W., McBryan, J., Harvey, H., Lajczak, N.,…Harvey, B. J. (2017). Bidirectional KCNQ1:β-catenin interaction drives colorectal cancer cell

differentiation. *Proc Natl Acad Sci U S A*, *114*(16), 4159-4164. https://doi.org/10.1073/pnas.1702913114
Rifes, P., & Thorsteinsdóttir, S. (2012). Extracellular matrix assembly and 3D organization during paraxial mesoderm development in the chick embryo. *Dev Biol*, *368*(2), 370-381. https://doi.org/10.1016/j.ydbio.2012.06.003
Robinson, K. R. (1985). The responses of cells to electrical fields: a review. *J Cell Biol*, *101*(6), 2023-2027. https://doi.org/10.1083/jcb.101.6.2023
Roblero, L., Biggers, J. D., & Lechene, C. P. (1976). Electron probe analysis of the elemental microenvironment of oviducal mouse embryos. *J Reprod Fertil*, *46*(2), 431-434. https://doi.org/10.1530/jrf.0.0460431
Roblero, L. S., & Riffo, M. D. (1986). High potassium concentration improves preimplantation development of mouse embryos in vitro. *Fertil Steril*, *45*(3), 412-416. https://doi.org/10.1016/S0015-0282(16)49227-7
Romero-Moreno, R., Czowski, B. J., Harris, L., Kuehn, J. F., & White, K. A. (2024). Intracellular pH differentially regulates transcription of metabolic and signaling pathways in normal epithelial cells. *J Biol Chem*, *300*(10), 107658. https://doi.org/10.1016/j.jbc.2024.107658
Rotsch, C., & Radmacher, M. (2000). Drug-induced changes of cytoskeletal structure and mechanics in fibroblasts: an atomic force microscopy study. *Biophys J*, *78*(1), 520-535. https://doi.org/10.1016/S0006-3495(00)76614-8
Russell, S., Xu, L., Kam, Y., Abrahams, D., Ordway, B., Lopez, A. S.,…Gillies, R. J. (2022). Proton export upregulates aerobic glycolysis. *BMC Biol*, *20*(1), 163. https://doi.org/10.1186/s12915-022-01340-0
Salker, M. S., Schierbaum, N., Alowayed, N., Singh, Y., Mack, A. F., Stournaras, C.,…Lang, F. (2016). LeftyA decreases Actin Polymerization and Stiffness in Human Endometrial Cancer Cells. *Sci Rep*, *6*, 29370. https://doi.org/10.1038/srep29370
Schaeffer, J., Weber, I. P., Thompson, A. J., Keynes, R. J., & Franze, K. (2022). Axons in the Chick Embryo Follow Soft Pathways Through Developing Somite Segments. *Front Cell Dev Biol*, *10*, 917589. https://doi.org/10.3389/fcell.2022.917589
Schmitz, M., Nelemans, B. K., & Smit, T. H. (2016). A Submerged Filter Paper Sandwich for Long-term Ex Ovo Time-lapse Imaging of Early Chick Embryos. *J Vis Exp*(118). https://doi.org/10.3791/54636
Schnell, S., & Maini, P. K. (2000). Clock and induction model for somitogenesis. *Dev Dyn*, *217*(4), 415-420. https://doi.org/10.1002/(SICI)1097-0177(200004)217:4<415::AID-DVDY8>3.0.CO;2-3
Schröter, C., & Oates, A. C. (2010). Segment number and axial identity in a segmentation clock period mutant. *Curr Biol*, *20*(14), 1254-1258. https://doi.org/10.1016/j.cub.2010.05.071
Sen, B., Xie, Z., Howard, S., Styner, M., van Wijnen, A. J., Uzer, G., & Rubin, J. (2022). Mechanically Induced Nuclear Shuttling of β-Catenin Requires Co-transfer of Actin. *Stem Cells*, *40*(4), 423-434. https://doi.org/10.1093/stmcls/sxac006
Sharma, A., Mir, R., & Galande, S. (2021). Epigenetic Regulation of the Wnt/β-Catenin Signaling Pathway in Cancer. *Front Genet*, *12*, 681053. https://doi.org/10.3389/fgene.2021.681053
Sharma, A., & Pollack, G. H. (2020). Healthy fats and exclusion-zone size. *Food Chem*, *316*, 126305. https://doi.org/10.1016/j.foodchem.2020.126305
Shepherd, V. A., & Goodwin, P. B. (1992). Seasonal patterns of cell-to-cell communication in Chara corallina Klein ex Willd. I. Cell-to-cell communication in vegetative lateral branches during winter and spring. *Plant, Cell & Environment*, *15*(2). https://doi.org/10.1111/j.1365-3040.1992.tb01468.x
Shim, S., Baskaran, M., Thai, E. H., & Stone, H. A. (2021). CO. *Lab Chip*, *21*(17), 3387-3400. https://doi.org/10.1039/d1lc00211b
Shimmen, T. (2001). Electrical perception of "death message" in Chara: involvement of turgor pressure. *Plant Cell Physiol*, *42*(4), 366-373. https://doi.org/10.1093/pcp/pce047

Shimmen, T. (2002). Electrical perception of "death message" in chara: analysis of rapid component and ionic process. *Plant Cell Physiol*, *43*(12), 1575-1584. https://doi.org/10.1093/pcp/pcf182
Shimmen, T. (2006). Electrophysiology in Mechanosensing and Wounding Response. *Plant Electrophysiology*. https://doi.org/10.1007/978-3-540-37843-3_14
Shimmen, T. (2008). Electrophysiological characterization of the node in Chara corallina: functional differentiation for wounding response. *Plant Cell Physiol*, *49*(2), 264-272. https://doi.org/10.1093/pcp/pcn002
Shimmen, T., Mimura, T., Kikuyama, M., & Tazawa, M. (1994). Characean cells as a tool for studying electrophysiological characteristics of plant cells. *Cell Struct Funct*, *19*(5), 263-278. https://doi.org/10.1247/csf.19.263
Shimmen, T., & Tazawa, M. (1981). Demonstration of Voltage Dependency of Light-induced Potential Change in Chara. *Plant and Cell Physiology*, *22*(5). https://doi.org/10.1093/oxfordjournals.pcp.a076226
Shimmen, T., & Wakabayashi, A. (2008). Involvement of membrane potential in alkaline band formation by internodal cells of Chara corallina. *Plant Cell Physiol*, *49*(10), 1614-1620. https://doi.org/10.1093/pcp/pcn136
Shin, S., Shardt, O., Warren, P. B., & Stone, H. A. (2017). Membraneless water filtration using CO. *Nat Commun*, *8*, 15181. https://doi.org/10.1038/ncomms15181
Shyer, A. E., Rodrigues, A. R., Schroeder, G. G., Kassianidou, E., Kumar, S., & Harland, R. M. (2017). Emergent cellular self-organization and mechanosensation initiate follicle pattern in the avian skin. *Science*, *357*(6353), 811-815. https://doi.org/10.1126/science.aai7868
Somero, G. N. (1985). Intracellular pH, Buffering Substances and Proteins: Imidazole Protona. *Proceedings in Life Sciences*. https://doi.org/10.1007/978-3-642-70613-4_38
Spencer, P. D., Riches, J. D., & Williams, E. D. (2018). Exclusion zone water is associated with material that exhibits proton diffusion but not birefringent properties. *Fluid Phase Equilibria*, *466*. https://doi.org/10.1016/j.fluid.2018.03.020
Stahlberg, R., & Cosgrove, D. J. (1992). Rapid alterations in growth rate and electrical potentials upon stem excision in pea seedlings. *Planta*, *187*(4), 523-531. https://doi.org/10.1007/BF00199972
Stern, C. D., Fraser, S. E., Keynes, R. J., & Primmett, D. R. (1988). A cell lineage analysis of segmentation in the chick embryo. *Development*, *104 Suppl*, 231-244. https://doi.org/10.1242/dev.104.Supplement.231
Stillwell, E. F., Cone, C. M., & Cone, C. D. (1973). Stimulation of DNA synthesis in CNS neurones by sustained depolarisation. *Nat New Biol*, *246*(152), 110-111. https://doi.org/10.1038/newbio246110a0
Sträuber, H., & Müller, S. (2010). Viability states of bacteria--specific mechanisms of selected probes. *Cytometry A*, *77*(7), 623-634. https://doi.org/10.1002/cyto.a.20920
Sundelacruz, S., Levin, M., & Kaplan, D. L. (2009). Role of membrane potential in the regulation of cell proliferation and differentiation. *Stem Cell Rev Rep*, *5*(3), 231-246. https://doi.org/10.1007/s12015-009-9080-2
Swetha Balakrishnan, R. G. (2020). Ultrastructural studies on the corticating filament of Chara zeylanica. *Environmental and Experimental Biology*, *18*, 169–174. https://doi.org/http://doi.org/10.22364/eeb.18.17
Tabatabaei, M., Tafazzoli-Shadpour, M., & Khani, M. M. (2021). Altered mechanical properties of actin fibers due to breast cancer invasion: parameter identification based on micropipette aspiration and multiscale tensegrity modeling. *Med Biol Eng Comput*, *59*(3), 547-560. https://doi.org/10.1007/s11517-021-02318-w
Tamagawa, H., & Delalande, B. (2022). The membrane potential arising from the adsorption of ions at the biological interface. *Biol Futur*, *73*(4), 455-471. https://doi.org/10.1007/s42977-022-00139-y

Tamagawa, H., & Ikeda, K. (2018). Another interpretation of the Goldman-Hodgkin-Katz equation based on Ling's adsorption theory. *Eur Biophys J*, *47*(8), 869-879. https://doi.org/10.1007/s00249-018-1332-0

Tan, S. C., Pan, W. X., Ma, G., Cai, N., Leong, K. W., & Liao, K. (2008). Viscoelastic behaviour of human mesenchymal stem cells. *BMC Cell Biol*, *9*, 40. https://doi.org/10.1186/1471-2121-9-40

Tassinari, R., Cavallini, C., Olivi, E., Facchin, F., Taglioli, V., Zannini, C.,…Ventura, C. (2022). Cell Responsiveness to Physical Energies: Paving the Way to Decipher a Morphogenetic Code. *Int J Mol Sci*, *23*(6). https://doi.org/10.3390/ijms23063157

Tazawa, M., & Shimmen, T. (2001).How characean cells have contributed to the progress of plant membrane biophysics. *Australian journal of plant physiology*, *28*(7). https://doi.org/10.1071/PP01027

Tester, M., Beilby, M. J., & Shimmen, T. (1987). Electrical Characteristics of the Tonoplast of Cham corallincr. A Study Using Permeabilised Cells. *Plant and Cell Physiology*, *28*(8). https://doi.org/10.1093/oxfordjournals.pcp.a077450

Tester, M., & Tester, M. (1988). Pharmacology of K+ channels in the plasmalemma of the green algaChara corallina. *The Journal of Membrane Biology 1988 103:2*, *103*(2). https://doi.org/10.1007/BF01870946

Theparambil, S. M., Weber, T., Schmälzle, J., Ruminot, I., & Deitmer, J. W. (2016). Proton Fall or Bicarbonate Rise: glycolytic rate in mouse astrocytes is paved by intracellular alkalinization. *J Biol Chem*, *291*(36), 19108-19117. https://doi.org/10.1074/jbc.M116.730143

Thompson, A. J., Pillai, E. K., Dimov, I. B., Foster, S. K., Holt, C. E., & Franze, K. (2019). Rapid changes in tissue mechanics regulate cell behaviour in the developing embryonic brain. *Elife*, *8*. https://doi.org/10.7554/eLife.39356

Torres, M. A., & Nelson, W. J. (2000). Colocalization and redistribution of dishevelled and actin during Wnt-induced mesenchymal morphogenesis. *J Cell Biol*, *149*(7), 1433-1442. https://doi.org/10.1083/jcb.149.7.1433

Vander Heiden, M. G., Cantley, L. C., & Thompson, C. B. (2009). Understanding the Warburg effect: the metabolic requirements of cell proliferation. *Science*, *324*(5930), 1029-1033. https://doi.org/10.1126/science.1160809

Veech, R. L., Kashiwaya, Y., Gates, D. N., King, M. T., & Clarke, K. (2002). The energetics of ion distribution: the origin of the resting electric potential of cells. *IUBMB Life*, *54*(5), 241-252. https://doi.org/10.1080/15216540215678

Veech, R. L., Kashiwaya, Y., & King, M. T. (1995). The resting membrane potential of cells are measures of electrical work, not of ionic currents. *Integr Physiol Behav Sci*, *30*(4), 283-307. https://doi.org/10.1007/BF02691602

Veech, R. L., King, M. T., Pawlosky, R., Bradshaw, P. C., & Curtis, W. (2019). Relationship between inorganic ion distribution, resting membrane potential, and the Δ. *FASEB J*, *33*(12), 13126-13130. https://doi.org/10.1096/fj.201901942R

Venters, S. J., Hultner, M. L., & Ordahl, C. P. (2008). Somite cell cycle analysis using somite-staging to measure intrinsic developmental time. *Dev Dyn*, *237*(2), 377-392. https://doi.org/10.1002/dvdy.21424

Villar, R., Held, A. A., & Merino, J. (1994). Comparison of Methods to Estimate Dark Respiration in the Light in Leaves of Two Woody Species. *Plant Physiol*, *105*(1), 167-172. https://doi.org/10.1104/pp.105.1.167

Vodovnik, L., Miklavcic, D., & Sersa, G. (1992). Modified cell proliferation due to electrical currents. *Med Biol Eng Comput*, *30*(4), CE21-28. https://doi.org/10.1007/BF02446174

von Dassow, M., & Davidson, L. A. (2009). Natural variation in embryo mechanics: gastrulation in Xenopus laevis is highly robust to variation in tissue stiffness. *Dev Dyn*, *238*(1), 2-18. https://doi.org/10.1002/dvdy.21809

von Dassow, M., Strother, J. A., & Davidson, L. A. (2010). Surprisingly simple mechanical behavior of a complex embryonic tissue. *PLoS One*, *5*(12), e15359. https://doi.org/10.1371/journal.pone.0015359

Walker, N. A., Beilby, M. J., Smith, F. A., Walker, N. A., Beilby, M. J., & Smith, F. A. (1979/03). Amine uniport at the plasmalemma of charophyte cells: I. Current-voltage curves, saturation kinetics, and effects of unstirred layers. *The Journal of Membrane Biology 1979 49:1*, *49*(1). https://doi.org/10.1007/BF01871038

Wang, F., Sampogna, R. V., & Ware, B. R. (1989). pH dependence of actin self-assembly. *Biophys J*, *55*(2), 293-298. https://doi.org/10.1016/S0006-3495(89)82804-8

Wang, H. Y., Huang, Y. X., Qi, Y. F., Zhang, Y., Bao, Y. L., Sun, L. G.,…Li, Y. X. (2013). Mathematical models for the Notch and Wnt signaling pathways and the crosstalk between them during somitogenesis. *Theor Biol Med Model*, *10*, 27. https://doi.org/10.1186/1742-4682-10-27

Wang, H. Y., Huang, Y. X., Zheng, L. H., Bao, Y. L., Sun, L. G., Wu, Y.,…Li, Y. X. (2015). Modelling coupled oscillations in the Notch, Wnt, and FGF signaling pathways during somitogenesis: a comprehensive mathematical model. *Comput Intell Neurosci*, *2015*, 387409. https://doi.org/10.1155/2015/387409

Wang, Y., Wang, G., Luo, X., Qiu, J., & Tang, C. (2012). Substrate stiffness regulates the proliferation, migration, and differentiation of epidermal cells. *Burns*, *38*(3), 414-420. https://doi.org/10.1016/j.burns.2011.09.002

Weiß, I., & Bohrmann, J. (2019a). Electrochemical gradients are involved in regulating cytoskeletal patterns during epithelial morphogenesis in the Drosophila ovary. *BMC Dev Biol*, *19*(1), 22. https://doi.org/10.1186/s12861-019-0203-y

Weiß, I., & Bohrmann, J. (2019b). Electrochemical patterns during Drosophila oogenesis: ion-transport mechanisms generate stage-specific gradients of pH and membrane potential in the follicle-cell epithelium. *BMC Dev Biol*, *19*(1), 12. https://doi.org/10.1186/s12861-019-0192-x

Whited, J. L., & Levin, M. (2019). Bioelectrical controls of morphogenesis: from ancient mechanisms of cell coordination to biomedical opportunities. *Curr Opin Genet Dev*, *57*, 61-69. https://doi.org/10.1016/j.gde.2019.06.014

Winer, J. P., Janmey, P. A., McCormick, M. E., & Funaki, M. (2009). Bone marrow-derived human mesenchymal stem cells become quiescent on soft substrates but remain responsive to chemical or mechanical stimuli. *Tissue Eng Part A*, *15*(1), 147-154. https://doi.org/10.1089/ten.tea.2007.0388

Xie, Y., Wang, M., Cheng, M., Gao, Z., & Wang, G. (2019). The viscoelastic behaviors of several kinds of cancer cells and normal cells. *J Mech Behav Biomed Mater*, *91*, 54-58. https://doi.org/10.1016/j.jmbbm.2018.11.029

Yamada, A., Gaja, N., Ohya, S., Muraki, K., Narita, H., Ohwada, T., & Imaizumi, Y. (2001). Usefulness and limitation of DiBAC4(3), a voltage-sensitive fluorescent dye, for the measurement of membrane potentials regulated by recombinant large conductance Ca2+-activated K+ channels in HEK293 cells. *Jpn J Pharmacol*, *86*(3), 342-350. https://doi.org/10.1254/jjp.86.342

Yang, M., & Brackenbury, W. J. (2013). Membrane potential and cancer progression. *Front Physiol*, *4*, 185. https://doi.org/10.3389/fphys.2013.00185

Yonezawa, N., Nishida, E., & Sakai, H. (1985). pH control of actin polymerization by cofilin. *J Biol Chem*, *260*(27), 14410-14412.

Zhang, G., & Levin, M. (2025). Bioelectricity is a universal multifaced signaling cue in living organisms. *Mol Biol Cell*, *36*(2), pe2. https://doi.org/10.1091/mbc.E23-08-0312

Zheng, J., & Pollack, G. H. (2006). Solute Exclusion and Potential Distribution Near Hydrophilic Surfaces. https://doi.org/10.1007/1-4020-4927-7_8

Zheng, J. M., Chin, W. C., Khijniak, E., & Pollack, G. H. (2006). Surfaces and interfacial water: evidence that hydrophilic surfaces have long-range impact. *Adv Colloid Interface Sci*, *127*(1), 19-27. https://doi.org/10.1016/j.cis.2006.07.002

Zheng, J. M., & Pollack, G. H. (2003). Long-range forces extending from polymer-gel surfaces. *Phys Rev E Stat Nonlin Soft Matter Phys*, *68*(3 Pt 1), 031408. https://doi.org/10.1103/PhysRevE.68.031408

Załącznik nr 10. Oświadczenie kandydata o jego merytorycznym udziale w powstanie pracy
Annex No. 10. *Statement of the candidate on their substantive contribution to the creation of a work*

Manohara Mahadeva
(imię i nazwisko/ *name and surname*)

Olsztyn, 18.09.2025
miejscowość, data/ *city, date*

0000-0002-6644-7281
[ORCID]

Oświadczenie
Statement

Niniejszym oświadczam, że w pracy "Dependence of cell's membrane potential on extracellular voltage observed in Chara globularis", Mahadeva Manohara, Niestępski Sebastian, & Kowacz Magdalena, Biophysical Chemistry, 2024, 307, art. no 107199 (10.1016/j.bpc.2024.107199) mój udział polegał na metodologii, walidacji, analizie danych, badaniach, opracowaniu danych, redakcji i przygotowaniu pierwszej wersji manuskryptu, przygotowaniu odpowiedzi na recenzje, wizualizacji.[7]

I hereby declare that in the scientific paper "Dependence of cell's membrane potential on extracellular voltage observed in Chara globularis", Mahadeva Manohara, Niestępski Sebastian, & Kowacz Magdalena, Biophysical Chemistry, 2024, 307, art. no 107199 (10.1016/j.bpc.2024.107199) my contribution consisted of Methodology, Validation, Formal analysis, Investigation, Data curation, Writing – Original draft, Writing – Review and Editing, Visualization[7]

Manohara Mahadeva
.....
podpis kandydata/ *signature of the candidate*

Podpisy współautora/współautorów
Signatures of the co-author/co-authors:
Sebastian Niestępski
.....
Magdalena Kowacz
.....
.....

[7]**Określenie merytorycznego udziału kandydata w powstanie artykułu naukowego/monografii naukowej (https://credit.niso.org/)**
W celu jednoznacznego określenia wkładu kandydatów w powstanie publikacji naukowej, przyjmuje się następującą klasyfikację:

- **Konceptualizacja:** Tworzenie idei; formułowanie lub rozwijanie głównych celów, hipotez i założeń badawczych.
- **Opracowanie danych:** Zarządzanie danymi, w tym ich anotacja (tworzenie metadanych), przechowywanie danych badawczych do użytku bieżącego i/lub ponownej analizy.
- **Analiza danych:** Zastosowanie technik statystycznych, matematycznych, obliczeniowych lub innych metod do analizy danych badawczych.

- **Pozyskanie finansowania**: Zdobycie środków finansowych na realizację projektu, który doprowadził do powstania publikacji.
- **Badania:** Prowadzenie procesu badawczego, w tym przeprowadzanie eksperymentów oraz zbieranie danych.
- **Metodologia:** Opracowanie metod badawczych; tworzenie modeli badawczych.
- **Zarządzanie projektem:** Koordynacja i zarządzanie planowaniem oraz realizacją działań badawczych.
- **Oprogramowanie:** Programowanie; projektowanie programów komputerowych; implementacja kodu komputerowego i wspierających algorytmów; testowanie istniejących komponentów kodu.
- **Zasoby:** Zapewnienie materiału badawczego, odczynników, narzędzi badawczych, pacjentów, próbek laboratoryjnych, zwierząt doświadczalnych, sprzętu, zasobów obliczeniowych lub innych narzędzi analitycznych.
- **Walidacja:** Weryfikacja powtarzalności i odtwarzalności wyników badań, eksperymentów oraz innych rezultatów naukowych.
- **Wizualizacja:** Przygotowanie, opracowanie i/lub prezentacja wyników badawczych, w szczególności wizualizacja danych.
- **Redakcja i przygotowanie pierwszej wersji manuskryptu:** Opracowanie, stworzenie i/lub prezentacja pracy naukowej, w szczególności napisanie pierwszej wersji manuskryptu.
- **Przygotowanie odpowiedzi na recenzje:** Opracowanie, stworzenie i/lub prezentacja pracy naukowej przez autorów manuskryptu, obejmująca krytyczną analizę, komentarze oraz poprawki.

To clearly define the candidate's contribution to the publication, the following taxonomy (as per credit.niso.org) is recommended:

- **Conceptualization:** Ideas; formulation or evolution of overarching research goals and aims.
- **Data curation:** Management activities to annotate (produce metadata), scrub data and maintain research data (including software code, where it is necessary for interpreting the data itself) for initial use and later re-use.
- **Formal analysis:** Application of statistical, mathematical, computational, or other formal techniques to analyze or synthesize study data.
- **Funding acquisition:** Acquisition of the financial support for the project leading to this publication
- **Investigation:** Conducting a research and investigation process, specifically performing the experiments, or data/evidence collection.
- **Methodology:** Development or design of methodology; creation of models.
- **Project administration:** Management and coordination responsibility for the research activity planning and execution.
- **Software:** Programming, software development; designing computer programs; implementation of the computer code and supporting algorithms; testing of existing code components.
- **Resources:** Provision of study materials, reagents, materials, patients, laboratory samples, animals, instrumentation, computing resources, or other analysis tools.
- **Validation:** Verification, whether as a part of the activity or separate, of the overall replication/reproducibility of results/experiments and other research outputs.
- **Visualization:** Preparation, creation and/or presentation of the published work, specifically visualization/data presentation.
- **Writing - Original Draft:** Preparation, creation and/or presentation of the published work, specifically writing the initial draft (including substantive translation).
- **Writing - Review & Editing:** Preparation, creation and/or presentation of the published work by those from the original research group, specifically critical review, commentary or revision – including pre- or post-publication stages.

Załącznik nr 10. Oświadczenie kandydata o jego merytorycznym udziale w powstanie pracy
Annex No. 10. *Statement of the candidate on their substantive contribution to the creation of a work*

Manohara Mahadeva
(imię i nazwisko/ *name and surname*)

Olsztyn, 18.09.2025
miejscowość, data/ *city, date*

0000-0002-6644-7281
[ORCID]

Oświadczenie
Statement

Niniejszym oświadczam, że w pracy " Modifying membrane potential synchronously controls the somite's formation periodicity and growth", Mahadeva Manohara, Niestępski Sebastian, & Kowacz Magdalena, Developmental Biology, 2025, 517, 317-326 (10.1016/j.ydbio.2024.11.002) mój udział polegał na metodologii, walidacji, analizie danych, badaniach, opracowaniu danych, redakcji i przygotowaniu pierwszej wersji manuskryptu, przygotowaniu odpowiedzi na recenzje, wizualizacji.[7]

I hereby declare that in the scientific paper "Modifying membrane potential synchronously controls the somite's formation periodicity and growth", Mahadeva Manohara, Niestępski Sebastian, & Kowacz Magdalena, Developmental Biology, 2025, 517, 317-326 (10.1016/j.ydbio.2024.11.002) my contribution consisted of Methodology, Validation, Formal analysis, Investigation, Data curation, Writing – Original draft, Writing – Review and Editing, Visualization[7]

Manohara Mahadeva
.....
podpis kandydata/ *signature of the candidate*

Podpisy współautora/współautorów
Signatures of the co-author/co-authors:
.....Sebastian Niestępski.....
Magdalena Kowacz
.....
.....

[7]**Określenie merytorycznego udziału kandydata w powstanie artykułu naukowego/monografii naukowej (https://credit.niso.org/)**
W celu jednoznacznego określenia wkładu kandydatów w powstanie publikacji naukowej, przyjmuje się następującą klasyfikację:

- **Konceptualizacja:** Tworzenie idei; formułowanie lub rozwijanie głównych celów, hipotez i założeń badawczych.
- **Opracowanie danych:** Zarządzanie danymi, w tym ich anotacja (tworzenie metadanych), przechowywanie danych badawczych do użytku bieżącego i/lub ponownej analizy.
- **Analiza danych:** Zastosowanie technik statystycznych, matematycznych, obliczeniowych lub innych metod do analizy danych badawczych.

- **Pozyskanie finansowania**: Zdobycie środków finansowych na realizację projektu, który doprowadził do powstania publikacji.
- **Badania:** Prowadzenie procesu badawczego, w tym przeprowadzanie eksperymentów oraz zbieranie danych.
- **Metodologia:** Opracowanie metod badawczych; tworzenie modeli badawczych.
- **Zarządzanie projektem:** Koordynacja i zarządzanie planowaniem oraz realizacją działań badawczych.
- **Oprogramowanie:** Programowanie; projektowanie programów komputerowych; implementacja kodu komputerowego i wspierających algorytmów; testowanie istniejących komponentów kodu.
- **Zasoby:** Zapewnienie materiału badawczego, odczynników, narzędzi badawczych, pacjentów, próbek laboratoryjnych, zwierząt doświadczalnych, sprzętu, zasobów obliczeniowych lub innych narzędzi analitycznych.
- **Walidacja:** Weryfikacja powtarzalności i odtwarzalności wyników badań, eksperymentów oraz innych rezultatów naukowych.
- **Wizualizacja:** Przygotowanie, opracowanie i/lub prezentacja wyników badawczych, w szczególności wizualizacja danych.
- **Redakcja i przygotowanie pierwszej wersji manuskryptu:** Opracowanie, stworzenie i/lub prezentacja pracy naukowej, w szczególności napisanie pierwszej wersji manuskryptu.
- **Przygotowanie odpowiedzi na recenzje:** Opracowanie, stworzenie i/lub prezentacja pracy naukowej przez autorów manuskryptu, obejmująca krytyczną analizę, komentarze oraz poprawki.

To clearly define the candidate's contribution to the publication, the following taxonomy (as per credit.niso.org) is recommended:

- **Conceptualization:** Ideas; formulation or evolution of overarching research goals and aims.
- **Data curation:** Management activities to annotate (produce metadata), scrub data and maintain research data (including software code, where it is necessary for interpreting the data itself) for initial use and later re-use.
- **Formal analysis:** Application of statistical, mathematical, computational, or other formal techniques to analyze or synthesize study data.
- **Funding acquisition:** Acquisition of the financial support for the project leading to this publication
- **Investigation:** Conducting a research and investigation process, specifically performing the experiments, or data/evidence collection.
- **Methodology:** Development or design of methodology; creation of models.
- **Project administration:** Management and coordination responsibility for the research activity planning and execution.
- **Software:** Programming, software development; designing computer programs; implementation of the computer code and supporting algorithms; testing of existing code components.
- **Resources:** Provision of study materials, reagents, materials, patients, laboratory samples, animals, instrumentation, computing resources, or other analysis tools.
- **Validation:** Verification, whether as a part of the activity or separate, of the overall replication/reproducibility of results/experiments and other research outputs.
- **Visualization:** Preparation, creation and/or presentation of the published work, specifically visualization/data presentation.
- **Writing - Original Draft:** Preparation, creation and/or presentation of the published work, specifically writing the initial draft (including substantive translation).
- **Writing - Review & Editing:** Preparation, creation and/or presentation of the published work by those from the original research group, specifically critical review, commentary or revision – including pre- or post-publication stages.

Załącznik nr 10. Oświadczenie kandydata o jego merytorycznym udziale w powstanie pracy
Annex No. 10. *Statement of the candidate on their substantive contribution to the creation of a work*

Manohara Mahadeva
(imię i nazwisko/ *name and surname*)

Olsztyn, 18.09.2025
miejscowość, data/ *city, date*

0000-0002-6644-7281
[ORCID]

Oświadczenie

Statement

Niniejszym oświadczam, że w pracy " Bioelectric control of tissue mechanics: Effect of membrane potential on somite deformability in chick embryos", Mahadeva Manohara, Niestępski Sebastian, & Kowacz Magdalena, przedłożonej do recenzji do czasopisma Developmental Biology mój udział polegał na metodologii, walidacji, analizie danych, badaniach, opracowaniu danych, redakcji i przygotowaniu pierwszej wersji manuskryptu, przygotowaniu odpowiedzi na recenzje, wizualizacji.[7]

I hereby declare that in the scientific paper "Bioelectric control of tissue mechanics: Effect of membrane potential on somite deformability in chick embryos", Mahadeva Manohara, Niestępski Sebastian, & Kowacz Magdalena, submitted to Developmental Biology, my contribution consisted of Methodology, Validation, Formal analysis, Investigation, Data curation, Writing – Original draft, Writing – Review and Editing, Visualization[7]

Manohara Mahadeva
.....
podpis kandydata/ *signature of the candidate*

Podpisy współautora/współautorów
Signatures of the co-author/co-authors:
...Sebastian Niestępski....
Magdalena Kowacz
.....

.....

[7]**Określenie merytorycznego udziału kandydata w powstanie artykułu naukowego/monografii naukowej (https://credit.niso.org/)**
W celu jednoznacznego określenia wkładu kandydatów w powstanie publikacji naukowej, przyjmuje się następującą klasyfikację:

- **Konceptualizacja:** Tworzenie idei; formułowanie lub rozwijanie głównych celów, hipotez i założeń badawczych.
- **Opracowanie danych:** Zarządzanie danymi, w tym ich anotacja (tworzenie metadanych), przechowywanie danych badawczych do użytku bieżącego i/lub ponownej analizy.
- **Analiza danych:** Zastosowanie technik statystycznych, matematycznych, obliczeniowych lub innych metod do analizy danych badawczych.
- **Pozyskanie finansowania**: Zdobycie środków finansowych na realizację projektu, który doprowadził do powstania publikacji.

- **Badania:** Prowadzenie procesu badawczego, w tym przeprowadzanie eksperymentów oraz zbieranie danych.
- **Metodologia:** Opracowanie metod badawczych; tworzenie modeli badawczych.
- **Zarządzanie projektem:** Koordynacja i zarządzanie planowaniem oraz realizacją działań badawczych.
- **Oprogramowanie:** Programowanie; projektowanie programów komputerowych; implementacja kodu komputerowego i wspierających algorytmów; testowanie istniejących komponentów kodu.
- **Zasoby:** Zapewnienie materiału badawczego, odczynników, narzędzi badawczych, pacjentów, próbek laboratoryjnych, zwierząt doświadczalnych, sprzętu, zasobów obliczeniowych lub innych narzędzi analitycznych.
- **Walidacja:** Weryfikacja powtarzalności i odtwarzalności wyników badań, eksperymentów oraz innych rezultatów naukowych.
- **Wizualizacja:** Przygotowanie, opracowanie i/lub prezentacja wyników badawczych, w szczególności wizualizacja danych.
- **Redakcja i przygotowanie pierwszej wersji manuskryptu:** Opracowanie, stworzenie i/lub prezentacja pracy naukowej, w szczególności napisanie pierwszej wersji manuskryptu.
- **Przygotowanie odpowiedzi na recenzje:** Opracowanie, stworzenie i/lub prezentacja pracy naukowej przez autorów manuskryptu, obejmująca krytyczną analizę, komentarze oraz poprawki.

To clearly define the candidate's contribution to the publication, the following taxonomy (as per credit.niso.org) is recommended:

- **Conceptualization:** Ideas; formulation or evolution of overarching research goals and aims.
- **Data curation:** Management activities to annotate (produce metadata), scrub data and maintain research data (including software code, where it is necessary for interpreting the data itself) for initial use and later re-use.
- **Formal analysis:** Application of statistical, mathematical, computational, or other formal techniques to analyze or synthesize study data.
- **Funding acquisition:** Acquisition of the financial support for the project leading to this publication
- **Investigation:** Conducting a research and investigation process, specifically performing the experiments, or data/evidence collection.
- **Methodology:** Development or design of methodology; creation of models.
- **Project administration:** Management and coordination responsibility for the research activity planning and execution.
- **Software:** Programming, software development; designing computer programs; implementation of the computer code and supporting algorithms; testing of existing code components.
- **Resources:** Provision of study materials, reagents, materials, patients, laboratory samples, animals, instrumentation, computing resources, or other analysis tools.
- **Validation:** Verification, whether as a part of the activity or separate, of the overall replication/reproducibility of results/experiments and other research outputs.
- **Visualization:** Preparation, creation and/or presentation of the published work, specifically visualization/data presentation.
- **Writing - Original Draft:** Preparation, creation and/or presentation of the published work, specifically writing the initial draft (including substantive translation).
- **Writing - Review & Editing:** Preparation, creation and/or presentation of the published work by those from the original research group, specifically critical review, commentary or revision – including pre- or post-publication stages.

Biophysical Chemistry 307 (2024) 107199

Contents lists available at ScienceDirect

Biophysical Chemistry

journal homepage: www.elsevier.com/locate/biophyschem

Dependence of cell's membrane potential on extracellular voltage observed in *Chara globularis*

Manohara Mahadeva, Sebastian Niestępski, Magdalena Kowacz *

Department of Reproductive Immunology & Pathology, Institute of Animal Reproduction and Food Research Polish Academy of Sciences, 10-748 Olsztyn, Poland

ARTICLE INFO

Keywords:
Chara globularis
Membrane potential
Extracellular voltage
Colloid exclusion
Microelectrode technique

ABSTRACT

The membrane potential (V_m) of a cell results from the selective movement of ions across the cell membrane. Recent studies have revealed the presence of a gradient of voltage within a few nanometers adjacent to erythrocytes. Very notably this voltage is modified in response to changes in cell's membrane potential thus effectively extending the potential beyond the membrane and into the solution. In this study, using the microelectrode technique, we provide experimental evidence for the existence of a gradient of negative extracellular voltage (V_z) in a wide zone close to the cell wall of algal cells, extending over several micrometers. Modulating the ionic concentration of the extracellular solution with CO_2 alters the extracellular voltage and causes an immediate change in V_m. Elevated extracellular CO_2 levels depolarize the cell and hyperpolarize the zone of extracellular voltage (ZEV) by the same magnitude. This observation strongly suggests a coupling effect between V_z and V_m. An increase in the level of intracellular CO_2 (dark respiration) leads to hyperpolarization of the cell without any immediate effect on the extracellular voltage. Therefore, the metabolic activity of a cell can proceed without inducing changes in V_z. Conversely, V_z can be modified by external stimulation without metabolic input from the cell. The evolution of the ZEV, particularly around spines and wounded cells, where ion exchange is enhanced, suggests that the formation of the ZEV may be attributed to the exchange of ions across the cell wall and cell membrane. By comparing the changes in V_m in response to external stimuli, as measured by electrodes and observed using a potential-sensitive dye, we provide experimental evidence demonstrating the significance of extracellular voltage in determining the cell's membrane potential. This may have implications for our understanding of cell membrane potential generation beyond the activities of ion channels.

1. Introduction

Membrane potential is a fundamental characteristic of a healthy cell, determined by an unequal distribution of ions across the semipermeable membrane [1]. The unequal distribution is controlled by ion channels and energy-consuming ion pumps embedded within the cell membrane. Mainly, K^+ ions move out from the cytosol at a higher rate than Na^+ ions penetrate into the cell, creating a difference in electric voltage across the cell membrane [2]. However, the existence of an ion concentration gradient and an electric potential difference across a gel membrane (an abiotic system, resembling plant cell wall and/or animal cytoskeleton from its porous structure and negative surface charge [3,4]) has been experimentally showed [5]. In our recent study, a negative voltage gradient, emerging adjacent to the charged hydrogel surface within a few hundred micrometers from its interface in the solution, has been experimentally demonstrated and theoretical explanation for the mechanism behind the phenomenon has been provided [6]. It should be noted that voltage extending over such large distance in ionic solution is not expected from the perspective of classical electrostatic theory due to charge screening effect [6]. The presence of voltage near the hydrogel has been substantiated by visual observation of the exclusion of colloids away from the gel surface. This region of voltage gradient has been termed the depletion zone or exclusion zone (EZ). Many studies have provided evidence for the development of EZ adjacent to hydrophilic and ion-exchanging surfaces in both biological and synthetic systems [5–14]. The formation of these zones is facilitated by the selective exchange of ions between the zone-inducing surface and its surrounding medium, driven by electrical and chemical forces [5,6]. We have suggested in our previous work that the formation of the depletion zone near the gel surface is controlled by the liquid junction potential across the gel/water interface due to the generation of electric repulsive force between the negatively charged gel surface and the negative terminal of

* Corresponding author.
E-mail address: m.kowacz@pan.olsztyn.pl (M. Kowacz).

https://doi.org/10.1016/j.bpc.2024.107199
Received 22 December 2023; Received in revised form 31 January 2024; Accepted 4 February 2024
Available online 5 February 2024

the liquid junction. The separation of ionic charges with different diffusion speeds plays a crucial role in generating voltage near the hydrogel [6]. Namely, it is the charge separation that generates diffusion (or liquid junction) potential within the aqueous solution [15,16]. For example, when atmospheric CO_2 dissolves in an aqueous solution, it dissociates into H^+ and HCO_3^- ions. Charge separation within the solution occurs due to the distinct diffusion rates of the dissolved ions (with a diffusivity of $9.3 \times 10^{-9} m^2 s^{-1}$ for H^+ ions and $1.2 \times 10^{-9} m^2 s^{-1}$ for HCO_3^- ions). As rapidly diffusing H^+ move in a specific direction due to the chemical gradient (out of equilibrium conditions) following them counterions (HCO_3^-) are left behind and the ionic charges become physically separated in space [15]. Charge separation translates into electric potential difference - junction potential.

Living cells are subjected to local chemical gradients, including those generated by fast diffusing protons and their slower counterions. Therefore, local charge separation at the cell interface (next to, but not necessarily across the membrane), accompanied by voltage generation, can be expected. Recent studies have recognized the presence of voltage beyond the cell membrane, but only within a few nanometers of the region adjacent to red blood cells, and have shown its close relation to their membrane potential [17,18]. This suggests that a cell's membrane potential may include an extracellular voltage component that exists away from the cell membrane, prompting us to examine the membrane potential of a cell from a different perspective. The voltage near the red blood cells was described as an electrical double layer (EDL) [18]. However, there is a substantial difference in the size between the EDL and the depletion zone having a voltage gradient adjacent to the gel surface. The depletion zone is larger by three orders of magnitude compared to EDL. Additionally, the behavior of the voltage within the depletion zone is completely different from that of the EDL in response to the external modifications in the ionic concentration of the bulk. The thickness of the depletion zone and its voltage increase with increase in ion concentration of the solution [6], whereas the EDL exhibits the exact opposite behavior [19]. In this work, we aim to explore the existence of extracellular voltage in living system and its behavior toward contributing to the cell membrane potential. We use *Chara globularis* as our experimental model. *Chara* is widely utilized as a model for electrophysiological measurements due to its large single-cell size and ease of manipulation [20–23]. Membrane potential of *Chara* species has been known for many decades, including its responses to environmental modifications such as changes in light/dark conditions, pH, and salinity of the extracellular solution [20,24–29]. Despite the extensive studies on *Chara*, none of them have mentioned extracellular voltage next to *Chara* cells.

In our previous work on hydrogel, we demonstrated that the voltage near the hydrogel can be modulated by external stimuli, such as CO_2 [6]. CO_2 as an external stimulant may possibly have an impact on the membrane potential of cells. For example, proliferative cells such as embryos and tumors always experience a higher extracellular CO_2 concentration than other cells and tend to be depolarized compared to terminally differentiated cells [30–33]. The apparent correlation between cell function, its membrane potential and microenvironment, brings the idea about possible bioelectrical modification of cell's behavior by means of modulating chemistry of its environment [34]. Therefore, we examine whether an elevated level of CO_2 is merely present in the cell's surrounding or it is also causing the cell's depolarization. We aim to determine whether the cell's depolarization, if induced by increased CO_2 level, is dependent on the extracellular voltage present adjacent to the cell. To achieve this, our study aims to accomplish the following: (i) assess the feasibility of manipulating extracellular voltage using external CO_2 in an algal cell model system, and (ii) investigate the influence of changes in extracellular and intracellular CO_2 concentrations on the cell's membrane potential in relation to extracellular voltage.

2. Materials and methods

2.1. Sample preparation

Freshwater green algae (*Chara globularis*) were cultivated in an aquarium. The soil used for algae cultivation was collected from a natural lake. Appropriate light conditions (1000–1450 lm, FLUVAL Plant 3.0) were provided in a 10:14 h (light: dark) cycle at room temperature (22 °C). A healthy sample was obtained by cutting a portion of the algae, including the cortex, and internodal (axial, branch, and non-corticated) cells (Fig. S1). The extracted samples were rinsed two to three times with artificial pond water (APW, 0.1 mM NaCl, 0.1 mM KCl, and 0.1 mM $CaCl_2$, adjusted to pH 7.3 with 0.5 M $NaHCO_3$) to effectively remove contaminants. All chemicals used were purchased from Sigma Aldrich (Germany). KCl (Lot: K52082136 115), NaCl (Lot: K52782804 134), $CaCl_2$ *$2H_2O$ (Lot: A1756882 205), $NaHCO_3$ (Lot: K52580129 136). The cleaned algae sample was then immobilized on a glass bottom plastic Petri dish (35 mm, Ibidi GmbH, Germany) using thin plastic wires and curable silicone adhesive. The Petri dish containing the immobilized sample was filled with 3 mL of APW and allowed to stabilize at room temperature for two to three hours. This stabilization minimizes the stress on the sample caused by the extraction process. Following the stabilization phase, the sample was used for electrophysiological measurements.

2.2. Fabrication of glass microelectrode

Borosilicate glass capillaries with filaments (OD = 1.2 mm, ID = 0.68 mm, length = 75 mm) (World Precision Instruments (WPI), USA) were used for microelectrode fabrication. The process involved pulling clean glass capillaries using a micropipette puller (PUL - 1000, WPI, USA) in a looped program (heat index: 390, force: 250 g, distance: 0.60 mm, delay: 100). The diameter of the microelectrode tip was (1 to 2) μm. The pulled microelectrode was filled with 3 M KCl solution saturated with silver chloride (# 102545885, Source – BCCJ4878, Sigma Aldrich, Germany). The filled microelectrode was then carefully inserted into a microelectrode holder (PEL, WPI, USA) prefilled with 3 M KCl, ensuring the absence of air bubbles.

2.3. Measurement of cellular voltages

APW (pH 7.3) was used as the conducting medium for all experiments performed in this study. The immobilized, unstressed sample was positioned on the stage of an inverted microscope (Nikon ECLIPSE Ti), with an Ag/AgCl electrode immersed in the bulk solution serving as a reference electrode. An electrode holder containing a glass microelectrode filled with KCl was attached to a potential measurement probe connected to a low-noise dual-channel differential electrometer (model FD-223a, WPI, USA). The entire experimental setup was placed on an optical table within a Faraday cage to shield it from external mechanical vibrations and electrical interference. Prior to measuring the cell membrane potential, the potential difference (offset voltage) relative to the reference electrode was set to zero. The measurement of the membrane potential of the algal cells was carried out under microscope light during the day at room temperature. To measure the extracellular voltage, the reference electrode was placed in the bulk solution while the microelectrode tip was carefully positioned near the cell surface with the help of the micromanipulator (Luigs & Neumann GmbH, Germany) (Fig. S6A). To assess the cell membrane potential, the microelectrode tip was carefully inserted into the cortex and internodal cells using the micromanipulator (Fig. S6B). LabScribe software (from iWorx, version 4.322) was used to display and record the potential values as waveforms (potential vs. time traces). Advanced Research software (NIS Elements, v 5.01) was used to visualize the microelectrode and live algal cells during potential recording. Glass microelectrodes may be sensitive to pH. Therefore, additional experiments were performed in the APW at pH 7.3

regulated by a pH buffer (5 mM HEPES (Lot: RNBK6522, Sigma Aldrich) [35]) in order to verify that the measurements made in the unbuffered APW were not affected by the possible pH sensitivity of the electrodes.

2.4. Effect of CO_2, HCl, and KCl

Experiments to verify the effect of metabolic activities (dark respiration and photosynthesis) on the membrane potential of algal cells were carried out in the light/dark conditions, using a microscope lamp as a light source. The darkness increases the concentration of intracellular CO_2 due to the dark respiration of the cell, while the light decreases the intracellular CO_2 due to photosynthesis. Experiments to verify the influence of extracellular CO_2 on cellular voltages of algae were carried out in both dark and light-treated cells by introducing CO_2 into the bulk solution containing immobilized samples. For this purpose, compressed CO_2 from a cylinder was supplied via a glass micro nozzle with a tip diameter of (10 to 15) μm at a pressure of (0.25–0.3) bar. The CO_2 concentration in the bulk solution was increased above its level in the APW in equilibrium with atmospheric CO_2. The concentration of dissolved CO_2 in the bulk solution was quantified by pH measurements (a change in pH from 7.3 to 6.3 indicated saturation of APW with CO_2). The effect of pH change, as the one induced in response to CO_2 influx, on cell membrane potential and extracellular voltage, was verified by reducing the pH of the solution from 7.3 to 6.3 using HCl. Further, to confirm that the change in measured extracellular voltage is not the effect of change in pH of the bulk solution by additional CO_2, the measurement of extracellular voltage and its alteration by additional CO_2 was performed in the presence of a pH buffer in APW. While measuring the changes in extracellular voltage in response to additional CO_2, we placed an additional electrode away from the cell within the bulk, along with the one near the cell, and measured voltage with respect to the reference electrode (Fig. S6C). We observed a change in voltage upon an increase in extracellular CO_2 concentration from the electrode near the cell and no change in voltage from the other electrode, which was in the bulk. Experiments to verify the effect of KCl on the cellular voltages were conducted by dissolving (0.2, 0.3, 0.4, 0.5) mM KCl (data not shown) in APW containing the algal sample. 0.3 mM concentration of KCl was selected in this study because it has induced the same degree of depolarization as additional CO_2 in APW when measured with microelectrodes.

2.5. Measurement of the width of the extracellular voltage zone and its visualization

The width of the extracellular voltage zone was measured using microelectrodes and a micromanipulator. As the electrode was brought closer to the algal cell, the point at which the voltage drop occurred indicated the boundary of the zone. The zone width was determined by measuring the distance the electrode moved from the boundary of the zone until it made contact with the algal cell wall. The extension of the zone in the vicinity of healthy, naturally or manually damaged internodal and spine cells was visualized by exclusion of microspheres. For that purpose, a microsphere suspension was prepared by diluting 50 μL (equivalent to 1 drop) of uncharged, non-functionalized polystyrene microsphere solution (1.0 μm; analytical standard; 89,904; Sigma Aldrich) in 15 mL APW. Algal samples immobilized on 35 mm glass-bottomed Petri dishes were immersed in 3 mL of the suspension, and formation of the zones void of microspheres adjacent to algal cells was observed under the microscope. Additionally, the zone of extracellular voltage near algal cells was observed with the use of smaller microspheres (0.5 μm; analytical standard; Cat# 19507–5; Polysciences, Inc., Germany). The reason for using smaller microspheres was that small ions can be excluded to a greater distance by the same magnitude of voltage near the surface compared to large charged particles [36]. Therefore, smaller microspheres were employed to examine the particle exclusion ability of the extracellular voltage.

2.6. Membrane potential observation using voltage-sensitive dye

The voltage-sensitive dye $DiBAC_4(3)$ (bis-(1, 3-dibutylbarbituric acid) trimethine oxonol) (Lot: MKCQ7455, Sigma Aldrich, Germany) was used to observe the changes in membrane potential induced by CO_2 and KCl. An increase in fluorescence intensity compared to the control sample (not treated with CO_2 or KCl) indicates cell depolarization, while a decrease in fluorescence indicates hyperpolarization [37,38]. $DiBAC_4(3)$ powder was dissolved in 70% ethanol at a concentration of 1 mg/mL and then diluted (1:10) in deionized water to a concentration of 100 μg/mL. The resulting dye solution was further diluted (1:10) in APW (pH 7.3) to give a final dye concentration of 10 μg/mL. Effect of CO_2 was verified by incubating the samples with the dye for 30 min under 5% of CO_2 inside the incubator at room temperature in the dark. To observe the effect of KCl, the samples were incubated with the dye solution containing (0.1, 0.2, 0.3, 0.4, 0.5) mM KCl for 30 min at room temperature in the dark (Fig. S4). Samples in the presence of CO_2 and also with 0.3 mM KCl were imaged using an inverted microscope (ZEISS, Germany) with the fluorescence imaging in the dark at room temperature. The intensity values of the fluorescence were estimated by plotting histograms for the selected area on algae cell's image using ZEN (V3.6) image analysis software. The area for plotting intensity histogram was selected as large as possible within the single cell using rectangular tool from the analysis software.

3. Results and discussion

3.1. Extracellular voltage and membrane potential of algal cells

Extracellular and cytoplasmic modifications, such as changes in ionic concentration, can influence the membrane potential of living cells [39,40]. To explore the changes in the cell's membrane potential in response to extracellular and intracellular modifications, we have used algal cells (*Chara globularis*) as our experimental model system, and employed the microelectrode technique for measuring cellular voltages. The resting membrane potentials (V_m) of internodal (a: axial, b: branch, and c: non-corticated) (Fig. S1 a, b, and c) cells measured against artificial pond water (pH 7.3) as a reference under microscope light during the day were as follows: a: (-184.52 ± 15.66) mV, b: (-180.20 ± 13.16) mV, and c: (-189.28 ± 12.52) mV (Fig. 1). These measured membrane potentials are in agreement with previously reported values for *Chara* cells [26,41–48]. The cortex cells (Fig. S1 d) of *C. globularis* exhibited a lower membrane potential of (-88.68 ± 6.09) mV (Fig. 1). To the best of our knowledge, this is the first report of the membrane potential observed in cortex cells that show very similar ultrastructure, but are smaller in volume in relation to the internodal cells they surround [49]. It has been suggested that cell volume is directly proportional to the concentration of impermeable intracellular anions, including anionic metabolites, and that these anions are among the factors that determine membrane potential of a cell [50,51]. An augmented metabolic rate in a cell raises the concentration of impermeable anions, leading to an increase in both the negative membrane potential and cell volume [52]. Therefore, cell metabolism, cell voltage, and cell volume are interrelated. Thus, less negative membrane potential of the cortex cells, correlating with their smaller volume, may reflect their lower metabolic activity. Further in this work we will show experimental evidence supporting notion of different metabolic rates of internodal and cortex cells.

During the measurement of the algal cell's membrane potential, as we were slowly approaching the cell with the microelectrode, a negative voltage was observed at a distance of (4.67 ± 1.21) μm from the cell wall with reference to the bulk solution (Fig. 1, inset). A gradient of negative voltage was recorded throughout this micron-sized region, which we refer to as the zone of extracellular voltage (ZEV) or simply "the zone". At the immediate vicinity of the cell wall, a maximum negative voltage of (-18.04 ± 1.99) mV was observed (Fig. 1, inset). The voltage of

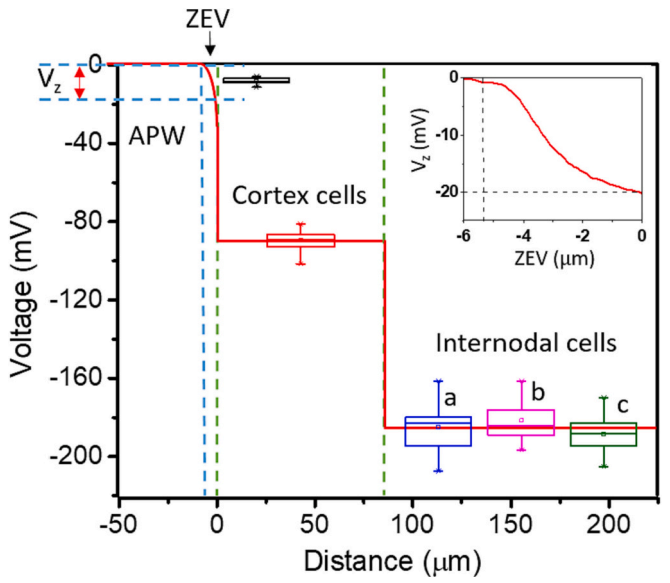

Fig. 1. Extracellular voltage and membrane potential of algal cells: The schematic illustrates the typical trace for extracellular voltage (V_z), and membrane potential at the cortex and internodal cell as a function of distance and the inset represents a zoomed-in view of the V_z at the zone of extracellular voltage (ZEV). Artificial pond water (APW) was the reference solution for all measured voltages. The boxes within the schematic show measured values of extracellular voltage, membrane potential for cortex cells, and internodal (a: axial, b: branch, and c: non-corticated) cells ($N = 25$ each).

(−18.67 ± 1.51) mV was measured at a distance of (4.83 ± 0.75) μm from the cell wall, even in the presence of a pH buffer in APW. The similarity in values of V_z and the width of the zone, both with and without the presence of a buffer in APW, suggests that the recorded voltage and the expanded zone were not influenced by changes in pH near the cell wall or within the bulk. Notably, the voltage gradient persisted despite the absence of any physical barrier between the zone and the bulk solution. We are reporting the existence of the extracellular voltage (V_z) phenomenon in algal cells for the first time. The presence of this zone of extracellular voltage indicates a localized electrochemical environment near the cell membrane/wall. This suggests that there is an electric potential beyond the cell membrane that must be considered when defining the membrane potential of a cell.

In order to understand the effect of the extracellular voltage on the cell membrane potential, it is necessary to consider the way in which the potential is actually measured. In our experiments, the potential difference is measured between a reference electrode placed in the bulk solution and the measuring electrode positioned either inside the cell or immediately outside it. Therefore, any changes induced in the cell's immediate environment, on the way of charge passage from the cell interior or its interfacial zone to the reference electrode [53], will necessarily affect the readings on both intracellular and extracellular electrodes relative to the reference. In the following sections, we will demonstrate the effect of an increase in ion concentration within the cell interior and exterior (induced by internal or external stimulations) on the zone of extracellular voltage and its correlation with the cell's membrane potential.

3.2. Effect of external and internal CO_2 on the extracellular voltage (V_z) and its influence on the membrane potential (V_m)

3.2.1. Effect of external CO_2

In our recent work, an interfacial zone, similar to the zone of extracellular voltage, but present near the charged hydrogel, was shown to be affected by CO_2 [6]. When a gradient of CO_2 was imposed between the gel interior and its surrounding solution, the size and the voltage of this zone became larger and more negative respectively. The mechanism of CO_2 action on increasing the negative voltage near the gel surface is described in our previous work [6]. In short, the voltage zone was enlarged due to charge separation (H^+ and HCO_3^- dissociated from CO_2) at the gel/water interface, driven by electrical and chemical forces that contribute to the directional movement of H^+ and HCO_3^- ions. H^+ ions are attracted to, while HCO_3^- ions are repelled from, the gel surface with its fixed negative charges. To verify this phenomenon in a living system, we introduced CO_2 into the bulk solution containing algal cells to manipulate the extracellular voltage (V_z). The goal was to explore the impact of changes in V_z on the cell's membrane potential, with the aim of understanding the correlation between them.

The increased CO_2 concentration in the bulk hyperpolarized the zone of extracellular voltage and depolarized the internodal cell. The changes in the extracellular voltage (ΔV_z) and membrane potential (ΔV_m) were (−15.91 ± 3.06) mV and (+16.84 ± 3.92) mV respectively (Fig. 2A, B). Conversely, upon reducing external CO_2 concentration to the one in equilibrium with atmospheric CO_2, the V_z and V_m returned to the initial values as in the resting condition (Fig. 2A, B). A lower magnitude of change in membrane potential of (+7.06 ± 3.08) mV, indicating less depolarization, was observed in cortex cells compared to internodal cells in response to an increase in external CO_2 concentration (Fig. 2C). Similar to the reaction of internodal cells, cortex cells responded immediately to the elevated extracellular CO_2 concentration; however, they took a longer time to reach the steady membrane potential value compared to the response of internodal cells (Fig. 2C). These measurements were performed for multiple cycles of increased and reduced concentration of external CO_2 (Fig. S2 A, B). The magnitude of changes in V_z and V_m is approximately the same, while the direction of changes is opposite (indicated by purple arrows in Fig. 2A and B). This suggests a coupling effect between extracellular voltage and the cell membrane potential in response to our extracellular modifications. This implies that the modulation of extracellular voltage can alter the cell membrane potential indicating the importance of accounting for extracellular voltage in defining the membrane potential of a cell.

Based on our results, it can be concluded that the measured membrane potential of the cell (V_m) encompasses both its internal electrogenic (voltage generated within the cell) (V_i) and extracellular voltage (V_z) components, and alterations in their values contribute to the depolarization or hyperpolarization of the cell. Our results indicate that the internal voltage (V_i) of internodal cells remains constant in response to extracellular modifications (Fig. 3 red dashed line). On the other hand, by adjusting ion concentration inside the internodal cell through light and dark treatments, we change V_i without affecting V_z (within the timeframe of our experiments) (Fig. 3 gold dashed line). This indicates that internal voltage and the extracellular voltage can be independently modified, what is reflected in the overall membrane potential of a cell. Both V_i and V_z emerge as crucial components of the cell membrane potential, with alterations in their values resulting in hyperpolarization or depolarization of the cell. Thus, electric potential difference across the cell membrane (V_m), defining a degree of membrane's polarization, can be represented as $V_m = V_i - V_z$ (Fig. 3). In this context, the smaller change in V_m of the cortex cell than that in V_z (in response to elevated extracellular CO_2 concentration) implies a concomitant change in the intracellular component (V_i) leading to the opposite effect on the net membrane potential. In our case, it suggests an increase in the internal negativity of the cortex cells in response to increased extracellular CO_2 concentration. On the other hand, as observed in internodal cells, the same in magnitude (but opposite in sign) concurrent changes of V_z and V_m imply that intracellular component (V_i) remains virtually unchanged in response to extracellular CO_2 (Fig. 3). The changes in voltages of internodal cells, cortex cells, and the zone of extracellular voltage (ZEV) in response to internal and extracellular modifications are summarized in Table S1.

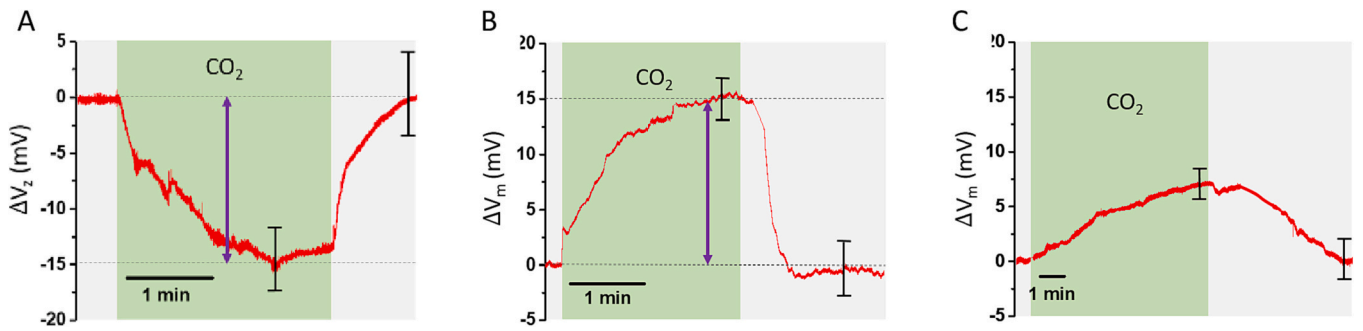

Fig. 2. Effect of extracellular CO_2 on extracellular voltage and membrane potential of algae: The graphs show the change in voltage (ΔV_z) and membrane potential (ΔV_m) in response to alternating increase (higher concentration than atmospheric CO_2) and reduced (in equilibrium with atmospheric CO_2) concentration of extracellular CO_2 for the zone of extracellular voltage (A), internodal (B), and cortex cells (C). The error bars in all the graphs represent the standard deviation of change in voltage values ($N = 4$).

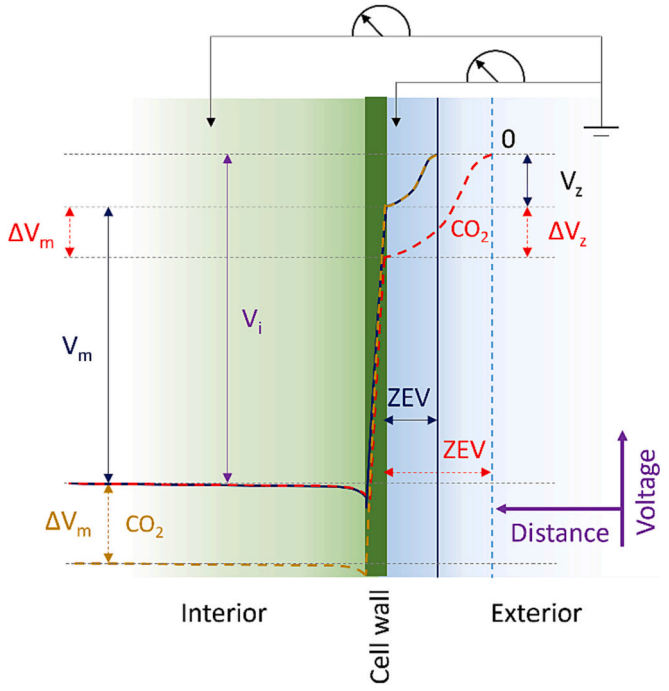

Fig. 3. Two-point concept of voltage measurement: Schematic representation of variation of the electrical potential difference (V_m) across the cell wall. $V_m = V_i - V_z$ represents the resting membrane potential (dark blue solid curve). The change in voltage (ΔV_z and ΔV_m) in response to elevated concentrations of extracellular CO_2 (red dashed curve) and intracellular CO_2 (gold dashed curve) are shown in exterior and interior of the cell, respectively. The zone of extracellular voltage (ZEV) is shown for the resting state (dark blue solid line) and in response to increased extracellular CO_2 concentration (blue dashed line). (For interpretation of the references to colour in this figure legend, the reader is referred to the web version of this article.)

3.2.2. *Effect of internal CO_2*

Cells were subjected to alternating periods of darkness and white light to explore their responses to changes in internal CO_2 concentration (Fig. S3). During the dark treatment, the cells undergo metabolic activities such as dark respiration, which increases the internal CO_2 concentration [54–56], while photosynthesis in the light reduces it [57,58]. Both internodal and cortex cells were hyperpolarized in response to the dark treatment. The change in membrane potential was (-31.82 ± 5.72) mV for internodal cells and (-9.05 ± 2.54) mV for cortex cells. Conversely, the cells depolarized and returned to their initial values upon illumination (Fig. 4A, B). Cortex cells took longer time to reach a steady membrane potential value in response to the dark and light treatments compared to the response of internodal cells (Fig. 4B). The smaller change in membrane potential of cortex cells compared to internodal cells and the longer time to reach a steady state in response to dark and light treatments suggest a slower metabolic rate of the cortex cells.

The extracellular voltage remained unchanged in response to the dark and light treatments, suggesting that the extracellular space is not reacting to the changes induced by the cell's metabolic activities (photosynthesis and respiration) within the timeframe of the experiments. This indicates that changes in intracellular CO_2 concentration modulate cell membrane potential without affecting extracellular voltage. On the other hand, variations in the extracellular CO_2 concentration affect both, membrane (V_m) and extracellular potentials. Changes in extracellular environment should affect the measurement of V_z. At the same time, intracellular changes proceeding without immediate electrogenic ion exchange with the environment, will not affect the reading between the electrode external to the cell and the reference one located further in the bulk solution (Fig. 3). Regarding the mechanism of negativity increase by additional CO_2, as induced both internally and externally (Fig. 2A, 4A), one has to consider the direction of the CO_2 concentration gradient and its interactions with barriers to cross: membrane and/or cell wall. Dark respiration increases the concentration of intracellular CO_2; prompting CO_2 outflow, while externally increased CO_2 concentration directs CO_2 inwardly to the cell. As explained in detail in our previous work [6], the movement of both H^+ and HCO_3^- ions in a specific direction (driven by chemical or electrical gradient), but at different diffusion rates, can lead to their separation near the cell wall/membrane. The separation of charges within the solution result in the generation of voltage. This separation of charges is then further supported by their interactions with a selectively permeable barrier that accommodates cations (due to its fixed negative charges), but repels anions. Such charge separation near the cell wall is expected to cause the negative extracellular voltage to increase in reference to the bulk solution (in a manner alike to the one near gels [6]). In response to increased internal CO_2 (dark treatment), a similar mechanism may act within the cell to increase internal negativity. In fact, such approach to membrane potential generation is corroborated by other studies showing contribution of selective ion partitioning, occurring independently at either side of the membrane, to the outcome voltage [59,60]. Selective, transient localization of protons, in particular, and its effect on induction of membrane polarization is also extensively discussed in a series of work by Lee [61–64].

3.2.3. *Combined effect of both external and internal CO_2*

Cells were further treated with dark and light conditions in the presence of a higher concentration of external CO_2 to understand the combined effect of both internal and external CO_2 on their membrane potential. The measurement began with an increased external CO_2

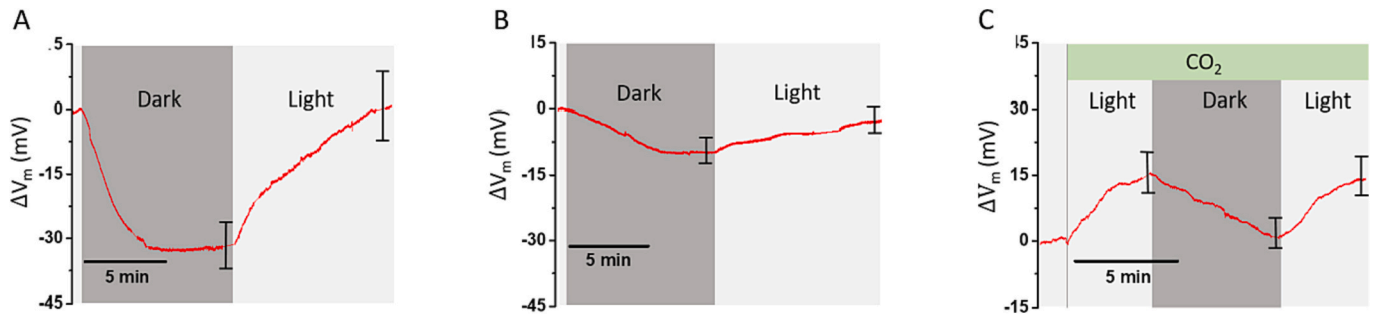

Fig. 4. Effect of intracellular and extracellular CO_2 on the membrane potential of algae: The graphs show the change in membrane potential (ΔV_m) in response to alternating dark and light treatments for internodal (A) and cortex cells (B) and in response to alternating dark and light treatments in the presence of increased concentration of extracellular CO_2 for internodal cells (C). The error bars in all the graphs represent the standard deviation of change in potential values ($N = 5$).

concentration, which depolarized the cell by (+16.33 ± 3.06) mV (Fig. 4C). Subsequent treatment with the darkness hyperpolarized the cell by (−14.33 ± 3.51) mV, bringing its potential back to a more negative value (Fig. 4C). Upon illuminating the cells, the membrane potential returned to a less negative value as it was induced by increased extracellular CO_2. The change in potential values resulting from the combined higher concentration of external CO_2 and the dark treatment was approximately half the value compared to the potential change by the dark treatment alone (in the absence of additional CO_2) (Fig. 4A). This is because the changes in membrane potential caused by external and internal CO_2 act in opposite directions. Thus, the CO_2 in the beginning of the experiment had already depolarized the cell by (+16.33 ± 3.06) mV (Fig, 4C), compensating for the change in membrane potential that was anticipated to be induced by the dark treatment alone. This indicates that the change in cell membrane potential occurs due to an additive effect of both external and internal changes in CO_2 concentrations. The same magnitude and sign of change in response to external CO_2 in dark and in light indicates that the immediate effect of external CO_2 is not related to the metabolic activities of a cell.

3.3. *Effect of external stimuli on the zone of extracellular voltage*

An increase in the concentration of CO_2 in the bulk solution altered the solution pH from 7.3 to 6.3. To verify whether the increase in

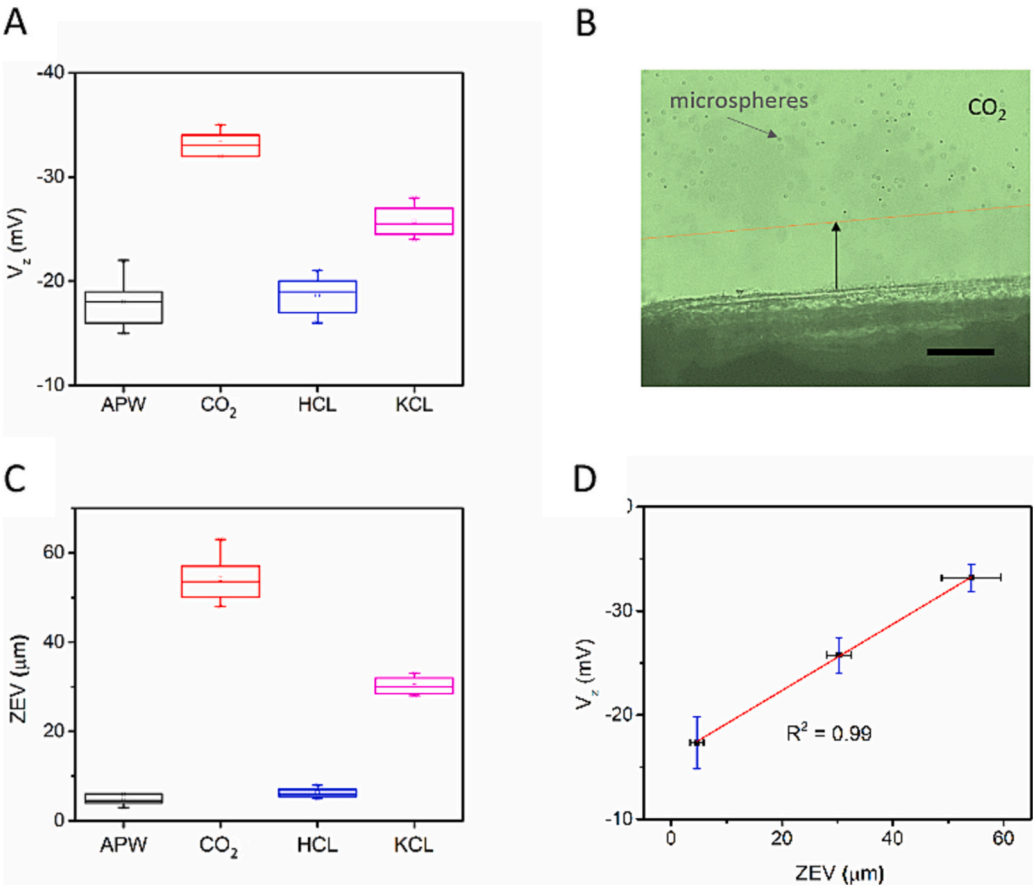

Fig. 5. Effect of external stimuli on the zone of extracellular voltage: A microscopic image shows the expanded zone of extracellular voltage (ZEV) upon influx of extracellular CO_2, observed with the help of microspheres (A). Box plots show the measured values of V_z (B) and the width of the zones (C) near the cell wall in APW (pH 7.3), APW + external CO_2 (pH 6.3), APW + 0.5 µM HCl (pH 6.3), and APW + 0.3 mM KCl (pH 7.3) respectively (B and C) ($N = 5$). Linear dependence of the size of the zone of extracellular voltage on V_Z (D). Scale bar in the image is 50 µm.

negative extracellular voltage was simply due to the change in external solution pH or it is the effect of charge separation at the cell membrane/wall as a result of increased concentration of external CO_2, measurements of V_z were taken at pH 6.3, adjusted using HCl. The cell membrane potential did not change in response to altered solution pH and it was found that V_z was remaining unchanged (Fig. 5A). This indicates that the increase in V_z was not the effect of a change in solution pH induced by CO_2 but as it was described previously (section 3.2), the increase in negative voltage could be due to the charge separation at the zone/bulk interface generated by ions with distinct diffusion rates (H^+ and HCO_3^- from CO_2 in water [6]). At higher negative V_z, resulting from an increased concentration of external CO_2 the increase in the width of the zone of extracellular voltage (ZEV) was observed. Since the ZEV is known to exclude colloids [6,65], polymer microspheres were used to visualize the zone enlargement (Movie S1). Additional CO_2 raised a maximum negative extracellular voltage recorded near the cell wall to (−33.20 ± 1.30) mV and expanded the zone to a distance of (54.17 ± 5.34) μm from the cell wall (Fig. 5A, B, and C). To further confirm that the change in zone parameters (zone width and voltage) was due to an enhanced ion exchange across the cell membrane/wall, the cells were treated with another depolarizing agent, which is KCl. Increasing the concentration of KCl in the external solution always depolarizes algal cell [66,67]. We verified that the addition of 0.3 mM KCl in APW induced the same degree of cell depolarization as that induced by external CO_2 in both light and dark conditions. However, the extracellular voltage increased in magnitude to (−25.75 ± 1.71) mV, and the zone extended up to (30.25 ± 2.22) μm in response to an additional 0.3 mM KCl (Fig. 5A, C), the changes being lower than those induced by CO_2. The above results suggest that the charge separation at the cell membrane/wall interface (caused by induced ion concentration gradient near the cell) affects the extracellular voltage and the size of the ZEV. The development of different zone widths near the algal cell wall in response to external stimuli (CO_2 and KCl in our case) is the result of the separation of ionic charges with different diffusion rates across the zone of extracellular voltage [6]. The linear dependence between extracellular voltage and width of the zone was observed (Fig. 5D). The width of the zone and the extracellular voltage differ for various stimuli ((54.17 ± 5.34) μm for CO_2 and (30.25 ± 2.22) μm for KCl), even though they induce the same change in membrane potential of the cell ((+16.84 ± 3.92) mV for CO_2 and (+16.66 ± 1.53) mV for 0.3 mM KCl in this case). In reality, the external stimuli do not actually elicit the same intracellular changes; rather, it is the net effect that remains the same. What we measure as the cell's membrane potential is, in fact, combination of intracellular and extracellular voltages, which confirms our earlier assumptions (Fig. 3).

Additional experiments were conducted to visualize the zone of extracellular voltage near algal cell wall at resting condition using smaller microspheres (diameter: 0.5 μm). Microspheres were excluded to a distance of (5.40 ± 1.14) μm from the cell wall. At the same time, it was not possible to visualize this zone by large microspheres (diameter: 1.0 μm). This implies that the generated voltage was not strong enough to push larger microspheres away from the cell wall, although the voltage gradient could be detected up to (4.67 ± 1.21) μm from the cell wall (Fig. 1 inset). We observed that the smaller particles move to a longer distance than the larger particles for the same voltage change induced by 0.3 mM KCl (Fig. S5). Similar phenomenon was also demonstrated in a study, indicating that small ions can be excluded to a larger distance by a voltage of the same magnitude than charged objects (particles) of a larger mass [36].

3.4. Comparison of V_m measured with microelectrodes and observed with voltage-sensitive dye: The importance of extracellular voltage

As outlined earlier, an increased concentration of both extracellular CO_2 and additional 0.3 mM KCl raised the extracellular voltage near the cell to a more negative value. However, the magnitude of change in extracellular voltage ((−33.20 ± 1.30) mV for extracellular CO_2 and (−25.75 ± 1.71) mV for 0.3 mM KCl) and the zone width ((54.17 ± 5.34) μm for extracellular CO_2 and (30.25 ± 2.22) μm 0.3 mM KCl) in response to additional CO_2 and 0.3 mM KCl were different (Fig. 5A, C). The change in membrane potential in response to an additional 0.3 mM KCl was (+16.66 ± 1.53) mV, virtually the same as in response to increased concentration of CO_2 ((+16.84 ± 3.92) mV), when measured using microelectrodes (indicated by purple arrows in Fig. 6A and B). Yet, when observed by voltage-sensitive dye [$DiBAC_4(3)$] [68–70], respective changes were different for the two depolarizing agents. 0.3 mM KCl reduces internal negativity of the cells more than additional CO_2 (as evidenced by increased fluorescence in the former case, – Fig. 6C and D). However, since the voltage-sensitive dye does not capture extracellular events, the observed net depolarization was likely incomplete. The membrane potential represents the electrical work required to transport ions across the cell membrane [71]. When using electrodes, it becomes necessary to incorporate the extracellular voltage zone within the circuit (Fig. 3). This indicates that the net cell membrane potential measured with respect to the external solution includes the zone existing near the cell wall, suggesting the dependence of cell membrane potential on extracellular voltage. The overall cell depolarization can be shown when extracellular voltages (measured by microelectrodes) are considered in addition to the cell depolarization observed by voltage sensitive dye. That is, (i) additional 0.3 mM KCl induces a higher depolarization (as indicated by higher fluorescence) inside the cell (Fig. 6D) and a lower hyperpolarization of the ZEV (as expressed in the zone width) (Fig. 5A), (ii) additional CO_2 induces a lower depolarization inside the cell (Fig. 6C) and a higher hyperpolarization of the ZEV (Fig. 5A). After considering the effect of extracellular voltage on cell membrane potential along with depolarization observed by fluorescent dye (for both 0.3 mM KCl and additional CO_2), the net depolarization may become equal as it was measured by microelectrode (coupling effect between V_z and V_m) (Fig. 6A and B). This indicates that the extracellular voltage is an important additional component that needs to be taken into account in defining a cell's membrane potential.

Along with the increased fluorescence, a pattern of bright spots was observed in the cells with an additional 0.3 mM KCl, whereas a homogenous pattern of fluorescence with lower intensity was observed in the cells with additional CO_2 (Fig. 6C and D). Additional CO_2 and dark respiration reduce the intracellular pH of the cell [72–75]. The cell's internal buffering system responds to changes in pH to maintain a stable pH level inside the cell. This system operates through the protonation and deprotonation of the protein components within the cell [76]. At low intracellular pH, protonation results in the development of a positive charge on the functional groups of proteins. This phenomenon may cause negatively charged dye molecules to bind to those positively charged protein residues [77,78], resulting in the generation of uniform fluorescence inside the cell. The bright spots observed upon the addition of KCl may possibly be the localized spots, resulting from salt treatment [79].

The results obtained from voltage-sensitive dye provide information only about intracellular changes. The potential values recorded by microelectrodes include the extracellular voltage and provide the net change in both intracellular and extracellular voltage in response to induced modifications. Alterations in the extracellular voltage component may affect cell physiology, as they can influence the exchange of charged metabolites or nutrients into and out of the cell.

3.5. The evolution of the zone of extracellular voltage at the places where ion exchange is enhanced

Apart from the zone of extracellular voltage induced by means of the imposed concentration gradient (with additional CO_2 and KCl) prompting diffusional ion flow toward the cell, the zones were also observed next to the spine and naturally damaged cells (Fig. 7A and B). Spine cells are elongated, finger-like projections that extend from the

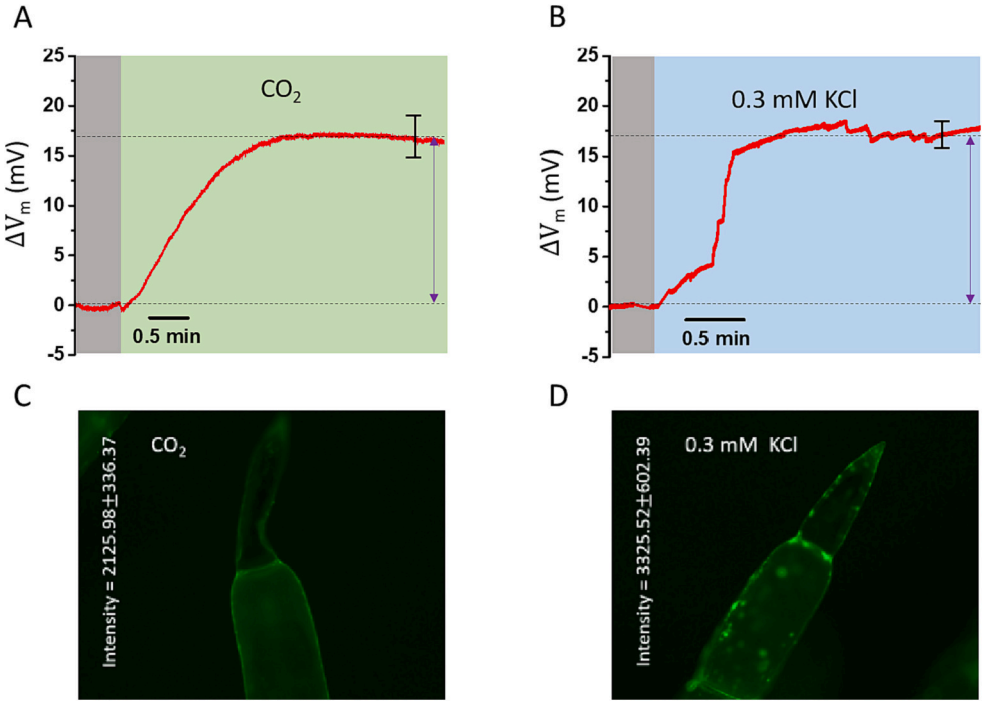

Fig. 6. Comparison of V_m measured with microelectrodes and observed with voltage-sensitive dye: Graphs show the same magnitude of change in membrane potential (ΔV_m) in response to additional 0.3 mM KCl ($N = 3$) and extracellular CO_2 (N = 4) in dark condition (A and B). Microscopic images show the change in fluorescence intensities upon addition of 0.3 mM KCl and extracellular CO_2 (C and D). An increase in fluorescence intensity from the dye indicates the cell depolarization. Conversely, hyperpolarization is indicated by decrease in fluorescence.

internodal cells of many species of algae, including *C. globularis*. These specialized structures may serve for the exchange of ions and nutrients required by the cell [80]. Similarly, there is an enhanced ion exchange next to damaged cells to support healing [81–83].

To verify the mechanism of ion exchange-induced zone formation, already established by us for gels [6], in living cells, algal cells were manually wounded at multiple sites on the cell surface to induce enhanced ion exchange. Within 10 min after wounding, zone enlargement was observed by the exclusion of colloidal particles (1.0 μm) near the wounded sites. The zones expanded to a maximum distance of (80.60 ± 8.02) μm from the cell wall measured with the help of micro electrodes (Fig. 7C, D). An increased negative extracellular voltage of (−42.75 ± 1.71) mV was recorded near the cell wall within these zones (Fig. 7E). These values follow the linear trend as shown earlier (Fig. 5D). The evolved zones were diminished over time (approximately 4 h after the cell was wounded). The wounded cells underwent depolarization from their resting potential value of (−184.52 ± 15.66) mV to (−151.40 ± 12.28) mV. Other studies have also reported a similar depolarization response of algal cells to wounding [43,84–86].

In our previous experiments, we enhanced directional ion diffusion toward the cell membrane/wall of algae by increasing the concentrations of extracellular CO_2 and KCl. This led to an increase in negative extracellular voltage and the zone width (Fig. 2A, 5A – C). The outcomes obtained from cell-wounding experiments also support the idea of zone expansion due to increased ion exchange at the injured sites. All of these results reinforce our expectation of ZEV expansion near surfaces with enhanced ion exchange. The extracellular voltage zone adjacent to wounded cells could potentially act as a protective barrier against pathogens, such as bacteria, viruses, or fungi, due to its ability to exclude colloids and bacteria [65,87–89]. This suggests an unrecognized strategy employed by algae to shield themselves from pathogen intrusion.

4. Conclusions

The existence of extracellular voltage (V_z) adjacent to *Chara* cells, as demonstrated in this work, reveals the extension of a cell's membrane potential (V_m) beyond its membrane. To the best of our knowledge, this work provides the first experimental evidence for the presence of extracellular voltage near the algal cell. We successfully manipulated the extracellular voltage using CO_2 as a stimulant. Modulation of V_z altered V_m, and a coupling effect between them was observed in response to changes in the extracellular CO_2 concentration. Our results suggest that changes in the extracellular environment modifying V_z and resulting in a net change in membrane potential may proceed without affecting intracellular voltage (V_i). In this context, observed cell depolarization, in response to augmented concentration of CO_2 in the extracellular environment, is ascribed to the increase in extracellular negativity that effectively diminishes voltage gradient across the membrane. On the other hand, an increase in intracellular CO_2 (induced by dark treatment) hyperpolarizes the cell by increasing internal negativity and without affecting V_z. These results suggest that the mechanism by which CO_2 increases the negativity of both extracellular and intracellular environments can be the same. A consistent degree of cell depolarization in response to increased extracellular CO_2 concentration in both dark- and light-treated cells further demonstrates that extracellular modifications in algae can influence the cell membrane potential independently of their metabolic activities.

Observations using a voltage-sensitive dye revealed alterations in intracellular voltage exclusively; nevertheless, the cell's membrane potential encompasses both intracellular and extracellular voltages. Therefore, the voltage measured by microelectrodes provides actual changes in membrane potential values that include changes in extracellular voltage in response to induced modifications. This indicates that extracellular voltage represents an essential additional component that contributes to defining the cell's membrane potential and may affect the selective exchange of ions across the cell membrane/wall. Enhanced ion exchange between the cell interior and exterior can increase the magnitude of extracellular voltage and expand the width of the zone of extracellular voltage (ZEV), as evidenced by the evolution of ZEV near the spines and wounded cells. The localized electrochemical

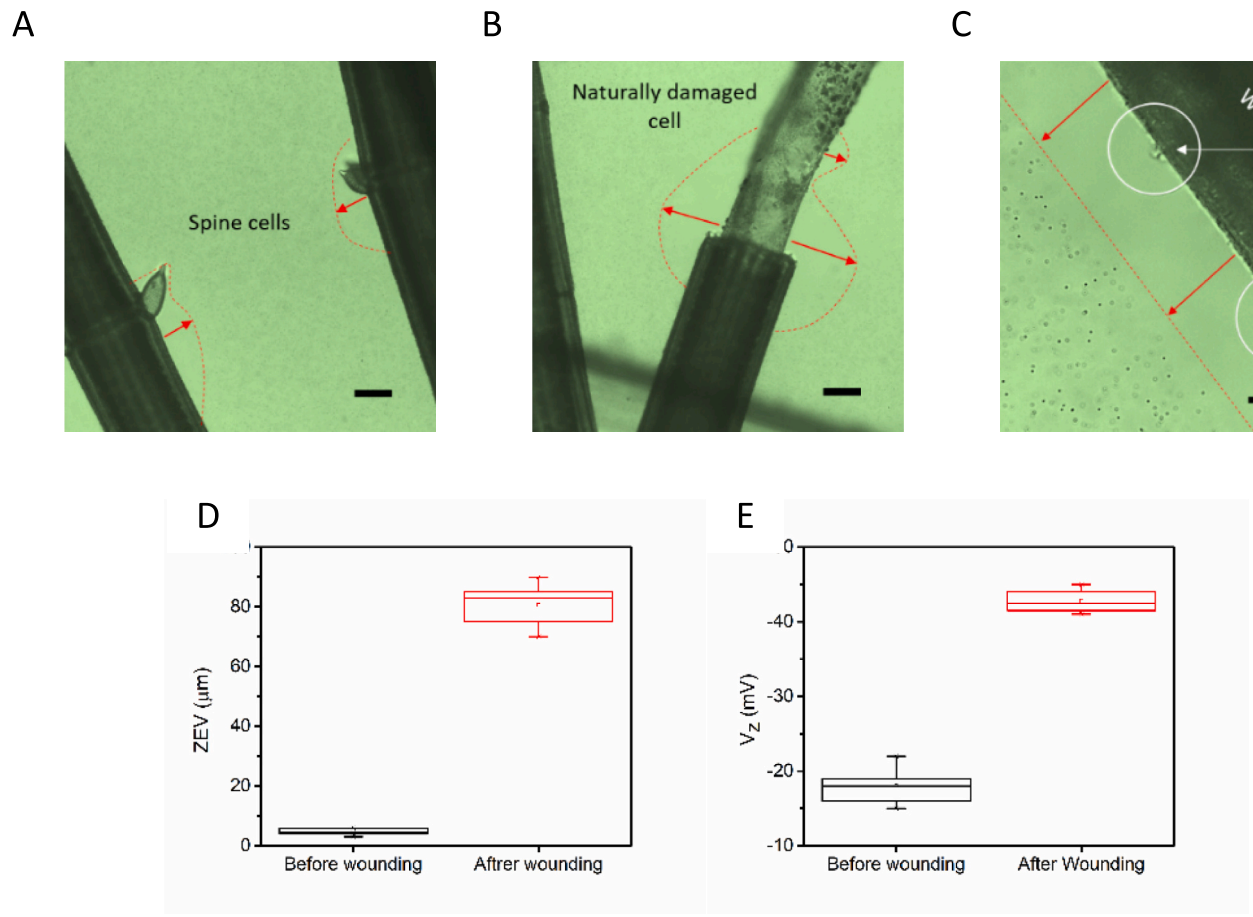

Fig. 7. Evolution of the zone of extracellular voltage near the spine and damaged cells of algae: Microscopic images show the existence of the zones near spine, naturally damaged, and manually wounded cells (A, B, and C). The box plots show the width of the zone of extracellular voltage and V_z near the cells before and after wounding them (D and E) (N = 5). Scale bar in the image A and B is 100 µm and C is 50 µm.

environment near the cells may play a crucial role in various cellular processes, including signal transmission, nutrient uptake, and maintaining cellular homeostasis. Furthermore, the zone of extracellular voltage may act as a protective barrier against pathogens (bacteria, viruses, or fungi) because it has the ability to expel colloids.

Supplementary data to this article can be found online at https://doi.org/10.1016/j.bpc.2024.107199.

Author contributions

M.K. conceptualized and supervised the project. M.M. conducted the laboratory work. M.M., M.K., and S.N. performed the data analysis and interpretations. S.N. supervised laboratory work. M.M., M.K., and S.N. wrote the original manuscript.

Funding

The National Science Centre of Poland under the grant number 2020/38/E/NZ3/00039 funded this work.

CRediT authorship contribution statement

Manohara Mahadeva: Writing – review & editing, Writing – original draft, Methodology, Formal analysis, Data curation. **Sebastian Niestępski:** Writing – review & editing, Writing – original draft, Supervision, Project administration, Methodology, Formal analysis. **Magdalena Kowacz:** Writing – review & editing, Writing – original draft, Supervision, Funding acquisition, Formal analysis, Conceptualization.

Declaration of competing interest

There are no conflicts to declare.

Acknowledgement

We thank Hydroidea Spółka z o.o. spółka Komandytowa Company for providing us the algae sample. We also thank Dr. Krzysztof Witek for supporting us with the fluorescence microscopy.

References

[1] S.A. Kempson, The plasma membrane, membrane transport, and the resting membrane potential and resting Membrana potential, Med. Physiol. Princ. Clin. Med. (2012) 19–36.
[2] D.A. McCormick, Membrane potential and action potential, from Mol. To networks an Introd. to cell, Mol. Neurosci. Third Ed. (2014) 351–376, https://doi.org/10.1016/B978-0-12-397179-1.00012-9.
[3] J. Fels, S.N. Orlov, R. Grygorczyk, The hydrogel nature of mammalian cytoplasm contributes to osmosensing and extracellular pH sensing, Biophys. J. 96 (2009) 4276–4285, https://doi.org/10.1016/j.bpj.2009.02.038.
[4] G. Michel, T. Tonon, D. Scornet, J.M. Cock, B. Kloareg, The cell wall polysaccharide metabolism of the brown alga Ectocarpus siliculosus. Insights into the evolution of extracellular matrix polysaccharides in Eukaryotes, New Phytol. 188 (2010) 82–97, https://doi.org/10.1111/J.1469-8137.2010.03374.X.
[5] M. Kowacz, G.H. Pollack, Cells in new light: ion concentration, voltage, and pressure gradients across a hydrogel membrane, ACS Omega 5 (2020) 21024–21031, https://doi.org/10.1021/acsomega.0c02595.
[6] M. Kowacz, S.R. Withanage, S. Niestępski, Voltage and concentration gradient across membraneless interface generated next to hydrogels: relation to glycocalyx, Soft Matter (2024), https://doi.org/10.1039/D3SM00889D.
[7] D. Florea, S. Musa, J.M.R. Huyghe, H.M. Wyss, Long-range repulsion of colloids driven by ion exchange and diffusiophoresis, Proc. Natl. Acad. Sci. U. S. A. 111

(2014) 6554–6559, https://doi.org/10.1073/PNAS.1322857111/SUPPL_FILE/PNAS.1322857111.SM02.MP4.
[8] B.V. Derjaguin, M.V. Golovanov, On long-range forces of repulsion between biological cells, Prog. Surf. Sci. 40 (1992) 210–217, https://doi.org/10.1016/0079-6816(92)90048-M.
[9] Z. Li, G.H. Pollack, Surface-induced flow: a natural microscopic engine using infrared energy as fuel, Sci. Adv. 6 (2020) 941–949, https://doi.org/10.1126/SCIADV.ABA0941.
[10] J. Ming Zheng, W.C. Chin, E. Khijniak, E. Khijniak, G.H. Pollack, Surfaces and interfacial water: evidence that hydrophilic surfaces have long-range impact, Adv. Colloid Interface Sci. 127 (2006) 19–27, https://doi.org/10.1016/J.CIS.2006.07.002.
[11] J. Ming Zheng, G.H. Pollack, Long-range forces extending from polymer-gel surfaces, Phys. Rev. E 68 (2003) 031408, https://doi.org/10.1103/PhysRevE.68.031408.
[12] A. Sharma, G.H. Pollack, Healthy fats and exclusion-zone size, Food Chem. 316 (2020) 126305, https://doi.org/10.1016/J.FOODCHEM.2020.126305.
[13] B. Chai, H. Yoo, G.H. Pollack, Effect of radiant energy on near-surface water, J. Phys. Chem. B 113 (2009) 13953–13958, https://doi.org/10.1021/JP908163W/ASSET/IMAGES/MEDIUM/JP-2009-08163W_0005.GIF.
[14] R. Pedregal-Cortés, G. Toriz, E. Delgado, G.H. Pollack, Interfacial water and its potential role in the function of sericin against biofouling 35 (2019) 732–741, https://doi.org/10.1080/08927014.2019.1653863.
[15] S. Shin, O. Shardt, P.B. Warren, H.A. Stone, Membraneless water filtration using CO2, Nat. Commun. 8 (2017) 1–6, https://doi.org/10.1038/ncomms15181.
[16] S. Shim, M. Baskaran, E.H. Thai, H.A. Stone, CO2-driven diffusiophoresis and water cleaning: similarity solutions for predicting the exclusion zone in a channel flow, Lab Chip 21 (2021) 3387–3400, https://doi.org/10.1039/D1LC00211B.
[17] M.P. Hughes, C.H. Fry, F.H. Labeed, Cytoplasmic anion/cation imbalances applied across the membrane capacitance may form a significant component of the resting membrane potential of red blood cells, Sci. Rep. 12 (2022) 1–10, https://doi.org/10.1038/s41598-022-19316-z.
[18] M.P. Hughes, E.J. Kruchek, A.D. Beale, S.J. Kitcatt, S. Qureshi, Z.P. Trott, O. Charbonnel, P.A. Agbaje, E.A. Henslee, R.A. Dorey, R. Lewis, F.H. Labeed, Vm-related extracellular potentials observed in red blood cells, Sci. Rep. 11 (2021) 1–13, https://doi.org/10.1038/s41598-021-98102-9.
[19] R. Hatsuki, F. Yujiro, T. Yamamoto, Direct measurement of electric double layer in a nanochannel by electrical impedance spectroscopy, Microfluid. Nanofluid. 14 (2013) 983–988, https://doi.org/10.1007/S10404-012-1105-5/FIGURES/6.
[20] T. Shimmen, T. Mimura, M. Kikuyama, M. Tazawa, Characean Cells as a Tool for Studying Electrophysiological of Plant Cells Characteristics 278, 1994, pp. 263–278.
[21] N. Kamiya, Cytoplasmic streaming in giant algal cells: a historical survey of experimental approaches, Bot. Mag. Tokyo. 99 (1986) 441–467, https://doi.org/10.1007/BF02488723/METRICS.
[22] N. Kamiya, Physical and chemical basis of cytoplasmic streaming 32 (2003) 205–236, https://doi.org/10.1146/ANNUREV.PP.32.060181.001225.
[23] M. Tazawa, T. Shimmen, How characean cells have contributed to the progress of plant membrane biophysics, Funct. Plant Biol. 28 (2001) 523–539, https://doi.org/10.1071/PP01027.
[24] T. Shimmen, M. Tazawa, Demonstration of voltage dependency of light-induced potential change in chara, Plant Cell Physiol. 22 (1981) 807–818.
[25] W.J. Lucas, Mechanism of acquisition of exogenous bicarbonate by internodal cells of Chara corallina, Planta. 156 (1982) 181–192, https://doi.org/10.1007/BF00395434/METRICS.
[26] A. Hope, Ionic relations of cells of Chara Australls X. Effects of bicarbonate ions on electrical properties, Aust. J. Biol. Sci. 18 (1965) 789–802, https://doi.org/10.1071/BI9650789.
[27] F. Baudenbacher, L.E. Fong, G. Thiel, M. Wacke, V. Jazbinsek, J.R. Holzer, A. Stampfl, Z. Trontelj, Intracellular axial current in Chara corallina reflects the altered kinetics of ions in cytoplasm under the influence of light, Biophys. J. 88 (2005) 690–697, https://doi.org/10.1529/biophysj.104.044974.
[28] A.A. Bulychev, N.A. Kamzolkina, Differential effects of plasma membrane electric excitation on H+ fluxes and photosynthesis in characean cells, Bioelectrochemistry. 69 (2006) 209–215, https://doi.org/10.1016/J.BIOELECHEM.2006.03.001.
[29] W.J. Lucas, K. Ogata, Hydroxyl– and bicarbonate-associated transport processes in Chara corallina: studies on the light-dark regulation mechanism, J. Exp. Bot. 36 (1985) 1947–1958, https://doi.org/10.1093/JXB/36.12.1947.
[30] R. Kikuchi, Y. Iwai, T. Tsuji, Y. Watanabe, N. Koyama, K. Yamaguchi, H. Nakamura, K. Aoshiba, Hypercapnic tumor microenvironment confers chemoresistance to lung cancer cells by reprogramming mitochondrial metabolism in vitro, Free Radic. Biol. Med. 134 (2019) 200–214, https://doi.org/10.1016/J.FREERADBIOMED.2019.01.014.
[31] K. Kirkegaard, J.J. Hindkjaer, H.J. Ingerslev, Effect of oxygen concentration on human embryo development evaluated by time-lapse monitoring, Fertil. Steril. 99 (2013) 738–744.e4, https://doi.org/10.1016/J.FERTNSTERT.2012.11.028.
[32] M. Oginuma, P. Moncuquet, F. Xiong, E. Karoly, J. Chal, K. Guevorkian, O. Pourquié, A gradient of glycolytic activity coordinates FGF and Wnt signaling during elongation of the body Axis in Amniote embryos, Dev. Cell 40 (2017) 342–353.e10, https://doi.org/10.1016/J.DEVCEL.2017.02.001.
[33] M. Levin, Molecular bioelectricity in developmental biology: new tools and recent discoveries, BioEssays. 34 (2012) 205–217, https://doi.org/10.1002/BIES.201100136.
[34] S. Sundelacruz, M. Levin, D.L. Kaplan, Role of membrane potential in the regulation of cell proliferation and differentiation, Stem Cell Rev. Reports. 5 (2009) 231–246, https://doi.org/10.1007/s12015-009-9080-2.
[35] Y. Okazaki, M. Tazawa, Y. Moriyama, N. Iwasaki, Bafilomycin inhibits vacuolar pH regulation in a fresh water Charophyte, Chora corallina, Bot. Acta 105 (1992) 421–426, https://doi.org/10.1111/J.1438-8677.1992.TB00323.X.
[36] M. Nooryani, A.M. Benneker, G. Natale, Self-generated exclusion zone in a dead-end pore microfluidic channel, Lab Chip 23 (2023) 2122–2130, https://doi.org/10.1039/D2LC01130A.
[37] K.R. Konrad, R. Hedrich, The use of voltage-sensitive dyes to monitor signal-induced changes in membrane potential–ABA triggered membrane depolarization in guard cells†, Plant J. 55 (2008) 161–173, https://doi.org/10.1111/J.1365-313X.2008.03498.X.
[38] J. Kim, Y. Sasaki, W. Yoshida, N. Kobayashi, A.J. Veloso, K. Kerman, K. Ikebukuro, K. Sode, Rapid cytotoxicity screening platform for amyloid inhibitors using a membrane-potential sensitive fluorescent probe, Anal. Chem. 85 (2013) 185–192, https://doi.org/10.1021/AC302442Q/SUPPL_FILE/AC302442Q_SI_001.PDF.
[39] R.H. Adrian, 658 the effect of internal and external potassium concentration on the membrane potential of frog muscle, J. Physiol. 33 (2024) 63.
[40] A.L. Hodgkin, P. Horowicz, The influence of potassium and chloride ions on the membrane potential of single muscle FIBRES, J. Physiol. 48 (2024) 27–60.
[41] M.J. Beilby, M.A. Bisson, S.C. Schneider, How Characean algae take up needed and excrete unwanted ions – an overview explaining how insights from electrophysiology are useful to understand the ecology of aquatic macrophytes, Aquat. Bot. 181 (2022) 103542, https://doi.org/10.1016/J.AQUABOT.2022.103542.
[42] B.R. Johnson, R.A. Wyttenbach, R. Wayne, R.R. Hoy, Action potentials in a giant algal cell: a comparative approach to mechanisms and evolution of excitability, J. Undergrad. Neurosci. Educ. 1 (2002).
[43] T. Shimmen, Electrical perception of “death message” in Chara: analysis of rapid component and ionic process, Plant Cell Physiol. 43 (2002) 1575–1584, https://doi.org/10.1093/pcp/pcf182.
[44] M.J. Beilby, Multi-scale characean experimental system : from electrophysiology of membrane transporters to cell-to-cell connectivity, Cytoplasmic Streaming and Auxin Metabolism 7 (2016) 1–20, https://doi.org/10.3389/fpls.2016.01052.
[45] M. Tester, Pharmacology of K+ channels in the plasmalemma of the green alga Chara corallina, J. Membr. Biol. 103 (1988) 159–169, https://doi.org/10.1007/BF01870946/METRICS.
[46] M. Tester, M.J. Beilby, T. Shimmen, Electrical characteristics of the tonoplast of Cham corallincr. A study using permeabilised cells, Plant Cell Physiol. 28 (1987) 1555–1568, https://doi.org/10.1093/OXFORDJOURNALS.PCP.A077450.
[47] N.A. Walker, M.J. Beilby, F.A. Smith, Amine uniport at the plasmalemma of charophyte cells: I. Current-voltage curves, saturation kinetics, and effects of unstirred layers, J. Membr. Biol. 49 (1979) 21–55, https://doi.org/10.1007/BF01871038/METRICS.
[48] V.A. Shepherd, P.B. Goodwin, Seasonal patterns of cell-to-cell communication in Chara corallina Klein ex Willd. I. Cell-to-cell communication in vegetative lateral branches during winter and spring, Plant Cell Environ. 15 (1992) 137–150, https://doi.org/10.1111/J.1365-3040.1992.TB01468.X.
[49] S. Balakrishnan, R. Govindarajan, L.J. Groves, L. Ruprecht, Ultrastructural studies on the corticating filament of Chara zeylanica, Environ. Exp. Biol. 18 (2020) 169–174, https://doi.org/10.22364/eeb.18.17.
[50] A.R. Kay, How cells can control their size by pumping ions, Front. Cell Dev. Biol. 5 (2017) 1–14, https://doi.org/10.3389/fcell.2017.00041.
[51] A.R. Kay, M.P. Blaustein, Evolution of our understanding of cell volume regulation by the pump-leak mechanism, J. Gen. Physiol. 151 (2019) 407–416, https://doi.org/10.1085/JGP.201812274.
[52] E. Jakobsson, Interactions of cell volume, membrane potential, and membrane transport parameters, Am. J. Physiol. - Cell Physiol. 7 (1980), https://doi.org/10.1152/AJPCELL.1980.238.5.C196.
[53] R.L. Veech, M.T. King, R. Pawlosky, P.C. Bradshaw, W. Curtis, Relationship between inorganic ion distribution, resting membrane potential, and the ΔG’ of ATP hydrolysis: a new paradigm, FASEB J. 33 (2019) 13126–13130, https://doi.org/10.1096/fj.201901942R.
[54] J.A. Bunce, Three new methods indicate that CO2concentration affects plant respiration in the range relevant to global change, AoB Plants. 13 (2021) 2–6, https://doi.org/10.1093/aobpla/plab004.
[55] H. Pfanz, G. Aschan, R. Langenfeld-Heyser, C. Wittmann, M. Loose, Ecology and ecophysiology of tree stems: Corticular and wood photosynthesis, Naturwissenschaften. 89 (2002) 147–162, https://doi.org/10.1007/s00114-002-0309-z.
[56] S. Lautner, M. Stummer, R. Matyssek, J. Fromm, T.E.E. Grams, Involvement of respiratory processes in the transient knockout of net CO2 uptake in Mimosa pudica upon heat stimulation, Plant Cell Environ. 37 (2014) 254–260, https://doi.org/10.1111/pce.12150.
[57] R. Villar, A.A. Held, J. Merino, Comparison of methods to estimate dark respiration in the light in leaves of two woody species, Plant Physiol. 105 (1994) 167–172, https://doi.org/10.1104/pp.105.1.167.
[58] D.D.E. Beer, A.W.D. Larkum, Photosynthesis and calcification in the calcifying algae, 2001, pp. 1209–1217.
[59] H. Tamagawa, B. Delalande, The membrane potential arising from the adsorption of ions at the biological interface, Biol. Futur. 73 (2022) 455–471, https://doi.org/10.1007/s42977-022-00139-y.
[60] T. Heimburg, Comment on Tamagawa and Ikeda’s reinterpretation of the Goldman–Hodgkin–Katz equation: are transmembrane potentials caused by

polarization? Eur. Biophys. J. 47 (2018) 865–867, https://doi.org/10.1007/s00249-018-1335-x.
[61] J.W. Lee, Transient protonic capacitor: Explaining the bacteriorhodopsin membrane experiment of Heberle et al. 1994, Biophys. Chem. 300 (2023) 107072, https://doi.org/10.1016/j.bpc.2023.107072.
[62] J.W. Lee, Electrostatically localized proton bioenergetics: better understanding membrane potential, Heliyon. 5 (2019) e01961, https://doi.org/10.1016/J.HELIYON.2019.E01961.
[63] J.W. Lee, Mitochondrial energetics with transmembrane electrostatically localized protons: do we have a thermotrophic feature? Sci. Reports 111 (11) (2021) 1–13, https://doi.org/10.1038/s41598-021-93853-x.
[64] J.W. Lee, Protonic conductor: better understanding neural resting and action potential, J. Neurophysiol. 124 (2020) 1029–1044, https://doi.org/10.1152/JN.00281.2020/ASSET/IMAGES/LARGE/Z9K0092055900005.JPEG.
[65] J. Zheng, G.H. Pollack, Solute exclusion and potential distribution near hydrophilic surfaces, Water Cell (2006) 165–174, https://doi.org/10.1007/1-4020-4927-7_8/COVER.
[66] T. Shimmen, Electrophysiology in mechanosensing and wounding response, plant Electrophysiol. Theory, Methods. (2006) 319–339, https://doi.org/10.1007/978-3-540-37843-3_14/COVER.
[67] D.W. Keifer, W.J. Lucas, Potassium channels in Chara corallina control and interaction with the electrogenic H+ pump, Plant Physiol. 69 (1982) 781–788, https://doi.org/10.1104/PP.69.4.781.
[68] D.F. Baxter, M. Kirk, A.F. Garcia, A. Raimondi, M.H. Holmqvist, K.K. Flint, D. Bojanic, P.S. Distefano, R. Curtis, Y. Xie, A Novel Membrane Potential-Sensitive Fluorescent Dye Improves Cell-Based Assays for Ion Channels 7, 2002, pp. 79–85, https://doi.org/10.1177/108705710200700110.
[69] A. Yamada, N. Gaja, S. Ohya, K. Muraki, H. Narita, T. Ohwada, Y. Imaizumi, Usefulness and limitation of DiBAC4(3), a voltage-sensitive fluorescent dye, for the measurement of membrane potentials regulated by recombinant large conductance Ca2+-activated K+ channels in HEK293 cells, Jpn. J. Pharmacol. 86 (2001) 342–350, https://doi.org/10.1254/JJP.86.342.
[70] D.S. Adams, S.G.M. Uzel, J. Akagi, D. Wlodkowic, V. Andreeva, P.C. Yelick, A. Devitt-Lee, J.F. Pare, M. Levin, Bioelectric signalling via potassium channels: a mechanism for craniofacial dysmorphogenesis in KCNJ2-associated Andersen–Tawil Syndrome, J. Physiol. 594 (2016) 3245–3270, https://doi.org/10.1113/JP271930.
[71] R.L. Veech, Y. Kashiwaya, M.T. King, The resting membrane potential of cells are measures of electrical work, not of ionic currents, Integr. Physiol. Behav. Sci. 30 (1995) 283–307, https://doi.org/10.1007/BF02691602.
[72] A.A. Bulychev, N.A. Krupenina, Interchloroplast communications in Chara are suppressed under the alkaline bands and are relieved after the plasma membrane excitation, Bioelectrochemistry. 129 (2019) 62–69, https://doi.org/10.1016/J.BIOELECHEM.2019.05.006.
[73] W.F. Boron, P. De Weer, Intracellular pH transients in squid giant axons caused by CO2, NH3, and metabolic inhibitors, J. Gen. Physiol. 67 (1976) 91–112, https://doi.org/10.1085/JGP.67.1.91.
[74] N.A. Nimer, C. Brownlee, M.J. Merrett, Carbon dioxide availability, intracellular pH and growth rate of the coccolithophore Emiliania huxleyi, Mar. Ecol. Prog. Ser. 109 (1994) 257–262, https://doi.org/10.3354/MEPS109257.
[75] J.R. Coleman, B. Colman, Photosynthetic carbon assimilation in the blue-green alga Coccochloris peniocystis, Plant Cell Environ. 4 (1981) 285–290, https://doi.org/10.1111/1365-3040.EP11604546.
[76] G.N. Somero, Intracellular pH, Buffering Substances and Proteins: Imidazole Protonation and the Conservation of Protein Structure and Function, 1985, pp. 454–468, https://doi.org/10.1007/978-3-642-70613-4_38.
[77] H. Sträuber, S. Müller, Viability states of bacteria-specific mechanisms of selected probes, Cytom. Part A. 77 (2010) 623–634, https://doi.org/10.1002/cyto.a.20920.
[78] T. Bräuner, D.F. Hülser, R.J. Strasser, Comparative measurements of membrane potentials with microelectrodes and voltage-sensitive dyes, Biochim. Biophys. Acta Biomembr. 771 (1984) 208–216, https://doi.org/10.1016/0005-2736(84)90535-2.
[79] T. Shimmen, A. Wakabayashi, Involvement of membrane potential in alkaline band formation by internodal cells of Chara corallina, Plant Cell Physiol. 49 (2008) 1614–1620, https://doi.org/10.1093/pcp/pcn136.
[80] S. Lambert, Stoneworts : their habitats, ecological requirements and conservation Integrated catchment science programme Science report : SC030202 The Environment Agency is the leading public body protecting and improving the environment in England 23, 2009.
[81] I. Foissner, G.O. Wasteneys, The characean internodal cell as a model system for studying wound healing, J. Microsc. 247 (2012) 10–22, https://doi.org/10.1111/j.1365-2818.2011.03572.x.
[82] A. Klima, I. Foissner, Actin-dependent deposition of putative endosomes and endoplasmic reticulum during early stages of wound healing in characean internodal cells, Plant Biol. 13 (2011) 590–601, https://doi.org/10.1111/j.1438-8677.2010.00413.x.
[83] J.W. La, C. Ii, 156: Planta Wound-healing motility in the green alga Ern calcium ions and metabolic energy are required 156 (2016) (1982) 466–474.
[84] R. Stahlberg, D.J. Cosgrove, Rapid alterations in growth rate and electrical potentials upon stem excision in pea seedlings, Planta. 187 (1992) 523–531, https://doi.org/10.1007/BF00199972.
[85] T. Shimmen, Electrophysiological characterization of the node in Chara corallina: functional differentiation for wounding response, Plant Cell Physiol. 49 (2008) 264–272, https://doi.org/10.1093/pcp/pcn002.
[86] T. Shimmen, Electrical perception of “death message” in Chara: involvement of TurgorPressure, Plant Cell Physiol. 42 (2001) 366–373, https://doi.org/10.1093/PCP/PCE047.
[87] P.D. Spencer, J.D. Riches, E.D. Williams, Fluid phase equilibria exclusion zone water is associated with material that exhibits proton diffusion but not birefringent properties, Fluid Phase Equilib. 466 (2018) 103–109, https://doi.org/10.1016/j.fluid.2018.03.020.
[88] Y. Cheng, C.I. Moraru, Long-range interactions keep bacterial cells from liquid-solid interfaces: evidence of a bacteria exclusion zone near Nafion surfaces and possible implications for bacterial attachment, Colloids Surfaces B Biointerfaces. 162 (2018) 16–24, https://doi.org/10.1016/J.COLSURFB.2017.11.016.
[89] M.J. Esplandiu, D. Reguera, J. Fraxedas, Electrophoretic origin of long-range repulsion of colloids near water/Nafion interfaces, Soft Matter 16 (2020) 3717–3726, https://doi.org/10.1039/D0SM00170H.

Developmental Biology 517 (2025) 317–326

Contents lists available at ScienceDirect

Developmental Biology

journal homepage: www.elsevier.com/locate/developmentalbiology

Original research article

Modifying membrane potential synchronously controls the somite's formation periodicity and growth

Manohara Mahadeva, Sebastian Niestępski, Magdalena Kowacz *

Department of Reproductive Immunology & Pathology, Institute of Animal Reproduction and Food Research Polish Academy of Sciences, 10-748, Olsztyn, Poland

ARTICLE INFO

Keywords:
Chick embryo
Membrane potentials
Periodicity of somite formation
Somite growth
Cell electrophysiology
Glass microelectrodes

ABSTRACT

Coordination between periodicity of somite formation and somite growth is crucial for regular body pattern formation during somitogenesis. Yet, the specific mechanism that links the two processes remains unclear. Using chick embryos, we demonstrate that both temporal and spatial features can be simultaneously controlled by membrane potential (V_m) of somite-forming cells. Our findings show that somites hyperpolarize as they mature, displaying step-like changes in V_m observed between specific groups of somites, reflecting the reported onset of biochemical and structural changes within them. We modify V_m by changing chemical compositions of the microenvironment of the embryo. Alteration of V_m sets a new pace of somite formation (cell migration and self-assembly) and its concurrent growth (cell proliferation) without disturbing the somite's regular aspect ratio. Our results therefore suggest that V_m has the ability to orchestrate cell proliferation, migration and self-assembly - processes that are hallmarks of embryogenesis, tumorigenesis and tissue regeneration.

1. Introduction

Somitogenesis is the rhythmic segmentation of somites, where pairs of paraxial mesoderm blocks, originating from somite-forming cells or presomitic mesoderm (PSM), form on either side of the embryo's anterior-posterior axis (Pourquié and Pourquié, 2001/11/01). This process is characterized by tissue- and species-specific periodicity (Carraco et al., 2022). Somite formation occurs with temporal cyclicity accompanied by corresponding somite's growth, leading to development of defined spatial pattern with segment's size proportional to overall body length (Dale and Pourquié, 2000; Pourquié, 2003). Temporal periodicity is regulated by gene oscillations known as the segmentation clock, driven by complex signalling pathways (Dequéant et al., 2006; Hubaud and Pourquié, 2014; Krol et al., 2011; Masamizu et al., 2006; Palmeirim et al., 1997). However, the mechanism setting the clock period and that synchronizes temporal periodicity with somite growth is not fully understood (Carraco et al., 2022; Ishimatsu et al., 2018). Studies have attempted to explain respective somite scaling and suggested that reduction in the somite formation interval should lead to larger somites with increasing the period having the reverse outcome (Juul et al., 2019; Lauschke et al., 2013). However, some experimental findings have shown the opposite effect: accelerating the timing of somite formation through genetic manipulation led to smaller somites, while slowing the segmentation resulted in larger segments (Harima et al., 2013; Schröter and Oates, 2010). Therefore, the question remains open: what precisely synchronizes periodicity of somite segmentation and somite growth rate to generate consistent early body pattern during embryonic development? To answer this question, it's crucial to understand the cellular processes involved in somitogenesis. A discrete number of cells from PSM need to migrate and self-assemble to form somite blocks, then proliferate to assure segment growth and differentiate to acquire structure-related function (Alvarez et al., 1989; Blomberg et al., 2008; Nakamura et al., 2007). All these fundamental processes must work in an orchestrated manner to generate somites with consistent size at precise time and space intervals. It has been demonstrated that the rate of cell proliferation and differentiation can be controlled by modifying the membrane potential of cells (Blackiston et al., 2009; Cone and Tongier, 1971). Also cell migration and structure/pattern formation during tissue regeneration and embryo development were shown to be regulated by membrane potential (Fukumoto et al., 2005; Levin, 2012; Nishiyama et al., 2008; Ozkucur et al., 2011). However, the possibility to couple proliferation with morphogenesis via bioelectric control of physiological processes is only beginning to be understood (Levin and Martyniuk, 2018). The membrane potential of different cell types has been measured and correlated with their proliferablity, revealing that proliferative cells are depolarized compared to

* Corresponding author.
E-mail addresses: m.mahadeva@pan.olsztyn.pl (M. Mahadeva), s.niestepski@pan.olsztyn.pl (S. Niestępski), m.kowacz@pan.olsztyn.pl (M. Kowacz).

https://doi.org/10.1016/j.ydbio.2024.11.002
Received 16 September 2024; Received in revised form 22 October 2024; Accepted 6 November 2024
Available online 8 November 2024

differentiated ones (Binggeli and Weinstein, 1986). Generally, cells in embryos or tumors are highly proliferative, depolarized, and also share common characteristics of the microenvironment, enriched in CO_2 and K^+ compared to the one of quiescent cells (Chen et al., 2022; Kikuchi et al., 2019; Oginuma et al., 2017; Roblero et al., 1976; Roblero and Riffo, 1986). This suggests that the chemical composition of cells' surrounding may play a role in defining their membrane potential. Supporting this notion, we have recently demostrated for the first time that cells can in fact be depolarized by increasing the external CO_2, in addition to the known depolarizing effect of KCl (Mahadeva et al., 2024). We have experimentally demonstrated the existence of a negative extracellular voltage adjacent to the cell and its evolution in response to depolarization induced by either CO_2 or KCl (Mahadeva et al., 2024). Increased concentration of those components in the cell's environment prompted development of electric potential at the outer cell wall/-membrane and caused corresponding changes in the overall transmembrane potential (TMP) value. By comparing the voltage measured using the direct microelectrode technique and observed using potential-sensitive dye, we have shown the importance of considering extracellular voltage in defining TMP of a cell. Increased concentration

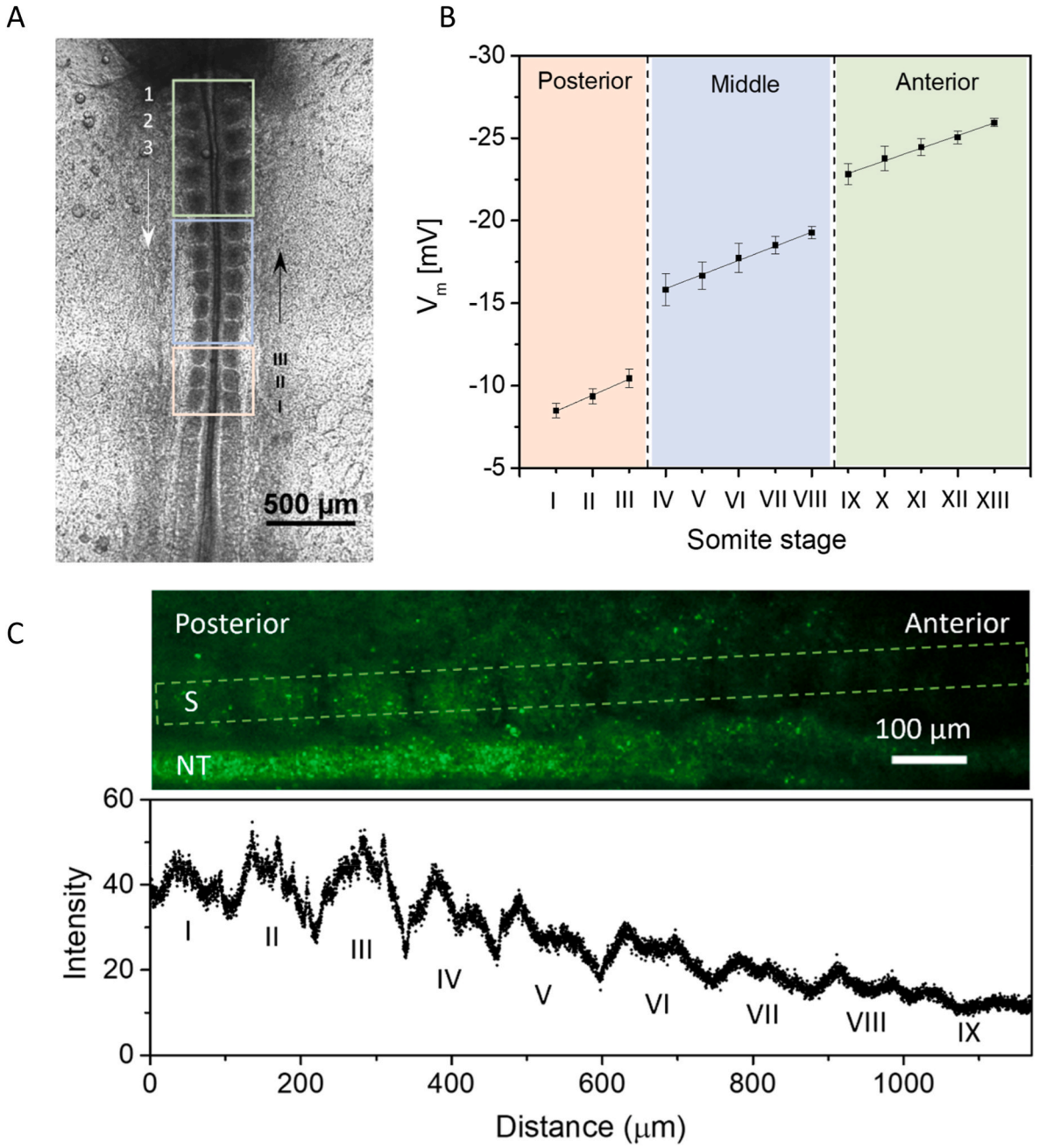

Fig. 1. Membrane potential (V_m) of somite-forming cells in chick embryo. A bright-field microscopy image shows embryo with 13 somite pairs, where somite stages are indicated by Roman numbers and somite positions are indicated by Arabic number. Posterior (SS I - III), middle, (SS IV - VIII) and anterior (SS IX – XIII) somite groups represented by orange, blue, and green boxes, respectively (A). Dependence of V_m on somite stages for embryos with 8–13 pairs of somites. The lines are linear fit for each somite group [$V_m = -0.95 \cdot SS - 7.4$, $R^2 = 0.99$ (posterior, orange), $V_m = -0.88 \cdot SS - 12.35$, $R^2 = 0.99$ (middle, blue), and $V_m = -0.75 \cdot SS - 16.11$, $R^2 = 0.99$ (anterior, green)] (N = 18) (B). Confocal microscopy image shows the change in fluorescence intensities of somites and fluorescence intensity versus distance graph shows the degree of hyperpolarization of somite-forming cells along anterior-posterior axis of chick embryo (9 somite pairs) (C) (N = 5). Decrease in fluorescence intensity of the dye indicates the cell hyperpolarization. S – somite, NT – neural tube.

of intracellular CO_2 (from metabolic output of a cell) also resulted in negativity increase, but at the inner side of the membrane, thus having the opposite effect on TMP than environmental CO_2 (Mahadeva et al., 2024). These experimental findings are consistent with the previously defined concept that cell's TMP, as measured by microelectrodes and described by classical Nernst equation (Hopper et al., 2022), comprises both intracellular and extracellular negative components (Vodovnik et al., 1992), emergence of which is also consistent with Ling's theory (Tamagawa and Ikeda, 2018). Based on those considerations, it has been suggested that the overall transmembrane potential can be altered by affecting independently only extracellular voltage and that this can be responsible for the observed effect of externally applied electric field on cell proliferation (Vodovnik et al., 1992). It has been also recognized that endogenous extraembryonic electric fields contribute to embryo development by influencing cell migration (Hotary and Robinson, 1990). However, it is not yet known if the elecrtic potential gradients can affect the timing of somite formation (cell migration and self-assembly) and their synchronous growth (proliferation). Therefore, in this study, we aim to verify whether changes in membrane potential of somite-forming cells, induced by adjusting composition of their microenvironment, can control early body pattern formation by affecting elemental processes underlying somitogenesis. For this purpose, we use CO_2 and KCl to modify the membrane potential of chick embryonic cells and then assess the effect of the induced changes on somite segmentation rate and somite growth. Our data reveal that CO_2 and KCl, naturally enriched in the embryo's environment, contribute to depolarization of embryonic cells. The membrane potential (V_m), adjusted by those environmental stimuli to a given level, sets the new timing of somite appearance coordinated with its adequate spatial expansion. The somite formation periodicity (τ) depends linearly, while somite growth rate (L(t)) depends exponentially on V_m, with depolarization accelerating fundamental events of early somitogenesis.

2. Results and discussion

2.1. Mapping the voltage of somites in the chick embryo along its anterior-posterior axis

The membrane potential measured in this study, designates the electric potential difference between the somite interior and its surrounding medium. In chick embryo, the somite stages (SS) are represented by Roman numbers. The somite position along the axis, counted from most rostral to caudal one, is represented by Arabic numbers (Venters et al., 2008) (Fig. 1a). In general, the somite stages reflect somite's intrinsic developmental time, while somite position along the axis (somite number) is related to its future fate in terms of giving rise to particular structures of vertebrate body. V_m was measured via microelectrode at control conditions of 5% CO_2 for all the somite stages (SS I - XIII) in embryos with 8–13 pairs of somites (Fig. 1a). Rostral somites have consistently exhibited more negative V_m compared to that of caudal ones (Fig. 1b). This indicates that somites become progressively hyperpolarized (acquiring more negative potential) with their maturation. This hyperpolarizing trend was also observed using a voltage-sensitive dye, showing that all the cells within the somites become hyperpolarized as they mature (Fig. 1c). Embryonic cells have been previously shown to be hyperpolarized with progressing development (Arcangeli et al., 1997). Along with the general hyperpolarizing trend we observed a step-like changes of V_m between specific groups of somites, specifically the youngest, most posterior ones (SS I – SS III), middle (SS IV – SS VIII), and most developmentally advanced, anterior somites (SS IX – SS XIII). We obtained the following V_m ranges for each somite group: (-8.49 ± 0.45 to -10.45 ± 0.47) mV for SS I – SS III, (-15.83 ± 0.98 to -19.28 ± 0.36) mV for SS IV – SS VIII, and (-22.82 ± 0.65 to -25.95 ± 0.25) mV for SS IX – SS XIII. Within each group, V_m exhibited a linear dependence on somite stage, with slopes of -0.95, -0.87, and -0.75 respectively for posterior, middle, and anterior somites, which shows that the developmental processes reflected in changes of V_m are more dynamic in caudal somites than in the rostral ones (Fig. 1b). The most dynamical, youngest somites are structurally and functionally identical and still silent in terms of morphogen expression (Maschner et al., 2016). Therefore, observed changes in membrane potential are most probably related to their metabolic output (Jakobsson, 1980; Mahadeva et al., 2024), what is in agreement with more posterior cells within the embryo showing the highest glycolytic activity (Oginuma et al., 2020). Intracellular anionic metabolites contribute to defining negative membrane potential of a cell (Jakobsson, 1980), while metabolism in general provides both precursor molecules and energy necessary for gene expression that directs further development (Carthew, 2021). It is worth noting that membrane potential is not only a product of cell metabolism, but also regulates metabolic performance because membrane polarization directly affects the transport of all charged species (including nutrients and waste products) into and out of the cell. As we will discuss further in this work, induced membrane potential changes may control cell's behavior via this feedback loop with metabolism.

The embryos examined in our study are in their early-stages where occipital (1–5 from the rostral end) and cervical (following 5–19) somites are formed. During this stage of embryogenesis, the onset of expression of transcription factors (TFs) as well as the onset of the following morphological changes were shown to be delayed in comparison to later stages (Ibarra-Soria et al., 2023; Maschner et al., 2016). This means that for the same intrinsic developmental time (somite stage), occipital and cervical somites are less developmentally advanced than their counterparts formed later in the somitogenesis. Our potential-based classification of somites (into groups separated by abrupt potential changes) in fact reflects the previously recognized differences in somite development, already at the level of the expression of morphogenic TFs or, later on, at the level of differentiation (Maschner et al., 2016). It has been shown that the expression of TFs in early embryogenesis starts only from the somite stage IV, what corresponds to the first step-like change in our V_m values. Then, differentiation begins from somite stage IX, thus corresponding exactly to the next step in otherwise linearly changing V_m. However, V_m is not specific for a given TF or a given morphological change. Expression of any TFs commences always at the same somite stage, but the identity of TFs being expressed differs for the same stage depending on somite position along the axis. Specifically, only *Pax1* was detected in SS IV – SS XI in embryos with 8–11 pairs of somites, while both *Pax1* and *MyoD* were expressed in those (and later) somite stages in embryos with 12 and 13 somite pairs. Yet, V_m values in those embryos are virtually constant for a given somite stage independently of its number along the axis. Morphological changes (manifested in the loosening of the epithelial integrity of occipital and cervical somites), on the other hand, begin always at SS IX, what is reflected in a step-like change of V_m. Nevertheless, then somites start to compartmentalize to form specific structures (here sclerotome), what is not mirrored by any abrupt change in V_m, that linearly increases within this (SS IX – SS XIII) morphologically nonuniform group. Therefore, the step-like changes of V_m, as reported in our study, closely reflect the onset (but not the identity) of either biochemical or structural changes within developing somites. In order to further verify this concept, we measured V_m in embryos having 4 to 7 pairs of somites, where all the somites are morphologically identical and do not show expression of any TFs (Maschner et al., 2016). In support of our conclusion, we observed no step-like change in V_m between SS III and SS IV, but linear hyperpolarizing trend (with the slope of -1.01) along anterior-posterior axis of the embryo (Fig. 2). Membrane potential marking the inception of different, non-specific changes again points toward the metabolism as the possible underlying factor. Once the level of energy and precursor materials is sufficient (and expressed in potential values), the processes can commence. In fact, it has been shown experimentally, that the rate of the whole embryo development is adjusted to the performance of its metabolism-limited slowest part

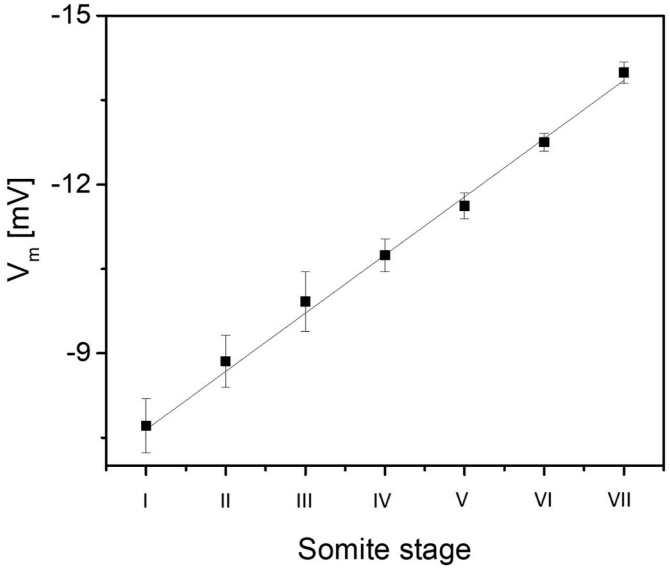

Fig. 2. Membrane potential (V_m) of somite-forming cells in early-stage chick embryos. Dependence of V_m on somite stages for the embryos with 4–7 pairs of somites. The line is the linear fit for the shown trend ($V_m = -1.011 \cdot SS - 6.75$, $R^2 = 0.99$) (N = 7).

(Carthew, 2021). The greater disparity in the step change of V_m values between the posterior and middle somite groups compared to that between the middle and anterior groups suggests that V_m is more sensitive to biochemical alterations than to structural ones (Fig. 1b). To the best of our knowledge, this is the first report showing the pattern of V_m alterations along the body axis of vertebrate embryo and its correlation with the onset of developmental events. In the following section we show the possibilities of affecting the V_m in order to later explore its ability to not only reflect, but also affect embryonic development, characterized by periodicity of somite formation and somite expansion rate.

2.2. The effect of external stimuli on the membrane potential of somite forming cells observed in the chick embryo

In this study, we have used CO_2 and KCl as the external stimuli to depolarize embryonic cells in early-stage chick embryos. Fertilized eggs were incubated (and analysed) at selected CO_2 levels (2%, 5%, and 7%) for a given experiment, while constant CO_2 (5%) level was maintained in experiments with additional (0.3 and 0.6) mM KCl to the medium (Pennett-Compton saline) containing 8.3 mM KCl (control). For the purpose of these experiments, somites were categorized, based on the V_m-bound groups along the embryo's body axis, into: posterior (SS I – SS III), middle (SS IV – SS VIII), and anterior (SSIX – SS XIII). To compare the effect of different stimuli on a given group of somites, V_m of selected representative somites from each group was measured and averaged for any experimental conditions. At 2% CO_2, the V_m of posterior, middle, and anterior somites were (−14.63 ± 1.58) mV, (−22.27 ± 2.73) mV, and (−26.70 ± 2.32) mV, (Fig. 3a). The somites in every group were depolarized by 42.78% to (−8.37 ± 1.31) mV, by 31.21% to (−15.32 ± 1.54) mV, and by 14.75% to (−22.76 ± 1.74) mV respectively, at 5% CO_2 (Fig. 3a). Somites were further depolarized by 55.32% to (−3.74 ± 1.09) mV, by 43.79% to (−8.61 ± 1.37) mV, and by 41.08% to (−13.41 ± 1.65) mV in caudal to rostral direction, in embryos developing at 7% CO_2 (Fig. 3a). The CO_2-induced depolarization was also shown by using potential-sensitive dye (Fig. S1). An increased level of CO_2 acidifies the cell's microenvironment (Gatenby and Gillies, 2004; Parkins et al., 1997). To verify whether the induced depolarization of somites could be the effect of change in pH of the bulk solution, we have adjusted the bulk pH to 6.3 (maximum change in pH brought by 7% CO_2) using HCl. The

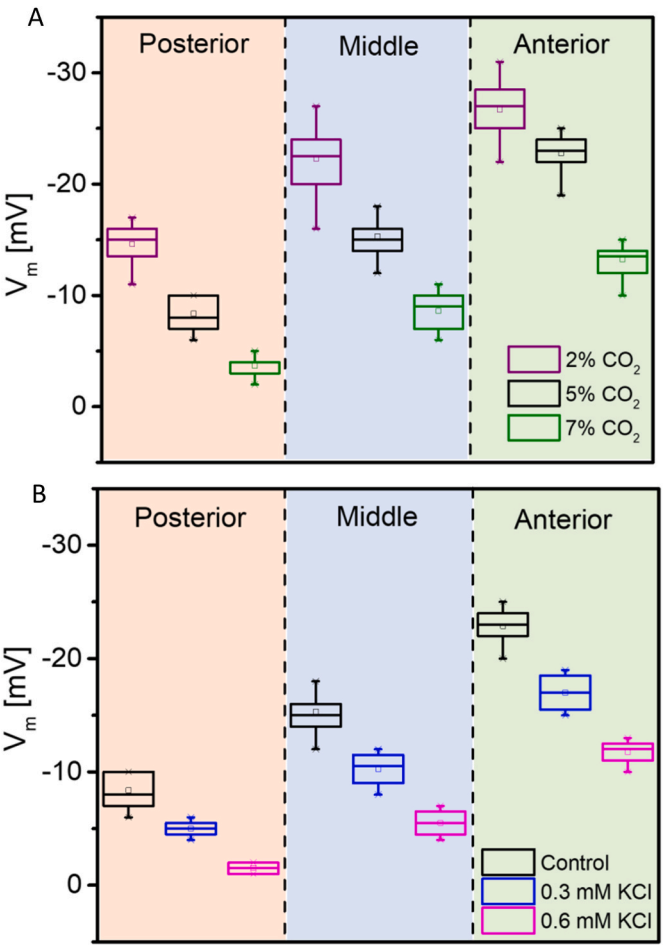

Fig. 3. Effect of CO_2 and KCl on the membrane potential (V_m) of somite-forming cells in chick embryo. Box plots show V_m for posterior (orange), middle (blue), and anterior (green) somites in response to change in concentrations of CO_2 and KCl. Depolarization and hyperpolarization of the somites were observed at 7% CO_2 (green) and 2% CO_2 (purple), respectively, compared to the control condition (5% CO_2) (black) (A) (N = 20 each). Depolarization of somites was observed at additional 0.3 mM KCl (blue) and additional 0.6 mM KCl (magenta), compared to the control condition (black) (B) (N = 4 each).

V_m of somites remained unchanged in response to additional HCl (Table S1). Therefore, the change in V_m in response to variations in CO_2 levels, as shown in our experiments, may not be attributed to changes in pH of the extracellular environment. Our results show that increasing levels of CO_2 in the embryo's surrounding always depolarize the somites. Next, the embryos grown at 5% CO_2 were treated with two different concentrations of KCl. Additional 0.3 mM KCl in the medium containing the embryo, has reduced (depolarized) V_m of posterior, middle, and anterior somites by 45.04% to (−4.60 ± 1.14) mV, by 34.73% to (−10.00 ± 1.58) mV, and by 23.55% to (−17.40 ± 1.82) mV, respectively, while, additional 0.6 mM KCl reduced V_m of corresponding somites by 80.88% to (−1.60 ± 0.55) mV, by 64.75% to (−5.40 ± 1.14) mV, and by 47.27% to (−12.00 ± 1.22) mV, compared to the control conditions (Fig. 3b). From the above results it can be noted that not only the dynamics of V_m changes at constant environmental conditions was the highest in the youngest somites (Fig. 1b), but also V_m response to the environmental stimuli is most expressed in this group (Fig. 3a and b). Our results confirmed that CO_2 and potassium-enriched microenvironment of embryos may contribute to defining their V_m.

Our previous work has shown that cell depolarization induced by either CO_2 or KCl is accompanied by the emergence of a negative extracellular voltage (V_z) adjacent to the cell surface and that the overall

membrane potential of a cell includes also V_z component (Mahadeva et al., 2024). V_z has the ability to exclude colloidal particles, the property that can be employed for its visual detection. Therefore, we used microspheres to verify the possible emergence of V_z near the embryonic cells in response to their induced depolarization. The microspheres (diameter: 0.5 μm) could be observed in the immediate vicinity of the somite surface at conditions of 5% CO_2 (Fig. 4a), while they have moved to a distance of approximately (16.73 ± 2.86) μm from the surface at 7% of CO_2 (Fig. 4b). The observed exclusion phenomenon could be either due to the anticipated electric field (V_z) developed in response to higher levels of CO_2 (Mahadeva et al., 2024), but possibly also due to an expansion of extracellular matrix (ECM). It has been recognized that microspheres (or other charged objects) of different sizes are excluded to different distances by the same magnitude of the interfacial voltage (Mahadeva et al., 2024; Nooryani et al., 2023). Therefore, to verify the mechanism behind the particle exclusion from the somite surface, we used smaller microspheres (diameter: 0.2 μm) and observed their exclusion to a larger distance of approximately (28.83 ± 2.79) μm (Fig. 4c) at 7% of CO_2 (N = 5, each). If the particle movement resulted from an expansion of ECM, both smaller and larger microspheres would have been excluded to the same distance or the smaller ones could penetrate more into ECM network, due to possible increase in pore size of ECM caused by its expansion. Our observations therefore indicate the emergence of V_z near the somite surface in response its CO_2-induced depolarization. Previous studies have shown the existence of an endogenous extracellular electric fields along the anterior-posterior axis of chick embryo, with a more positive voltage gradient at the rostral end compared to caudal end (Hotary and Robinson, 1990; Nuccitelli, 2003). It has been suggested that the more positive charges are mainly due to Na^+ ions being pumped out by cells (Hotary and Robinson, 1990). When positive ions are moved from the cells, their membrane potential becomes more negative (hyperpolarization) (Gadsby and Cranefield, 1979), what is consistent with reported by us trend of changes in membrane potential of somite-forming cells along the body axis. The endogenous electric fields have been suggested to provide directional information for growing and migrating cells in chick embryo (Hotary and Robinson, 1990). It is important to note however, that the direction of an electric field related to the emergence of V_z, as suggested in our

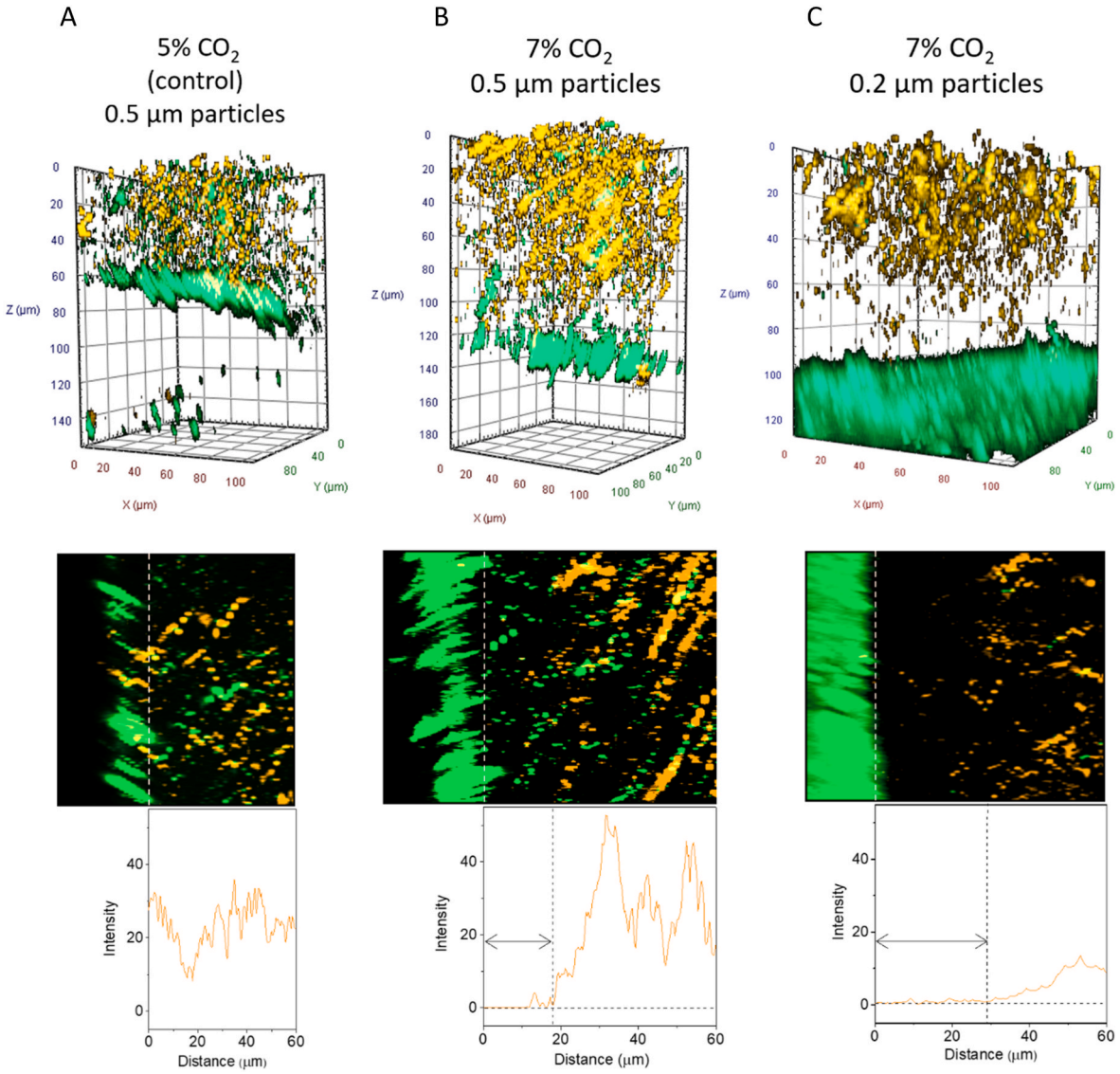

Fig. 4. Particle exclusion zone near somite's surface. Three dimensional graphs and two-dimensional confocal images show microspheres (0.5 μm, orange) attached to somite's surface (green) at control (5% CO_2) condition (A) and particle exclusion zones at 7% CO_2 for (0.5 and 0.2) μm, microspheres (orange) (B and C respectively). The line graphs show the intensity of the fluorescence of microspheres versus distance, where the arrows indicate the width of the zone largely devoid of microspheres.

study, would be normal to the somite surface, thus affecting charge movement in/out of the somite. This is in contrast to the previously reported extraembryonic fields driving ionic current flow parallel to the somite surface. V_z, as defined by us (Mahadeva et al., 2024) and akin to the previously recognized outer membrane potential (Vodovnik et al., 1992), is the component of transmembrane potential (Mahadeva et al., 2024) (here the electric potential difference measured across the somite surface), and as such may play yet unrecognized role in embryonic development.

2.3. Depolarization increases the pace of somite emergence and promotes its growth in the chick embryo

During somitogenesis, discrete clusters of cells organize and undergo segmentation to form somites. The segmentation of somites occurs at regular intervals of time. Studies have shown that the first five pairs of somites in chick embryo form approximately every 75 min, while somites of sixth pair onwards are formed at an average time of 90 min (measured at 5% CO_2) (Maia-Fernandes et al., 2024; Palmeirim et al., 1997). In our experiments, we have also observed the same temporal pattern, with somite formation occurring at a comparable periodicity of (89.80 ± 3.83) minutes across the examined embryo stages (7–13 pairs of somites) at control conditions (5% CO_2). In this study, to understand the contribution of V_m to the periodicity of the somite formation and its growth, we manipulated the membrane potential of early-stage chick embryos. As in the case of experiments examining the effect of specific stimuli on V_m, embryos were incubated and analysed at a given CO_2 concentration set to respective level for the whole experiment, or in the presence of a given concentration of KCl in the medium at constant 5% CO_2.

Modifications in V_m of somite forming cells prompted a shift in the pace of somite formation. At 2% of CO_2 level, the somite segmentation occurred in (121.60 ± 5.94) minutes. The somite segmentation time was reduced by 26% to (89.80 ± 3.83) minutes upon V_m depolarization induced in embryos developing at 5% CO_2. Somite segmentation time was accelerated by another 21% to (70.40 ± 3.84) minutes in response to further V_m depolarization in embryos growing at 7% CO_2. Depolarization induced in cells by KCl reduced the segmentation time by 12% to (79.00 ± 2.58) minutes and by subsequent 27% to (64.75 ± 4.04) minutes, in response to additional (0.3 and 0.6) mM KCl, respectively (Fig. S2) (N = 5 for each CO_2, and N = 4 for each KCL treatment). In general, the time required for the segmentation of somites depends linearly on the membrane potential of somite-forming cells with less negative membrane potential setting the faster tempo (Fig. 5).

Alterations in V_m affected somite's expansion/growth rate (Fig. 5). At 2% of CO_2 level the rate of expansion of somites (changes in the width of the somite measured along anterior-posterior axis) was (2.58 ± 0.22) μm per hour. The expansion rate increased by 92% to (4.97 ± 0.84) μm per hour upon depolarization of V_m induced in embryos exposed to 5% CO_2 (Fig. 5) and by further 103% to (10.11 ± 1.02) μm per hour as a result of even stronger depolarization experienced by embryos developing at 7% CO_2. Depolarization induced by additional 0.3 mM KCl has increased the somite expansion rate by 51% to (7.55 ± 0.45) μm per hour, whereas additional 0.6 mM KCl further accelerated it by 168% to (13.32 ± 0.60) μm per hour compared to control conditions (Fig. 5, S2) (N = 7 for CO_2, and N = 4 for KCL treatments, respectively). The rate of somite growth, in terms of changes in somite's diameter (estimated based on previously reported data on changes of somite's volume by assuming that the somites are spherical in shape) (McColl et al., 2018), in later stages of embryogenesis is (3.31 ± 1.97) μm per hour (average growth rate of SS I – III) (McColl et al., 2018). In our case, the rate of increase in somite's diameter for SS II at control conditions is (4.97 ± 0.84) μm per hour. This discrepancy could be due to the fact that the previously reported growth rate of somites was calculated for more developed embryos (22–28 somite pairs) (McColl et al., 2018) compared to the ones used in our work (4–13 somite pairs). In fact, the

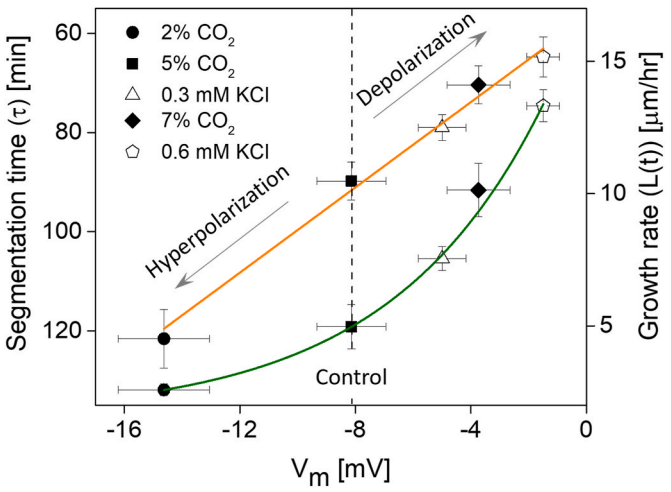

Fig. 5. Dependence of periodicity of somite formation (τ) and somite's growth rate (L(t)) on membrane potential (V_m) of somite-forming cells. The linear fit, $\tau = -4.30 \cdot V_m + 56.64$, $R^2 = 0.98$, (N = 5 for each point) corresponds to the periodicity of somite formation (orange), whereas the exponential fit, $L(t) = 1.58 + 15.65 \cdot e^{0.18 \cdot Vm}$, $R^2 = 0.99$ (N = 4 for each point) corresponds to the rate of individual somite expansion (green). Individual data points represent the values at 2% CO_2 (solid circle), 5% CO_2 (solid square), additional 0.3 mM KCl (empty triangle), 7% CO_2 (solid diamond), and additional 0.6 mM KCl (empty pentagon).

developmental processes reflected in changes of V_m are more dynamic in early embryogenesis, as indicated by the slopes of V_m versus SS trends: −1.01 for embryos with 4–7 somite pairs, and −0.95 (for SS I – III) in embryos with 8–13 somite pairs, respectively (Figs. 1 b, 2). This may possibly translate into faster growth rate of somites in early embryogenesis. In general, our data show that the rate of somite expansion changes exponentially as a function of V_m (Fig. 5) and, as in the case of segmentation periodicity, depolarization speeds up the process.

The revealed dependencies of somite formation and growth on V_m follow their respective trend lines, independently of the stimuli used to alter V_m, thus confirming that the observed effects are not stimuli-specific, but rather potential-specific (Fig. 5). The different trends reflect the fact that the two processes are distinct in nature. The segmentation occurs as a result of cell migration and self-assembly, while volume expansion is governed by cell proliferation and growth. Earlier study has shown that increase in the size of somites of epithelial morphology (as the ones addressed in our work) is mainly due to the increase in the number of epithelial cells (Bagnall and Berdan, 1994). It has been also demonstrated that the number of cells within somites increases exponentially with somite stage (maturation) (Venters et al., 2008). Therefore, the exponential dependence of somite expansion on V_m (Fig. 5), suggests that V_m should affect cell proliferation rate. The rate of cell proliferation has been shown to be accelerated by depolarizing the cells, and reduced by hyperpolarizing them (Blackiston et al., 2009; Cone and Tongier, 1971). Such observations are consistent with our findings showing increased and reduced somite expansion (cell proliferation) in response to induced depolarization and hyperpolarization respectively (Fig. 5). There are no preceding data on the effect of membrane potential changes on somite segmentation periodicity – a developmental process determined by cell migration and self-assembly (in the time course of our experiment, where all precursor cells are already present in the PSM). We are showing the possibility to shorten segmentation interval by unprecedented 27%, accompanied by a simultaneous increase in the somites' growth rate, thus maintaining their regular aspect ratio. Up to now the only way enabling somitogenesis acceleration was direct gene manipulation, which however resulted in only up to 9% increase in the respective tempo (Harima et al., 2013; Liao et al., 2016). Furthermore, faster segmentation periodicity

led to narrower segments, as somite growth did not adjust to the newly established somite birth rate (Harima et al., 2013; Liao et al., 2016). In contrast, membrane potential alterations, as applied in our work, allow for the synchronous control of both somite formation and growth. This is expressed in the undisturbed body pattern formation at any given somitogenesis rate set by membrane potential. This conclusion is further strengthened by our observations that embryos incubated *in ovo* at different CO_2 conditions (related to differences in V_m) reach expected, more or less advanced development stage by the same time of incubation, yet they do not show any morphological abnormalities. It is generally recognized that somite size scales with the length of PSM (Ishimatsu et al., 2018; Lauschke et al., 2013). Recently it has been proposed that this is due to gene oscillation dynamics (underlying also periodicity of somite formation) scaling with the size of embryo axis (Juul et al., 2019; Lauschke et al., 2013). Those results therefore revealed tight coupling between segmentation rate and somite growth. Our findings, showing somite size scaling accordingly with somite formation period, support such interdependence. However, this was not the case for somitogenesis accelerated by direct manipulation of oscillatory genes, where smaller somites were generated (Harima et al., 2013). It might be due to the fact that alterations of V_m affect cell proliferation in the whole embryo, including the PSM (thus supporting its steady-state length), allowing somites to adjust to the new pace of segmentation without any size disruptions.

Cell proliferation and migration/self-assembly are the processes that are known to be regulated by β-catenin/Wnt signalling pathway that controls somitogenesis, but also tumorigenesis and tissue regeneration (Qin et al., 2007; Sharma et al., 2021). In this study, we have shown that cell proliferation (in terms of change in the rate of somite expansion) and migration/self-assembly (in terms of change in periodicity of somite formation) could be synchronously altered by modifying V_m using external stimuli (Fig. 5). Our results show that the step-like changes in V_m reflect the onset of transcription factors expression and the onset of cells differentiation. This suggests that V_m might control the expression of genes that drive somitogenesis. In support of this, it has been previously shown that induced depolarization in cells results in the translocation of β-catenin (a protein molecule that transduces signal in Wnt signalling pathway) from the cytoplasm into the nucleus, prompting the onset of expression of TFs that lead to cell proliferation and differentiation (Rapetti-Mauss et al., 2017). β-catenin was also shown to be activated by increase in intracellular pH resulting from aerobic glycolysis (the prevalent metabolic pathway in early embryos). This process releases lactic acid, which carries its counterions (protons) out of the cells, thereby increasing intracellular pH (Oginuma et al., 2020). In our case, the induced depolarization of somite-forming cells, should facilitate the outward movement of protons due to lower electric force (less intracellular negativity) counteracting their expulsion. Simultaneously, the negative V_z near the depolarized cells should also aid proton removal, by providing electric force attracting positive charges into extracellular space. This possibility is supported by previous studies, arguing that application of an external electric field causes the cell membrane facing the negative electrode, analogous to our V_z, to become depolarized (Jaffe and Nuccitelli, 1977; Robinson, 1985; Vodovnik et al., 1992). The induced depolarization, in turn, reduces resistance of the membrane and increases transmembrane ionic current, thus supporting e.g. proton efflux (Vodovnik et al., 1992). Proton export, the predicted effect of lower membrane polarization, upregulates aerobic glycolysis (Man et al., 2022; Russell et al., 2022) pointing toward membrane potential acting upstream of metabolism. Therefore, modifications of the electric field running across the somite boundary shown in our study might support pH changes leading to activation of β-catenin/Wnt signalling pathway and thereby accelerating the periodicity of somite formation and growth. Thus, alterations in membrane potential of embryonic cells could potentially control the somitogenesis via β-catenin/Wnt signalling pathway.

Apart from biochemical factors, modulations in the softness of cells and the stiffness of the substrate can affect the developmental processes such as cell proliferation, migration, and differentiation (Kim et al., 2017, 2020; Wang et al., 2012). Achieving an optimal ratio of stiffness between the cells and extracellular matrix is crucial for supporting those processes (Marchant et al., 2022). Highly proliferative cells, such as those of embryos or tumors are more deformable or softer than differentiated cells (Chowdhury et al., 2010) and also relatively depolarized (Chen et al., 2022). Further to this end, it has been shown that induced depolarization of cells makes them softer (Callies et al., 2011). In our preliminary experiments, we have also observed an enhanced deformability of somites in chick embryo upon depolarizing them (data not shown). Cells may become softer as a result of depolarization-induced depolymerization of actin filaments in cytoskeleton of cells (Chifflet et al., 2003; Nin et al., 2009). Depolymerized actin facilitates the translocation of β-catenin into the nucleus, activating the Wnt signalling pathway, which in turn regulates cell proliferation, migration, and differentiation (Sen et al., 2022; Torres and Nelson, 2000). Also, the stiffness of extracellular matrix guides cell migration (durotaxis) and increases the rate of cell proliferation and differentiation (Jacob et al., 1991; Li et al., 2013; Pek et al., 2010; Peyton et al., 2006; Wang et al., 2012; Winer et al., 2009). It might be possible to alter the stiffness of ECM by modifying the extracellular voltage. Such possibility is corroborated by our previous findings showing that the voltage that runs through a hydrogel (a material which resembles the extracellular matrix by its porous structure and surface charge), makes the hydrogel resistant to hydrostatic and osmotic pressure (characteristic of a stiff material) (Kowacz and Pollack, 2020). Therefore, an increase in negative voltage (V_z) near the embryonic cells, as inferred from our experiments (Fig. 4), might enhance the stiffness of the ECM and thereby contribute to embryo development. Therefore, increase in cell migration/self-assembly (shift in periodicity of somite formation) and cell proliferation and growth (somite expansion) shown in our study could also be correlated to electric potential-induced changes in mechanics of cells and ECM.

The above considerations suggest that changes in the pace of somite segmentation and growth in response to induced alterations of V_m may be related to: i) the indirect modifications in gene expression, via β-catenin/Wnt signalling pathway triggered by supporting metabolic outcome of glycolysis and/or to ii) changes in tissue mechanics in the direction characteristic for morphing and spreading tissues.

3. Conclusions

In this study, we present for the first time the electric potential pattern of somites along the rostro-caudal axis of the chick embryo. We demonstrate that the changes in V_m reflect somites' maturation state as well as the reported onset of expression of morphogenic transcription factors and the onset of differentiation. V_m not only reflects these developmental transitions but also regulates the underlying processes. This is manifested in the fact that modifying V_m, via physiologically relevant environmental stimuli, establishes a new tempo of somitogenesis. To the best of our knowledge, this study is the first to show that V_m can synchronize both periodicity of somite formation (cell migration and self-assembly) and somite growth (cell proliferation), thereby producing a consistent body pattern during early embryogenesis. Our results, therefore, provide a new perspective for understanding the regulatory mechanisms involved in somitogenesis. Furthermore, characteristics such as cell proliferation, motility, depolarized membrane potentials, CO_2- and K^+-enriched microenvironment, tissue softening, as well as specific signalling pathways and genetic factors, are common to embryogenesis, tumorigenesis and tissue regeneration. Therefore, the unravelled correlations between V_m, microenvironment and early development, may help to understand also those other physiological and pathological processes.

4. Materials and methods

4.1. Embryo culture and extraction

Fertilized chicken eggs (Ross 308) from a farm were incubated in a humidified incubation chamber at 37.5 °C with 2%, 5% (control) and 7% CO_2 until they reached Hamburger-Hamilton stages 7 to 11 (4–13 pairs of somites) (Hamburger and Hamilton, 1992). When the embryos reached the required stage, they were extracted using filter paper and placed on the prepared albumin agar medium as previously described by Chapman (Chapman et al., 2001). The embryos were oriented with the ventral side facing up to avoid the vitelline membrane interference while approaching the somite with the microelectrode during the membrane potential measurement. The filter paper holding the embryo was immobilized with a metal ring, and the Petri dish was filled with Pennett-Compton (PC) saline, serving as the conducting medium for measuring the membrane potential of embryonic cells. PC saline is a mixture consisting of two aqueous solutions: 4% of Solution A (2.07 M NaCl, 207.91 mM KCl, 70.88 mM $CaCl_2{\cdot}H_2O$, and 62.47 mM $MgCl_2{\cdot}6H_2O$), and 6% of Solution B (13.29 mM $Na_2HPO_4{\cdot}2H_2O$ and 1.21 mM $NaH_2PO_4{\cdot}2H_2O$), mixed with deionized water (Schmitz et al., 2016). Experiments to verify the effect of KCl on V_m were conducted on embryos grown at 5% CO_2 by adding (0.3 and 0.6) mM KCl to the PC saline. All chemicals were purchased from Sigma Aldrich (Germany). The prepared samples were then used for V_m measurement.

4.2. Preparation of glass microelectrodes

Microelectrodes were prepared using borosilicate glass capillaries (OD = 1.2 mm, ID = 0.68 mm, length = 75 mm) (World Precision Instruments (WPI), USA). The capillaries were pulled using a micropipette puller (Model P-1000, Sutter Instruments, USA) with the following set parameters: heat index: 480, pull: 250, velocity: 420, delay: 70, pressure: 500. The pulled microelectrode was filled with 3 M KCl solution and inserted into a microelectrode holder (PEL, WPI, USA), without introducing air bubbles.

4.3. Measurement of membrane potential of somite-forming cells

The Petri dish containing the embryo and PC saline was positioned on a heating unit with an aperture (Bioscience Tools, USA), placed on the stage of an inverted microscope (Nikon ECLIPSE Ti, Japan), allowing visualization of the embryo. An Ag/AgCl electrode (WIP, USA) was immersed in the PC saline, serving as a reference electrode. The entire setup was placed on an optical table (MCI Air, NeuroGig Limited, UK) equipped with a Faraday cage (NG-FC-Custom-104, NeuroGig Limited, UK) to prevent external mechanical vibrations and electrical interference during the voltage measurement. A low-noise dual-channel differential electrometer (FD-223a, WPI, USA) was used to measure the membrane potential of somite-forming cells. During the measurement, the temperature of the medium containing the embryo was set to 37.5 °C, and the condition of PC solution was maintained by continuously replacing it with PC solution equilibrated with the atmosphere of the required levels of CO_2 (2%, 5%, and 7%), using a peristaltic pump. An electrode holder with a KCl-filled glass microelectrode was attached to a voltage measuring probe connected to the electrometer. V_m was measured by carefully inserting the glass microelectrode into the somite with the help of a micromanipulator (Luigs & Neumann GmbH, Germany). Voltage vs. time trace was recorded and analysed using LabScribe software (iWorx, version 4.322). Advanced Research software (NIS Elements, v 5.01) was used to visualize the glass microelectrode and the embryo during V_m recording.

4.4. Determination of periodicity of somite formation, and somite growth

To define the periodicity of somite formation (τ), the time between the appearance of two new pairs of somites of embryos cultured under appropriate experimental conditions was measured. The new segment formation was examined in embryos with initial 7 or more somite pairs. The rate of somite growth (L(t)) was determined by measuring the change in width (L) of the somite, along the anterior-posterior axis of the embryo, over time (t). For that purpose, the somite in SS II was tracked over the period of 2 h (therefore transitioning into SS III during the measurement) under the given incubation conditions.

4.5. Membrane potential of somite-forming cells observed using potential-sensitive dye

The potential-sensitive dye $DiBAC_4(3)$ (bis-(1, 3-dibutylbarbituric acid) trimethine oxonol) (Lot: MKCQ7455, Sigma Aldrich, Germany) was used to observe the membrane potential of somite-forming cells along the anterior-posterior axis of chick embryo. As the intensity of fluorescence increases, the cell becomes more hyperpolarized (Kim et al., 2013; Konrad and Hedrich, 2008). The dye solution was prepared by dissolving $DiBAC_4(3)$ in 70% ethanol to a concentration of 1 mg/mL. This stock solution was diluted (1:10) in deionized water to achieve a concentration of 100 μg/mL. This solution was then further diluted (1:10) in PC saline to reach a final concentration of 10 μg/mL. To observe V_m, eggs were initially incubated under given conditions (37.5 °C, 5% and 7% of CO_2). The embryos were then extracted into a Petri dish (without culture medium) using filter paper and immersed in the PC-dye solution for 30 min under the same CO_2 conditions. Following incubation, the embryos were washed with PC saline and imaged using confocal microscopy on an inverted microscope (ZEISS, Germany). Imaging was conducted by placing the embryos inside an incubator chamber set at 37.5 °C with 5% or 7% of CO_2 on the microscope stage. All images were captured at the same acquisition settings and all calculations were performed at raw source images. The image editing, in the form of adjusting intensity threshold, was employed solely for the better visualization of the representative image shown in the Supplementary Information (Fig S1 A), where relatively low sample fluorescence (as expected due to cells hyperpolarization) was obscured by normal background fluorescence. The fluorescence intensity values for somites were estimated from an intensity profile graph based on the intensities collected from the rectangular area encompassing somites along the anterior-posterior axis of the embryo (Fig. 1C) or encompassing a single somite area (Fig. S1), using ZEN (V3.6) image analysis software. It should be noted that advanced state-of-the-art systems employing voltage-sensitive dyes could also be used to obtain absolute membrane potential values (Brinks et al., 2015; Gest et al., 2024; Lazzari-Dean et al., 2019; Lazzari-Dean and Miller, 2021; McMillen and Levin, 2024) that in this work were measured using direct microelectrode method. The dyes have the advantage of additionally providing spatial information and $DiBAC_4(3)$ was used for such purpose in this work.

To observe the zone of extracellular voltage adjacent to the somite's surface, as demonstrated in our previous study using algal cells (Mahadeva et al., 2024), embryos were grown, extracted, and stained as mentioned above. Subsequently, the embryos were washed with PC saline and transferred into a new Petri dish with 2 mL PC saline. The evolution of the zone in the vicinity of the somite surface was visualized by exclusion of microspheres. For this purpose, suspensions of particles of two different sizes (0.5 μm and 0.2 μm) were prepared by diluting 100 μL of uncharged, non-functionalized polystyrene microspheres solutions (analytical standard; cat# 19507-5; Cat# 24050-5; Polyscience, Inc.)] in 5 mL PC saline. The Petri dish containing embryo was kept inside the incubation chamber (set to 37.5 °C and 5% or 7% CO_2) positioned on the microscope stage and filled with microsphere suspension (0.5 μm or 0.2 μm). Confocal images were captured using an inverted microscope (ZEISS, Germany). Additional experiments were performed with 0.5 μm particles to track dynamic exclusion of microspheres by changing the atmosphere in the chamber from initial 5% CO_2 to 7% CO_2 and

observing the movement of particles away from the surface. The width of the particle exclusion zone was estimated by plotting the fluorescence intensity of microspheres versus distance from the somite surface using ZEN (V3.6) image analysis software. The exclusion distance was determined by the deflection point of the intensity curve, after which the intensity (indicating microsphere concentration) started to increase from the near-zero value adjacent to the surface.

CRediT authorship contribution statement

Manohara Mahadeva: Writing – review & editing, Writing – original draft, Methodology, Formal analysis, Data curation. **Sebastian Niestępski:** Writing – review & editing, Writing – original draft, Supervision, Project administration, Methodology, Formal analysis. **Magdalena Kowacz:** Writing – review & editing, Writing – original draft, Visualization, Validation, Supervision, Resources, Project administration, Methodology, Investigation, Funding acquisition, Formal analysis, Conceptualization.

Funding

The National Science Centre (Poland) under the grant number 2020/38/E/NZ3/00039 funded this work.

Acknowledgement

We thank Prof. Jan Jankowski and AWB Spółka Fermowa sp. z o.o. Wola Szydłowska 44, 06–561 Stupsk, Ferma Drobiu Trzcianka Kolonia 39 and Turza Mała 45a for providing fertilized chicken eggs, Prof. Raquel P. Andrade for training us in chick embryo culture and extraction techniques. We also thank Cell and Tissue Analysis and Imaging Laboratory, especially Dr. Krzysztof Witek for his support with fluorescence microscopy.

Appendix A. Supplementary data

Supplementary data to this article can be found online at https://doi.org/10.1016/j.ydbio.2024.11.002.

Data availability

No data was used for the research described in the article.

References

Alvarez, I.S., Martín-Partido, G., Rodríguez-Gallardo, L., González-Ramos, C., Navascués, J., 1989. Cell proliferation during early development of the chick embryo otic anlage: quantitative comparison of migratory and nonmigratory regions of the otic epithelium. J. Comp. Neurol. 290, 278–288.
Arcangeli, A., Rosati, B., Cherubini, A., Crociani, O., Fontana, L., Ziller, C., Wanke, E., Olivotto, M., 1997. HERG- and IRK-like inward rectifier currents are sequentially expressed during neuronal development of neural crest cells and their derivatives. Eur. J. Neurosci. 9, 2596–2604.
Bagnall, K.M., Berdan, R.C., 1994. Increases in the number of cells in different areas of epithelial somites related to changes in morphology and development. Anat. Embryol. 190, 495–500.
Binggeli, R., Weinstein, R.C., 1986. Membrane potentials and sodium channels: hypotheses for growth regulation and cancer formation based on changes in sodium channels and gap junctions. J. Theor. Biol. 123, 377–401.
Blackiston, D.J., McLaughlin, K.A., Levin, M., 2009. Bioelectric controls of cell proliferation: ion channels, membrane voltage and the cell cycle. Cell Cycle 8, 3527–3536.
Blomberg, L., Hashizume, K., Viebahn, C., 2008. Blastocyst elongation, trophoblastic differentiation, and embryonic pattern formation. Reproduction 135, 181–195.
Brinks, D., Klein, A.J., Cohen, A.E., 2015. Two-photon lifetime imaging of voltage indicating proteins as a probe of absolute membrane voltage. Biophys. J. 109, 914–921.
Callies, C., Fels, J., Liashkovich, I., Kliche, K., Jeggle, P., Kusche-Vihrog, K., Oberleithner, H., 2011. Membrane potential depolarization decreases the stiffness of vascular endothelial cells. J. Cell Sci. 124, 1936–1942.
Carraco, G., Martins-Jesus, A.P., Andrade, R.P., 2022. The vertebrate Embryo Clock: common players dancing to a different beat. Front. Cell Dev. Biol. 10, 944016.
Carthew, R.W., 2021. Gene regulation and cellular metabolism: an essential partnership. Trends Genet. 37, 389–400.
Chapman, S.C., Collignon, J., Schoenwolf, G.C., Lumsden, A., 2001. Improved method for chick whole-embryo culture using a filter paper carrier. Dev Dyn 220, 284–289.
Chen, S., Cui, W., Chi, Z., Xiao, Q., Hu, T., Ye, Q., Zhu, K., Yu, W., Wang, Z., Yu, C., Pan, X., Dai, S., Yang, Q., Jin, J., Zhang, J., Li, M., Yang, D., Yu, Q., Wang, Q., Yu, X., Yang, W., Zhang, X., Qian, J., Ding, K., Wang, D., 2022. Tumor-associated macrophages are shaped by intratumoral high potassium via Kir2.1. Cell Metab 34, 1843–1859.e1811.
Chifflet, S., Hernández, J.A., Grasso, S., Cirillo, A., 2003. Nonspecific depolarization of the plasma membrane potential induces cytoskeletal modifications of bovine corneal endothelial cells in culture. Exp. Cell Res. 282, 1–13.
Chowdhury, F., Na, S., Li, D., Poh, Y.C., Tanaka, T.S., Wang, F., Wang, N., 2010. Material properties of the cell dictate stress-induced spreading and differentiation in embryonic stem cells. Nat. Mater. 9, 82–88.
Cone, C.D., Tongier, M., 1971. Control of somatic cell mitosis by simulated changes in the transmembrane potential level. Oncology 25, 168–182.
Dale, K.J., Pourquié, O., 2000. A clock-work somite. Bioessays 22, 72–83.
Dequéant, M.L., Glynn, E., Gaudenz, K., Wahl, M., Chen, J., Mushegian, A., Pourquié, O., 2006. A complex oscillating network of signaling genes underlies the mouse segmentation clock. Science 314, 1595–1598.
Fukumoto, T., Blakely, R., Levin, M., 2005. Serotonin transporter function is an early step in left-right patterning in chick and frog embryos. Dev. Neurosci. 27, 349–363.
Gadsby, D.C., Cranefield, P.F., 1979. Electrogenic sodium extrusion in cardiac Purkinje fibers. J. Gen. Physiol. 73, 819–837.
Gatenby, R.A., Gillies, R.J., 2004. Why do cancers have high aerobic glycolysis? Nat. Rev. Cancer 4, 891–899.
Gest, A.M.M., Grenier, V., Miller, E.W., 2024. Optical estimation of membrane potential values using fluorescence lifetime imaging microscopy and hybrid chemical-genetic voltage indicators. Bioelectricity 6, 34–41.
Hamburger, V., Hamilton, H.L., 1992. A series of normal stages in the development of the chick embryo. 1951. Dev Dyn 195, 231–272.
Harima, Y., Takashima, Y., Ueda, Y., Ohtsuka, T., Kageyama, R., 2013. Accelerating the tempo of the segmentation clock by reducing the number of introns in the Hes7 gene. Cell Rep. 3, 1–7.
Hopper, A., Beswick-Jones, H., Brown, A.M., 2022. The Nernst equation: using physico-chemical laws to steer novel experimental design. Adv. Physiol. Educ. 46, 206–210.
Hotary, K.B., Robinson, K.R., 1990. Endogenous electrical currents and the resultant voltage gradients in the chick embryo. Dev. Biol. 140, 149–160.
Hubaud, A., Pourquié, O., 2014. Signalling dynamics in vertebrate segmentation. Nat. Rev. Mol. Cell Biol. 15, 709–721.
Ibarra-Soria, X., Thierion, E., Mok, G.F., Münsterberg, A.E., Odom, D.T., Marioni, J.C., 2023. A transcriptional and regulatory map of mouse somite maturation. Dev. Cell 58, 1983–1995.e1987.
Ishimatsu, K., Hiscock, T.W., Collins, Z.M., Sari, D.W.K., Lischer, K., Richmond, D.L., Bessho, Y., Matsui, T., Megason, S.G., 2018. Size-reduced embryos reveal a gradient scaling-based mechanism for zebrafish somite formation. Development 145.
Jacob, M., Christ, B., Jacob, H.J., Poelmann, R.E., 1991. The role of fibronectin and laminin in development and migration of the avian Wolffian duct with reference to somitogenesis. Anat. Embryol. 183, 385–395.
Jaffe, L.F., Nuccitelli, R., 1977. Electrical controls of development. Annu. Rev. Biophys. Bioeng. 6, 445–476.
Jakobsson, E., 1980. Interactions of cell volume, membrane potential, and membrane transport parameters. Am. J. Physiol. 238, C196–C206.
Juul, J.S., Jensen, M.H., Krishna, S., 2019. Constraints on somite formation in developing embryos. J. R. Soc. Interface 16, 20190451.
Kikuchi, R., Iwai, Y., Tsuji, T., Watanabe, Y., Koyama, N., Yamaguchi, K., Nakamura, H., Aoshiba, K., 2019. Hypercapnic tumor microenvironment confers chemoresistance to lung cancer cells by reprogramming mitochondrial metabolism in vitro. Free Radic. Biol. Med. 134, 200–214.
Kim, H.Y., Jackson, T.R., Davidson, L.A., 2017. On the role of mechanics in driving mesenchymal-to-epithelial transitions. Semin. Cell Dev. Biol. 67, 113–122.
Kim, H.Y., Jackson, T.R., Stuckenholz, C., Davidson, L.A., 2020. Tissue mechanics drives regeneration of a mucociliated epidermis on the surface of Xenopus embryonic aggregates. Nat. Commun. 11, 665.
Kim, J., Sasaki, Y., Yoshida, W., Kobayashi, N., Veloso, A.J., Kerman, K., Ikebukuro, K., Sode, K., 2013. Rapid cytotoxicity screening platform for amyloid inhibitors using a membrane-potential sensitive fluorescent probe. Anal. Chem. 85, 185–192.
Konrad, K.R., Hedrich, R., 2008. The use of voltage-sensitive dyes to monitor signal-induced changes in membrane potential-ABA triggered membrane depolarization in guard cells. Plant J. 55, 161–173.
Kowacz, M., Pollack, G.H., 2020. Cells in new light: ion concentration, voltage, and pressure gradients across a hydrogel membrane. ACS Omega 5, 21024–21031.
Krol, A.J., Roellig, D., Dequéant, M.L., Tassy, O., Glynn, E., Hattem, G., Mushegian, A., Oates, A.C., Pourquié, O., 2011. Evolutionary plasticity of segmentation clock networks. Development 138, 2783–2792.
Lauschke, V.M., Tsiairis, C.D., François, P., Aulehla, A., 2013. Scaling of embryonic patterning based on phase-gradient encoding. Nature 493, 101–105.
Lazzari-Dean, J.R., Gest, A.M., Miller, E.W., 2019. Optical estimation of absolute membrane potential using fluorescence lifetime imaging. Elife 8.
Lazzari-Dean, J.R., Miller, E.W., 2021. Optical estimation of absolute membrane potential using one- and two-photon fluorescence lifetime imaging microscopy. Bioelectricity 3, 197–203.
Levin, M., 2012. Molecular bioelectricity in developmental biology: new tools and recent discoveries: control of cell behavior and pattern formation by transmembrane potential gradients. Bioessays 34, 205–217.

Levin, M., Martyniuk, C.J., 2018. The bioelectric code: an ancient computational medium for dynamic control of growth and form. Biosystems 164, 76–93.
Li, Z., Gong, Y., Sun, S., Du, Y., Lü, D., Liu, X., Long, M., 2013. Differential regulation of stiffness, topography, and dimension of substrates in rat mesenchymal stem cells. Biomaterials 34, 7616–7625.
Liao, B.K., Jörg, D.J., Oates, A.C., 2016. Faster embryonic segmentation through elevated Delta-Notch signalling. Nat. Commun. 7, 11861.
Mahadeva, M., Niestępski, S., Kowacz, M., 2024. Dependence of cell's membrane potential on extracellular voltage observed in Chara globularis. Biophys. Chem. 307, 107199.
Maia-Fernandes, A.C., Martins-Jesus, A., Borralho-Martins, N., Pais-de-Azevedo, T., Magno, R., Duarte, I., Andrade, R.P., 2024. Spatio-temporal dynamics of early somite segmentation in the chicken embryo. PLoS One 19, e0297853.
Man, C.H., Mercier, F.E., Liu, N., Dong, W., Stephanopoulos, G., Jiang, L., Jung, Y., Lin, C.P., Leung, A.Y.H., Scadden, D.T., 2022. Proton export alkalinizes intracellular pH and reprograms carbon metabolism to drive normal and malignant cell growth. Blood 139, 502–522.
Marchant, C.L., Malmi-Kakkada, A.N., Espina, J.A., Barriga, E.H., 2022. Cell clusters softening triggers collective cell migration in vivo. Nat. Mater. 21, 1314–1323.
Masamizu, Y., Ohtsuka, T., Takashima, Y., Nagahara, H., Takenaka, Y., Yoshikawa, K., Okamura, H., Kageyama, R., 2006. Real-time imaging of the somite segmentation clock: revelation of unstable oscillators in the individual presomitic mesoderm cells. Proc. Natl. Acad. Sci. U. S. A. 103, 1313–1318.
Maschner, A., Krück, S., Draga, M., Pröls, F., Scaal, M., 2016. Developmental dynamics of occipital and cervical somites. J. Anat. 229, 601–609.
McColl, J., Mok, G.F., Lippert, A.H., Ponjavic, A., Muresan, L., Münsterberg, A., 2018. 4D imaging reveals stage dependent random and directed cell motion during somite morphogenesis. Sci. Rep. 8, 12644.
McMillen, P., Levin, M., 2024. Optical estimation of bioelectric patterns in living embryos. Methods Mol. Biol. 2745, 91–102.
Nakamura, Y., Yamamoto, Y., Usui, F., Mushika, T., Ono, T., Setioko, A.R., Takeda, K., Nirasawa, K., Kagami, H., Tagami, T., 2007. Migration and proliferation of primordial germ cells in the early chicken embryo. Poultry Sci. 86, 2182–2193.
Nin, V., Hernández, J.A., Chifflet, S., 2009. Hyperpolarization of the plasma membrane potential provokes reorganization of the actin cytoskeleton and increases the stability of adherens junctions in bovine corneal endothelial cells in culture. Cell Motil Cytoskeleton 66, 1087–1099.
Nishiyama, M., von Schimmelmann, M.J., Togashi, K., Findley, W.M., Hong, K., 2008. Membrane potential shifts caused by diffusible guidance signals direct growth-cone turning. Nat. Neurosci. 11, 762–771.
Nooryani, M., Benneker, A.M., Natale, G., 2023. Self-generated exclusion zone in a dead-end pore microfluidic channel. Lab Chip 23, 2122–2130.
Nuccitelli, R., 2003. Endogenous electric fields in embryos during development, regeneration and wound healing. Radiat. Protect. Dosim. 106, 375–383.
Oginuma, M., Harima, Y., Tarazona, O.A., Diaz-Cuadros, M., Michaut, A., Ishitani, T., Xiong, F., Pourquié, O., 2020. Intracellular pH controls WNT downstream of glycolysis in amniote embryos. Nature 584, 98–101.
Oginuma, M., Moncuquet, P., Xiong, F., Karoly, E., Chal, J., Guevorkian, K., Pourquié, O., 2017. A gradient of glycolytic activity coordinates FGF and Wnt signaling during elongation of the body Axis in amniote embryos. Dev. Cell 40, 342–353.e310.
Ozkucur, N., Perike, S., Sharma, P., Funk, R.H., 2011. Persistent directional cell migration requires ion transport proteins as direction sensors and membrane potential differences in order to maintain directedness. BMC Cell Biol. 12, 4.
Palmeirim, I., Henrique, D., Ish-Horowicz, D., Pourquié, O., 1997. Avian hairy gene expression identifies a molecular clock linked to vertebrate segmentation and somitogenesis. Cell 91, 639–648.
Parkins, C.S., Stratford, M.R., Dennis, M.F., Stubbs, M., Chaplin, D.J., 1997. The relationship between extracellular lactate and tumour pH in a murine tumour model of ischaemia-reperfusion. Br. J. Cancer 75, 319–323.
Pek, Y.S., Wan, A.C., Ying, J.Y., 2010. The effect of matrix stiffness on mesenchymal stem cell differentiation in a 3D thixotropic gel. Biomaterials 31, 385–391.
Peyton, S.R., Raub, C.B., Keschrumrus, V.P., Putnam, A.J., 2006. The use of poly (ethylene glycol) hydrogels to investigate the impact of ECM chemistry and mechanics on smooth muscle cells. Biomaterials 27, 4881–4893.
Pourquié, O., 2003. The segmentation clock: converting embryonic time into spatial pattern. Science 301, 328–330.
Pourquié, O., Pourquié, O., 2001. Vertebrate somitogenesis. Annu. Rev. Cell Dev. Biol. 17.
Qin, X., Zhang, H., Zhou, X., Wang, C., Zhang, X., Ye, L., 2007. Proliferation and migration mediated by Dkk-1/Wnt/beta-catenin cascade in a model of hepatocellular carcinoma cells. Transl. Res. 150, 281–294.
Rapetti-Mauss, R., Bustos, V., Thomas, W., McBryan, J., Harvey, H., Lajczak, N., Madden, S.F., Pellissier, B., Borgese, F., Soriani, O., Harvey, B.J., 2017. Bidirectional KCNQ1:β-catenin interaction drives colorectal cancer cell differentiation. Proc. Natl. Acad. Sci. U. S. A. 114, 4159–4164.
Robinson, K.R., 1985. The responses of cells to electrical fields: a review. J. Cell Biol. 101, 2023–2027.
Roblero, L., Biggers, J.D., Lechene, C.P., 1976. Electron probe analysis of the elemental microenvironment of oviducal mouse embryos. J. Reprod. Fertil. 46, 431–434.
Roblero, L.S., Riffo, M.D., 1986. High potassium concentration improves preimplantation development of mouse embryos in vitro. Fertil. Steril. 45, 412–416.
Russell, S., Xu, L., Kam, Y., Abrahams, D., Ordway, B., Lopez, A.S., Bui, M.M., Johnson, J., Epstein, T., Ruiz, E., Lloyd, M.C., Swietach, P., Verduzco, D., Wojtkowiak, J., Gillies, R.J., 2022. Proton export upregulates aerobic glycolysis. BMC Biol. 20, 163.
Schmitz, M., Nelemans, B.K., Smit, T.H., 2016. A submerged filter paper sandwich for long-term ex ovo time-lapse imaging of early chick embryos. J. Vis. Exp.
Schröter, C., Oates, A.C., 2010. Segment number and axial identity in a segmentation clock period mutant. Curr. Biol. 20, 1254–1258.
Sen, B., Xie, Z., Howard, S., Styner, M., van Wijnen, A.J., Uzer, G., Rubin, J., 2022. Mechanically induced nuclear shuttling of β-catenin requires Co-transfer of actin. Stem Cell. 40, 423–434.
Sharma, A., Mir, R., Galande, S., 2021. Epigenetic regulation of the wnt/β-catenin signaling pathway in cancer. Front. Genet. 12, 681053.
Tamagawa, H., Ikeda, K., 2018. Another interpretation of the Goldman-Hodgkin-Katz equation based on Ling's adsorption theory. Eur. Biophys. J. 47, 869–879.
Torres, M.A., Nelson, W.J., 2000. Colocalization and redistribution of dishevelled and actin during Wnt-induced mesenchymal morphogenesis. J. Cell Biol. 149, 1433–1442.
Venters, S.J., Hultner, M.L., Ordahl, C.P., 2008. Somite cell cycle analysis using somite-staging to measure intrinsic developmental time. Dev Dyn 237, 377–392.
Vodovnik, L., Miklavcic, D., Sersa, G., 1992. Modified cell proliferation due to electrical currents. Med. Biol. Eng. Comput. 30, CE21–28.
Wang, Y., Wang, G., Luo, X., Qiu, J., Tang, C., 2012. Substrate stiffness regulates the proliferation, migration, and differentiation of epidermal cells. Burns 38, 414–420.
Winer, J.P., Janmey, P.A., McCormick, M.E., Funaki, M., 2009. Bone marrow-derived human mesenchymal stem cells become quiescent on soft substrates but remain responsive to chemical or mechanical stimuli. Tissue Eng. 15, 147–154.